

**SPEED-SENSORLESS ESTIMATION AND POSITION CONTROL OF INDUCTION
MOTORS FOR MOTION CONTROL APPLICATIONS**

A

THESIS

Presented to the Faculty

of the University of Alaska Fairbanks

in Partial Fulfillment of the Requirements

for the Degree of

DOCTOR OF PHILOSOPHY

By

Murat Barut, M.S.

Fairbanks, Alaska

December 2006

UMI Number: 3251422

INFORMATION TO USERS

The quality of this reproduction is dependent upon the quality of the copy submitted. Broken or indistinct print, colored or poor quality illustrations and photographs, print bleed-through, substandard margins, and improper alignment can adversely affect reproduction.

In the unlikely event that the author did not send a complete manuscript and there are missing pages, these will be noted. Also, if unauthorized copyright material had to be removed, a note will indicate the deletion.

UMI[®]

UMI Microform 3251422

Copyright 2007 by ProQuest Information and Learning Company.

All rights reserved. This microform edition is protected against unauthorized copying under Title 17, United States Code.

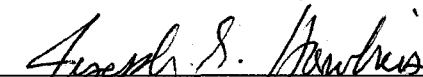
ProQuest Information and Learning Company
300 North Zeeb Road
P.O. Box 1346
Ann Arbor, MI 48106-1346

SPEED-SENSORLESS ESTIMATION AND POSITION CONTROL OF INDUCTION
MOTORS FOR MOTION CONTROL APPLICATIONS

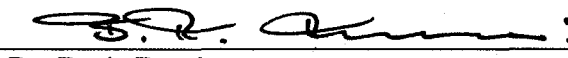
By

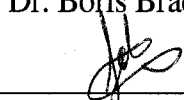
Murat Barut

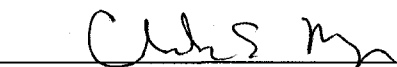
RECOMMENDED:


Dr. Joseph G. Hawkins

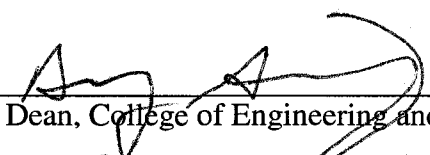

Dr. Richard W. Wies


Dr. Boris Bracio


Dr. Seta Bogosyan, Advisory Committee Chair


Chair, Department of Electrical and Computer Engineering

APPROVED:


Dean, College of Engineering and Mines


Dean of the Graduate School


Date

ABSTRACT

High performance sensorless position control of induction motors (IMs) calls for estimation and control schemes which offer solutions to parameter uncertainties as well as to difficulties involved with accurate flux and velocity estimation at very low and zero speed. In this thesis, novel control and estimation methods have been developed to address these challenges. The proposed estimation algorithms are designed to minimize estimation error in both transient and steady-state conditions over a wide velocity range, including very low and persistent zero speed operation. To this aim, initially single Extended Kalman Filter (EKF) algorithms are designed to estimate the flux, load torque, and velocity, as well as the rotor, R_r' or stator, R_s resistances. The temperature and frequency related variations of these parameters are well-known challenges in the estimation and control of IMs, and are subject to ongoing research. To further improve estimation and control performance in this thesis, a novel EKF approach is also developed which can achieve the simultaneous estimation of R_r' and R_s for the first time in the sensorless IM control literature. The so-called *Switching* and *Braided* EKF algorithms are tested through experiments conducted under challenging parameter variations over a wide speed range, including under persistent operation at zero speed. Finally, in this thesis, a sensorless position control method is also designed using a new sliding mode controller (SMC) with reduced chattering. The results obtained with the proposed control and estimation schemes appear to be very compatible and many times superior to existing literature results for sensorless control of IMs in the very low and zero speed range. The developed estimation and control schemes could also be used with a variety of the sensorless speed and position control applications, which are challenged by a high number of parameter uncertainties.

Table of Contents

	Page
Signature Page.....	i
Title Page.....	ii
Abstract.....	iii
Table of Contents.....	iv
List of Figures.....	viii
List of Tables.....	xi
List of Appendices.....	xii
Acknowledgements.....	xiii
Chapter 1: General Introduction.....	1
1.1 The objective of the thesis.....	1
1.2 Induction motors.....	4
1.3 Control methods for induction motors.....	6
1.4 Direct torque control vs. field oriented control.....	12
1.5 Requirements for speed or position-sensorless FOC and DTC systems of IMs...	13
1.6 Problems associated with observer/estimator design for IMs.....	15
1.7 Observers/estimators designed for the speed sensorless control of IMs.....	16
1.8 Controllers designed for the sensorless position control of IMs.....	25
1.9 Studies performed in the scope of this thesis.....	26
1.10 Organization of the thesis.....	34
References.....	34
Chapter 2: EKF Based Sensorless Direct Torque Control of IMs in the Low Speed	
Range.....	48
Abstract.....	48

Index Terms.....	48
2.1 Introduction.....	48
2.2 Mathematical Model of the IM.....	50
2.3 Development of the EKF Algorithm.....	52
2.4 The Speed-Sensorless DTC System.....	53
2.5 Simulation Results and Observations.....	53
2.6 Conclusion.....	57
References.....	58

Chapter 3: Sensorless Low/Zero Speed Control of Induction Motors with EKF

Estimation.....	61
Abstract.....	61
Index Terms.....	61
3.1 Introduction.....	61
3.2 Mathematical Model of the IM.....	63
3.3 Development of the EKF Algorithm.....	64
3.4 The Speed-Sensorless DTC System.....	65
3.5 Simulation Results and Observations.....	66
3.6 Conclusion.....	70
References.....	71

Chapter 4: A Switching Technique for Rotor and Stator Resistance Estimation in

Speed-Sensorless Control of IMs.....	73
Abstract.....	73
Index Terms.....	74
4.1 Introduction.....	74
4.2 Extended Mathematical Models of the IM.....	77
4.3 Development of the Switching EKF Algorithm.....	80
4.4 The Speed-Sensorless DTC System.....	83

4.5	Simulation Results and Observations.....	84
4.6	Conclusion.....	98
	References.....	100
Chapter 5: Experimental Evaluation of Braided EKF for Sensorless Control of		
	Induction Motors.....	105
	Abstract.....	105
	Index Terms.....	105
5.1	Introduction.....	105
5.2	Extended Mathematical Models for Braided EKF.....	109
5.3	Development of the Braided EKF Algorithm.....	112
5.4	Experimental Results and Observations.....	114
5.5	Conclusion.....	125
	References.....	128
Chapter 6: Sensorless Sliding Mode Position Control of Induction Motors Using		
	Braided Extended Kalman Filters.....	131
	Abstract.....	131
	Index Terms.....	131
6.1	Introduction.....	131
6.2	Mathematical Model of the IM.....	133
6.3	Proposed Position Control System.....	134
	A. Design of SMCs design with reduced chattering.....	135
	B. Braided EKF Based Observers.....	137
6.4	Simulation Results and Observations	139
6.5	Conclusion.....	144
	References.....	145
Chapter 7: General Conclusion.....		
	References.....	153

Appendices.....	155
------------------------	------------

List of Figures

	Page
Fig. 1.1 Per phase sinusoidal steady-state (equivalent circuit) model of the IMs.....	5
Fig. 1.2 Classification of IM control methods (Buja and Kazmierkowski, 2004).....	7
Fig. 1.3 Closed-loop IM drive with constant V/ Hz control strategy.....	7
Fig. 1.4 Sensorless direct field oriented (vector) control of IMs.....	9
Fig. 1.5 Indirect field oriented (vector) control of IMs.....	10
Fig. 1.6 Sensorless direct torque control (DTC) of IMs.....	12
Fig. 1.7 Structure of EKF algorithm for speed-sensorless estimation in IMs.....	23
Fig. 1.8 The proposed sliding-mode position control system.....	30
Fig. 2.1 The speed-sensorless DTC system.....	53
Fig. 2.2 Simulation results for the estimations of the EKF based estimator and the DTC system.....	55
Fig. 2.3 Simulation results for the estimation errors of the EKF based estimator and the DTC system.....	56
Fig. 2.4 Trajectory of $\hat{\psi}_{s\alpha}$ and $\hat{\psi}_{s\beta}$	57
Fig. 3.1 The rotor oriented sensorless DVC system.....	65
Fig. 3.2 Simulation results for the estimations of the EKF based estimator and the DVC system.....	68
Fig. 3.3 Simulation results for the estimation errors of the EKF based estimator and the DVC system.....	69
Fig. 4.1 Flow-chart of the novel Switching EKF algorithm.....	82
Fig. 4.2 The speed-sensorless DVC system.....	83
Fig. 4.3 Variation of the stator/rotor resistances, R_s/R_r , the reference speed value, n_m^{ref} , and applied load torque, t_L	86
Fig. 4.4 Simulation results for the estimation of velocity obtained with the Switching EKF estimator and DVC system.....	88
Fig. 4.5 Simulation results for the estimation of the load torque using the Switching EKF estimator.....	89

Fig. 4.6	Simulation results for the estimation of the stator resistance using the Switching EKF estimator.....	90
Fig. 4.7	Simulation results for the estimation of rotor resistance using the Switching EKF estimator.....	91
Fig. 4.8	Simulation results for the estimation of flux obtained with the Switching EKF estimator and DVC.....	92
Fig. 4.9	Simulation results for combined Switching EKF estimation and DVC for the zero speed range.....	93
Fig. 4.10	Comparative results in the high and low velocity range with the EKF- \hat{R}_s , EKF- \hat{R}_r and proposed method.....	97
Fig. 5.1	Flow-chart of the Braided EKF algorithm.....	114
Fig. 5.2	Schematic representation of the experimental setup.....	115
Fig. 5.3	Stator currents and voltages applied to the IM through the AC drive.....	117
Fig. 5.4	Experimental results of $EKF - R_r$ for load torque & stator resistance variations.....	119
Fig. 5.5	Experimental results of $EKF - R_s$ for load torque & rotor resistance variations.....	121
Fig. 5.6	Experimental results of Braided EKF for load torque variations at constant velocity.....	123
Fig. 5.7	Experimental results of Braided EKF for steady state with incorrect $R_s(0^+) = 2 \times R_{sn}$	124
Fig. 5.8	Experimental results for Braided EKF for low speed operation.....	126
Fig. 6.1	The proposed SM position control system.....	134
Fig. 6.2	Flow-chart of the Braided EKF algorithm.....	139
Fig. 6.3	Step-type tracking performance for proposed SMC and CF SMC.....	141
Fig. 6.4	Sinusoidal tracking performance for proposed SMC and CF SMC.....	142
Fig. 6.5	The performance of the proposed SM control system under variation of stator resistance, rotor resistance and load torque.....	143
Fig. A-1	Structure of the proposed EKF algorithm.....	160

Fig. A-2 Schematic representation of the experimental setup.....	161
Fig. A-3 Stator currents and voltages applied to the IM through the AC drive.....	164
Fig. A-4 Experimental results demonstrating R_r' update requirement.....	166
Fig. A-5 Experimental results demonstrating 4 region operation.....	167
Fig. A-6 Experimental results at high speed with EKF- R_r' and without R_s estimation..	169
Fig. A-7 Experimental results at high speed with R_s estimation and R_r' look-up table..	171
Fig. A-8 Experimental results at very low speed without R_s estimation.....	173
Fig. A-9 Experimental results at very low/zero speed with R_s estimation.....	174
Fig. B-1 Braided EKF algorithm block diagram.....	186
Fig. B-2 Variation of velocity estimation errors, e_{nm} , at high speed operation under load torque variations, for three methods.....	188
Fig. B-3 Variation of e_{nm} for zero speed and zero load for three methods.....	189
Fig. B-4 Schematic representation of the experimental setup.....	190
Fig. B-5 EKF- R_r' results for high speed operation.....	191
Fig. B-6 EKF- R_r' results for low/zero speed operation.....	192
Fig. B-7 EKF- R_s results for low/zero speed operation.....	193
Fig. B-8 EKF- R_s results for high speed operation.....	194
Fig. B-9 Braided EKF results for high speed operation.....	196
Fig. B-10 Braided EKF results for zero speed operation.....	197

List of Tables

	Page
Table 1.1 Summary of requirements for speed or position-sensorless FOC and DTC of IMs.....	14
Table 4.1 Rated values and parameters of the induction motor used in the experiments.....	84
Table 5.1a Rated values and parameters of the induction motor used in the experiments.....	115
Table 5.1b. Rated values and parameters of the DC machine used in the experiments.....	116
Table A-1 An interpolation (2-D) table with prelook-up index search to obtain variations in rotor resistance.....	160
Table A-2a Rated values and parameters of the induction motor used in the experiments.....	162
Table A-2b Rated values and parameters of the DC machine used in the experiments.....	163
Table B-1a Rated values and parameters of the induction motor used in the experiments.....	187
Table B-1b Rated values and parameters of the DC machine used in the experiments.....	187

List of Appendices

	Page
Appendix A: Sensorless-Estimation of Induction Motors in Wide Speed Range..	155
Abstract.....	155
Index Terms.....	156
A.1 Introduction.....	156
A.2 Extended Mathematical Model of the IM.....	156
A.3 Development of the EKF Algorithm.....	158
A.4 Hardware Configuration.....	161
A.5 Experimental Results and Observations.....	162
A.6 Conclusion.....	175
References.....	175
Appendix B: Braided Extended Kalman Filters for Sensorless Estimation in	
Induction Motors at High-Low/Zero Speed.....	177
Abstract.....	177
Index Terms.....	177
B.1 Introduction.....	177
B.2 Extended Mathematical Models of the IM.....	182
B.3 Development of the Braided EKF Algorithm.....	184
B.4 Simulation and Experimental Results.....	187
B.5 Conclusion.....	198
References.....	199
Appendix C: Definitions of Acronyms.....	203

Acknowledgements

First of all, I would like to thank my advisor, Dr. Seta Bogosyan, for her exceptional guidance, recommendations, help, and friendship. I would also like to express my gratitude to Dr. Metin Gokasan for his valuable help with the experimental setup, and friendliness.

Moreover, I would like to acknowledge gratefully my committee members Dr. Joseph G. Hawkins, Dr. Richard W. Wies, and Dr. Boris Bracio for their valuable suggestions and comments in the review of this thesis.

Once again, thanks to Dr. Bogosyan and Dr. Wies for providing me the experimental equipment through the establishment and improvement of the Power Electronics Laboratory at UAF, based on the NSF Grant, entitled “A Novel Approach in Improving Power Electronics and Electric Drives Courses, Curriculum, and Laboratories: Multi-University Adaptation and Implementation” which made this thesis possible.

I would like to extend my sincerest appreciation to the UAF Graduate School for funding my research with *Graduate Research Fellowships* between fall 2004 and spring 2006 and awarding me a *Thesis Completion Fellowship* and *Travel Grant* in fall 2006.

I am also grateful to the UAF Electrical and Computer Engineering Department and the UAF Office of International Programs members for their assistance and kindness.

I want to say special thanks to all members of my big family as well as to my dear friends for their constant encouragement and moral support throughout my studying at the UAF.

Last but not least, I would like to thank my wife Natavan for her love, help and understanding, and I want to dedicate this thesis to her and our future baby.

Chapter 1:

General Introduction

1.1 The objective of the thesis

The objective of this thesis is to develop robust estimation and control methods for the sensorless position and speed control of induction motors (IMs) to address the well-known challenges of parameter uncertainties and problems related to wide speed range operation, particularly persistent operation at and around zero speed.

Mechanical uncertainties, mainly due to the load torque and friction and electrical uncertainties mostly arising from the temperature and frequency dependent variations of the rotor and stator resistances, have well-known performance degrading effects on the accurate estimation of flux and velocity in the sensorless motion control applications of IMs over a wide speed range.

An additional challenge in IM sensorless position and velocity control exists at very low and zero speed in steady-state under no-load condition. In this case, the stator current, which is the only source of feedback, ceases to convey information on the rotor angular velocity, thereby giving rise to significant estimation and control errors.

Another ongoing problem is to improve the dynamic behavior of the IM control system, which constitutes a highly nonlinear and fifth order system. To this aim, controllers that are robust to the parameter, load, and model uncertainties of the IM have to be designed.

Five journal and two conference papers are prepared within the context of this thesis to address the above problems, which are the estimation and control objectives of this work. The studies performed in the scope of this dissertation are listed below:

- *Study 1:* EKF based estimation of $[i_{s\alpha} i_{s\beta} \psi_{s\alpha} \psi_{s\beta} \omega_m t_L R_s]$ for the direct torque control of IM is proposed in Chapter 2. This is the first reported study performing the simultaneous estimation of the *stator fluxes*, $\psi_{s\alpha}$ and $\psi_{s\beta}$, angular velocity, ω_m , load torque, t_L , and the stator resistance, R_s , of the IM besides the stator currents, $i_{s\alpha}$ and $i_{s\beta}$, (referred to the stator stationary frame), which are also measured as output.
- *Study 2:* EKF based estimation of $[i_{s\alpha} i_{s\beta} \psi_{r\alpha} \psi_{r\beta} \omega_m t_L R_s]$ for the sensorless direct vector control of IMs is proposed in Chapter 3. This is the first reported study performing the simultaneous estimation of the *rotor fluxes*, $\psi_{r\alpha}$ and $\psi_{r\beta}$, angular velocity, ω_m , load torque, t_L , and the stator resistance, R_s , of the IM besides the stator currents, $i_{s\alpha}$ and $i_{s\beta}$, (referred to the stator stationary frame), which are also measured as output.
- *Study 3:* EKF based estimation of $[i_{s\alpha} i_{s\beta} \psi_{r\alpha} \psi_{r\beta} \omega_m t_L R_s]$ & *look up table* – R_r' for the sensorless direct vector control (DVC) of IMs is proposed in Appendix A. This is the first study using the *combined EKF and look-up table* approach for the speed-sensorless control of IMs in real-time experiments.
- *Study 4:* Switching EKF for the estimation of $[i_{s\alpha} i_{s\beta} \psi_{r\alpha} \psi_{r\beta} \omega_m t_L R_s]$ & $[i_{s\alpha} i_{s\beta} \psi_{r\alpha} \psi_{r\beta} \omega_m t_L R_r']$ in the sensorless rotor flux oriented DVC of IMs is proposed in Chapter 4. This is the first reported study estimating R_s and R_r' for the sensorless *rotor flux* based control of IMs both in the transient and steady state *in simulations*, while also estimating the unknown load torque, velocity, rotor flux and stator current components without the need for signal injection or algorithm changes as in most previous studies.

- *Study 5:* Braided EKF based estimation of $[i_{s\alpha} i_{s\beta} \psi_{r\alpha} \psi_{r\beta} \omega_m t_L R_s]$ & $[i_{s\alpha} i_{s\beta} \psi_{r\alpha} \psi_{r\beta} \omega_m t_L R_r']$ for the sensorless rotor flux oriented DVC of IMs is proposed in Chapter 5. This is the first reported study estimating R_s and R_r' for the sensorless *rotor flux* based control of IMs both in the transient and steady state *in real-time experiments* besides the accurate estimation of the unknown load torque, velocity, rotor flux and stator current components without the need for signal injection or algorithm changes as in most previous studies.
- *Study 6:* Braided EKF for the estimation of $[i_{s\alpha} i_{s\beta} \psi_{s\alpha} \psi_{s\beta} \omega_m t_L R_s]$ & $[i_{s\alpha} i_{s\beta} \psi_{s\alpha} \psi_{s\beta} \omega_m t_L R_r']$ is proposed in Appendix B. This is the first reported study estimating R_s and R_r' for the sensorless *stator flux* based control of IMs both in the transient and steady state *in simulations and real-time experiments*, while also estimating the unknown load torque, velocity, rotor flux and stator current components without the need for signal injection or algorithm changes as in most previous studies.
- *Study 7:* Sensorless position control of IMs integrating a novel reduced chattering sliding-mode controller (SMC) with Braided EKFs is proposed in Chapter 6. This is the first reported study presenting a novel reduced chattering SMC law which combines the concept of the *power rate reaching law* and the *average-equivalent control law* for the sensorless position control of IMs.

The major contributions of this thesis are the following:

- * Novel single EKF schemes are developed to estimate R_s or R_r' as well as the load torque, velocity and flux. These schemes yield improved results over existing sensorless IM control literature results in terms of estimation and control accuracy.

- * Novel “switching” and “braided” EKF techniques are developed which benefit from the high convergence rate, persistency of excitation, and smoothing performance inherent in EKFs. However, these multi-EKF techniques also offer a solution to the well-known problem of single EKFs in estimating a high number of parameters. With the design of these novel estimation techniques, the simultaneous estimation of R_s and R_r' has been possible for the first time in the sensorless IM control literature, without the need for signal injection. The results demonstrate an improved estimation accuracy over the whole speed range, particularly at and around zero speed, even under challenging parameter uncertainties and load variations. The resulting peer-reviewed journal publications (Barut et al., 2006b; Barut et al., 2006c; Barut et al., 2006d) and conference publications (Barut et al., 2005c; Barut and Bogosyan, 2007) are presented in the main body of the thesis, and Bogosyan et al. (2006a) and Bogosyan et al. (2006b) are presented in the Appendix section.
- * A novel sliding mode control (SMC) technique with reduced chattering is developed for the sensorless position control of IMs. The approach demonstrates improved performance against parameter and load variations in comparison to another high performance chattering-free SMC technique used for sensorless IM position control (Sahin et al., 1995) and other demanding motion control applications (Bogosyan et al., 1997; Bogosyan et al., 1999). The chattering-free SMC taken as benchmark has already proven to outperform classical control methods in motion control, such as proportional-integral-derivative (PID) control.

1.2 Induction motors

Induction motors (IMs) are the well-known work horses of the industry. This is due to their low cost and longevity in addition to their simplicity in terms of manufacturing. Another attraction of IMs is that the motor and drive system requires very little or no maintenance.

IMs are represented by the “standard” per phase sinusoidal steady-state (equivalent circuit) model based on the concept of a “rotating transformer” shown in Fig. 1.1 (Barnes and Gross, 1995). Here, L_{ls} and R_s are the stator leakage inductance and resistance, respectively. L_{lr}' and R_r' are the rotor leakage inductance and resistance, referred to the stator side, respectively. L_m is the magnetizing inductance. V_s and I_s are the amplitude of stator voltage and current. I_r' is the amplitude of rotor current referred to the stator side and s is the slip.

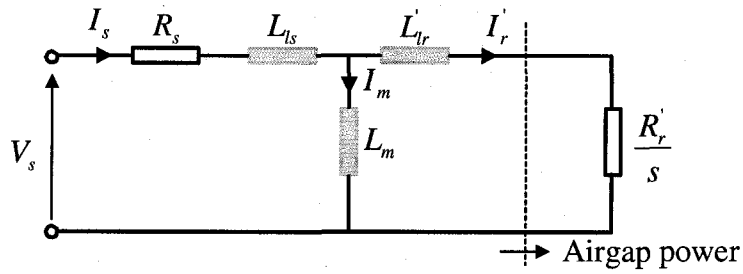


Fig. 1.1 Per phase sinusoidal steady-state (equivalent circuit) model of the IMs

This model is valid when the IM runs in the steady state with constant rotor speed and under sinusoidal supply voltage. If an IM is used within a closed-loop motion control application, its transient behavior also has to be taken into consideration (Bose, 2002). Therefore, high performance control of the IMs calls for using a dynamic model of the IM, which is known as the *two-phase* or *fundamental* IM model, described by

$$\frac{d}{dt} \begin{bmatrix} i_{sx} \\ i_{sy} \\ \psi_{rx} \\ \psi_{ry} \\ \omega_m \end{bmatrix} = \begin{bmatrix} -\left(\frac{R_s}{L_s} + \frac{L_m^2 R_r'}{L_s L_r'^2}\right) & 0 & \frac{L_m R_r'}{L_s L_r'^2} & \frac{L_m}{L_s L_r'} p_p \omega_m & 0 \\ 0 & -\left(\frac{R_s}{L_s} + \frac{L_m^2 R_r'}{L_s L_r'^2}\right) & -\frac{L_m R_r'}{L_s L_r'^2} & \frac{L_m}{L_s L_r'} p_p \omega_m & 0 \\ \frac{R_r'}{L_r'} L_m & 0 & -\frac{R_r'}{L_r'} & -p_p \omega_m & 0 \\ 0 & \frac{R_r'}{L_r'} L_m & p_p \omega_m & -\frac{R_r'}{L_r'} & 0 \\ -\frac{1}{J_L} \frac{3}{2} p_p \frac{L_m}{L_r'} \psi_{ry} & \frac{1}{J_L} \frac{3}{2} p_p \frac{L_m}{L_r'} \psi_{rx} & 0 & 0 & -\frac{B_L}{J_L} \end{bmatrix} \begin{bmatrix} i_{sx} \\ i_{sy} \\ \psi_{rx} \\ \psi_{ry} \\ \omega_m \end{bmatrix} + \begin{bmatrix} \frac{1}{L_s} & 0 \\ 0 & \frac{1}{L_s} \\ 0 & 0 \\ 0 & 0 \\ 0 & 0 \end{bmatrix} \begin{bmatrix} v_{sx} \\ v_{sy} \end{bmatrix} + \begin{bmatrix} 0 \\ 0 \\ 0 \\ 0 \\ -\frac{1}{J_L} \end{bmatrix} t_L \quad (1.1)$$

Here, $L_s = L_{ls} + L_m$ and $L_r' = L_{lr}' + L_m$ are the stator and rotor inductance, respectively. $L_\sigma = \sigma L_s = \left(L_s - \frac{L_m^2}{L_r'}\right)$ is the stator transient inductance. σ is the leakage factor. $v_{s\alpha}$ and $v_{s\beta}$ are the stator stationary axis components of stator voltages. $i_{s\alpha}$ and $i_{s\beta}$ are the stator stationary axis components of stator currents. $\psi_{r\alpha}$ and $\psi_{r\beta}$ are the stator stationary axis components of rotor flux. ω_m is the angular velocity. p_p is the pole pair. t_L is the load torque. J_L is the total inertia. B_L is the total viscous friction coefficient.

Eq. (1.1) is valid both in the steady-state and transient state. Considering this model, an IM is a *dynamic* system due to the differential operations, an *uncertain time-varying* system due to the variations in load torque and other system parameters, such as temperature and frequency based variations of rotor and stator resistances, and a *nonlinear* system due to the products of the states (Shi, 2001). Therefore, the control of IMs presents significant challenges due to this highly nonlinear and coupled fifth order dynamics of the system under strong parameter and model uncertainties, and with only three state variables ($i_{s\alpha}$, $i_{s\beta}$ and ω_m) that are available for measurement. In this respect, IMs represent a theoretically attractive and practically significant class of nonlinear systems and their control is regarded as a benchmark problem in the area of nonlinear control (Ortega et al., 2001). That is why high performance control and estimation techniques of IMs (Bose, 1997) have been developing very fast and receiving a lot of attention in the literature.

1.3 Control methods for induction motors

Induction motor control methods are classified into two major categories: *scalar* and *vector* control (Buja and Kazmierkowski, 2004). Fig. 1.2 demonstrates the general classification of the variable frequency methods. In this figure, control methods within the scope of this thesis are drawn with bold lines.

Fig 1.3 shows the closed-loop scalar control (V/Hz) strategy. In this figure, the difference between the reference rotor angular speed value, ω_m^* , and the actual rotor angular

velocity, ω_m , which is speed error, is processed through a controller, usually a proportional-integral (PI) controller, and a limiter to obtain the slip-speed reference, ω_{sl}^r . Then, the slip-speed reference and electrical rotor angular velocity are added together to generate the fundamental stator frequency reference. Thereafter, the fundamental stator frequency reference also determines the amplitude of the fundamental stator voltage reference, V_s^r . Namely, in the scalar control (V/Hz) principle, IM is fed with a 3-phase

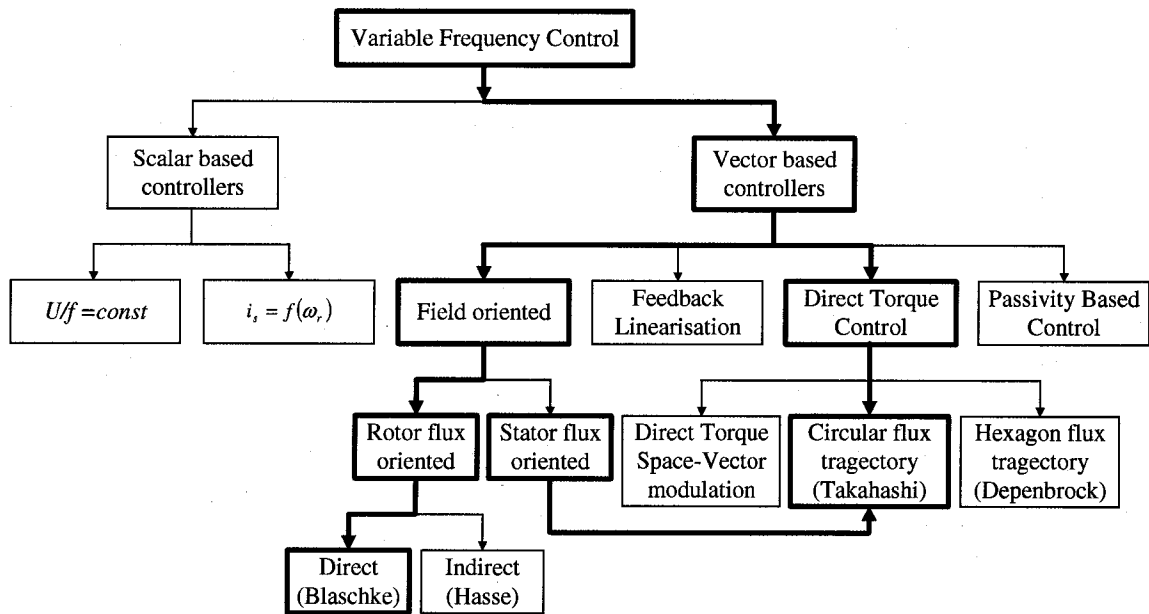


Fig. 1.2 Classification of IM control methods (Buja and Kazmierkowski, 2004)

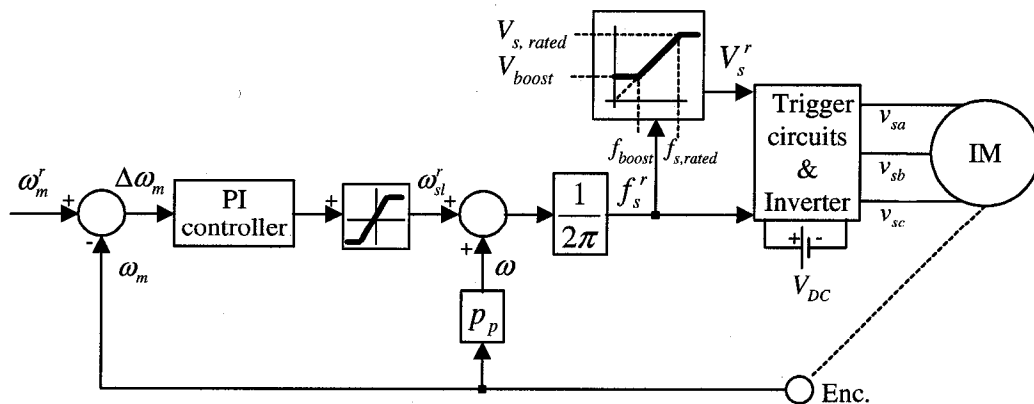


Fig. 1.3 Closed-loop IM drive with constant V/ Hz control strategy

sinusoidal voltage whose amplitude is proportional to the frequency, except below the boost frequency and over the rated frequency, as shown in Fig. 1.3.

However, scalar control (V/Hz) of IMs results in quasi steady-state control (Martins and Carvalho, 2001). The most important variables, such as torque and flux, are neither directly nor indirectly controlled in this case (Nash, 1997; Martins and Carvalho, 2001). The control is provided with a frequency and voltage reference generator which produces an output of constant volts per hertz and, hence, drives a pulse width modulation (PWM). Although simple, two of the main drawbacks are limited speed accuracy, especially in the low speed range, and poor torque response (Nash, 1997; Martins and Carvalho, 2001). The reaction of the motor to the applied frequency and voltage governs flux and torque levels which are not under the control of the drive. Briefly, this control principle allows using a sinusoidal steady-state model of the IMs (AVR494, 2005) which is not valid for the transient state. Therefore, it satisfies only moderate dynamic demands and performances (Holtz, 2002).

On the contrary, vector control uses a state space model of the IMs. Therefore, it provides the control of not only the magnitude and frequency (angular velocity) of the voltage, current, and flux, but also instantaneous positions of their space vectors. Hence, the vector control method offers the correct orientation of these vectors both in transient and steady state (Buja and Kazmierkowski, 2004). That is why vector control is called a high-performance control method.

As stated by the definition above, vector control is a general control philosophy that can be performed in many different ways (Buja and Kazmierkowski, 2004). The greatest breakthrough, known as *field-oriented control* (FOC) or *vector control* (VC), has been proposed by Hasse in 1969 and Blaschke in 1971 in Germany (Buja and Kazmierkowski, 2004). The utilization of the FOC method, which converts the control of the IM to that of a separately excited DC motor by keeping the rotor (or stator) flux constant on the d-axis,

[illegible]

On the other hand, for the indirect field-oriented control of IMs demonstrated in Fig. 1.5, accurate knowledge of the slip frequency (calculated as a function of the rotor time constant) is required in addition to the rotor speed. Moreover, the main difference between the FOC methods is based on the calculation of the decoupling angle or field angle of the oriented flux, which is $\hat{\theta}_{rf}$ and θ_{rf} in Fig. 1.4 and 1.5, respectively. However, the performance of both field orientation methods depends primarily on accurate values of the motor parameters used in field orientation (Shieh et al., 1998).

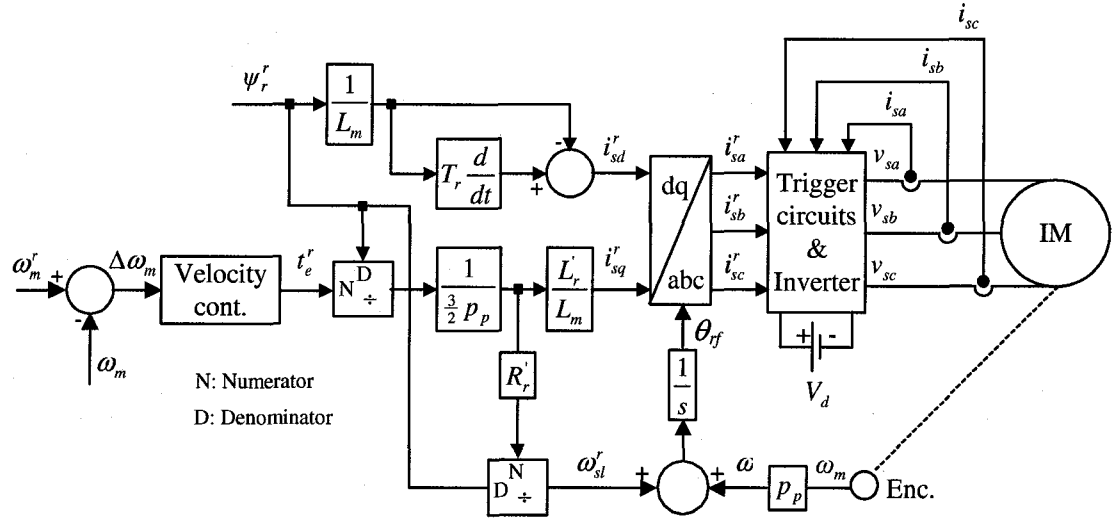


Fig. 1.5 Indirect field oriented (vector) control of IMs

A drawback of FOC is the assumption of a constant rotor flux that leads to an only “asymptotically” decoupled rotor velocity from the flux (Bodson et al., 1994). From the theoretical perspective, it is possible that a variety of coordinate or nonlinear transformations can be proposed to obtain decoupling and linearization of the IM equations (Buja and Kazmierkowski, 2004). This has originated in methods known as modern nonlinear control. In studies such as Krzeminski (1987), Marino et al. (1990), and Marino et al. (1993) a nonlinear transformation is developed which aims at the independent control of the speed and rotor flux magnitude in the new coordinates by the use of the so-called *input–output linearization (feedback linearization or input–output decoupling)* controller (or by a SMC (Sabanovic and Izosimov, 1981)) (Novotnak et al., 1999; Buja and Kazmierkowski, 2004). Although the decoupling condition is always kept in this method, the performance of the feedback linearization methods depends on how well the system parameters are known (Wang and Chen, 2005).

The FOC or feedback linearization control provides the IM with almost the same dynamic behavior as in the case of a separately excited dc motor, but both of the control

schemes are sensitive to parameter and load torque variations of the IM. Furthermore, globally defined control laws are required for FOC of IMs (Wang and Chen, 2005).

The passivity approach is another scheme for stability analysis of feedback systems. In the passivity based control (PBC) approach, an IM is described in terms of the Euler-Lagrange equations expressed in generalized coordinates (Buja and Kazmierkowski, 2004). Although the controller in PBC is globally stable, the control performance is still affected by the parametric uncertainties and external disturbances like the load torque of the IM (Wang and Chen, 2005).

In the mid-80s, the *direct-torque control* (DTC) method was proposed by Takahashi and Noguchi (1986), and Depenbrock (1988), which departs from the idea of coordinate transformation and the dc motor control analogy (Buja and Kazmierkowski, 2004). DTC replaces the decoupling control with hysteresis band comparators, which is highly suitable for the on-off operation of inverters in IM control. This control strategy is commonly referred to as DTC. Depenbrock's control method, also called *direct self-control*, is preferable in the high power range applications, where a lower inverter switching frequency can justify higher current distortion (Casadei et al., 2002). In this thesis, the attention will be mainly focused on Takahashi and Noguchi's control scheme, as shown in Fig 1.6, which is more suitable in the small and medium power range applications and is also called DTC.

DTC has three distinctive properties (Ortega et al., 2001):

- 1) It concentrates on *stator* (instead of rotor) flux regulation.
- 2) Contrary to classical FOC, it does not aim at an asymptotically stable nonlinear transformation (and thus it does not involve additional current control loops).
- 3) It simply takes into account the discrete nature of the control actions, which resembles a *switching logic*.

Currently, both FOC and DTC drives are widely used and are made available on the market by several producers (Schofield, 1995; Tiitinen and Surandra, 1996; Casadei et al., 2002), but their robust (to parameter and model uncertainties) and speed-sensorless solutions, generally established for different applications that require very low or zero speed, still do not exist. However, in spite of theoretical issues to be solved, there is a noticeable interest from industry, transportation and civil applications for low cost and precise speed-sensorless systems able to efficiently drive IMs at very low speed and, specifically, at zero speed (Consoli et al., 2003).

The DTC method (Fig. 1.6) involves the direct choice of the appropriate optimum switching modes in order to keep the flux and torque errors within a predetermined band limit (in a hysteresis band) (Casadei et al., 2002). The errors are defined as the difference between the reference and the measured (estimated) values of flux and torque.

Unlike FOC methods (Fig. 1.4 and 1.5), the DTC technique requires utilization of hysteresis band comparators instead of flux and torque controllers, PIs. To replace the coordinate transformations and pulse width modulation (PWM) signal generators of FOC, DTC uses look-up tables to select the switching procedure based on the inverter states. Therefore, the configuration of the DTC is much simpler than the FOC system (Idris and Yatim, 2004). Because of the delays removed in DTC, which are related to the PWM modulator stage and PIs (current control loops), torque response is better than that available with either dc or field oriented control (Schofield, 1995; Nash, 1997; Casadei et al., 2002).

However, the response during steady-state operation of DTC drives includes considerable torque, flux, and current ripples or spikes, and acoustical noise arises during operation. Actually, the two major problems associated with DTC drives have been addressed in the literature: the variation of the switching frequency of the inverter used in the drives with operating conditions and the high torque ripple (Idris and Yatim, 2004). However, using space-vector modulation (SVM), instead of the switching logic in the conventional DTC, offers better control and helps improve the steady-state behavior of the drive (Lascu et al., 2004a). Finally, DTC drives with SVM provide excellent performance in terms of reduced torque and flux pulsations, reliable startup and low speed operation, a well-defined harmonic spectrum, and quiet operation (Lascu et al., 2004a; Buja and Kazmierkowski, 2004). Thus, the switching frequency is constant and the switching pattern can be further optimized.

1.5 Requirements for speed or position-sensorless FOC and DTC systems of IMs

Both control methods could be developed with reference to stator, air-gap and rotor flux. However, rotor oriented control that allows for the independent control of flux and torque is preferred for FOC. Stator based control, which is less sensitive to parameter variations offers a simpler solution and is, therefore, more adequate for DTC (Barut et al., 2005a).

To achieve high efficiency control, both FOC and DTC require the accurate knowledge of the amplitude and angular position of the flux with reference to the stationary stator axis (in Cartesian coordinates). Additionally, information on the rotor angular velocity is required for velocity control over a wide speed range and in the low and zero-speed range for position control applications. In the conventional approach, the flux vector is obtained utilizing the Hall effect or search coil sensors, while incremental encoders are used for rotor angular velocity (Barut et al., 2005a). A problem with the utilization of measurement devices is the increased hardware complexity and cost. Additionally, those sensors are usually affected by mechanical vibrations and high temperatures of the operating environment. Thus, it is often more practical to attain the states by observers or estimators. However, the fifth-order nonlinear and time-varying nature of the mathematical model of the IM poses some problems in the observer design, mainly arising from modeling errors, parameter uncertainties and changing operating conditions. Finally, all requirements for the velocity and position control applications of the speed or position-sensorless FOC and DTC IM drives are summarized in Table 1.1 (Casadei et al., 2002; Wai, 2002; Consoli et al, 2003; Buja and Kazmierkowski, 2004).

Table 1.1 Summary of requirements for speed or position-sensorless FOC and DTC of IMs

	Indirect FOC	Direct FOC	DTC
Flux information	-	✓	✓
Speed information	✓	✓	✓
Summary of control task	1) To obtain robust estimations of <i>speed</i> and <i>rotor time</i> constant in the ranges of zero, low and high velocities for both in steady and transient states of IM. 2) To design robust controllers like PI/PID or other type	1) To obtain robust estimations of <i>speed</i> and <i>flux</i> in the ranges of zero, low and high velocities for both steady and transient states of IM. 2) To design robust controllers like PI/PID or other type	1) To obtain robust estimations of <i>speed</i> and <i>flux</i> in the ranges of zero, low and high velocities for both steady and transient states of IM. 2) To design robust controllers like PI/PID or other type

PI is a proportional-integral controller.

PID is a proportional-integral-derivative controller

1.6 Problems associated with observer/estimator design for IMs

The design of reliable observers and estimators for highly uncertain, time-varying, high order, nonlinear and dynamic systems such as IMs is a difficult task due to temperature and frequency dependent system parameters as well as instantaneous variations of load torque and velocity. Uncertainties in the IM parameter estimates are the most crucial factors in the design of an observer or estimator. From the general point of view, uncertainties in an electric motor can be classified in two groups—electrical and mechanical. The stator and rotor resistances are the most important sources of electrical uncertainty in an IM due to their dependence on temperature and frequency. For the stator side, the variation of the resistance could be determined by measuring or estimating the temperature (Al-Tayie and Acarnley, 1997), but there are physical difficulties in determining the rotor resistance in a squirrel cage IM. The performance of speed-sensorless control systems is also affected by mechanical uncertainties related to load torque and friction. Therefore, uncertainties related to the resistances and the mechanical side should be identified or estimated simultaneously to achieve an improved control performance.

On the other hand, the performance of estimation and hence speed-sensorless control still constitutes a persisting challenge at low and zero speed (Holtz, 2006). Besides parameter uncertainties, problems arise due to increased noise-to-signal ratios in measured output voltage and input currents, especially under low or no load conditions. An additional difficulty is encountered at zero speed in steady-state, when the stator currents, which are measured as output in sensorless control, cease to convey information on the rotor angular velocity around zero stator frequency (Holtz, 2000; Holtz and Quan, 2003). This is mainly due to the fact that all flux estimation methods rely on the effect of the rotor induced voltages on the measured variables of the stator side and those effects almost vanish with decreasing stator frequency (Holtz, 2000; Holtz, 2006). Thus, in the design of observers for sensorless control of IMs, not only robustness against parameter and

model uncertainties must be achieved, but solutions must be sought for operation at and around zero speed.

1.7 Observers/estimators designed for the speed-sensorless control of IMs

In the conventional estimation approach, the flux vector is obtained from the voltage (V-I) model using the measured stator voltages and currents and/or the current (I- ω) model requiring the measured stator current and rotor angular velocity (Jansen and Lorenz, 1994). The V-I estimator utilizing open-loop pure integration suffers from increased noise on voltage and current and quantization errors in the digital system, in addition to problems related to the offset, gain and conversion factors especially in the low speed operation range (Vas, 1998), even with the correct knowledge of the stator resistance. As a solution to the problem, the integrator is replaced by a low-pass filter. However, in this case, as the stator excitation frequency approaches the corner frequency of the filter, the filter gain decreases and more importantly, because the 90° phase shift is not maintained, the accurate determination of the flux position with respect to the stationary stator axis is not possible (Holtz, 2002). The I- ω estimator, on the other hand, is highly sensitive to rotor time constant variations, particularly in the high velocity range (at no-load) where slip rate assumes very small values and small errors in the velocity measurement give rise to considerable errors in the determination of flux position (Habetler et al., 1998). In velocity control applications, the design of both I- ω and V-I flux estimators require knowledge of the rotor mechanical velocity. However, open-loop flux and velocity estimators (Vas, 1998) designed to meet this requirement are highly sensitive to parameter variations. Therefore, closed-loop parameter and state estimators are developed for an improved performance against errors in the initial values of the states as well as parameter and model uncertainties.

Among the first reported studies on closed-loop velocity estimation, Schauder (1992) takes a Model-Reference Adaptive System (MRAS) approach based on Popov's stability criterion assuming the slower variation of velocity with respect to the electrical states.

Improvements have been made to this study in terms of parameter variation and integration in Fang-Zheng and Fukao (1994). However, the estimation performance in Schauder (1992), and Fang-Zheng and Fukao (1994) and in a more recent study (Vasic and Vukosavic, 2001), is not quite satisfactory in the very low or zero speed region due to the open loop flux estimation and/or the utilization of the back electro-motive force (EMF) vector for the estimation of velocity.

To achieve an improved performance, closed-loop estimators and observers have been designed for the determination of flux as well as velocity. Among the first reported studies taking this approach, Sangwongwanich et al. (1990) uses SMC, Tajima and Hori (1993) develops a Gopinath's reduced-order observer, while Kubota et al. (1993) and Yang and Chin (1993) utilize the Lyapunov and Popov criteria, respectively. Stable observers have not been achieved with these approaches, for the very low and zero frequency range in the regenerative region (Sangwongwanich et al., 1990; Tajima and Hori, 1993; Kubota et al., 2002; Suwankawin and Sangwongwanich, 2002), except in Hinkkanen (2004). Additionally, with the speed adaptive full-order flux observer in Kubota et al. (1993) and Yang and Chin (1993), the observer gain matrix requires adjustment to suppress the oscillations on the estimated velocity resulting from the variation of velocity references and load conditions in the steady-state (Kojabadi et al., 2002). Sliding-Mode Observers (SMO), as in Utkin (1993) and Sahin et al. (1995), have also been designed with the error correction term reflected in the observer model as a multiplicative term. In theory, the switching frequency should be infinite to prevent chattering on the sliding surface (Rodic and Jezernik, 2002), which poses problems in some applications. A recent study given in Lascu et al. (2004a) uses a sliding-mode flux observer with chattering that does not require speed adaptation and SMO based stator resistance adaptation for speed-sensorless control. Satisfactory results are presented in the 3-6 rpm operation region, but no results are presented in the zero speed region. Derdiyok et al. (2002) present a chattering-free SMO observing the rotor flux and

velocity as well as the rotor time constant. However, persistent operation at zero speed has not been addressed.

Another method utilized for the closed-loop state and parameter estimation of IMs is the Extended Luenberger Observer (ELO). In studies, such as Du et al. (1995), the velocity is reflected in the model as a slow varying or constant parameter. In spite of an improved performance in the steady-state, this approach has given rise to a significant observer error in the velocity during the transient state. Additionally, to improve the system response for various speeds, the observer gain matrix is adjusted based on the rotor speed. Differently, in Du and Brdys (1993), the estimation of the angular velocity is carried out using the equation of motion. However, similar to other ELO based studies on speed-sensorless control, performance in the low speed region has not been addressed.

To address the problems in the low and zero speed range, the motor anisotropies are exploited, either via the injection of continuous high frequency signals or by direct use of the inverter PWM signals, which cause repetitive transient excitation (Holtz and Quan, 2003). These methods using the anisotropic properties of the machine (Holtz, 2006; Caruana et al., 2006) and model based methods using induction motor state equations have been competing for the improvement of the zero and low speed performance of sensorless IM drives (Holtz, 2006). Speed-sensorless control methods based on the signal injection are capable of long-term stability at zero stator frequency. However, they are highly sophisticated and require customized designs for a particular motor drive (Holtz and Quan, 2003; Holtz, 2006). Because of these restrictions, improving the estimation accuracy of the fundamental model becomes highly attractive again.

Therefore, for the solution of the problem at zero and very low speed, new model based estimation methods have been proposed recently, such as those in Cirrincione and Pucci (2005), Cirrincione et al. (2006), and Edelbaher et al. (2006), specifically addressing persistent operation at zero speed. Among those studies, Cirrincione and Pucci (2005)

use MRAS based linear neural networks presenting results with a maximum velocity estimation error of 95 [rpm] during a persistent operation interval of 60 [sec] at zero speed. Cirrincione et al. (2006) use a total least square (TLS) based speed adaptive flux observer which enables zero stator frequency operation over an interval of 60 [sec], with mean and maximum estimation error values of 1.34 [rpm] and 38 [rpm], respectively, at zero load. Edelbaher et al. (2006) utilize a continuous sliding mode approach, for which zero stator frequency results are obtained under load and presented only for a very short interval of 4 [sec].

As is well known, temperature and frequency based variations of stator (R_s) and rotor (R_r') resistances play an important role in the rotor and stator oriented IM models and their variations influence the estimation and control performance significantly besides variations in load torque. Some studies seeking an observer-based solution to the problem of the parameter variations could be listed as follows. In Lascu et al. (2004a), besides a speed estimator, a sliding mode based flux observer and an online sliding-mode adaptation for the stator resistance is designed for the DTC of IMs, but the speed estimator and the resistance adaptation suffer from variations of the rotor resistance and the load torque, respectively. In the speed-sensorless study based on a speed adaptive flux observer (Guidi and Umida, 2000), the stator resistance has been estimated based on a two-time scale approach, while in the ELO in Du and Brdys (1993), the rotor fluxes and rotor velocity are estimated, as well as the step-type load torque. However, no estimation has been conducted for the stator resistance. Also, neither of the studies in Guidi and Umida (2000) and Du and Brdys (1993) have taken the rotor resistance into consideration. On the other hand in Faiz and Sharifian (2001), the angular velocity and slip frequency (reflecting in the effect of the load torque) have been taken into account in addition to the rotor resistance, only with an initial value of $R_r'(0)=0.85 R_m'$.

Among studies reported so far on R_s and R_r' estimation, Faiz and Sharifian (2001) state that the simultaneous estimation of the stator and rotor resistances gives rise to instability

in the speed-sensorless case. On the other hand, in studies such as Ha and Lee, (2000), and Tajima et al. (2002) the speed and rotor flux are estimated besides stator resistance and rotor resistance by injecting high frequency signals to the flux and magnetizing current commands, respectively. However, in Ha and Lee (2000), the algorithm identifying the resistances used in a feedback linearization controller is applicable only when the sensorless speed control system is in steady state, but not when the load torque is varying largely or when the speed command is being changed, as stated by the authors. On the other hand, in Tajima et al. (2002), it is stated that persistent operation at zero frequency is not possible and that the proposed drive can compete with a speed sensor equipped drive only if accuracy in steady-state is not essential and operation under high loads is not a requirement. Zhen and Xu (1998) present a MRAS based on 3 models, one of which is used for the estimation of the rotor time constant via high frequency signal injection. The other 2 models are used interchangeably, by enabling the stator resistance estimation only during short intervals, during which the rotor speed has reached the steady state. Recently, Edelbaher et al. (2006) present a sensorless control scheme using an open-loop estimator to calculate R_r' and a model reference adaptation for R_s . However, the performance of the parameter estimation is not demonstrated and only evaluated indirectly via the estimated velocity and flux. Among other studies performing R_s and R_r' estimation, in Cirrincione et al. (2006), Lascu et al. (2005), Ohyama et al. (2005), Lascu et al. (2004a) and Lascu and Trzynadlowski (2004b), R_r' estimation is conducted by adjusting its value in proportion to the estimated R_s .

In addition to the above mentioned group of studies taking a deterministic approach to the design of closed-loop observers, there are also Extended Kalman Filter (EKF) based applications in the literature, taking a stochastic approach for the control of IMs with velocity sensors (Lin, 1996; Wade et al., 1997; Finch et al., 1998) and without sensors.

The Kalman filter (KF) is a well-known recursive algorithm that takes the stochastic state space model of the system into account, together with measured outputs to achieve the

optimal estimation of states (Chen and Dunnigan, 2002) in multi-input, multi-output systems. The system and measurement noises are considered to be in the form of white noise. These noises represent computational inaccuracies, modelling errors and errors in the measurements. The optimality of the state estimation is achieved with the minimization of the covariance of the estimation error. For nonlinear problems, such as IMs, the KF is not strictly applicable, since linearity plays an important role in its derivation and performance as an optimal filter. The EKF attempts to overcome this difficulty by using a linearized approximation where the linearization is performed about the current state estimate (Goodwin and Sin, 1984). This process requires a discrete model of the IM, which can be given in the following general form:

$$\begin{aligned}\underline{x}_e(k+1) &= \underline{f}_e(\underline{x}_e(k), \underline{u}_e(k)) + \underline{w}_1(k) \\ &= \underline{A}_e(\underline{x}_e(k))\underline{x}_e(k) + \underline{B}_e\underline{u}_e(k) + \underline{w}_1(k)\end{aligned}\quad (1.2)$$

$$\begin{aligned}\underline{Z}(k) &= \underline{h}_e(\underline{x}_e(k)) + \underline{w}_2(k) \\ &= \underline{H}_e\underline{x}_e(k) + \underline{w}_2(k)\end{aligned}\quad \text{(measurement equation)} \quad (1.3)$$

Here \underline{f}_e is the nonlinear function of the states. \underline{x}_e is the extended state vector. \underline{A}_e is the system matrix. \underline{u}_e is the control input vector. \underline{B}_e is the input matrix. \underline{h}_e is the function of the outputs. \underline{H}_e is the measurement matrix. \underline{w}_1 and \underline{w}_2 are the process and measurement noise, respectively.

As mentioned before, EKF involves the linearized approximation of the nonlinear model (1.2-1.3) and uses the current estimation of states $\hat{\underline{x}}_e(k)$ and inputs $\hat{\underline{u}}_e(k)$ in linearization by using,

$$\underline{F}_e(k) = \left. \frac{\partial \underline{f}_e(\underline{x}_e(k), \underline{u}_e(k))}{\partial \underline{x}_e(k)} \right|_{\hat{\underline{x}}_e(k), \hat{\underline{u}}_e(k)} \quad (1.4)$$

Different from standard EKF applications, in this thesis the EKF scheme is derived with the consideration of control input error for increased estimation accuracy, based on a study (Bogosyan et al., 2001) on EKF applications to motion control systems. This approach involves the addition of the following term:

$$\underline{F}_u(k) = \frac{\partial \underline{f}_e(\underline{x}_e(k), \underline{u}_e(k))}{\partial \underline{u}_e(k)} \bigg|_{\hat{\underline{x}}_e(k), \hat{\underline{u}}_e(k)} \quad (1.5)$$

With this addition, the EKF algorithm can be given in the following recursive relations:

$$\underline{N}(k) = \underline{F}_e(k) \underline{P}(k) \underline{F}_e(k)^T + \underline{F}_u(k) \underline{D}_u \underline{F}_u(k)^T + \underline{Q} \quad (1.6a)$$

$$\underline{P}(k+1) = \underline{N}(k) - \underline{N}(k) \underline{H}_e^T (\underline{D}_\xi + \underline{H}_e \underline{N}(k) \underline{H}_e^T)^{-1} \underline{H}_e \underline{N}(k) \quad (1.7b)$$

$$\hat{\underline{x}}_e(k+1) = \hat{\underline{f}}_e(\underline{x}_e(k), \hat{\underline{u}}_e(k)) + \underline{P}(k+1) \underline{H}_e^T \underline{D}_\xi^{-1} (\underline{Z}(k) - \underline{H}_e \hat{\underline{x}}_e(k)) \quad (1.8c)$$

Here, \underline{Q} is the covariance matrix of the system noise, namely model error. \underline{D}_ξ is the covariance matrix of the output noise, namely measurement noise. \underline{D}_u is the covariance matrix of the control input noise ($v_{s\alpha}$ and $v_{s\beta}$), namely input noise. \underline{P} and \underline{N} are the covariance matrix of state estimation error and extrapolation error, respectively.

The algorithm involves two main stages: prediction and filtering. In the prediction stage, the next predicted states $\hat{\underline{f}}_e(\cdot)$ and predicted state error covariance matrices, $\underline{P}(\cdot)$ and $\underline{N}(\cdot)$ are processed, while in the filtering stage, next estimated states, $\hat{\underline{x}}_e(k+1)$, obtained as the sum of the next predicted states and the correction term (2nd term in (1.8c)) are calculated.

The EKF algorithm utilizes the extended or augmented model in (1.2) and (1.3) to generate all states required for the sensorless control system, by using the measured

phase currents, $i_{s,\alpha\beta}$, and voltages, $v_{s,\alpha\beta}$. The schematic representation of the algorithm is given in Fig. 1.7.

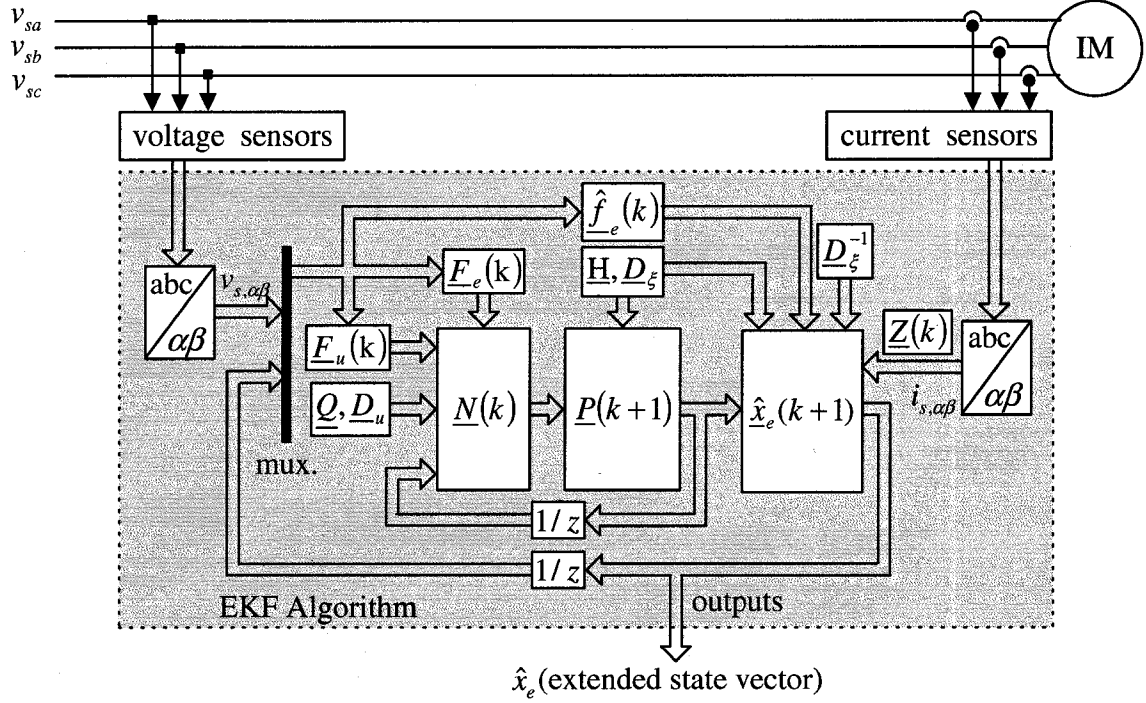


Fig. 1.7 Structure of EKF algorithm for speed-sensorless estimation in IMs.

Different from the other methods, the model uncertainties and nonlinearities inherent in IMs are well suited to the stochastic nature of EKF (Wade et al., 1995; Cupertino et al., 1999). With this method, it is possible to make the online estimation of states while performing the simultaneous identification of parameters in a relatively short time interval (Salvatore et al., 1993), by also taking system and process and measurement noises directly into account. This is the reason why the EKF has found wide application in sensorless control of IMs, in spite of its computational complexity. However, with the developments in high performance processor technology, the computational burden and speed of EKF has ceased to be a problem. Among recent sensorless studies using EKF estimation for IMs, Kim et al. (1994) and Shi et al. (2002) estimate the flux and velocity, while Lee and Chen (1998) uses an adaptive flux observer in combination with a reduced

second order Kalman filter for the same purpose. None of these studies estimate the load and motor resistances, resulting in a performance that is sensitive to the variation of these parameters. In the reduced order EKF studies in Wenqiang et al. (2001), Qiongxuan and Zhiyue (2000), Garcia Soto et al. (1999), and El Moucary et al. (1999), the velocity is estimated as a constant parameter, which gives rise to a significant estimation error in the velocity during the transient state, especially under instantaneous load variations, although the performance is improved in the steady state. While Wenqiang et al. (2001), Qiongxuan and Zhiyue (2000), and Garcia Soto et al. (1999) methods are sensitive to the resistance variations, El Moucary et al. (1999) also estimate the rotor resistance only. However, the estimation of rotor resistance is performed by the injection of low amplitude, high frequency signals to the flux reference in the direct vector control (DVC) of IMs. This has caused fluctuations in the motor flux, torque and speed. The other studies such as Chen and Dunnigan (2002) with speed sensors, and Du and Brdys (1993) without speed sensors compare the results of EKF using the IM model in the rotating axes (the synchronous frame) with that of SMO and ELO for high speed operation, respectively. Finally, Zhou and Lai (2000) perform the low speed performance comparison of open-loop speed estimator, MRAS, ELO, and EKF based estimators. A common feature in all these studies is the estimation of velocity, which is taken into consideration as a slow varying or constant parameter, except in Du and Brdys (1993). Although good results have been obtained in those studies in the relatively low and high speed operation region, the performance at zero stator frequency or at very low speed is not satisfactory or not addressed at all.

Finally, our previous studies on the sensorless velocity control of IMs, which estimate all states required for speed-sensorless FOC or DTC of the IM, as well as the load torque including viscous friction (Barut et al., 2002b; Barut et al., 2003a; Barut et al. 2003b; Barut et al., 2004; Barut et al., 2006a) or the load torque and rotor resistance (Barut et al., 2002a; Barut et al., 2003c; Barut et al., 2003d; Barut et al., 2005a, Barut et al., 2005b), demonstrate improved results both in simulations and experiments performed in a wide

speed range, including high, low and zero speed. In these studies, the velocity has been estimated via the consideration of the equation of motion in the EKF models. However, all of the results in our previous studies are noted to be sensitive to variations in stator resistance, especially at very low velocity and zero speed.

1.8 Controllers designed for the sensorless position control of IMs

As mentioned previously in Section 1.5, control objectives mainly involve the development of robust controllers against parameter and model uncertainties. This could be achieved by adaptive feedback linearization methods provided the system model and parameters are known accurately. However, considering the uncertainties involved with the IM model, SMC based robust control methods may be viewed as more viable solutions for sensorless IM control.

PID controllers are widely used in motor control and other industrial applications because they provide simple structure, design and implementation, while also ensuring a good control performance (Astrom and Hagglund, 2001; Kukolj et al., 2001; Kim and Han, 2006). However, the parameter-tuning of the controller is quite a difficult task for highly nonlinear systems, such as IMs under parameter variations and external disturbances, when the aim is to track desired dynamics (Heber et al., 1997; Wai, 2003). Therefore, artificial intelligence based studies as in Wai (2003), Wai and Chang (2004), and Khaorapapong and Ariyadirek (2004) recently have also been proposed for the position control of IMs. However, these methods need computationally complex algorithms, network architecture or fuzzy rules which are constructed by a time-consuming trial-and-error tuning procedure.

The SMC is a very effective approach for the solution of the problem due to its well-established design criteria, easy implementation, fast dynamic response, and robustness to parameter variations, when a system is in a sliding mode (Utkin, 1993; Hung et al., 1993; Kaynak et al., 2001; Shiau and Lin, 2001). However, the well-known drawback of

the SMC is chattering, which is due to high-frequency control activity and may excite unmodeled plant dynamics. Thus, to reduce the chattering, several modifications have been proposed in previous work related to the sliding mode position control of IMs. Dunnigan et al. (1998), Xia et al. (2000), Goh et al. (2004), and Wang and Chen (2005) use Slotine's sliding mode control approach, first-order low-pass filter (LPF), a pseudo sliding technique, and an adaptive law for estimating the load torque disturbance, respectively. In Dunnigan et al. (1998), the tracking error is kept in a thin boundary layer, while the work of Xia et al. (2000) gives a sluggish response in the transient state. While electrical uncertainty effects on performance of the controller were not addressed at all in Goh et al. (2004), the method used in Wang and Chen (2005) is sensitive to variations in the rotor time constant and no sinusoidal tracking control results were presented. Moreover, in all studies mentioned above, position sensors have been used.

Among previous studies using SMC for the sensorless position control of IMs, Sahin et al. (1995) present a chattering-free SMC based on the average-equivalent control approach. The simulation results have been obtained under variations of 20% and 8% in rotor and stator resistance at rated load, respectively. However, zero load-zero speed operation, which is very critical in the sensorless position control of IMs, has not been addressed at all. Moreover, it should be noted that there is a trade-off between robustness and chattering reduction (Suyitno et al., 1993).

1.9 Studies performed in the scope of this thesis

In this thesis, to meet the challenges in sensorless position control, initially methods are sought to address problems related to accurate estimation of parameters and states, particularly at low and zero speed within the context of sensorless velocity control. To this aim, first, two new EKF based observers (Barut et al., 2005c; Barut et al., 2006b) are developed for speed-sensorless DTC and direct FOC (or also called DVC) in order to improve the estimation performance at very low and zero speed operation by achieving robustness against variations in the stator resistance and load torque. The differences

between these two studies are the proposed IM models used in each EKF algorithm and their simulation based testing for DTC in the former, and DVC in the latter paper in order to evaluate the performance of the obtained EKF algorithm. To provide solutions for both types of flux orientations, Barut et al. (2005c) provide the independent control of flux and torque for DVC, while Barut et al. (2006b) consider the stator flux based IM model offering a simpler solution by DTC. Hence, the results obtained with different sensorless control methods in both studies indicate that the proposed EKF based observers perform well with different switching procedures of inverters required by the control methods in each study. Additionally, due to the system noise (model errors) inherently introduced in EKF schemes, there has been no need to add white noise to the measured states (in this case stator currents). The estimation of the motor velocity via the equation of motion in combination with the PWM originated dynamics of the current help reflect the rotor information to the stator side via the mechanical torque. This aspect of EKF becomes particularly useful in sensorless estimation in the problematic low and zero speed operation region. For improved estimation accuracy, The proposed EKF algorithms also take into consideration the control input error due to the limited wordlength of the analog-to-digital converter (ADC), as first implemented for high precision motion control in Bogosyan et al. (2001). Thus, both Barut et al. (2005c) and (2006b) have yielded good results through simulations by removing the deteriorating effects of stator resistance and load torque uncertainties, particularly in low and zero speed operation, without the need for signal injection as is commonly the case in previous studies. However, the results have also demonstrated that the frequency and temperature uncertainties related to the rotor resistance are significant throughout the whole velocity range. Hence, they should also be estimated to improve estimation accuracy for high performance sensorless motion control.

Thus, as a simple solution, in Bogosyan et al. (2006a) an algorithm is developed, which combines the estimations of the stator resistance, R_s , load torque, t_L , velocity and rotor flux with an offline-estimation of rotor resistance, R_r' . To this aim, the extended model is

continuously updated with R_r' values from a look-up table, which is constructed via the EKF estimation in Barut et al. (2005b). As demonstrated by the successful experimental results obtained with the combined EKF and look-up table approach, the estimated states and parameters undergo a very short transient and attain their steady-state values accurately, with no need for signal injection due to the inherent noise introduced by EKF. The significant improvement achieved with the estimation scheme over a wide speed range motivates the utilization of the approach in practice, in cases where one single EKF might not be adequate to handle the high number of parameters to be estimated, thereby compromising estimation accuracy. However, the performance of the approach should be further improved by increasing the “sensitivity” of the R_r' look-up table to velocity, torque and temperature variations or better yet by incorporating a second on-line EKF scheme, which runs in parallel (or consecutively) with the first, to estimate the additional parameters. This solution also addresses the well-known limitations of a single EKF estimating a high number of parameters.

Estimation of a high number of parameters and states was first implemented by using the parallel processing capability of supercomputers in Bogosyan (2004) and promising results were obtained. However, due to the practical aims of the sensorless IM control and considering the limitations of current microcontroller technologies, the consecutive use of the EKF algorithms (instead of parallel) was seen as a more realistic option in this thesis. Thus, another novel concept of EKF implementation has been introduced in Barut et al. (2006c) and Barut et al. (2006d), leading to the first reported studies for the simultaneous on-line estimation of the stator and rotor resistances in sensorless control of IMs.

The resulting *Switching* and *Braided EKF* estimation techniques offer different variations for the implementation of multiple EKF algorithms to estimate accurately a higher number of parameters than would be possible with any single EKF or other algorithm. The technique is based on the consecutive execution of two EKF algorithms having

exactly the same configuration and being derived based on the same extended model, except for one state where R_s in one is replaced by R_r' in the other. The number of sampling periods, n , is determined based on the desired system performance. The Switching EKF approach thus applied provides the accurate estimation of an increased number of parameters than would be possible with a single EKF algorithm. The Braided EKF, on the other hand, intends to keep a “close eye” on the estimation error in case of faster or unmatched parameter variations (uncertainties occurring in parameters that are not estimated in that interval), and switches the EKF algorithms on and off at every sampling period. Both Braided and Switching EKF algorithms perform the simultaneous and accurate estimation of rotor, R_r' and stator, R_s resistances, both in the transient and steady state, and in both high and low or zero speed operation, which is seen as an important challenge in speed-sensorless IM control. Both methods are tested with simulations and experiments under challenging variations of the load torque, velocity references and with both matched and unmatched parameter variations. The new algorithms yield improved R_r' and R_s estimation performance, both in the transient and steady state of speed and load torque variations, over previous methods requiring signal injection and algorithm changes for different parameters at constant speed.

The major difference between Barut et al. (2006d) and Bogosyan et al. (2006b) is that in the latter braided technique, the two EKFs use their own covariance matrix of state estimation error, which is different from previous studies (Barut et al., 2006c; Barut et al., 2006d) where the two EKF algorithms running in turn use the same covariance matrix of state estimation error. Another difference is that while Barut et al. (2006d) is tested experimentally for the DVC control strategy and mostly in low and high speed regions, Bogosyan et al. (2006b) is tested experimentally for DTC of IMs and in the whole speed range, with particular emphasis on persistent operation in the zero speed range and under no load conditions. All EKF schemes also estimate the velocity via the equation of motion, and not as a constant term as is common with most past studies.

Lastly, a novel reduced chattering SMC law is developed for the sensorless position control of IMs (Fig. 1.8) in Barut and Bogosyan (2007).

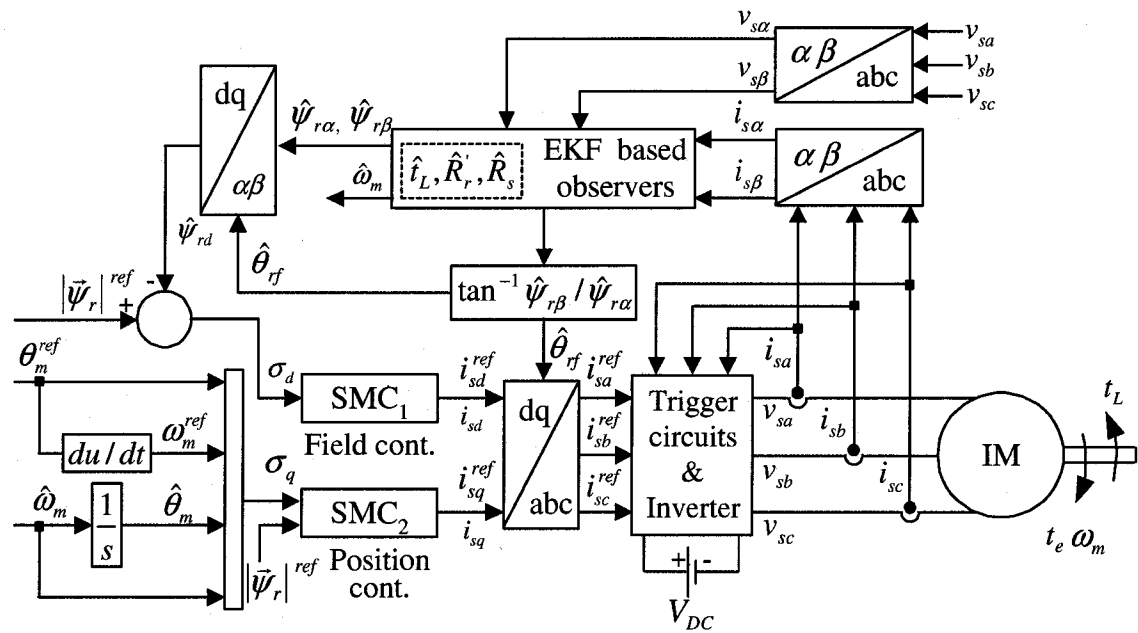


Fig. 1.8 The proposed sliding-mode position control system.

The developed control combines the concept of the power rate reaching law in Hung et al. (1993) and the average-equivalent control law in Bogosyan et al. (1997) and Bogosyan et al. (1999). In the proposed control law, the equivalent control represents the average control signal which is required to keep the switching variable on the switching surface. The power rate switching term is considered to make the controller robust against matched uncertainties and to attain sliding mode in a short time interval. However, although the control law is robust against parameter variations, in sensorless control, the performance is very much dependent on how well the states are estimated. This, in turn, calls for reliable estimation methods that can account for stator and rotor resistance variations as well as the load torque. To this aim, the developed controller is combined with the novel Braided EKF estimation technique developed in Barut et al. (2006d). Finally, the obtained simulation results show that the proposed SMC and

estimator combination provides a superior performance over the SMC and observer in Sahin et al. (1995).

Below is a per paper summary of the main contributions of the thesis:

- **Study 1:** *EKF based estimation of $[i_{s\alpha} i_{s\beta} \psi_{s\alpha} \psi_{s\beta} \omega_m t_L R_s]$ for the DTC of IM.*

The major contribution of this study is the development of an Extended Kalman Filter (EKF) based speed-sensorless direct torque control (DTC) of induction motors (IMs) for an improved performance, especially at low and zero speed operation by achieving robustness against variations in the stator resistance and load torque. This is achieved by the EKF based simultaneous estimation of the stator fluxes, $\psi_{s\alpha}$ and $\psi_{s\beta}$, angular velocity, ω_m , load torque, t_L , and the stator resistance, R_s , as well as the stator currents, $i_{s\alpha}$ and $i_{s\beta}$, (referred to the stator stationary frame), which are also measured as output.

Resulting conference papers: Barut, M., Bogosyan, S. and Gokasan, M. (2005c) (in Chapter 2).

- **Study 2:** *EKF based estimation of $[i_{s\alpha} i_{s\beta} \psi_{r\alpha} \psi_{r\beta} \omega_m t_L R_s]$ for the sensorless DVC of IMs.*

The major contribution of this study is the development of an EKF based rotor flux oriented speed-sensorless direct vector control (DVC) system of induction motors (IMs). The approach taken in the study increases robustness against stator resistance, R_s , and load torque, t_L , uncertainties, the effects of which are known to give rise to performance deteriorations in the sensorless control of IMs, especially at very low and zero speed operation. This is achieved by the EKF based simultaneous estimation of the rotor fluxes, $\psi_{r\alpha}$ and $\psi_{r\beta}$, angular velocity, ω_m , load torque, t_L , and the stator resistance, R_s , of the IM besides the stator currents, $i_{s\alpha}$ and $i_{s\beta}$, (referred to the stator stationary frame), which are also measured as output.

Resulting journal papers: Barut, M., Bogosyan, S. and Gokasan, M. (2006b) (in Chapter 3).

- **Study 3:** *EKF based estimation of $[i_{s\alpha} i_{s\beta} \psi_{r\alpha} \psi_{r\beta} \omega_m t_L R_s]$ & look up table – R_r' for the sensorless DVC of IMs.*

The major contribution of this study is the development of an EKF based scheme, which aims to solve the R_s and R_r' estimation problem in IM sensorless control. This is achieved by the combined EKF and look-up table approach for the speed-sensorless control of IMs in real-time experiments. That is, to further improve estimation accuracy, the extended model of the EKF algorithm is continuously updated with R_r' values from a look-up table, which is also constructed via a self-commissioning EKF scheme.

Resulting journal papers: Bogosyan, S., Barut, M., and Gokasan, M. (2006a) (in Appendix A).

- **Study 4:** *Switching EKF for the estimation of $[i_{s\alpha} i_{s\beta} \psi_{r\alpha} \psi_{r\beta} \omega_m t_L R_s]$ & $[i_{s\alpha} i_{s\beta} \psi_{r\alpha} \psi_{r\beta} \omega_m t_L R_r']$ in the sensorless rotor flux oriented DVC of IMs.*

The major contribution of this study is the development of a “switching” EKF based estimation technique, which aims at the accurate estimation of an increased number of parameters both in the transient and steady state for sensorless control of IMs. It is based on two EKF algorithms that are switched *on* and *off* every n sampling periods ($n \times T$). The novel technique is specifically used for the estimation of rotor and stator resistances, R_r' and R_s , besides the unknown load torque, velocity, rotor flux and stator current components without signal injection, and performs the simultaneous estimation of R_s and R_r' for the sensorless rotor flux based control of IMs both in the transient and steady state in simulations. The proposed algorithm is run in combination with the speed-sensorless rotor flux oriented direct vector control (DVC) of IMs.

Resulting journal papers: Barut, M., Bogosyan, S. and Gokasan, M. (2006c) (in Chapter 4)

- **Study 5:** *Braided EKF based estimation of $[i_{s\alpha} i_{s\beta} \psi_{r\alpha} \psi_{r\beta} \omega_m t_L R_s]$ & $[i_{s\alpha} i_{s\beta} \psi_{r\alpha} \psi_{r\beta} \omega_m t_L R_r']$ for the sensorless rotor flux oriented DVC of IMs.*

The major contribution of this study is the development of a “braided” EKF based observer approach for the speed-sensorless *rotor flux* based control of IMs. The observer involves the consecutive use of two EKF algorithms at every time step and achieves the simultaneous estimation of R_s and R_r' as well as flux, torque and velocity, without the need for signal injection or algorithm changes as in most previous studies. In this study, the effectiveness of the method is demonstrated by real-time experiments in the low and high speed range.

Resulting journal papers: Barut, M., Bogosyan, S. and Gokasan, M. (2006d) (in Chapter 5).

- **Study 6:** *Braided EKF for the estimation of $[i_{s\alpha} i_{s\beta} \psi_{s\alpha} \psi_{s\beta} \omega_m t_L R_s]$ & $[i_{s\alpha} i_{s\beta} \psi_{s\alpha} \psi_{s\beta} \omega_m t_L R_r']$.*

The major contribution of this study is the development of the Braided EKF technique for speed-sensorless *stator flux* based control of IMs. The algorithm is once again used for the simultaneous estimation of R_s and R_r' to improve the estimation accuracy of flux and velocity both in the transient and steady state. The performance of the Braided EKF technique is demonstrated using simulations and real-time experiments over a wide speed range, and particularly for persistent operation at zero speed. It has been noted that the new algorithm outperforms, or is at least comparable to the few past studies in all speed ranges and particularly at and around zero speed.

Resulting journal papers: Bogosyan, S., Barut, M., and Gokasan, M. (2006b) (in Appendix B).

- **Study 7:** *Sensorless position control of IMs integrating a novel reduced chattering sliding mode controller (SMC) with Braided EKFs.*

The major contribution of this study is the development of a sensorless sliding mode position control method for the rotor flux oriented DVC of IMs. The reduced-order sliding mode controller (SMC) combines the power rate reaching law with the average-equivalent control law. In this study, the new SMC is integrated with the Braided EKF

to demonstrate the performance of the combined estimation and control for the sensorless position control of IMs. The simulation results demonstrate a very promising performance over a wide speed range, including persistent operation at zero speed under no load.

Resulting conference papers: Barut, M., Bogosyan, S. and Gokasan, M. (2007) (in Chapter 6)

1.10 Organization of the thesis

The thesis is organized as follows. After a discussion of previous literature on sensorless estimation and control of IMs in Chapter 1, Chapter 2 proceeds with the “*EKF Based Sensorless Direct Torque Control of IMs in the Low Speed Range*”. Next, Chapter 3 introduces “*Sensorless Low/Zero Speed Control of Induction Motors with EKF Estimation*”. Chapter 4 describes “*Switching EKF Technique for Rotor and Stator Resistance Estimation in Speed-Sensorless Control of IMs*”. Chapter 5 offers “*Experimental Evaluation of Braided EKF for Sensorless Control of Induction Motors*”, followed by Chapter 6 presenting “*Sensorless Sliding Mode Position Control of Induction Motors Using Braided Extended Kalman Filters*”. The obtained results, contributions, and future directions are discussed in Chapter 7, and finally, “*Sensorless-Estimation of Induction Motors in Wide Speed Range*”, “*Braided Extended Kalman Filters for Sensorless Estimation in Induction Motors at High-Low/Zero*”, and “*Definitions of Acronyms*”, are presented in Appendix A, Appendix B, and Appendix C, respectively.

References

Al-Tayie, J.K. and Acarnley, P. P. (1997), “Estimation of speed, stator temperature and rotor temperature in cage induction motor drive using the Extended Kalman Filter algorithm”, *IEE Proceedings—Electric Power Applications*, Vol. 144 No. 5, pp. 301–309.

Astrom, K.J. and Hagglund, T. (2001), “The future of PID control”, *Control Engineering Practice*, Vol. 9 No. 11, pp. 1163–1175.

AVR494: Atmel Corporation application notes (2005), AC induction motor control using the constant V/f principle and a natural PWM algorithm.

Barnes, M.L. and Gross, C.A. (1995), "Comparison of induction machine equivalent circuit models," *Proceedings of IEEE-The 27th Southeastern Symposium on System Theory*, pp. 14–17.

Barut, M., Bogosyan, S. and Gokasan, M. (2002a), "EKF based estimation for direct vector control of induction motors", *Proceedings of the IEEE-IECON'02 Annual Meeting*, Vol. 2, pp. 1710–1715.

Barut, M., Bogosyan, S. and Gokasan, M. (2002b), "Genişletilmiş Kalman Filtresi tabanlı akı, hız ve yük momenti kestiricisi", *Proceedings of the Turkish National Automatic Control Committee Conference (TOK 2002)*, pp. 211–217 (In Turkish).

Barut, M., Bogosyan, S. and Gokasan, M. (2003a), "Sensorless direct vector control of induction motors using EKF algorithm", *Proceedings of the International Conference on Mathematics and Informatics for Industry (MII-2003)*, pp. 22–29.

Barut, M., Gokasan, M. and Bogosyan, S. (2003b), "EKF based speed sensorless direct torque control system for induction motors", *Proceedings of the Third International Conference on Electrical and Electronics Engineering (ELECO'03)*, Electric-Control part, pp. 319–323.

Barut, M., Bogosyan, S. and Gokasan, M. (2003c), "EKF based sensorless direct vector control of induction motors", *Proceedings of the IEEE-IECON'03 Annual Meeting*, Vol. 1, pp. 318–322.

Barut, M., Bogosyan, S. and Gokasan, M. (2003d), "An EKF based reduced order estimator for the sensorless control of IM's", *Proceedings of the IEEE-Conference on Control Applications (CCA'03)*, Vol. 2, pp. 1256–1261.

Barut, M., Bogosyan, S. and Gokasan, M. (2004), "EKF based estimator for sensorless direct torque control of induction motors", *Proceedings of the International Aegean Conference on Electrical Machines and Power Electronics (ACEMP 04)*, pp. 515–520.

Barut, M., Bogosyan, S. and Gokasan, M. (2005a), "Speed sensorless direct torque control of IMs with rotor resistance estimation", *Energy Conversion and Management (Elsevier)*, Vol. 46 No. 3, pp. 335–349.

Barut, M., Bogosyan, S. and Gokasan, M. (2005b), "An EKF based estimator for speed sensorless vector control of induction motors", *Electric Power Components & Systems, formerly Electric Machines and Power Systems (Taylor–Francis)*, Vol. 33 No. 7, pp. 727–744.

Barut, M., Bogosyan, S. and Gokasan, M. (2005c), "EKF based sensorless direct torque control of IMs in the low speed range", *Proceedings of the IEEE International symposium on Industrial Electronics (ISIE 2005)*, Vol. 3, pp. 969–974.

Barut, M., Bogosyan, S. and Gokasan, M. (2006a), "Speed sensorless estimation for induction motors using Extended Kalman Filters", *IEEE Transactions on Industrial Electronics*. (In press)

Barut, M., Bogosyan, S. and Gokasan, M. (2006b), "Sensorless low/zero speed control of induction motors with EKF estimation", *World Scientific and Engineering Academy and Society (WSEAS) Transactions on Systems*, Vol. 5 No. 11, pp. 2530–2535.

Barut, M., Bogosyan, S. and Gokasan, M. (2006c), "A Switching technique for rotor and stator resistance estimation in speed-sensorless control of IMs", *Energy Conversion and Management (Elsevier)*. (In review)

Barut, M., Bogosyan, S. and Gokasan, M. (2006d), "Experimental evaluation of Braided EKF for sensorless control of induction motors", *IEEE Transactions on Industrial Electronics*. (In press)

Barut, M. and Bogosyan, S. (2007), "Sensorless sliding mode position control of induction motors using Braided Extended Kalman Filters", *Proceedings of the IEEE International symposium on Industrial Electronics (ISIE 2007)*. (To be submitted)

Bodson, M., Chiasson, J. and Novotnak, R. (1994), "High-performance IM control via input-output linearization", *IEEE Control Systems Magazine*, Vol. 14 No. 4, pp. 25–33.

Bogosyan, S., Gokasan M., and Sabanovic A. (1997), "Robust-adaptive linearization with torque ripple minimization for a PMSM driven single link arm," *Proceedings of the IEEE-IECON'97 Annual Meeting*, Vol. 1, pp. 102–107.

Bogosyan S., Gokasan M., and Jafarov E.M. (1999), "A sliding mode controllers for a nonlinear time-varying motion control system", *Proceedings of the IEEE-IECON'97 Annual Meeting*, Vol. 2, pp. 1008–1013.

Bogosyan, S., Gokasan, M. and Hajiyeve, C. (2001), "An application of EKF for the position control of a single link arm", *Proceedings of IEEE-IECON'01 Annual Meeting*; Vol. 1, pp. 564–569.

Bogosyan, S. (2004), Parallel Kalman Filters for state/parameter estimation in nuclear power plants, ARSC Faculty Camp Report.

Bogosyan, S., Barut, M., and Gokasan, M. (2006a), "Sensorless estimation of induction motors in wide speed range", *The International Journal for Computation and Mathematics in Electrical and Electronic Engineering (COMPEL)*. (In review)

Bogosyan, S., Barut, M., and Gokasan, M. (2006b), "Braided Extended Kalman Filters for sensorless estimation in induction motors at high-low/zero", *IEE Proceedings- Control Theory & Applications*. (In review)

Bose, B.K. (1997), "High performance control and estimation in AC drives", *Proceedings of the IEEE-IECON'97 Annual Meeting*, Vol. 2, pp. 377–385.

Bose B.K. (2002), Modern power electronics and AC drives, Prentice Hall Inc., New Jersey.

Buja, G.S. and Kazmierkowski, M.P. (2004), "Direct torque control of PWM inverter-fed AC motors-a survey", *IEEE Transactions on Industrial Electronics*, Vol. 51 No. 4, pp.744–757.

Caruana, C., Asher, G.M. and Sumner, M. (2006), "Performance of HF signal injection techniques for zero-low-frequency vector control of induction machines under sensorless conditions", *IEEE Transactions on Industrial Electronics*, Vol. 53 No. 1, pp. 225-238.

Casadei, D., Profumo, F., Serra, G. and Tani, A. (2002), "FOC and DTC: two viable schemes for induction motors torque control", *IEEE Transactions on Power Electronics*, Vol. 17 No. 5, pp. 779-787.

Chen, F. and Dunnigan, M.W. (2002), "Comparative study of a sliding-mode observer and Kalman Filters for full state estimation in an induction machine", *IEE Proceedings-Electric Power Applications*, Vol. 149 No. 1, pp. 53-64.

Cirrincione, M. and Pucci, M. (2005), "An MRAS-based sensorless high-performance induction motor drive with a predictive adaptive model", *IEEE Transactions on Industrial Electronics*, Vol. 52 No. 2, pp 532-551.

Cirrincione, M., Pucci, M., Cirrincione, G. and Capolino, G.-A. (2006), "An adaptive speed observer based on a new total least-squares neuron for induction machine drives", *IEEE Transactions on Industry Applications*, Vol. 42 No. 1, pp 89-104.

Consoli, A., Scarcella, G. and Testa, A. (2003), "Using the induction motor as a flux sensor: new control perspectives for zero-speed operation of standard drives", *IEEE Transactions on Industrial Electronics*, Vol. 50 No. 5, pp.1052-1061.

Cupertino, F., Lattanzi, A., Salvatore, L. and Stasi, S. (1999), "Induction motor control in the low-speed range using EKF- and LKF-based algorithms", *Proceedings of the IEEE-ISIE'99 Annual Meeting*, Vol. 3, pp. 1244-1249.

Depenbrock, M. (1988), "Direct self-control (DSC) of inverter-fed induction machine", *IEEE Transactions on Power Electronics*, Vol. 3 No. 4, pp. 420-429.

Derdiyok, A., Guven, M.K., Rehman, H., Inanc, N. and Xu, L. (2002), "Design and implementation of a new sliding-mode observer for speed-sensorless control of induction motor", *IEEE Transactions on Industrial Electronics*, Vol. 49 No. 5, pp. 1177-1182.

Du, T. and Brdys, M.A. (1993), "Shaft speed, load torque and rotor flux estimation of induction motor drive using an extended Luenberger observer", *Proceedings of the 6th IEEE International Conference on Electrical Machines and Drives*, Conf. Publ. No. 376, pp. 179–184.

Du, T., Vas, P. and Stronach, F. (1995), "Design and application of extended observers for joint state and parameter estimation in high-performance AC drives", *IEE Proceedings-Electric Power Applications*, Vol. 142 No. 2, pp. 71–78.

Dunnigan, M.W., Wade, S., Williams, B.W. and Yu, X. (1998), "Position control of a vector controlled induction machine using Slotine's sliding mode control approach", *IEE Proceedings-Electric Power Applications*, Vol. 145 No. 3, pp. 231–238.

Edelbaher, G., Jezernik, K. and Urlep, E. (2006), "Low-speed sensorless control of induction machine", *IEEE Transactions on Industrial Electronics*, Vol. 53 No. 1, pp. 120–129.

El Moucary, Ch., Garcia Soto, G. and Mendes, E. (1999), "Robust rotor flux, rotor resistance and speed estimation of an induction machine using the Extended Kalman Filter", *Proceedings of IEEE ISIE'99 Annual Meeting*, Vol. 2, pp. 742–746.

Faiz, J. and Sharifian, M.B.B. (2001), "Different techniques for real time estimation of an induction motor rotor resistance in sensorless direct torque control for electric vehicle", *IEEE Transactions on Energy Conversion*, Vol. 16 No. 1, pp. 104–109.

Fang-Zheng, P. and Fukao, T. (1994), "Robust speed identification for speed-sensorless vector control of induction motors", *IEEE Transactions on Industry Applications*, Vol. 30 No.5, pp. 1234–1240.

Finch, J.W., Atkinson, D.J. and Acarnley, P.P. (1998), "Full-order estimator for induction motor states and parameters", *IEE Proceedings—Electric Power Applications*, Vol. 145 No. 3, pp. 169–179.

Garcia Soto, G., Mendes, E. and Razek, A. (1999), "Reduced-order observers for rotor flux, rotor resistance and speed estimation for vector controlled induction motor drives

using the Extended Kalman Filter technique”, *IEE Proceedings–Electric Power Applications*, Vol. 146 No. 3, pp. 282–288.

Goodwin, G.C. and Sin, K.S. (1984), *Adaptive filtering prediction and control*, Prentice-Hall Inc., New Jersey.

Goh, K.B., Dunnigan, M.W. and Williams, B.W. (2004), “Sliding mode position control of a vector-controlled induction machine with nonlinear load dynamics”, *Proceedings of the IEEE–PEMD 2004*, Vol. 1, pp. 87–92.

Guidi, G and Umida, H (2000), “A novel stator resistance estimation method for speed-sensorless induction motor drives”, *IEEE Transactions on Industry Applications*; Vol. 36 No. 6, pp. 1619–1627.

Ha, I.-J. and Lee, S.-H. (2000), “An online identification method for both stator-and rotor resistances of induction motors without rotational transducers”, *IEEE Transactions on Industrial Electronics*, Vol. 47 No. 4, pp. 842–853.

Habetler, T.G., Profumo, F., Griva, G., Pastorelli, M. and Bettini, A. (1998), “Stator resistance tuning in a stator-flux field-oriented drive using an instantaneous hybrid flux estimator,” *IEEE Transactions on Power Electronics*, Vol. 13 No. 1, pp. 125–133.

Heber, B., Longya, X. and Tang, Y. (1997), “Fuzzy logic enhanced speed control of an indirect field-oriented induction machine drive”, *IEEE Transactions on Power Electronics*, Vol. 12 No. 5, pp. 772–778.

Hinkkanen M. 2004, “Analysis and design of full-order flux observers for sensorless induction motors”, *IEEE Transactions on Industrial Electronics*, Vol. 51 No. 5, pp. 1033–1040.

Holtz, J. (2000), “Sensorless control of induction motors-performance and limitations”, *Proceedings of the IEEE–ISIE 2000 Annual Meeting*, Vol. 1, pp. PL12–PL20.

Holtz, J. (2002), "Sensorless control of induction motor drives", *Proceedings of the IEEE*, Vol. 90 No.8, pp. 1359–1394.

Holtz, J. and Quan, J. (2003), "Drift- and parameter-compensated flux estimator for persistent zero-stator-frequency operation of sensorless-controlled induction motors", *IEEE Transactions on Industry Applications*, Vol. 39 No. 4, pp. 1052–1060.

Holtz, J. (2006), "Sensorless control of induction machines —with or without signal injection?", *IEEE Transactions on Industrial Electronics*, Vol. 53 No. 1, pp. 7–30.

Hung, J.Y., Gao, W. and Hung J.C. (1993), "Variable structure control: a survey", *IEEE Transactions on Industrial Electronics*, Vol. 40 No. 1, pp. 2–22.

Idris, N.R.N. and Yatim, A.H.M. (2004), "Direct torque control of induction machines with constant switching frequency and reduced torque ripple", *IEEE Transactions on Industrial Electronics*, Vol. 51 No. 4, pp. 758–767

Jansen, P.L. and Lorenz, R.D. (1994), "A physically insightful approach to the design and accuracy assessment of flux observers for field oriented induction machine drives", *IEEE Transactions on Industry Applications*, Vol. 30 No. 1, pp. 101–110.

Kaynak, O., Erbatur, K. and Ertugrul, M. (2001), "The fusion of computationally intelligent methodologies and sliding-mode control-a survey", *IEEE Transactions on Industrial Electronics*, Vol. 48 No. 1, pp. 4–17.

Khaorapong, T. and Ariyadirek P. (2004), "Application of fuzzy logic in the position control of induction motor for bending and cutting machine", *Proceedings of the IEEE–ISCIT 2004*, Vol. 1, pp. 378–382.

Kim, S.-M. and Han W.-Y. (2006), "Induction motor servo drive using robust PID-like neuro-fuzzy controller", *Control Engineering Practice*, Vol. 14, No. 5, pp. 481–487.

Kim, Y.-R., Sul, S.-K. and Park, M.-H. (1994), "Speed sensorless vector control of induction motor using Extended Kalman Filter", *IEEE Transactions on Industry Applications*, Vol. 30 No. 5, pp. 1225–1233.

Kojabadi, H.M., Chang, L. and Doriaswami, R. (2002), "Recent progress in sensorless vector-controlled induction motor drives", *Proceedings of the IEEE–Large Eng. Syst. Conf. on Power Eng. (LESCOPE 02)*, pp. 80–85.

Krzeminski, Z. (1987), "Nonlinear control of the induction motor," *Proceedings of the 10th IFAC World Congr.*, pp. 349–354.

Kubota, H., Matsuse, K. and Nakano, T. (1993), "DSP-based speed adaptive flux observer of induction motor," *IEEE Transactions on Industry Applications*, Vol. 29 No. 2, pp. 344–348.

Kubota, H., Sato, I., Tamura, Y., Matsuse, K., Ohta, H. and Hori, Y. (2002), "Regenerating-mode low-speed operation of sensorless induction motor drive with adaptive observer", *IEEE Transactions on Industry Applications*, Vol. 38 No. 4, pp. 1081–1086.

Kukolj, D.D., Kuzmanovi, S.B. and Levi E. (2001), "Design of a PID-like compound fuzzy logic controller", *Engineering Applications of Artificial Intelligence*, Vol. 14 No. 6, pp. 785–803.

Lascu, C., Boldea, I. and Blaabjerg, F. (2004a), "Direct torque control of sensorless induction motor drives: a sliding-mode approach", *IEEE Transactions on Industry Applications*, Vol. 40 No. 2, pp. 582–590.

Lascu, C. and Trzynadlowski, A.M. (2004b), "Combining the principles of sliding mode, direct torque control, and space-vector modulation in a high-performance sensorless AC drive", *IEEE Transactions on Industry Applications*, Vol. 40 No. 1, pp. 170–177.

Lascu, C., Boldea, I. and Blaabjerg, F. (2005), "Very-low-speed variable-structure control of sensorless induction machine drives without signal injection", *IEEE Transactions on Industry Applications*, Vol. 41 No. 2, pp. 591–598.

Lee, C.-M. and Chen, C.-L. (1998), "Observer-based speed estimation method for sensorless vector control of induction motors", *IEE Proceedings—Control Theory and Applications*, Vol. 145 No. 3, pp. 359–363.

Lin F.-J. (1996), "Robust speed-controlled induction motor drive using EKF and RLS estimators", *IEE Proceedings—Electric Power Applications*, Vol. 143 No. 3, pp. 186–192.

Marino, R., Peresada, S. and Valigi, P. (1990), "Adaptive partial feedback linearization of induction motors", *Proceedings of the IEEE Conference on Decision and Control*, Vol. 6, pp. 3313 – 3318.

Marino, R., Peresada, S. and Valigi, P. (1993), "Adaptive input-output linearizing control of induction motors", *IEEE Transactions on Automatic Control*, Vol. 38 No. 2, pp. 208–221.

Martins, C.A. and Carvalho, A.S. (2001), "Technological trends in induction motor electrical drives", *Proceedings of the IEEE Porto Power Tech Conference*, Vol. 2, p. 7

Nash, J.N. (1997), "Direct torque control, induction motor vector control without an encoder", *IEEE Transactions on Industry Applications*, Vol. 33 No. 2, pp. 333–341.

Novotnak, R.T., Chiasson, J. and Bodson, M. (1999), "High-performance motion control of an induction motor with magnetic saturation", *IEEE Transactions on Control Systems Technology*, Vol. 7 No. 3, pp. 315–327.

Ohya, K., Asher, G.M. and Sumner, M. (2005) "Comparative analysis of experimental performance and stability of sensorless induction motor drives", *IEEE Transactions on Industrial Electronics*, Vol. 53 No. 1, pp. 178–186.

Ortega, R., Barabanov, N., Escobar, G. and Valderrama, E. (2001), "Direct torque control of induction motors: stability analysis and performance improvement", *IEEE Transactions on Automatic Control*, Vol. 46 No. 8, pp. 1209–1222.

Qiongxuan, G. and Zhiyue, F. (2000), "Speed estimated for vector control of induction motor using reduced-order Extended Kalman Filter", *Proceedings of IEEE-PIEMC 2000 Annual Meeting*, Vol. 1, pp. 138–142.

Rashed, M. and Stronach, A.F. (2004) "A stable back-EMF MRAS-based sensorless low speed induction motor drive insensitive to stator resistance variation", *IEE Proceedings-Electric Power Applications*, Vol. 151 No.6, pp. 685–693.

Rodic, M. and Jezernik, K. (2002), "Speed-sensorless sliding-mode torque control of an induction motor", *IEEE Transactions on Industrial Electronics*, Vol. 49 No. 1, pp. 87–95.

Sabanovic, A. and Izosimov, D.B. (1981), "Application of sliding modes to induction motor control", *IEEE Transactions on Industry Applications*, Vol. IA-17, pp. 41–49.

Sahin, C., Sabanovic, A. and Gokasan, M. (1995), "Robust position control based on chattering-free sliding modes for induction motors", *Proceedings of the IEEE-IECON'95 Annual Meeting*, Vol. 1, pp. 512–517.

Salvatore, L., Stasi, S and Tarchioni, L. (1993), "A New EKF-based algorithm for flux estimation in induction machines", *IEEE Transactions on Industrial Electronics*, Vol. 40 No. 5, pp. 496–504.

Sangwongwanich, S., Doki, S., Yonemoto, T. and Okuma, S. (1990), "Adaptive sliding observers for direct field-oriented control of induction motor", *Proceedings of the IEEE-IECON'90 Annual Meeting*, Vol. 2, pp. 915–920.

Schauder, C. (1992), "Adaptive speed identification for vector control of induction motors without rotational transducers", *IEEE Transactions on Industry Applications*, Vol. 28 No. 5, pp. 1054–1061.

Schofield, J.R.G. (1995), "Direct torque control-DTC [of induction motors]", *IEE Colloquium on Vector Control and Direct Torque Control of Induction Motors*, pp. 1/1–1/3.

Shi, K.L. (2001), "Intelligent control for an induction motor," *PhD Thesis*, Hong Kong Polytechnic University, China.

Shi, K.L., Chan, T.F., Wong, Y.K. and Ho, S.L. (2002), "Speed estimation of an induction motor drive using an optimized Extended Kalman Filter", *IEEE Transactions on Industrial Electronics*, Vol. 49 No. 1, pp. 124–133.

Shiau, L.-G. and Lin, J.-L. (2001), "Stability of sliding-mode current control for high performance induction motor position drives", *IEE Proceedings–Electric Power Applications*, Vol. 148 No. 1, pp. 69–75.

Shieh, H.-J., Shyu, K.-K. and Lin, F.-J. (1998), "Adaptive estimation of rotor time constant for indirect field-oriented induction motor drive", *IEE Proceedings–Electric Power Applications*, Vol. 145 No. 2, pp. 111–118.

Suwankawin, S. and Sangwongwanich, S. (2002), "A speed-sensorless IM drive with decoupling control and stability analysis of speed estimation", *IEEE Transactions on Industrial Electronics*, Vol. 49 No. 2, pp. 444–455.

Suyitno, A., Fujikawa, J., Kobayashi, H., and Dote, Y. (1993), "Variable-structured robust controller by fuzzy logic for servomotors", *IEEE Transactions on Industrial Electronics*, Vol. 40 No. 1, pp. 80–88.

Tajima, H. and Hori, Y. (1993), "Speed sensorless field-orientation control of the induction machine", *IEEE Transactions on Industry Applications*, Vol. 29 No. 1, pp. 175–180.

Tajima, H., Guidi, G. and Umida, H. (2002), "Consideration about problems and solutions of speed estimation method and parameter tuning for speed-sensorless vector control of induction motor drives", *IEEE Transactions on Industry Applications*, Vol. 38 No. 5, pp. 1282–1289.

Takahashi, I. and Noguchi, T. (1986), "A new quick-response and high-efficiency control strategy of an induction motor", *IEEE Transactions on Industry Applications*, Vol. 22 No. 5, pp. 820–827.

Tiitinen, P. and Surandra, M. (1996), "The next generation motor control method, DTC direct torque control", *Proceedings of the IEEE-Power Electronics, Drives and Energy Systems for Industrial Growth*, Vol. 1, pp. 37–43.

Utkin, V.I. (1993), "Sliding mode control design principles and applications to electric drives", *IEEE Transactions on Industrial Electronics*, Vol. 40 No. 1, pp. 23–36.

Vas P. (1998), *Sensorless vector and direct torque control*, Oxford University Press, New York.

Vasic, V. and Vukosavic, S. (2001) "Robust MRAS-based algorithm for stator resistance and rotor speed identification", *IEEE Power Engineering Review*, Vol. 21 No. 11, pp. 39–41.

Wade, S., Dunnigan, M.W. and Williams, B.W. (1995), "Comparison of stochastic and deterministic parameter identification algorithms for indirect vector control", *IEE Colloquium on Vector Control and Direct Torque Control of Induction Motors*, Vol. 2, pp. 1–5.

Wade, S., Dunnigan, M.W. and Williams, B.W. (1997), "Modeling and simulation of induction machine vector control with rotor resistance identification", *IEEE Transactions on Power Electronics*, Vol. 12 No. 3, pp. 495–506.

Wai R.-J. (2002), "Development of new training algorithms for neuro-wavelet systems on the robust control of induction servo motor drive", *IEEE Transactions on Industrial Electronics*, Vol. 49 No. 6, pp. 1323–1341

Wai, R.-J. (2003), "Supervisory genetic evolution control for indirect field-oriented induction motor drive", *IEE Proceedings—Electric Power Applications*, Vol. 150 No. 2, pp. 215–226.

Wai R.-J. and Chang H.-H. (2004), "Backstepping wavelet neural network control for indirect field-oriented induction motor drive", *IEEE Transactions on Neural Networks*, Vol. 15 No. 2, pp. 367–382.

Wang, W.-J. and Chen, J.-Y. (2005), "Passivity-based sliding mode position control for induction motor drives", *IEEE Transactions on Energy Conversion*, Vol. 20 No. 2, pp. 316–321.

Wenqiang, Y., Zhengchun, J. and Qiang, X. (2001), "A new algorithm for flux and speed estimation in induction machine", *Proceedings of IEEE-ICEMS 2001 Annual Meeting*, Vol. 2, 698–701.

Xia, Y., Yu, X. and Oghanna, W. (2000), "Adaptive robust fast control for induction motors", *IEEE Transactions on Industrial Electronics*, Vol. 47 No. 4, pp. 854–862.

Yang, G. and Chin, T.-H. (1993), "Adaptive-speed identification scheme for a vector-controlled speed sensorless inverter-induction motor drive", *IEEE Transactions on Industry Applications*, Vol. 29 No. 4, pp. 820–825.

Zhen, L. and Xu, L. (1998), "Sensorless field orientation control of induction machines based on a mutual MRAS scheme", *IEEE Transactions on Industrial Electronics*, Vol. 45 No. 5, pp. 824–831.

Zhou R. and Lai J.-S. (2000), "Low-speed performance comparison of induction motor sensorless control methods", *Proceedings of IEEE Computers in Power Electronics (COMPEL 2000)*, pp. 247–252.

Chapter 2:

EKF Based Sensorless Direct Torque Control of IMs in the Low Speed Range*

Abstract— This study aims to improve the performance of the speed-sensorless direct-torque control (DTC) of induction motors (IMs), specifically in low and zero speed operation. To this aim, the estimation of the stator resistance is performed using an Extended Kalman filter based estimator, which also performs the estimation of the stator flux, angular velocity and load torque. Simulation results demonstrate a good performance and robustness.

Index Terms— *Induction motor, Extended Kalman Filter, estimator, observer, identification, load torque, stator resistance, sensorless control, low speed operation.*

2.1 Introduction

High efficiency control and estimation techniques related to induction motors (IM's) have been finding more and more application fields with Blaschke's well-known field-oriented control (FOC) established in 1971. There has been an intensive amount of work to improve the dynamic response and reduce the complexity of FOC methods. One such method is the Direct Torque Control (DTC) method developed by Takahashi in 1984 [1], and it has been getting increased attention due to the improved dynamic performance and simplified control strategy that it offers with respect to the FOC methods. However, both FOC and DTC require the accurate knowledge of the amplitude of the controlled flux and angular position (with respect to the stationary stator axis) in addition to the angular velocity for velocity control applications.

As it is well known, speed sensors like tachometers or incremental encoders increase the size and cost of systems unnecessarily. Similar problems arise with the addition of

* Barut, M., Bogosyan, S. and Gokasan, M. (2005c), "EKF Based Sensorless Direct Torque Control of IMs in the Low Speed Range", *Proceedings of the IEEE International Symposium on Industrial Electronics (ISIE 2005)*, Vol. 3, pp. 969–974.

search coils or Hall effect sensors to the motor for the measurement of flux, hindering functionality in terms of implementation. In addition to those considerations, various factors such as temperature and mechanical vibrations arising from the operation of the IM have undesirable effects on sensors; thus, to improve the overall system performance, state estimators and observers are usually more preferable than physical measurements.

However, the design of reliable observers and estimators for this highly nonlinear [2], 5th order system is a difficult task due to temperature [3] and frequency [4] dependent system parameters as well as instantaneous variations of torque and velocity and remains a challenge in the low velocity range, particularly at zero speed. The problems are due to parameter uncertainties, signal acquisition errors and noise [5, 6] in the very low speed range, with an additional difficulty encountered at zero speed in steady-state, when the stator current ceases to convey information on the rotor angular velocity [7]. Another feature affecting the performance at low speed operation is the information on the stator resistance; therefore, its estimation becomes crucial for the accurate estimation of velocity [8].

Current state-of-the-art close-loop techniques conducting simultaneous stator flux and velocity estimation in the low speed operation of the DTC include Sliding Mode Observers (SMO) as in [9], Adaptive Flux Observers (AFO) as in [10], Extended Luenberger Observers [11], and Extended Kalman Filters (EKF). Unlike the other methods, model uncertainties and nonlinearities inherent to IM's are well-suited to the stochastic nature of EKFs [12]. With this method, it is possible to make an on-line estimation of states while simultaneously performing identification of parameters in a relatively short time interval [13-15], also taking system process and measurement noises directly into account. This is the reason why EKF has found wide application in the sensorless control of IM's, in spite of its computational complexity. Among previous EKF based DTC studies, [16] estimates the stator flux components and velocity under the assumption of known load, while in [17, 18], the velocity is estimated as a constant parameter. In spite of an improved performance in the steady-state, the latter approach has given rise to a significant observer error in the velocity during the transient state. In

our previous study in [19], additional estimation of the load torque is performed. However, all these studies are sensitive to variations in stator resistance.

The major contribution of this study is the development of an EKF based speed-sensorless DTC system for improved performance, especially at low and zero speed operation, by achieving robustness against variations in the stator resistance and load torque. The developed EKF algorithm involves the estimation of stator flux, angular velocity, load torque and stator resistance in addition to the stator currents (referred to the stator stationary frame), which are also measured as output. With the square shaped voltage obtained by switching the inverter on and off, there has been no need for the addition of white noise to the measured states; thus, a more realistic approach has been taken to the solution of the problem. The performance of the control system with the proposed EKF algorithm has been demonstrated with simulations, taking into consideration load torque variations that are step like or linearly varying with the rotor velocity.

The paper is organized as follows. After the introduction in Section I, the mathematical model of the IM is presented in Section II. Next, the development of the EKF algorithm and the DTC scheme are given in Section III and IV, respectively. Finally, simulation results and conclusions are presented in Section V and Section VI, respectively.

2.2 Mathematical Model of the IM

The discrete model of the IM in the stator stationary axis can be given as follows:

$$\begin{aligned}\underline{x}_e(k+1) &= \underline{f}_e(\underline{x}_e(k), \underline{u}_e(k)) + \underline{w}_1(k) \\ &= \underline{A}_e(\underline{x}_e(k))\underline{x}_e(k) + \underline{B}_e\underline{u}_e(k) + \underline{w}_1(k)\end{aligned}\quad (2.1)$$

$$\begin{aligned}\underline{y}(k) &= \underline{h}_e(\underline{x}_e(k)) + \underline{w}_2(k) \text{ (measurement equation)} \\ &= \underline{H}_e\underline{x}_e(k) + \underline{w}_2(k)\end{aligned}\quad (2.2)$$

$$\underline{A}_e = \begin{bmatrix} 1-a_1R_s(k)-a_4 & -a_5\omega_m(k) & a_3 & a_6\omega_m(k) & 0 & 0 & 0 \\ a_5\omega_m(k) & 1-a_1R_s(k)-a_4 & -a_6\omega_m(k) & a_3 & 0 & 0 & 0 \\ -TR_s(k) & 0 & 1 & 0 & 0 & 0 & 0 \\ 0 & -TR_s(k) & 0 & 1 & 0 & 0 & 0 \\ -a_7\psi_{s\beta}(k) & a_7\psi_{s\alpha}(k) & 0 & 0 & 1 & -a_8 & 0 \\ 0 & 0 & 0 & 0 & 0 & 1 & 0 \\ 0 & 0 & 0 & 0 & 0 & 0 & 1 \end{bmatrix},$$

$$\underline{B}_e = \begin{bmatrix} a_1 & 0 & 0 & 0 & 0 & 0 & 0 \\ 0 & a_1 & 0 & 0 & 0 & 0 & 0 \end{bmatrix}^T, \quad \underline{H}_e = \begin{bmatrix} 1 & 0 & 0 & 0 & 0 & 0 & 0 \\ 0 & 1 & 0 & 0 & 0 & 0 & 0 \end{bmatrix},$$

$$\underline{x}_e(k) = [i_{s\alpha}(k) \quad i_{s\beta}(k) \quad \psi_{s\alpha}(k) \quad \psi_{s\beta}(k) \quad \omega_m(k) \quad t_L(k) \quad R_s(k)]^T, \quad \underline{u}_e(k) = [v_{s\alpha}(k) \quad v_{s\beta}(k)]^T$$

$$a_1 = T/(L_s - L_m^2/L_r), \quad a_2 = R_r/L_r, \quad a_3 = a_1 a_2, \quad a_4 = L_s a_3, \quad a_5 = p_p T, \quad a_6 = p_p a_1, \\ a_7 = 1.5 a_5 / J_L, \quad a_8 = T / J_L$$

where \underline{f}_e is the nonlinear function of the states. \underline{x}_e is the extended state vector. \underline{A}_e is the system matrix. \underline{u}_e is the control input vector. \underline{B}_e is the input matrix. \underline{h}_e is the function of the outputs. \underline{H}_e is the measurement matrix. \underline{w}_1 and \underline{w}_2 are the process and measurement noise, respectively. p_p is the number of pole pairs. L_s and R_s are stator inductance and resistance, respectively. L_r and R_r are the rotor inductance and resistance, referred to the stator side, respectively. L_m is the magnetizing inductance. $v_{s\alpha}$ and $v_{s\beta}$ are the stator stationary axis components of stator voltages. $\psi_{s\alpha}$ and $\psi_{s\beta}$ are the stator stationary axis components of stator flux. $i_{s\alpha}$ and $i_{s\beta}$ are the stator stationary axis components of stator currents. ω_m is the angular velocity. t_L is the load torque. T is the sampling time. J_L is the total inertia.

2.3 Development of the EKF Algorithm

The Kalman filter is a well-known recursive algorithm that takes the stochastic state space model of the system together with measured outputs to achieve the optimal estimation of states [20] in multi-input, multi-output systems. The filter takes system and measurement noises into account in the form of white noise. The optimality of the state estimation is achieved with the minimization of the mean estimation error. In this study, EKF, which is a form of a Kalman filter that could be used for nonlinear systems is used for the estimation $i_{s\alpha}, i_{s\beta}, \psi_{s\alpha}, \psi_{s\beta}, t_L$ and R_s .

$$\underline{F}_e(k) = \left. \frac{\partial f_e(\underline{x}_e(k), \underline{u}_e(k))}{\partial \underline{x}_e(k)} \right|_{\hat{\underline{x}}_e(k), \hat{\underline{u}}_e(k)} \quad (2.3)$$

$$\underline{F}_u(k) = \left. \frac{\partial f_e(\underline{x}_e(k), \underline{u}_e(k))}{\partial \underline{u}_e(k)} \right|_{\hat{\underline{x}}_e(k), \hat{\underline{u}}_e(k)} \quad (2.4)$$

Thus, the EKF algorithm can be given in the following recursive relations [14]:

$$\underline{N}(k) = \underline{F}_e(k) \underline{P}(k) \underline{F}_e(k)^T + \underline{F}_u(k) \underline{D}_u \underline{F}_u(k)^T + \underline{Q} \quad (2.5a)$$

$$\underline{P}(k+1) = \underline{N}(k) - \underline{N}(k) \underline{H}_e^T (\underline{D}_\varepsilon + \underline{H}_e \underline{N}(k) \underline{H}_e^T)^{-1} \underline{H}_e \underline{N}(k) \quad (2.5b)$$

$$\hat{\underline{x}}_e(k+1) = \hat{\underline{f}}_e(\underline{x}_e(k), \hat{\underline{u}}_e(k)) + \underline{P}(k+1) \underline{H}_e^T \underline{D}_\varepsilon^{-1} (\underline{Z}(k) - \underline{H}_e \hat{\underline{x}}_e(k)) \quad (2.5c)$$

Here, \underline{Q} is the covariance matrix of the system noise, namely model error. $\underline{D}_\varepsilon$ is the covariance matrix of the output noise, namely measurement noise. \underline{D}_u is the covariance matrix of the control input ($v_{s\alpha}$ and $v_{s\beta}$) noise, namely input noise. $\underline{P}(\cdot)$ and $\underline{N}(\cdot)$ are the covariance matrix of state estimation error and extrapolation error, respectively.

a system covariance matrix, $\underline{Q} = \text{diag}\{10^{-9} \ 10^{-9} \ 10^{-9} \ 10^{-9} \ 10^{-9} \ 10^{-5} \ 10^{-5}\}$,
and variances, $\underline{D}_\xi = \text{diag}\{10^{-6} \ 10^{-6}\}$ $\underline{D}_u = \text{diag}\{10^{-5} \ 10^{-5}\}$.

The bandwidth (b_ψ) of the flux comparator is 0.02, while that of the torque comparator (b_{t_e}) is 0.01. Simulations are performed for 13 different scenarios, aiming to force the developed algorithm with random variations imposed on the system. For this purpose, random variations are given to the reference velocity, stator resistance and load torque as illustrated in Fig. 2.2-2.3(a). Fig. 2.4 depicts the stator flux. Fig. 2.2(b), (c), (d) and (e) depict the variations of $|\hat{\psi}_s|$, \hat{n}_m , \hat{t}_L , and \hat{R}_s , while Fig. 2.3(b), (c), (d), (e) and (f) show the variations of $|\psi_s| - |\hat{\psi}_s|$, $n_m - \hat{n}_m$, $t_L - \hat{t}_L$, $R_s - \hat{R}_s$ and $|\psi_s|^r - |\hat{\psi}_s|$, respectively. The $e_{(\cdot)}$ error signals illustrate the deviation between the actual and the estimated parameter or state.

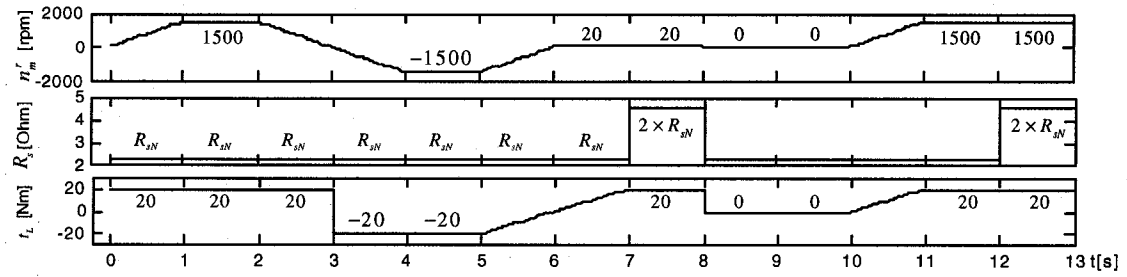
Analysing the simulation results, the following observations are made:

- With initial values taken as zero, it has been demonstrated that the EKF based estimation and control perform quite well even in spite of instantaneous variations in the load, velocity and stator resistance both in the high and in the low and zero speed region.
- Another advantage of the developed scheme is the ability to account for various other constant uncertainties (the viscous friction, in this case), within the estimated constant load value. For the viscous friction coefficient $\beta_L = 0.001$ used in the model, but considered as $\beta_L = 0$ in the EKF,

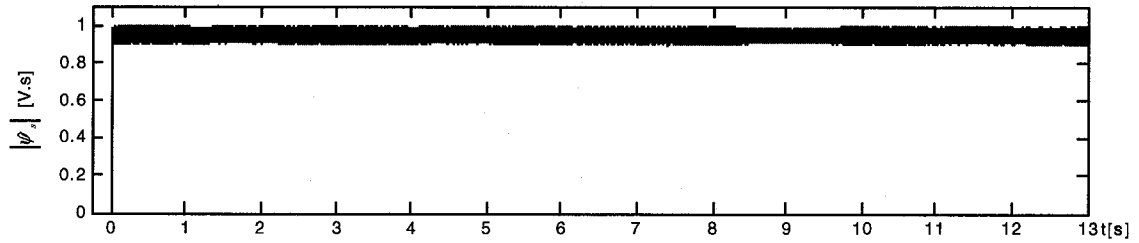
$$\begin{aligned} \omega_m(\infty) &= \hat{\omega}_m(\infty) + e_{\omega_m(\infty)} \\ &= 2\pi(1500.4 - 1.06 \times 10^{-5})/60 = 157.1215 [\text{rad/s}] \end{aligned} \quad (2.6)$$

and

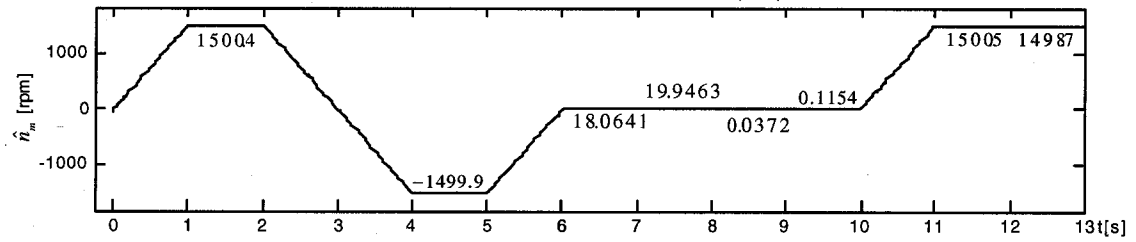
$$\begin{aligned} e_{tL} &= -\beta_L \omega_m(\infty) \rightarrow -0.1571 = -0.001 \times 157.1215 \\ &= -0.1571 [\text{Nm}] \cong -0.1571215 [\text{Nm}], \end{aligned} \quad (2.7)$$



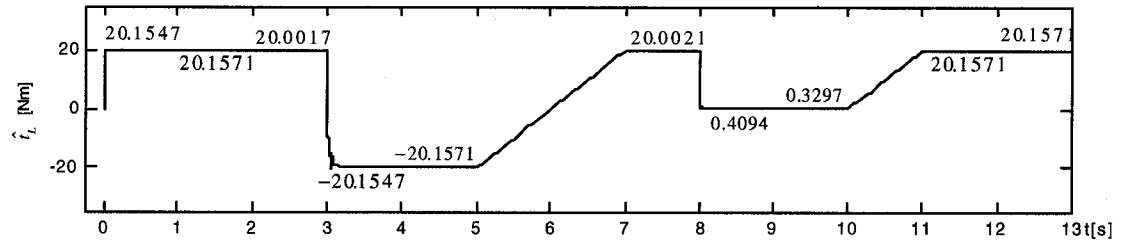
(a) Variation of the reference speed value, n_m^r , stator resistance, R_s , and applied load torque, t_L for performance test



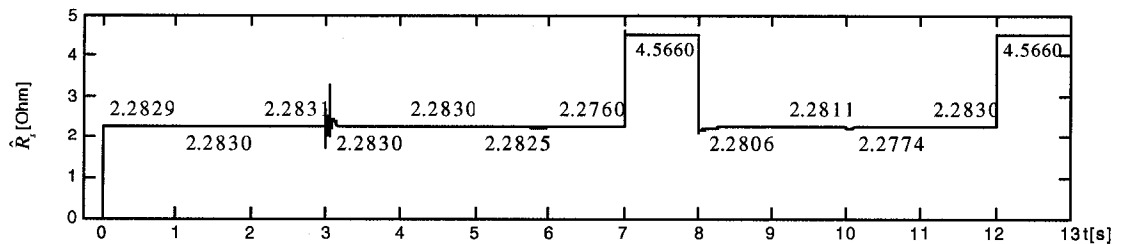
(b) Variation of the estimated $|\psi_s|$



(c) Variation of the estimated n_m

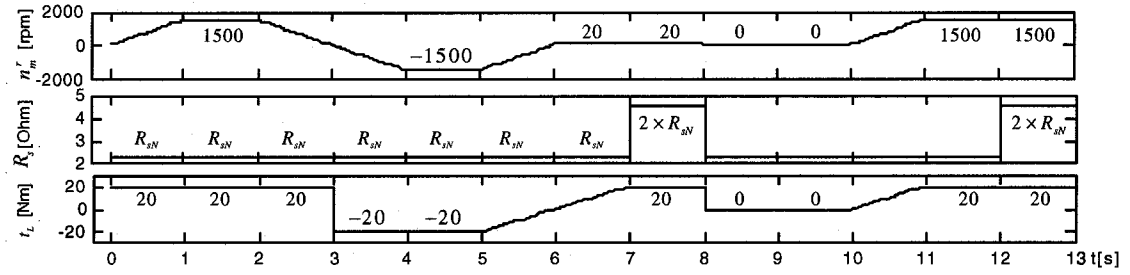


(d) Variation of the estimated t_L

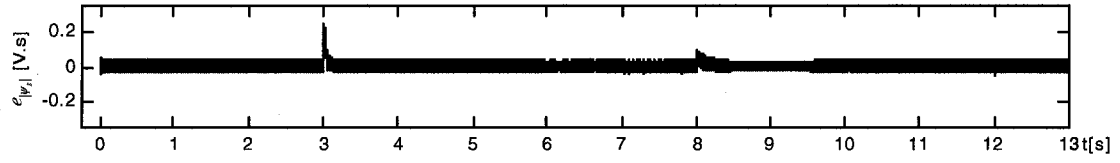


(e) Variation of the estimated R_s

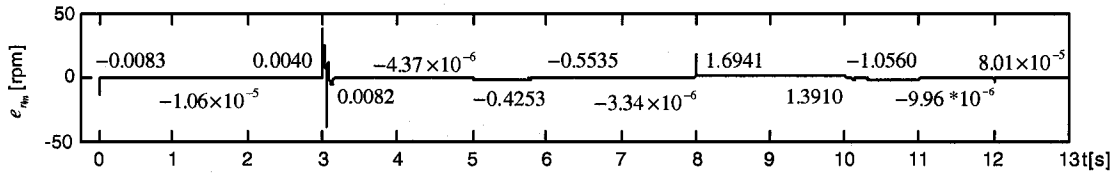
Fig. 2.2 Simulation results for the estimations of the EKF based estimator and the DTC system



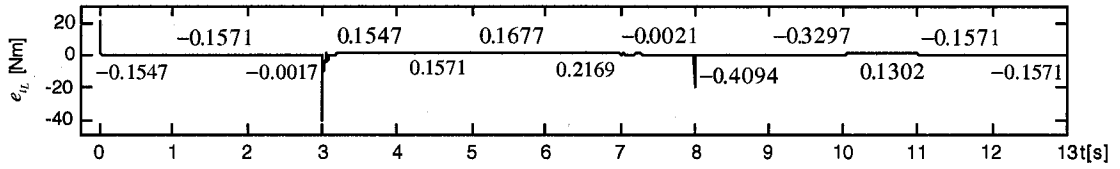
(a) Variation of the reference speed value, n_m^* , stator resistance, R_s , and applied load torque, t_L for performance test



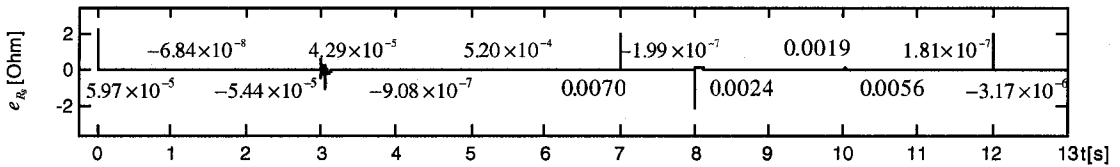
(b) Variation of the estimation error of $|\psi_s|$, $e_{|\psi_s|}$



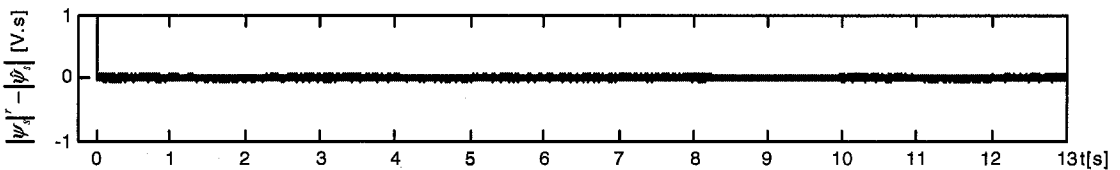
(c) Variation of the estimation error of n_m , e_{n_m}



(d) Variation of the estimation error of t_L , e_{t_L}



(e) Variation of the estimation error of R_s , e_{R_s}



(f) Variation of the flux comparator input

Fig. 2.3 Simulation results for the estimation errors of the EKF based estimator and the DTC system.

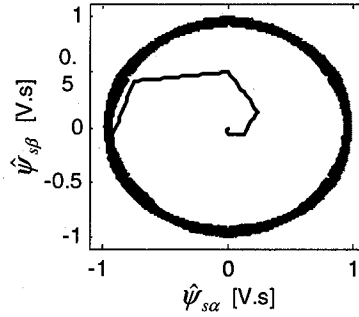


Fig. 2.4 Trajectory of $\hat{\psi}_{s\alpha}$ and $\hat{\psi}_{s\beta}$

e_{t_L} is equal to $-\beta_L \omega_m$, as can be seen in the second time interval (1-2 s) of Fig. 2.3(d) and as expected.

- A hysteresis based flux comparator and switching table result in high-frequency switching activity; therefore, noise limited with the band of the hysteresis comparator exists in Fig. 2.2b, 2.3b and 2.4. Moreover, the trajectory of $\hat{\psi}_{s\alpha}$ and $\hat{\psi}_{s\beta}$ in Fig. 2.4 are obtained in a circular form, as expected, because of their sinusoidal variations.
- Considering the limitations of previous model based estimations of IMs [5, 21], simulation results, especially those obtained at the zero velocity and load torque (worst set of conditions for state and parameter estimations of IMs) are quite satisfactory.
- The developed algorithm is sensitive to variations in the unestimated rotor resistance, R_r . Thus, it is noted that R_r estimation should also be included into the algorithm.

In summary, the speed-sensorless DTC system has demonstrated a good performance, in the whole velocity range, also including zero speed, in the face of instantaneous variations in stator resistance and step-like and linear variations of the load torque with the angular velocity.

2.6 Conclusion

In this study, we present results demonstrating improved performance in the speed-sensorless DTC of IMs, especially in the low and zero speed region. For this purpose, an EKF algorithm is designed estimating the stator as well as the load torque. The

simulation results have demonstrated good performance and robustness throughout a wide velocity range, including low and zero speed operation under challenging variations of the load and stator resistance. However, the experiments have also demonstrated the well-known effect of the rotor resistance; therefore, its estimation should also be performed with an EKF algorithm or otherwise.

References

- [1] I. Takahashi and T. Noguchi, "A new quick-response and high-efficiency control strategy of an induction motor", *IEEE Tran. on Industry Applications*, vol. IA-22, no. 5, Sept.-Oct.1986, pp. 820-827.
- [2] D.E. Bogard, G. Olsson and R.D. Lorenz, "Accuracy issues for parameter estimation of field oriented induction machine drives," *IEEE Tran. on Industry Applications*, vol. 31, no. 4, July-Aug.1995, pp. 795-801.
- [3] E. Akin, H.B. Ertan and M.Y. Uctug, "A method for stator resistance measurement suitable for vector control," in *Proc. IEEE-IECON'94 Annual Meeting*, vol. 3, Bologna, 1994, pp. 2122-2126.
- [4] H. Kabbaj, X. Roboam, Y. Lefevre and J. Faucher, "Skin effect characterization induction machine," in *Proc. IEEE-ISIE'97 Annual Meeting*, vol. 2, Guimarães, 1997, pp. 532-536.
- [5] J. Holtz, "Sensorless control of induction motors-performance and limitations," in *Proc. IEEE-ISIE 2000 Annual Meeting*, vol. 1, México, 2000, pp. PL12-PL20.
- [6] N. Hur, K. Hong and K. Nam, "Sensorless vector control in the presence of voltage and current measurement errors by dead-time [induction motors]," in *Proc. IEEE-IAS'97 Annual Meeting*, vol. 1, New Orleans, 1997, pp. 433-438.
- [7] J. Holtz and J. Quan, "Drift- and parameter-compensated flux estimator for persistent zero-stator-frequency operation of sensorless-controlled induction motors," *IEEE Tran. on Industry Applications*, vol. 39 , no. 4, July-Aug.2003, pp. 1052-1060.

- [8] G. Guidi and H. Umida, "A novel stator resistance estimation method for speed-sensorless induction motor drives," *IEEE Tran. on Industry Applications*, vol. 36, no. 6, Nov.-Dec. 2000, pp.1619–1627.
- [9] C. Lascu, I. Boldea and F. Blaabjerg, "Direct torque control of sensorless induction motor drives: a sliding- mode approach," *IEEE Tran. on Industry Applications*, vol. 40, no. 2, March-April 2004, pp. 582–590.
- [10] K.B. Lee, J.H. Song, I. Choy and J.Y. Choi, "An observer-based DTC of induction motors driven by 3-level inverter for improving low speed operation," in *Proc. IEE–Power Electronics and Variable Speed Drives*, London, 2000, pp. 170–175.
- [11] Y.-O. Choi, K.-Y. Lee, K.-S. Seo, G.-B. Kim, B.-H. Jung, G.-B. Cho, H.-L. Baek, and S.-Y. Jeong, "Performance analysis of the DTC using a closed loop stator flux observer for induction motor in the low speed range," in *Proc. IEEE–ICEMS 2001 Annual Meeting*, vol. 1, Shenyang, 2001, pp. 89–93.
- [12] S. Wade, M.W. Dunnigan, and B.W. Williams, "Comparison of stochastic and deterministic parameter identification algorithms for indirect vector control," in *Proc. IEE Colloquium on Vector Control and Direct Torque Control of Induction Motors*, vol. 2, London, 1995, pp. 1–5.
- [13] L. Salvatore, S. Stasi, and L. Tarchioni, "A New EKF-based algorithm for flux estimation in induction machines," *IEEE Tran. on Industrial Electronics*, vol. 40, no. 5, October 1993, pp. 496–504.
- [14] O.S. Bogosyan, M. Gokasan, and C. Hajiyev, "An Application of EKF for the position control of a single link arm," in *Proc. IEEE–IECON'01 Annual Meeting*, Denver, 2001, vol.1, pp. 564–569.
- [15] M. Barut, O.S. Bogosyan, and M. Gokasan, "EKF based estimation for direct vector control of induction motors," in *Proc. IEEE–IECON'02 Annual Meeting*, vol. 2, Sevilla, 2002, pp. 1710–1715.

- [16] D. Pai A, L. Umanand, and N.J. Rao, "Direct torque control of induction motor with Extended Kalman Filter," in *Proc. IEEE-PIEMC 2000 Annual Meeting*, vol. 1, Beijing, 2000, pp. 132–137.
- [17] J. El Hassan, E.V. Westerholt, X. Roboam, and B. De Fornel, "Comparison of different state models in direct torque control of induction machines operating without speed sensor," in *Proc. IEE-IAS 2000*, vol. 3, Rome, 2000, pp. 1345–1352.
- [18] X. Ma and Y. Gui, "Extended Kalman Filter for speed sensor-less DTC based on DSP," in *Proc. IEEE-Intelligent Control and Automation*, vol. 1, Shanghai, 2002, pp.119–122.
- [19] M. Barut, M. Gokasan, and O. S. Bogosyan, "EKF based speed sensorless direct torque control system for IMs," in *Proc. International conference on Electrical and Electronics Engineering (ELECO'2003) Annual Meeting*, Istanbul, 2003, vol. 1, pp. 319–323.
- [20] F. Chen and M.G. Dunnigan, "Comparative study of a sliding-mode observer and Kalman Filters for full state estimation in an induction machine," *IEE Proceedings-Electric Power Applications*, Vol. 149, No. 1, Jan. 2002, pp. 53 – 64.
- [21] J. Holtz , "Sensorless control of induction motor drives," *Proceedings of the IEEE*, vol. 90, No. 8, Aug. 2002, pp.1359–1394.

Chapter 3:

Sensorless Low/Zero Speed Control of Induction Motors with EKF Estimation*

Abstract— This study aims at improved estimation performance for the speed-sensorless control of induction motors (IMs) over a very low to zero speed range. For this purpose, an Extended Kalman Filter (EKF) observer is designed to overcome the difficulties of flux and speed estimation at and around zero speed. The estimation problems related to low speed operation are further emphasized due to stator resistance, R_s uncertainties. Thus, the observer is designed to estimate the stator resistance, load torque and velocity, which is taken into account via the equation of motion. With this approach, the rotor flux information is reflected to the stator, thus improving the estimation accuracy. The simulation results obtained for the EKF approach in combination with the Direct Vector Control (DVC) of an IM, indicate improved performance.

Index Terms— *Induction motor, Extended Kalman Filter, sensorless control, low and zero speed operation, stator resistance and load torque estimation.*

3.1 Introduction

Sensorless vector control [1] and direct torque control (DTC) [2] of induction motors (IMs) require the accurate estimation of speed and torque, as well as the rotor or stator flux. The performance of estimation and hence, control in IMs is also dependent on system parameters [3, 4] that vary significantly with temperature and frequency. Additional problems arise with estimation at very low and zero speed, mainly due to the fact that the stator currents which are measured as output in sensorless control cease to convey information on the reduced levels of rotor currents and voltages around zero

* Barut, M., Bogosyan, S. and Gokasan, M. (2006b), "Sensorless Low/Zero Speed Control of Induction Motors with EKF Estimation," *WSEAS Transactions on Systems*, Vol. 5 No. 11, pp. 2530–2535.

stator frequency [5]. Parameter sensitivity also becomes more relevant with sensorless control at very low speeds.

Model based methods that model the induction motor by its state equations and signal injection methods based on exploited anisotropic properties of the machine have been competing in the zero and very low speed performance of sensorless IM drives [6]. Although speed-sensorless control based on the signal injection methods are capable of long-term stability at zero stator frequency, they are highly sophisticated, and their design is not general as it must be customized for a particular drive motor [6].

Recently, for the solution of the problem at zero and very low speed, studies using model based estimation methods using Adaptive Flux Observers (AFO) as in [7], Model Reference Adaptive Systems (MRAS) as in [8], Sliding Mode Observers (SMO) as in [9] and Extended Kalman Filters (EKF) as in [10] have been proposed. Unlike the other methods, model uncertainties and nonlinearities inherent to IMs are well-suited to the stochastic nature of EKF [11]. With this method, it is possible to make the on-line estimation of states while simultaneously performing identification of parameters in a relatively short time interval [12], also taking system process and measurement noises directly into account. This is the reason why EKF has found wide application in the sensorless control of IM's, in spite of its computational complexity.

In this study, the problems of parameter sensitivity and low and zero speed operation in IMs is addressed with an EKF algorithm which estimates stator resistance, R_s , as its temperature dependent uncertainties have well-known performance degrading effects on estimation at low speeds. The EKF also estimates the load torque, T_L as well as angular velocity, ω_m , which is taken into account with the equation of motion, unlike most past studies taking the velocity into account as a constant. This approach helps the estimation performance by conveying the rotor-stator relationship which is otherwise lost at low and zero speed as is the case with most estimators used in past studies. The simulation results

demonstrate the good performance of the EKF observer used in combination with the direct vector control of IMs.

3.2 Mathematical Model of the IM

The discrete model of IM in stator stationary axis can be given as follows:

$$\begin{aligned}\underline{x}_e(k+1) &= \underline{f}_e(\underline{x}_e(k), \underline{u}_e(k)) + \underline{w}_1(k) \\ &= \underline{A}_e(\underline{x}_e(k))\underline{x}_e(k) + \underline{B}_e\underline{u}_e(k) + \underline{w}_1(k)\end{aligned}\quad (3.1)$$

$$\begin{aligned}\underline{y}(k) &= \underline{h}_e(\underline{x}_e(k)) + \underline{w}_2(k) \text{ (measurement equation)} \\ &= \underline{H}_e\underline{x}_e(k) + \underline{w}_2(k)\end{aligned}\quad (3.2)$$

$$\underline{A}_e = \begin{bmatrix} 1 - a_1 R_s(k) - a_2 & 0 & a_2 & a_3 \omega_m(k) & 0 & 0 & 0 \\ 0 & 1 - a_1 R_s(k) - a_2 & -a_3 \omega_m(k) & a_2 & 0 & 0 & 0 \\ a_5 & 0 & 1 - a_4 & -a_6 \omega_m(k) & 0 & 0 & 0 \\ 0 & a_5 & a_6 \omega_m(k) & 1 - a_4 & 0 & 0 & 0 \\ -a_7 \psi_{r\beta}(k) & a_7 \psi_{r\alpha}(k) & 0 & 0 & 1 & -a_8 & 0 \\ 0 & 0 & 0 & 0 & 0 & 1 & 0 \\ 0 & 0 & 0 & 0 & 0 & 0 & 1 \end{bmatrix}$$

$$\underline{B}_e = \begin{bmatrix} a_1 & 0 & 0 & 0 & 0 & 0 & 0 \\ 0 & a_1 & 0 & 0 & 0 & 0 & 0 \end{bmatrix}^T, \quad \underline{H}_e = \begin{bmatrix} 1 & 0 & 0 & 0 & 0 & 0 & 0 \\ 0 & 1 & 0 & 0 & 0 & 0 & 0 \end{bmatrix}$$

$$\underline{x}_e(k) = [i_{s\alpha}(k) \ i_{s\beta}(k) \ \psi_{r\alpha}(k) \ \psi_{r\beta}(k) \ \omega_m(k) \ t_L(k) \ R_s(k)]^T, \quad \underline{u}_e(k) = [v_{s\alpha}(k) \ v_{s\beta}(k)]^T$$

$$a_1 = T/(L_s - L_m^2/L_r), \quad a_2 = L_m^2 R_r a_1 / L_r^2, \quad a_3 = L_m p_p a_1 / L_r, \quad a_4 = R_r T / L_r, \quad a_5 = L_m a_4,$$

$$a_6 = p_p T, \quad a_7 = 1.5 p_p a_5 / (R_r J_L), \quad a_8 = T / J_L$$

where \underline{f}_e is the nonlinear function of the states. \underline{x}_e is the extended state vector. \underline{A}_e is the system matrix. \underline{u}_e is the control input vector. \underline{B}_e is the input matrix. \underline{h}_e is the function of the outputs. \underline{H}_e is the measurement matrix. \underline{w}_1 and \underline{w}_2 are the process and measurement noise, respectively. p_p is the number of pole pairs. L_s and R_s are stator inductance and resistance, respectively. L_r and R_r are the rotor inductance and resistance, referred to the stator side, respectively. L_m is the magnetizing inductance. $v_{s\alpha}$ and $v_{s\beta}$ are the stator stationary axis components of stator voltages. $\psi_{r\alpha}$ and $\psi_{r\beta}$ are the stator stationary axis components of rotor flux. $i_{s\alpha}$ and $i_{s\beta}$ are the stator stationary axis components of stator currents. ω_m is the angular velocity. t_L is the load torque. T is the sampling time. J_L is the total inertia.

3.3 Development of the EKF Algorithm

The Kalman filter is a well-known recursive algorithm that takes the stochastic state space model of the system together with measured outputs to achieve the optimal estimation of states [13] in multi-input, multi-output systems. The filter takes system and measurement noises into account in the form of white noise. The optimality of the state estimation is achieved with the minimization of the mean estimation error. In this study, an EKF estimator is developed, which is a form of a Kalman filter that could be used for nonlinear systems. The filter performs the estimation of the extended vector $\underline{x}_e(k) = [i_{s\alpha}(k) \ i_{s\beta}(k) \ \psi_{r\alpha}(k) \ \psi_{r\beta}(k) \ \omega_m(k) \ t_L(k) \ R_s(k)]^T$ as below [3]

$$\underline{F}_e(k) = \left. \frac{\partial \underline{f}_e(\underline{x}_e(k), \underline{u}_e(k))}{\partial \underline{x}_e(k)} \right|_{\hat{\underline{x}}_e(k), \hat{\underline{u}}_e(k)} \quad (3.3)$$

$$\underline{F}_u(k) = \left. \frac{\partial \underline{f}_e(\underline{x}_e(k), \underline{u}_e(k))}{\partial \underline{u}_e(k)} \right|_{\hat{\underline{x}}_e(k), \hat{\underline{u}}_e(k)} \quad (3.4)$$

angular velocity of the rotating d - q axis. The velocity, field and torque controllers given in the diagram are conventional proportional-integral controllers (PIs).

3.5 Simulation Results and Observations

To test the performance of the estimation method, simulations were performed on an IM with the following rated parameters;

$$\begin{aligned} R_{sN} &= 2.283 \Omega, \quad R'_{rN} = 2.133 \Omega, \quad L_s = 0.23 H, \quad L'_r = 0.23 H, \quad L_m = 0.22 H, \\ J_L &= 0.005 \text{ kg.m}^2, \quad p_p = 2, \quad t_{LN} = 20 \text{ Nm}, \quad N_{mN} = 1430 \text{ rpm} \\ \beta_L &= 0.001 \text{ Nm/(rad/s)} \text{ (total viscous friction coefficient),} \end{aligned}$$

Covariance matrixes are selected as below:

$$\begin{aligned} \underline{Q} &= \text{diag} \{10^{-9} \quad 10^{-9} \quad 10^{-9} \quad 10^{-9} \quad 10^{-4} \quad 10^{-4} \quad 10^{-5}\}, \quad \underline{P} = \text{diag} \{9 \quad 9 \quad 9 \quad 9 \quad 9 \quad 9 \quad 9\}, \\ \underline{D}_\xi &= \text{diag} \{10^{-6} \quad 10^{-6}\}, \quad \underline{D}_u = \text{diag} \{10^{-5} \quad 10^{-5}\}. \end{aligned}$$

The simulations are performed considering four different group of scenarios for certain time intervals:

- i) Start-up and transition to zero speed: ($0 \leq t \leq 3 \text{ sec}$)
- ii) Persistent operation at zero speed under variations of R_{sN} and *non-zero* t_L : ($3 \text{ sec} \leq t \leq 69 \text{ sec}$)
- iii) Persistent operation at zero speed with linear R_s variations and *zero* t_L : ($69 \text{ sec} \leq t \leq 135 \text{ sec}$)
- iv) Demonstration of repeatability ($135 \text{ sec} \leq t \leq 137 \text{ sec}$)

For this purpose, scenarios are developed by incurring simultaneous changes to the velocity reference, load torque value and stator resistance values used in the extended

model as demonstrated in Fig. 3.2-3.3(a). Both step-type and linear variations are given to R_s , although it is taken into consideration as a constant parameter in the EKF scheme. The resulting system performance for all scenarios is given with Fig. 3.2(b), (c), (d), (e), (f), and (g), which represent the estimated values of the velocity (\hat{n}_m), load torque (\hat{t}_L), stator resistance (\hat{R}_s), α -component of the rotor flux ($\hat{\psi}_{r\alpha}$), β -component of the rotor flux ($\hat{\psi}_{r\beta}$), and the position of the flux with reference to the stationary axis ($\hat{\theta}_{rf}$). Fig. 3.3(b), (c), (d), (e), (f), (g) and (h) demonstrate the variations of estimation errors for the estimated states and parameters and the errors of the velocity and the flux controller inputs given as $e_{n_m} = n_m - \hat{n}_m$, $e_{t_L} = t_L - \hat{t}_L$, $e_{R_s} = R_s - \hat{R}_s$, $e_{\psi_{r\alpha}} = \psi_{r\alpha} - \hat{\psi}_{r\alpha}$, $e_{\psi_{r\beta}} = \psi_{r\beta} - \hat{\psi}_{r\beta}$, $n_m^{ref} - \hat{n}_m$, and $|\psi_r|^{ref} - |\hat{\psi}_r|$, respectively.

Analysing the simulation results, the following observations are made:

- With no a priori information on the initial values and by taking them as zero, it has been demonstrated that the EKF based estimation and control perform quite well despite instantaneous variations in the load, velocity and stator resistance both in the high and in the low to zero speed region.
- Another advantage of the developed scheme is the ability to account for various other constant uncertainties (the viscous friction, in this case), within the estimated constant load value, \hat{t}_L . Therefore, e_{t_L} should be expected to be equal to $-\beta_L \omega_m$, and as can be seen in the first time interval (0-2 sec.) of Fig. 3.3(c)

$$\omega_m(\infty) = \hat{\omega}_m(\infty) + e_{\omega_m(\infty)} = 2\pi(10.1945 - 2.4 \times 10^{-6})/60 = 1.0676 [\text{rad/s}] \quad (3.6)$$

$$\begin{aligned} e_{t_L} &= -\beta_L \omega_m(\infty) \\ &= -0.001 = -0.001 \times 1.0676 \rightarrow -0.001 [\text{Nm}] \cong -0.0010676 [\text{Nm}] \end{aligned} \quad (3.7)$$

(g) Variation of the estimated θ_{rf}

Reproduced with permission of the copyright owner. Further reproduction prohibited without permission.

Figure 1 displays three panels of time-resolved IR spectra showing the change in absorbance (ΔA) in molar extinction coefficient units ($M^{-1} cm^{-1}$) versus time (t) in femtoseconds (fs). The panels show the evolution of the photochemical reaction of 1 over time, with arrows indicating the time delay between the pump and probe pulses. The data points are labeled with their corresponding time delays in fs.

- Left Panel (1500-1700 cm^{-1}):** Shows a broad absorption band around 1600 cm^{-1} . The time delays are: -0.1945, 0.1574, 0.1522, -0.1292, 0.0731, and -0.0714 fs.
- Middle Panel (1200-1400 cm^{-1}):** Shows a broad absorption band around 1300 cm^{-1} . The time delays are: 0.0904, -0.2099, -0.0817, -0.1240, 0.1490, and 0.0735 fs.
- Right Panel (1000-1100 cm^{-1}):** Shows a broad absorption band around 1050 cm^{-1} . The time delays are: 0.2659 and -0.0217 fs.

Figure 10 shows three subplots of the time evolution of the normalized difference of the squared norm of the wave function, $|\psi_c|^2 - |\psi_s|^2$, over time t [s]. The y-axis ranges from -1 to 1. The x-axis ranges from 0 to 9 s for the first plot, 68 to 137 s for the second, and 134 to 137 s for the third. Arrows indicate specific values at various time points.

Time t [s]	Value of $ \psi_c ^2 - \psi_s ^2$
0.0042	0.0042
4 * 10 ⁻⁴	4 * 10 ⁻⁴
8.1 * 10 ⁻⁴	8.1 * 10 ⁻⁴
0.0020	0.0020
-9.5 * 10 ⁻⁴	-9.5 * 10 ⁻⁴
0.0010	0.0010
-0.0016	-0.0016
2.5 * 10 ⁻³	2.5 * 10 ⁻³
5.2 * 10 ⁻³	5.2 * 10 ⁻³
8.9 * 10 ⁻⁴	8.9 * 10 ⁻⁴
0.0013	0.0013
-1.6 * 10 ⁻³	-1.6 * 10 ⁻³
0.0022	0.0022
0.0019	0.0019

Fig. 3.3 Simulation results for the estimation errors of the EKF based estimator and the DVC system

- The limitations of model based estimations of IMs in [5] is true when considering the fundamental frequency component only. However, the effect of current harmonics incurred by the PWM operation should also be taken into account. In this study, to increase the information transfer from the rotor to the stator side, the velocity is taken into account with the equation of motion unlike most previous studies taking velocity into consideration as a constant state in the extended model. With the equation of motion in the extended model, the harmonic components of the current and flux in the torque term reflect the rotor information to the stator side, which in turn helps the estimation of the velocity by the EKF algorithm. To highlight this feature of the proposed algorithm, the motor is operated at $n_m^{ref} = 0$ and $t_L = 0$ in the interval of $69\text{sec} \leq t \leq 135\text{sec}$. The simulation results are quite satisfactory under this set of conditions which is recognized to be the major challenge in the sensorless estimation of IMs.
- The EKF scheme is also tested for estimation in the high to very low speed range. However, those results are not presented here due to space limitation.
- The developed algorithm is sensitive to variations in the unestimated rotor resistance, R_r' . Thus, it is noted that R_r' estimation should also be included into the algorithm.

In summary, the EKF based speed-sensorless DVC system has demonstrated a good performance, in the whole velocity range including at zero speed, in the face of instantaneous variations in stator resistance and the load torque.

3.6 Conclusion

In this study, an Extended Kalman Filter (EKF) algorithm is developed for the rotor oriented sensorless direct vector control system.

The major contribution of the study is the approach taken to increase robustness against stator resistance, R_s , and load torque, t_L uncertainties, the effects of which are known to give rise to performance deteriorations in the sensorless control of IMs, especially at very low and zero speed operation. This is achieved by the EKF based estimation of R_s , t_L and ω_m , which is taken into account through the use of the equation of motion and not as a constant state as in most past studies. The PWM based switching and resulting flux and current fluctuations that reflect the rotor information to the stator side via the mechanical torque in the equation of motion are the benefits of this approach, particularly in the very low and zero speed region. Simulation results obtained over a large speed range indicate the expected benefits of the approach, also including zero speed, zero load torque operation depicted as being problematic in most past literature [5, 6] on sensorless control. The results can further be improved by also taking into account the well-known frequency and temperature uncertainties related to the rotor resistance. Hence, an approach that combines the estimation of both stator and rotor resistances should be considered for high performance sensorless motion control.

References

- [1] G. Guidi, and H. Umida, A novel stator resistance estimation method for speed-sensorless induction motor drives, *IEEE Trans on Industry Applications*, Vol. 36, No. 6, 2000, pp. 1619–1627.
- [2] C. Lascu, I. Boldea, and F. Blaabjerg, Direct torque control of sensorless induction motor drives: a sliding-mode approach, *IEEE Trans on Industry Applications*, Vol. 40, No. 2, 2004, pp. 582–590.
- [3] M. Barut, O.S. Bogosyan and M. Gokasan, Speed sensorless direct torque control of IMs with rotor resistance estimation, *Energy Conversion and Management (Elsevier)*, Vol. 46, No. 3, 2005, pp. 335–349.
- [4] H. Wang, W. Xu, T. Shen, and G. Yang, Stator flux and torque decoupling control for induction motors with resistances adaptation, *IEE Proceedings-Control Theory Applications*, Vol. 152, No. 4, 2005, pp. 363–370.

- [5] J. Holtz, Sensorless control of induction motors-performance and limitations, *Proc. of IEEE-ISIE2000*, Vol. 1, 2000, pp. PL12–PL20.
- [6] J. Holtz, Sensorless control of induction machines —with or without signal injection?, *IEEE Trans on Industrial Electronics*, Vol. 53, No. 1, 2006, pp.7–30.
- [7] M. Cirrincione, M. Pucci, G. Cirrincione, and G.-A.Capolino, An adaptive speed observer based on a new total least-squares neuron for induction machine drives, *IEEE Trans on Ind. App.*, Vol. 42, No. 1, 2006, pp. 89–104.
- [8] M. Cirrincione and M Pucci, An MRAS-based sensorless high-performance induction motor drive with a predictive adaptive model, *IEEE Trans on Industrial Electronics*, Vol. 52, No. 2, 2005, pp. 532–551.
- [9] G. Edelbaher, K. Jezernik and E. Urlep, Low-speed sensorless control of induction Machine, *IEEE Trans on Industrial Electronics*, Vol. 53, No. 1, 2006, pp. 120–129.
- [10] M. Barut, M. Gokasan and O.S. Bogosyan, EKF based estimator for sensorless direct torque control of IMs, *Proc. of the International Aegean Conference on Electrical Machines and Power Electronics (ACEMP 04)*, 2004, pp. 515–520.
- [11] S. Wade, M.W. Dunnigan, B.W. Williams, Comparison of stochastic and deterministic parameter identification algorithms for indirect vector control, *Proc. of IEE Colloquium on Vector Control and Direct Torque Control of Induction Motors*, Vol. 2, 1995, pp. 1–5.
- [12] L. Salvatore, S. Stasi and L. Tarchioni, A New EKF-based algorithm for flux estimation in induction machines, *IEEE Trans on Industrial Electronics*, Vol. 40, No. 5, 1993, pp. 496–504.
- [13] F. Chen and M.G. Dunnigan, Comparative Study of a sliding-mode observer and Kalman filters for full state estimation in an induction machine, *IEE Proceedings-Electric Power Applications*, Vol. 149, No. 1, 2002, pp. 53–64.
- [14] O.S. Bogosyan, M. Gokasan, and C. Hajiyeve, An Application of EKF for the position control of a single link arm, *Proc. of IEEE-IECON'01 Annual Meeting*, Vol.1, 2001, pp. 564–569.

Chapter 4:

A Switching Technique for Rotor and Stator Resistance Estimation in Speed-Sensorless Control of IMs *

Abstract— High performance speed-sensorless control of induction motors (IMs) calls for estimation and control schemes which offer solutions to parameter uncertainties as well as to difficulties involved with accurate flux and velocity estimation at very low and zero speed. In this study, a new Extended Kalman Filter (EKF) based estimation algorithm is proposed for the solution of both problems and is applied in combination with speed-sensorless Direct Vector Control (DVC). The technique is based on the consecutive execution of two EKF algorithms, by switching from one algorithm to another at every n sampling periods. The number of sampling periods, n , is determined based on the desired system performance. The Switching EKF approach thus applied provides the accurate estimation of an increased number of parameters than it would be possible with a single EKF algorithm. The simultaneous and accurate estimation of rotor, R_r , and stator, R_s , resistances, both in the transient and steady state, is an important challenge in speed-sensorless IM control and reported studies achieving satisfactory results are only a few, if any. With the proposed technique in this study, the sensorless estimation of R_r and R_s is achieved in transient and steady state and in both high and low speed operation, while also estimating the unknown load torque, velocity, flux and current components. The performance demonstrated by the simulation results at zero speed, as well as at low and high speed operation is very promising when compared with individual EKF algorithms performing either R_r or R_s estimation or with the few other approaches taken in past studies, which require either signal injection and/or change of

* Barut, M., Bogosyan, S. and Gokasan, M. (2006c), "A Switching Technique for Rotor and Stator Resistance Estimation in Speed-Sensorless Control of IMs", *Energy Conversion and Management (Elsevier)*. (In review)

algorithms based on the speed range. The results also motivate the utilization of the technique for multiple parameter estimation in a variety of control methods.

Index Terms— *Induction motor; Extended Kalman Filter with switching; sensorless control; load torque estimation, rotor resistance and stator resistance estimation; zero speed operation.*

4.1 Introduction

Industry workhorse induction motors (IMs) constitute a theoretically interesting and practically important class of nonlinear systems, and hence, a benchmark problem for nonlinear control [1]. IMs enjoy several inherent advantages, like simplicity, reliability, low cost, and almost maintenance-free electrical drives [2]. However, the speed-sensorless high performance control of IMs currently continues to be a challenge due to the highly coupled nonlinearities and the multi-input, multi output nature of the motor model. The problem has been addressed by a variety of methods such as, *field-oriented control* (FOC) or *vector control* [3], *direct torque control* (DTC) [4], *input-output linearization (feedback linearization) control* [3, 5], *sliding mode control* (SMC) [6] and *passivity-based control* (PBC) [3], each of which aims at independent control of the torque and flux. Additional difficulties are due to unknown load disturbances, and parameter uncertainties mostly related to the stator and rotor resistances varying with the operating conditions. There are also well-known problems related to high performance control, particularly in the very low and zero speed region, mainly due to lost rotor information on the stator side as well as noise and signal acquisition errors [1, 7, 8]. In this regard, it is essential to design estimation and control methods that provide robustness predominantly against the variations of R_s , R_r , and t_L , while also providing solutions to problems at and around zero speed.

Some recent studies seeking an observer-based solution to the problem of parameter variations are listed as follows. In [9], beside a speed estimator, a sliding mode based

flux observer and an online sliding-mode adaptation for the stator resistance is designed for DTC of IMs, but the speed estimator and the resistance adaptation suffer from variations of the rotor resistance and the load torque, respectively. In the speed-sensorless study based on speed adaptive flux observer in [10], the stator resistance has been estimated based on a two-time scale approach, while in the Extended Luenberger observer (ELO) in [11], the rotor fluxes and rotor velocity are estimated, as well as the step-type load torque; however, no estimation has been conducted for the stator resistance. Also, neither of the studies in [10] and [11] have taken the rotor resistance into consideration. On the other hand in [12], the angular velocity, and slip frequency (reflecting in the effect of the load torque) have been taken into account in addition to the rotor resistance only with an initial value of $R_r'(0) = 0.85R_m'$.

There are also Extended Kalman Filter (EKF) applications in the literature for the control of IMs with velocity sensors [13–15] and without sensors. Different from the other methods, the model uncertainties and nonlinearities inherent in IMs are well suited to the stochastic nature of EKFs [16]. With this method, it is possible to make the online estimation of states while performing the simultaneous identification of parameters in a relatively short time interval [17–19], by also taking system process and measurement noises directly into account. This is the reason why the EKF has found wide application in sensorless control of IMs, in spite of its computational complexity. Among recent sensorless studies using EKF estimation for IMs, [20] and [21] estimate the flux and velocity, while [22] uses an adaptive flux observer in combination with a second order Kalman filter for the same purpose. None of these studies estimate the load and motor resistances, resulting in a performance that is sensitive to the variation of these parameters. In [23–25], the velocity is estimated as a constant parameter, which gives rise to a significant estimation error in the velocity during the transient state, especially under instantaneous load variations, although the performance is improved in the steady state. While [23] and [24] are sensitive to rotor resistance variations, [25] also estimates the rotor resistance. However, the estimation of rotor resistance is performed by the

injection of low amplitude, high frequency signals to the flux reference in the DVC of IMs. This has caused fluctuations in the motor flux, torque and speed. Finally, recent studies of the authors [26, 27] estimating the velocity via the consideration of the equation of motion in the EKF model, together with the estimation of rotor resistance and mechanical uncertainties demonstrate improved results. However, the results are sensitive to variations of stator resistance, indicating the necessity of an approach that estimates rotor resistance and stator resistance simultaneously and accurately beside the load torque for high performance control in a wide operation range, including very low and zero speed.

Among studies reported so far on R_s and R_r estimation, [12] states that the simultaneous estimation of the stator and rotor resistances gives rise to instability in the speed-sensorless case. On the other hand, in studies such as [28] and [29], the stator and rotor resistances are estimated by injecting high frequency signals to the flux and magnetizing current commands, while also estimating the speed and rotor flux. However, in [28], the algorithm identifying the resistances used in a feedback linearization controller is applicable only when the sensorless speed control system is in steady state, but not when the load torque is varying largely or when the speed command is being changed, as stated by the authors. On the other hand, in [29], it is stated that persistent operation at zero frequency is not possible and that the proposed drive can compete with a speed sensor equipped drive only if accuracy in steady-state is not essential and operation under high loads is not a requirement. In [30], a model reference adaptive system (MRAS) is presented based on 3 models, of which one is used for the estimation of rotor time constant via high frequency signal injection. The other 2 models are used interchangeably, by enabling the stator resistance estimation only during short intervals, during which the rotor speed has reached the steady state. As for the remaining few studies performing R_s and R_r estimation, as in [31], [32] and [33], R_r estimation is conducted only by adjusting its value in proportion to the estimated R_s .

The major contribution of this study is the development of a novel EKF based estimation technique, which aims at the accurate estimation of an increased number of parameters both in the transient and steady state for sensorless IM control. The technique does not require signal injection and/or algorithm changes for different parameters or speed ranges as is commonly practised in similar past studies. It is based on two EKF algorithms that are switched *on* and *off* every n sampling periods, the output parameters and states of which are used in the direct-vector control (DVC) of IMs. In this study, the accurate estimation of both R_s and R_r is achieved as a novelty in sensorless control of IMs, together with the unknown load torque, velocity, flux and current components. Simulation results are presented using the new algorithm for the DVC of IMs with the switching period taken as $100 \times T$ for the desired transient and steady-state performance. The results highlight the significant improvement achieved with the simultaneous estimation of R_s and R_r , over EKF results obtained by either R_s or R_r estimation only.

This paper is organized as follows. After the introduction in section I, section II gives the extended mathematical models considered at each step of the EKF estimation. Next, section III describes the development of the EKF algorithm, followed by section IV presenting a brief description of the Direct Vector Control (DVC) scheme. The performance of the proposed approach is tested by simulations with results presented in section V and finally, conclusions are listed in section VI.

4.2 Extended Mathematical Models of the IM

The sensorless DVC scheme developed for IMs requires the estimation of stator flux components, $\psi_{r\alpha}$, $\psi_{r\beta}$, angular velocity, ω_m and stator current components $i_{s\alpha}$ and $i_{s\beta}$, which are also measured as output. In this study, two extended models are developed, one which includes the rotor resistance, R_r and one, with the stator resistance, R_s . The rest of the variables are the same for both extended vectors, \underline{x}_{ei} , used in the two EKF

algorithms which run consecutively. The extended models can be given (as referred to the stator stationary frame) in the following general form:

$$\dot{\underline{x}}_{ei}(t) = \underline{f}_{ei}(\underline{x}_{ei}(t), \underline{u}_e(t)) + \underline{w}_{i1}(t) = \underline{A}_{ei}(\underline{x}_{ei}(t))\underline{x}_{ei}(t) + \underline{B}_e \underline{u}_e(t) + \underline{w}_{i1}(t) \quad (4.1)$$

$$\underline{Z}(t) = \underline{h}_{ei}(\underline{x}_{ei}(t)) + \underline{w}_{i2}(t) = \underline{H}_e \underline{x}_{ei}(t) + \underline{w}_{i2}(t) \quad (\text{measurement equation}) \quad (4.2)$$

Where, $i = 1, 2$, extended state vector \underline{x}_{ei} represents the estimated states and load torque, t_L , which is included in the extended state vector as a constant state with the assumption of a slow variation with time. \underline{f}_{ei} is the nonlinear function of the states and inputs; \underline{A}_{ei} is the system matrix. \underline{u}_e is the control input vector. \underline{B}_e is the input matrix. \underline{w}_{i1} is the process noise. \underline{h}_{ei} is the function of the outputs. \underline{H}_e is the measurement matrix. \underline{w}_{i2} is the measurement noise.

Based on the general form in (4.1) and (4.2), the detailed matrix representation of the two IM models can be given as below:

Model 1: Extended model of IM derived for the estimation of R_s , (Model- R_s):

$$\begin{bmatrix} \dot{i}_{s\alpha} \\ \dot{i}_{s\beta} \\ \dot{\psi}_{r\alpha} \\ \dot{\psi}_{r\beta} \\ \dot{\omega}_m \\ \dot{t}_L \\ \dot{R}_s \end{bmatrix} = \underbrace{\begin{bmatrix} -\left(\frac{R_s}{L_\sigma} + \frac{L_m^2 R_r'}{L_\sigma L_r'^2}\right) & 0 & \frac{L_m R_r'}{L_\sigma L_r'^2} & \frac{L_m}{L_\sigma L_r'} p_p \omega_m & 0 & 0 & 0 \\ 0 & -\left(\frac{R_s}{L_\sigma} + \frac{L_m^2 R_r'}{L_\sigma L_r'^2}\right) & \frac{L_m}{L_\sigma L_r'} p_p \omega_m & \frac{L_m R_r'}{L_\sigma L_r'^2} & 0 & 0 & 0 \\ L_m \frac{R_r'}{L_r'} & 0 & \frac{R_r'}{L_r'} & -p_p \omega_m & 0 & 0 & 0 \\ 0 & L_m \frac{R_r'}{L_r'} & p_p \omega_m & \frac{R_r'}{L_r'} 0 & 0 & 0 & 0 \\ \frac{3 p_p L_m}{2 J_L L_r'} \psi_{r\beta} & \frac{3 p_p L_m}{2 J_L L_r'} \psi_{r\alpha} & 0 & 0 & 0 & \frac{1}{J_L} & 0 \\ 0 & 0 & 0 & 0 & 0 & 0 & 0 \\ 0 & 0 & 0 & 0 & 0 & 0 & 0 \end{bmatrix}}_{\underline{A}_{ei}} \begin{bmatrix} i_{s\alpha} \\ i_{s\beta} \\ \psi_{r\alpha} \\ \psi_{r\beta} \\ \omega_m \\ t_L \\ R_s \end{bmatrix} + \underbrace{\begin{bmatrix} \frac{1}{L_\sigma} & 0 \\ 0 & \frac{1}{L_\sigma} \\ 0 & 0 \\ 0 & 0 \\ 0 & 0 \\ 0 & 0 \\ 0 & 0 \end{bmatrix}}_{\underline{B}_{ei}} \begin{bmatrix} v_{s\alpha} \\ v_{s\beta} \end{bmatrix} + \underline{w}_{i1}(t) \quad (4.3)$$

$$\underbrace{\begin{bmatrix} i_{s\alpha} \\ i_{s\beta} \end{bmatrix}}_{\underline{Z}} = \underbrace{\begin{bmatrix} 1 & 0 & 0 & 0 & 0 & 0 & 0 \\ 0 & 1 & 0 & 0 & 0 & 0 & 0 \end{bmatrix}}_{\underline{H}_e} \begin{bmatrix} i_{s\alpha} \\ i_{s\beta} \\ \psi_{r\alpha} \\ \psi_{r\beta} \\ \omega_m \\ t_L \\ R_s \end{bmatrix} + \underline{w}_{12}(t) \quad (4.4)$$

Model 2: Extended model of IM derived for the estimation of R_r' , (Model- R_r'):

$$\underbrace{\begin{bmatrix} \dot{i}_{s\alpha} \\ \dot{i}_{s\beta} \\ \dot{\psi}_{r\alpha} \\ \dot{\psi}_{r\beta} \\ \dot{\omega}_m \\ \dot{t}_L \\ \dot{R}_r' \end{bmatrix}}_{\underline{\dot{z}}_{e2}} = \underbrace{\begin{bmatrix} -\left(\frac{R_s}{L_\sigma} + \frac{L_m^2 R_r'}{L_\sigma L_r'^2}\right) & 0 & \frac{L_m R_r'}{L_\sigma L_r'^2} & \frac{L_m}{L_\sigma L_r'} p_p \omega_m & 0 & 0 & 0 \\ 0 & -\left(\frac{R_s}{L_\sigma} + \frac{L_m^2 R_r'}{L_\sigma L_r'^2}\right) & \frac{L_m}{L_\sigma L_r'} p_p \omega_m & \frac{L_m R_r'}{L_\sigma L_r'^2} & 0 & 0 & 0 \\ L_m \frac{R_r'}{L_r'} & 0 & \frac{R_r'}{L_r'} & -p_p \omega_m & 0 & 0 & 0 \\ 0 & L_m \frac{R_r'}{L_r'} & p_p \omega_m & \frac{R_r'}{L_r'} & 0 & 0 & 0 \\ \frac{3 p_p L_m}{2 J_L L_r'} \psi_{r\beta} & \frac{3 p_p L_m}{2 J_L L_r'} \psi_{r\alpha} & 0 & 0 & 0 & \frac{1}{J_L} & 0 \\ 0 & 0 & 0 & 0 & 0 & 0 & 0 \\ 0 & 0 & 0 & 0 & 0 & 0 & 0 \end{bmatrix}}_{\underline{A}_{e2}} \underbrace{\begin{bmatrix} i_{s\alpha} \\ i_{s\beta} \\ \psi_{r\alpha} \\ \psi_{r\beta} \\ \omega_m \\ t_L \\ R_r' \end{bmatrix}}_{\underline{x}_{e2}} + \underbrace{\begin{bmatrix} \frac{1}{L_\sigma} & 0 \\ 0 & \frac{1}{L_\sigma} \\ 0 & 0 \\ 0 & 0 \\ 0 & 0 \\ 0 & 0 \\ 0 & 0 \end{bmatrix}}_{\underline{B}_{e2}} \underbrace{\begin{bmatrix} v_{s\alpha} \\ v_{s\beta} \end{bmatrix}}_{\underline{u}_e} + \underline{w}_{21}(t) \quad (4.5)$$

$$\underbrace{\begin{bmatrix} i_{s\alpha} \\ i_{s\beta} \end{bmatrix}}_{\underline{Z}} = \underbrace{\begin{bmatrix} 1 & 0 & 0 & 0 & 0 & 0 & 0 \\ 0 & 1 & 0 & 0 & 0 & 0 & 0 \end{bmatrix}}_{\underline{H}_e} \begin{bmatrix} i_{s\alpha} \\ i_{s\beta} \\ \psi_{r\alpha} \\ \psi_{r\beta} \\ \omega_m \\ t_L \\ R_r' \end{bmatrix} + \underline{w}_{22}(t) \quad (4.6)$$

Here, p_p is the number of pole pairs. $L_\sigma = \sigma L_s$ is the stator transient inductance.

$\sigma = 1 - \frac{L_m^2}{L_s L_r'}$ is the leakage or coupling factor. L_s and R_s are the stator inductance and

resistance, respectively. L_r' and R_r' are the rotor inductance and resistance, referred to the stator side, respectively. $v_{s\alpha}$ and $v_{s\beta}$ are the stator stationary axis components of stator voltages. $i_{s\alpha}$ and $i_{s\beta}$ are the stator stationary axis components of stator currents. $\psi_{r\alpha}$ and $\psi_{r\beta}$ are the stator stationary axis components of rotor flux. J_L is the total inertia of the IM and load. ω_m is the angular velocity; As can be seen from (4.3)-(4.4) and (4.5)-(4.6), the only difference between the two extended vectors, \underline{x}_{e1} and \underline{x}_{e2} , are the constant states R_s and R_r' , respectively. Additionally, as in both algorithms $i_{s\alpha}$ and $i_{s\beta}$ are the measured variables, the measurement noises, w_{12} and w_{22} , are equal.

4.3 Development of the Switching EKF Algorithm

An EKF algorithm is developed for the estimation of the states in the extended IM model given in (4.1) and (4.2), to be used in the sensorless DVC of the IM. The Kalman filter is a well-known recursive algorithm that takes the stochastic state space model of the system into account, together with measured outputs to achieve the optimal estimation of states [34] in multi-input, multi-output systems. The system and measurement noises are considered to be in the form of white noise. The optimality of the state estimation is achieved with the minimization of the covariance of the estimation error. For nonlinear problems the KF is not strictly applicable since linearity plays an important role in its derivation and performance as an optimal filter. The EKF attempts to overcome this difficulty by using a linearized approximation where the linearization is performed about the current state estimate [35]. This process requires the discretization of (4.3) and (4.4) – or (4.5) and (4.6) as below:

$$\underline{x}_{ei}(k+1) = \underline{f}_{ei}(\underline{x}_{ei}(k), \underline{u}_e(k)) + \underline{w}_{i1}(k) \quad (4.7)$$

$$\underline{Z}(k) = \underline{H}_e \underline{x}_{ei}(k) + \underline{w}_{i2}(k) \quad (4.8)$$

As mentioned before, EKF involves the linearized approximation of the nonlinear model (4.7-4.8) and uses the current estimation of states $\hat{\underline{x}}_{ei}(k)$ and inputs $\hat{\underline{u}}_e(k)$ in linearization by using,

$$\underline{F}_{ei}(k) = \left. \frac{\partial \underline{f}_{ei}(\underline{x}_{ei}(k), \underline{u}_e(k))}{\partial \underline{x}_{ei}(k)} \right|_{\hat{\underline{x}}_{ei}(k), \hat{\underline{u}}_e(k)} \quad (4.9)$$

$$\underline{F}_{ui}(k) = \left. \frac{\partial \underline{f}_{ei}(\underline{x}_{ei}(k), \underline{u}_e(k))}{\partial \underline{u}_e(k)} \right|_{\hat{\underline{x}}_{ei}(k), \hat{\underline{u}}_e(k)} \quad (4.10)$$

Thus, the EKF algorithm can be given in the following recursive relations;

$$\underline{N}_i(k) = \underline{F}_{ei}(k) \underline{P}_i(k) \underline{F}_{ei}(k)^T + \underline{F}_{ui}(k) \underline{D}_u \underline{F}_{ui}(k)^T + \underline{Q} \quad (4.11a)$$

$$\underline{P}_i(k+1) = \underline{N}_i(k) - \underline{N}_i(k) \underline{H}_e^T (\underline{D}_\xi + \underline{H}_e \underline{N}_i(k) \underline{H}_e^T)^{-1} \underline{H}_e \underline{N}_i(k) \quad (4.11b)$$

$$\hat{\underline{x}}_{ei}(k+1) = \hat{\underline{f}}_{ei}(\underline{x}_{ei}(k), \hat{\underline{u}}_e(k)) + \underline{P}_i(k+1) \underline{H}_e^T \underline{D}_\xi^{-1} (\underline{Z}(k) - \underline{H}_e \hat{\underline{x}}_{ei}(k)) \quad (4.11c)$$

Here, \underline{Q}_i is the covariance matrix of the system noise, namely model error. \underline{D}_ξ is the covariance matrix of the output noise, namely measurement noise. \underline{D}_u is the covariance matrix of the control input noise ($v_{s\alpha}$ and $v_{s\beta}$), namely input noise. \underline{P}_i and \underline{N}_i are the covariance matrix of state estimation error and extrapolation error, respectively.

The algorithm involves two main stages: prediction and filtering. In the prediction stage, the next predicted states $\hat{\underline{f}}_{ei}(\cdot)$ and predicted state error covariance matrices, $\underline{P}_i(\cdot)$ and $\underline{N}_i(\cdot)$ are processed, while in the filtering stage, the next estimated states, $\hat{\underline{x}}_{ei}(k+1)$, obtained as the sum of the next predicted states and the correction term (2nd term in (4.11c)) are calculated.

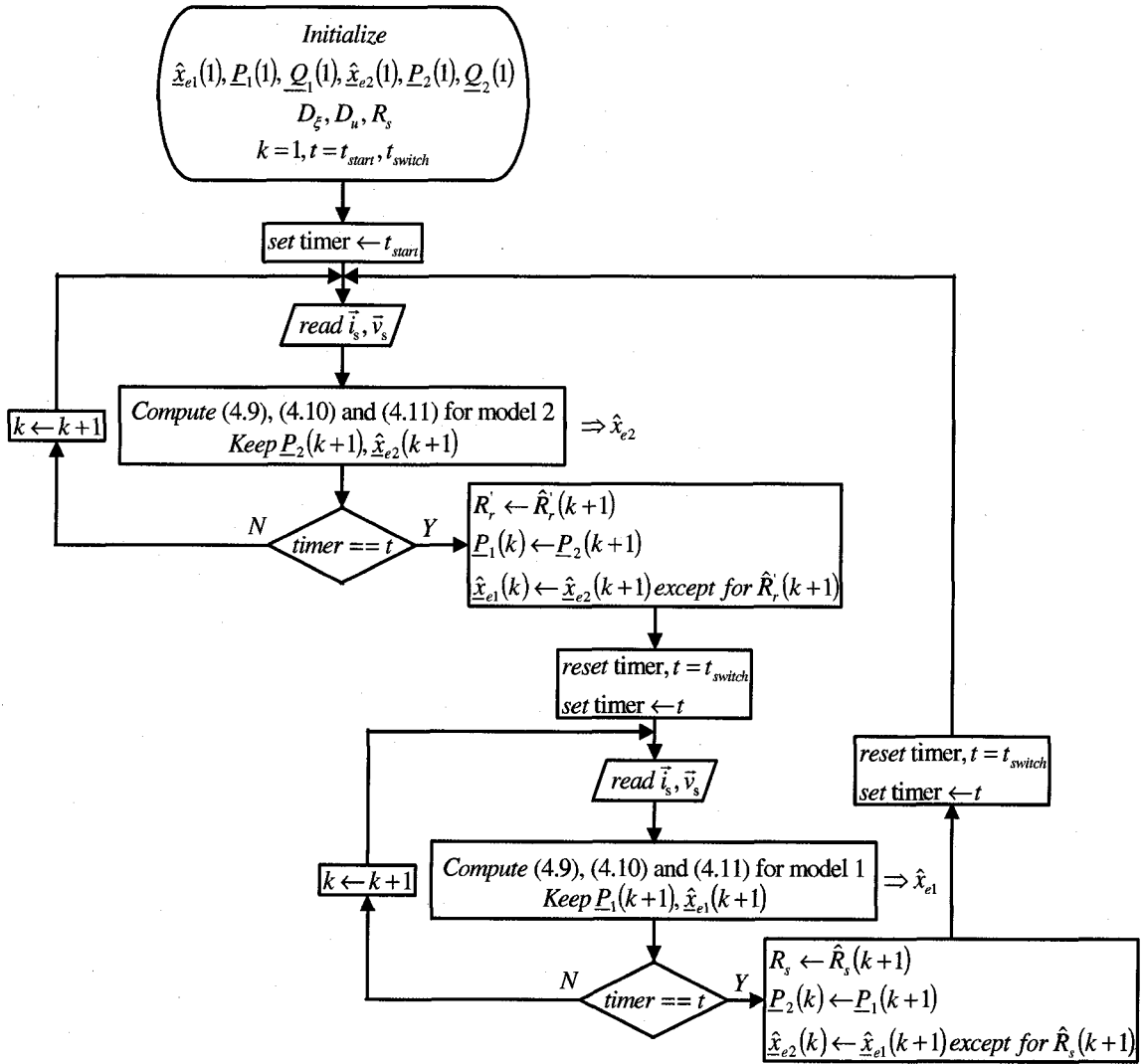


Fig. 4.1 Flow-chart of the novel Switching EKF algorithm

The schematic representation of the new EKF based switching estimation algorithm is given in Fig. 4.1. As can be seen in Fig. 4.1, two EKF algorithms with two different extended models are run consecutively, –one for the estimation of R_s and one for the estimation of R_r in this case. Thus, both algorithms estimate the same state variables except for the resistances. Therefore, one of the EKFs estimates the rotor resistance during one switching period and the other estimates the stator resistance in the next

switching interval and so on. After the initialization of the states and determination of t_{start} and t_{switch} , which is the start time and duration of the EKF algorithms, respectively, the algorithms are run by switching them on and off, consecutively and for equal durations. The final values of $\underline{P}_i(k+1)$ and $\hat{\underline{x}}_{ei}(k+1)$ calculated at the end of each switching period are passed over to the next EKF algorithm at the end of the period, as the initial values of the covariances and states for the new switching period, during which the other algorithm will be running. The estimated resistance during the previous period is also passed on to the new algorithm and is assumed constant in the other EKF model throughout the whole switching period, during which the other resistance value is calculated as well as the state variables.

4.4 The Speed-Sensorless DVC System

Fig. 4.2 demonstrates the speed-sensorless DVC system based on rotor flux. Here, $\hat{\theta}_{rf}$ stands for the position of the flux with reference to the stationary axis, while $\frac{d}{dt}\hat{\theta}_{rf}$ is the

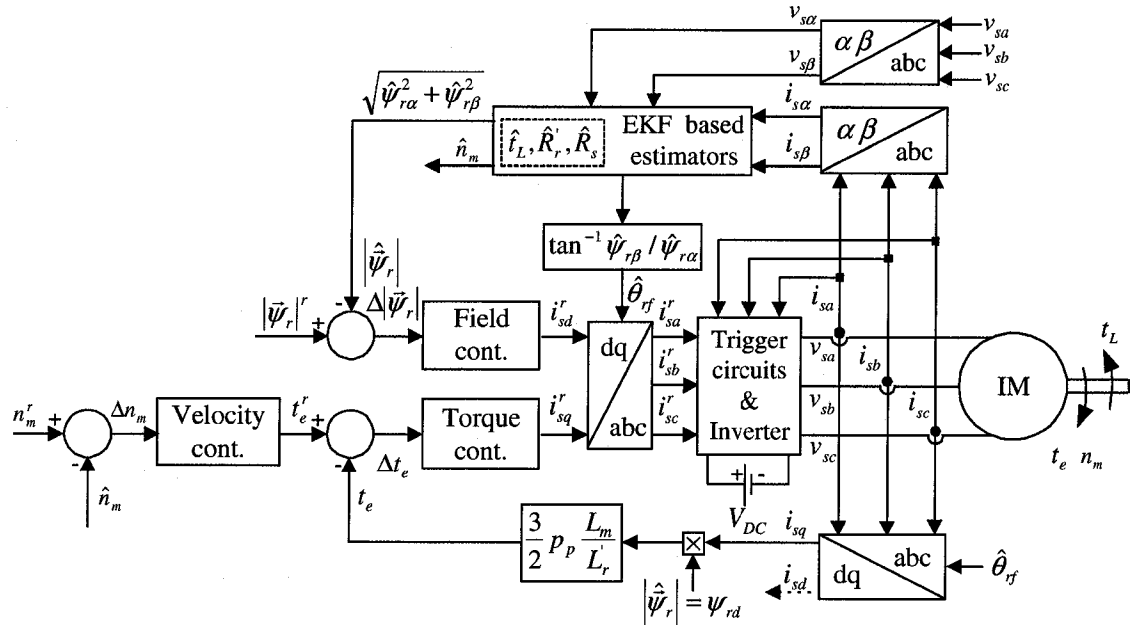


Fig. 4.2 The speed-sensorless DVC system

angular velocity of the rotating d - q axis. The velocity, field, and torque controllers given in the diagram are conventional Proportional-Integral (PI) controllers.

4.5 Simulation Results and Observations

To test the performance of the proposed estimation method, simulations are performed on an IM with the rated parameters given in Table 4.1.

Table 4.1 Rated values and parameters of the induction motor used in the experiments

P [kW]	f [Hz]	J_L [kg.m ²]	B_L [Nm/(rad/s)]	p_p	V [V]	I [A]
3	50	0.006	0.001	2	380	6.9

R_s [Ω]	R_r [Ω]	L_s [H]	L_r [H]	L_m [H]	N_m [rpm]	T_e [Nm]
2.283	2.133	0.2311	0.2311	0.22	1430	20

The values of system parameters and covariance matrix elements have a significant effect on the performance of the EKF estimation. In this study, to avoid computational complexity, the covariance matrix of the system noise \underline{Q}_i is chosen in diagonal form, also satisfying the condition of positive definiteness. According to the Kalman filter theory, the \underline{Q}_i , \underline{D}_ξ (measurement error covariance matrix) and \underline{D}_u (input error covariance matrix) have to be obtained by considering the stochastic properties of the corresponding noises [36]. However, since these are usually not known, in most cases the covariance matrix elements are used as weighting factors or tuning parameters. In this study, for both EKF algorithms, the tuning of the initial values of the \underline{P}_i and \underline{Q}_i is done by trial-and-error to achieve a rapid initial convergence and the desired transient and steady state behaviors of the estimated states and parameters, while the \underline{D}_ξ and \underline{D}_u are determined taking into account the measurement errors of the current and voltage sensors and the quantization errors of the ADCs as given below:

For Model- R_s ;

$$\underline{Q}_1 = \text{diag} \{ 10^{-9}[A^2] \quad 10^{-9}[A^2] \quad 10^{-9}[Wb^2] \quad 10^{-9}[Wb^2] \quad 10^{-4}[(rad/s)^2] \quad 10^{-4}[(Nm)^2] \quad 10^{-5}[\Omega^2] \}$$

$$\underline{P}_1 = \text{diag} \{ 9[A^2] \quad 9[A^2] \quad 9[Wb^2] \quad 9[Wb^2] \quad 9[(rad/s)^2] \quad 9[(Nm)^2] \quad 9[\Omega^2] \}$$

For Model- R_r :

$$\underline{Q}_2 = \text{diag} \{ 10^{-9}[A^2] \quad 10^{-9}[A^2] \quad 10^{-9}[Wb^2] \quad 10^{-9}[Wb^2] \quad 10^{-4}[(rad/s)^2] \quad 10^{-4}[(Nm)^2] \quad 10^{-5}[\Omega^2] \}$$

$$\underline{P}_2 = \text{diag} \{ 9[A^2] \quad 9[A^2] \quad 9[Wb^2] \quad 9[Wb^2] \quad 9[(rad/s)^2] \quad 9[(Nm)^2] \quad 9[\Omega^2] \}$$

For both models,

$$\underline{D}_\xi = \text{diag} \{ 10^{-6}[A^2] \quad 10^{-6}[A^2] \}$$

$$\underline{D}_u = \text{diag} \{ 10^{-6}[V^2] \quad 10^{-6}[V^2] \}$$

and sampling time $T = 100 \mu s$.

As can be seen from the time axis in Fig. 4.3, seventeen different scenarios are created to test the performance of the estimation and control algorithm in the time interval of $0 \leq t \leq 24 \text{ sec}$.

These scenarios are developed with simultaneous changes imposed on the stator and the rotor resistance (Fig. 4.3a), on the velocity reference (Fig. 4.3b), and the load torque values (Fig. 4.3c) used in the simulation model.

As it is well-known, it is difficult to obtain the initial value of the rotor resistance in a squirrel-cage IM, but that of the stator resistance can easily be determined by the DC test. Therefore, it is assumed that the initial value of the stator resistance is known at the outset of the scenarios while the estimation of the other parameters and all the states is started with an initial value of zero, as a more reasonable approach. Thus, the EKF

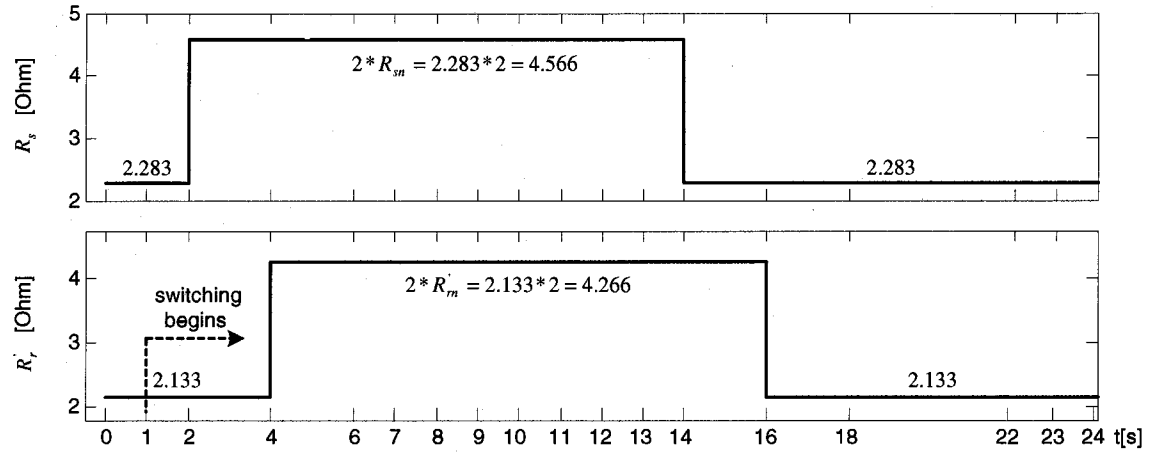
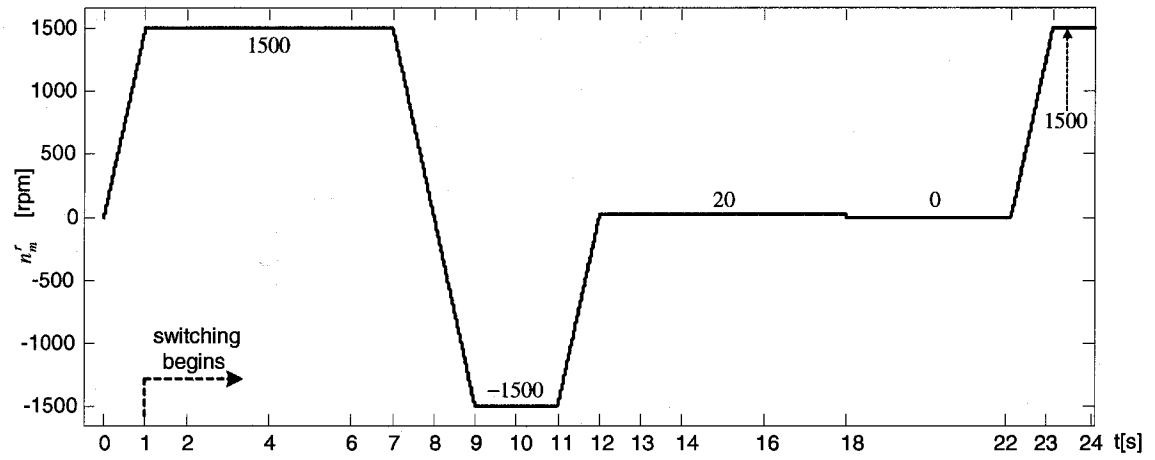
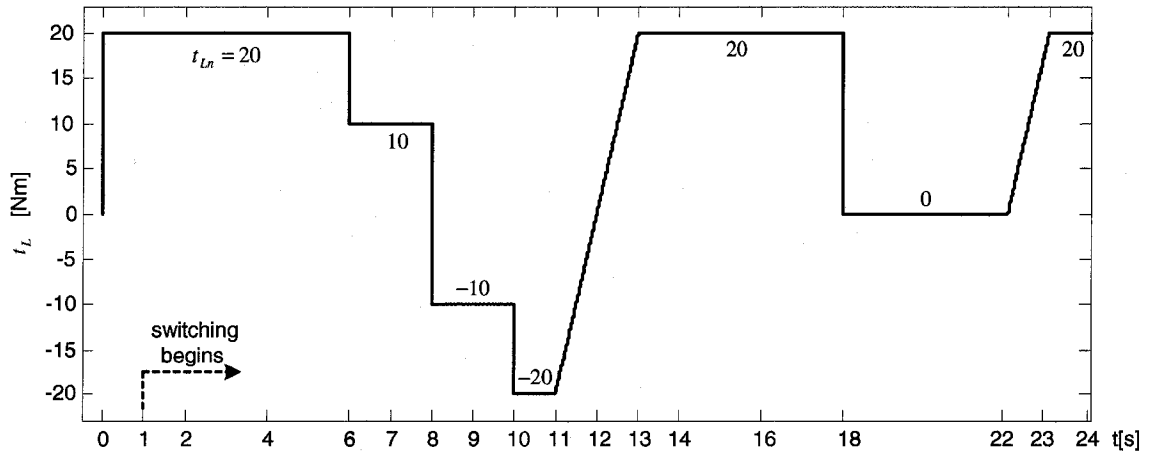
(a) Variation of the stator/rotor resistances, R_s / R_r (b) Variation of the reference speed value, n_m^{ref} (c) Variation of the applied load torque, t_L

Fig. 4.3 Variation of the stator/rotor resistances, R_s / R_r , the reference speed value, n_m^{ref} , and applied load torque, t_L

algorithm for the Model- \hat{R}_r' is started, and after $t_{start} = 1$ [sec] as shown in Fig. 4.3, the two EKF algorithms are used consecutively by switching from one to the other at the end of a constant time interval of duration, t_{switch} , in order to estimate the rotor and stator resistances beside all the other variables required by the control scheme. For the desired transient and steady-state performance criteria of this system, the t_{switch} is selected as $100 \times T$ (T : sampling period). The switching duration, t_{switch} is determined based on the following procedure:

- i) Tune \underline{P}_i and \underline{Q}_i until the desired estimation performance is achieved by each EKF algorithm; namely EKF- \hat{R}_s and EKF- \hat{R}_r' .
- ii) After the tuning stage, increase $t_{switch} = n \times T$ (where $n = 1, 2, 3, \dots$ and T : sampling period) by increasing n , until the desired estimation performance is reached.

In this study, t_{switch} is increased to $100 \times T$ in order to achieve an improved performance in transient and steady-state under *unmatched* variations of R_s and \hat{R}_r' , which is the most challenging case for both EKF algorithms. Intervals with *unmatched* variations describe intervals during which, while one type of resistance is being estimated, the other one is given a major variation. In this study, the best “ n ” is also determined under unmatched variations with the following scenario given in Fig. 4.3, in which EKF- \hat{R}_r' is switched *on* at $t = 2.01$ [sec] when $R_s : 2 * R_{sn} \rightarrow R_{sn}$ or similarly EKF- \hat{R}_s is switched *on* at $t = 4$ [sec] when $\hat{R}_r' : R_{rn}' \rightarrow 2 * R_{rn}'$.

The resulting system performance for all scenarios is given with Fig. 4.4a representing the velocity estimate, \hat{n}_m , with Fig. 4.4b depicting the velocity error, $(n_m^{ref} - \hat{n}_m)$ and Fig. 4.4c giving the estimation error, $n_m - \hat{n}_m$.

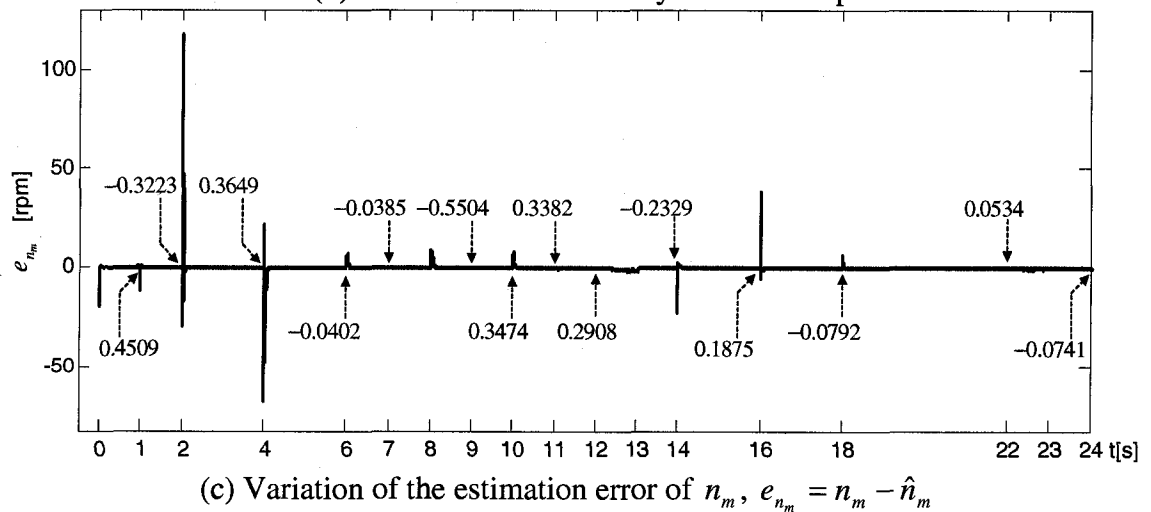
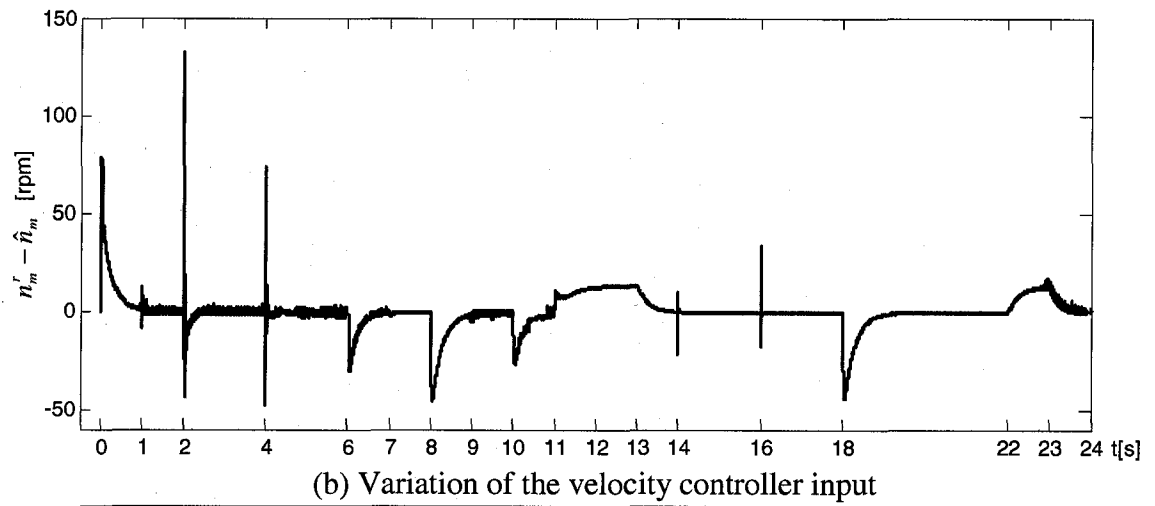
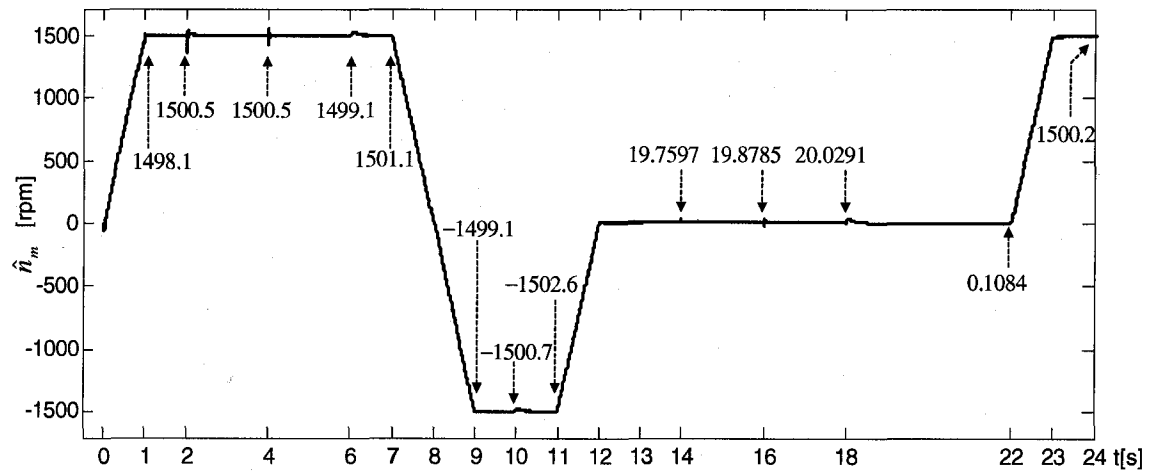
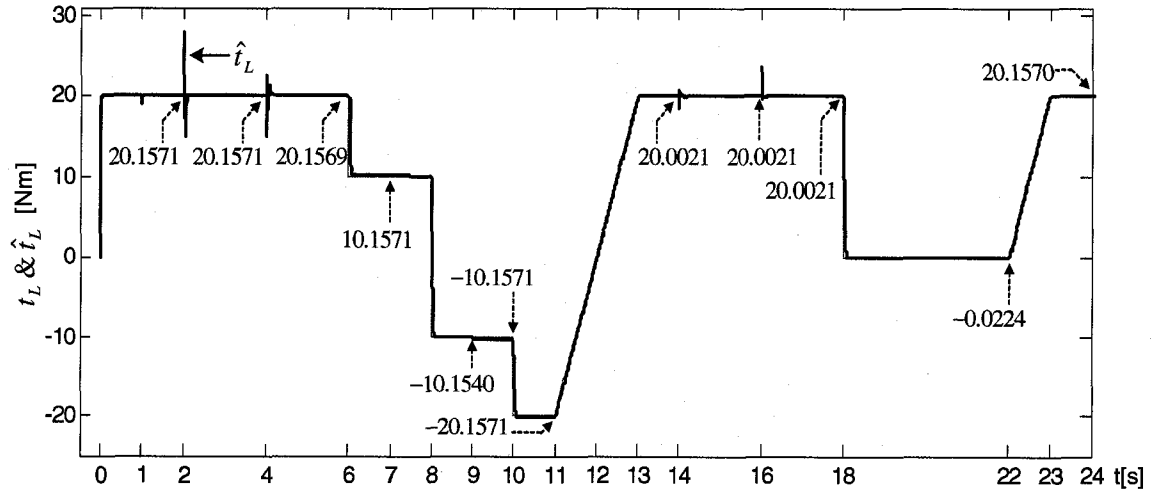
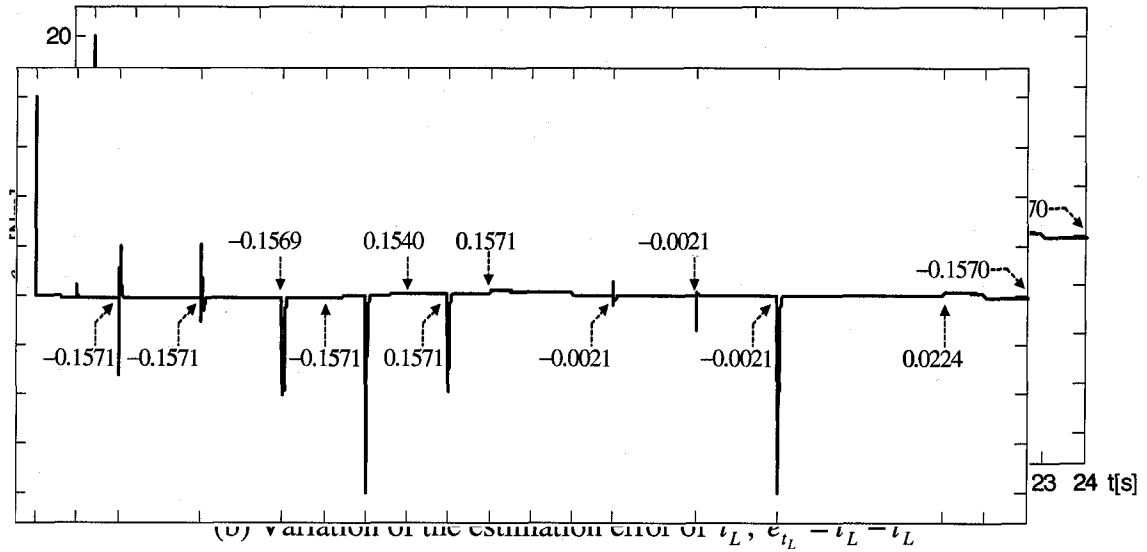


Fig. 4.4 Simulation results for the estimation of velocity obtained with the Switching EKF estimator and DVC system

The variation of the applied and estimated load torque is given in Fig. 4.5a, with Fig. 4.5b representing the estimation error, $(t_L - \hat{t}_L)$ for t_L .



(a) Variation of the t_L and \hat{t}_L



(b) Variation of the estimation error of t_L , $e_{t_L} = t_L - \hat{t}_L$

Fig. 4.5 Simulation results for the estimation of the load torque using the Switching EKF estimator

The variations related to the R_s are given in Fig. 4.6a and Fig. 4.6b, with the former plot representing the actual and estimated variations of R_s , while the latter plot represents the estimation error, $R_s - \hat{R}_s$.

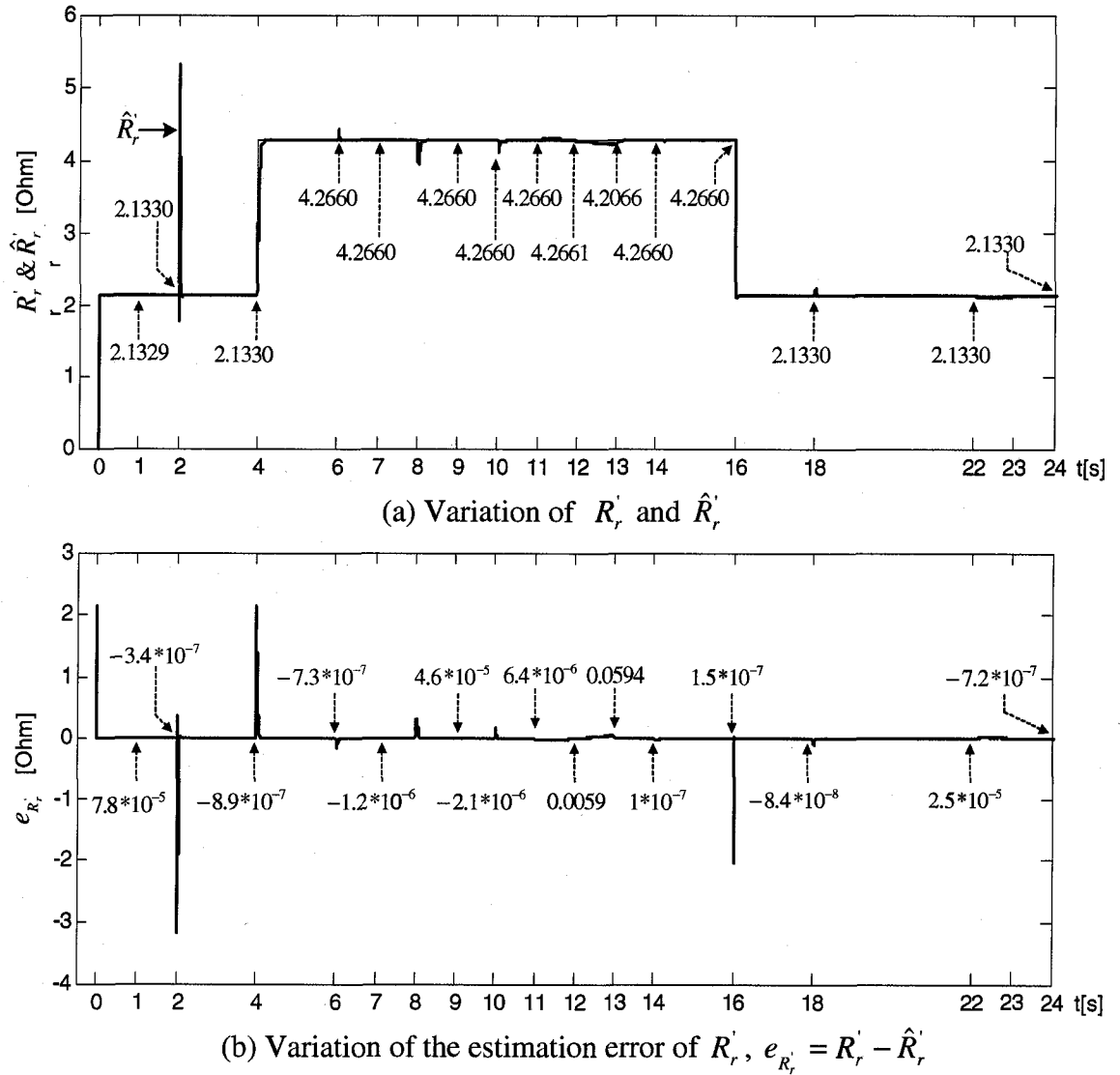


Fig. 4.7 Simulation results for the estimation of rotor resistance using the Switching EKF estimator

Finally, the system performance in the zero speed range under the scenarios given in Fig. 4.9a is demonstrated in Fig. 4.9b for the estimation error, $n_m - \hat{n}_m$, and in Fig. 4.9c for the variation of the estimated θ_{rf} , which is the position of the flux with reference to the stator stationary axis.

Analysing the simulation results, the following observations are made:

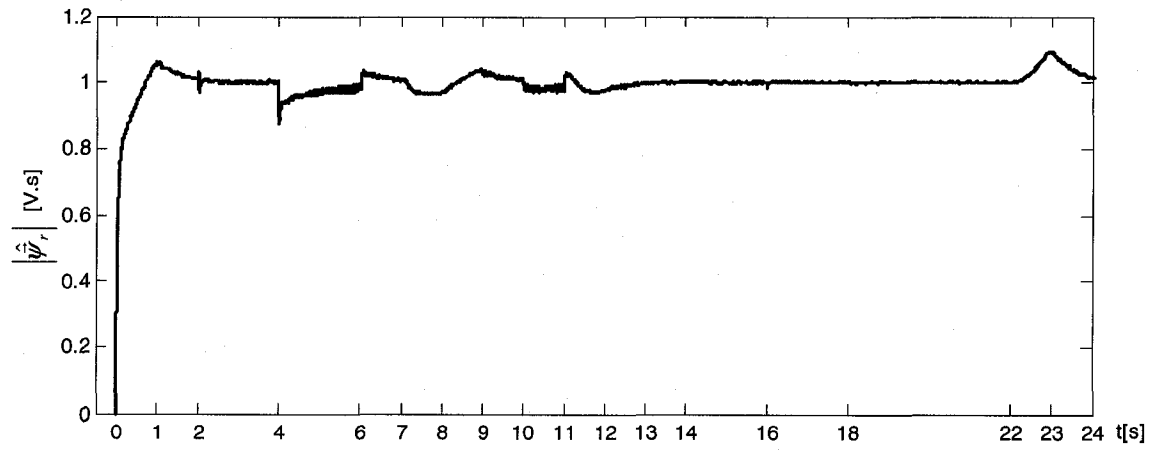
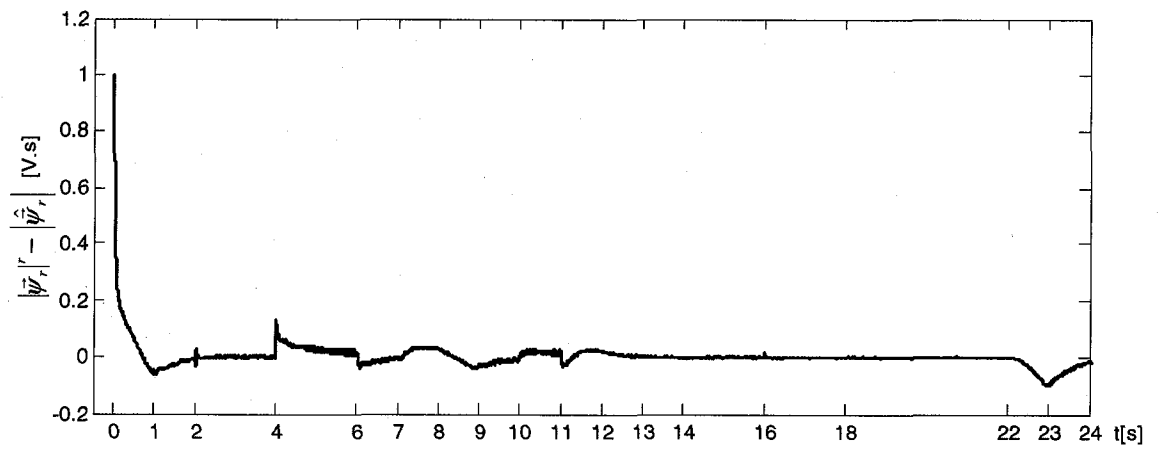
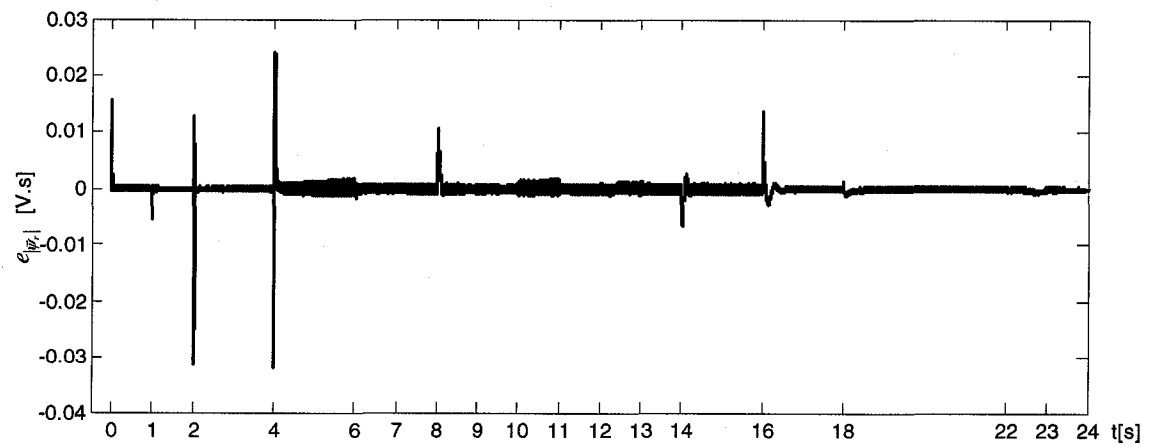
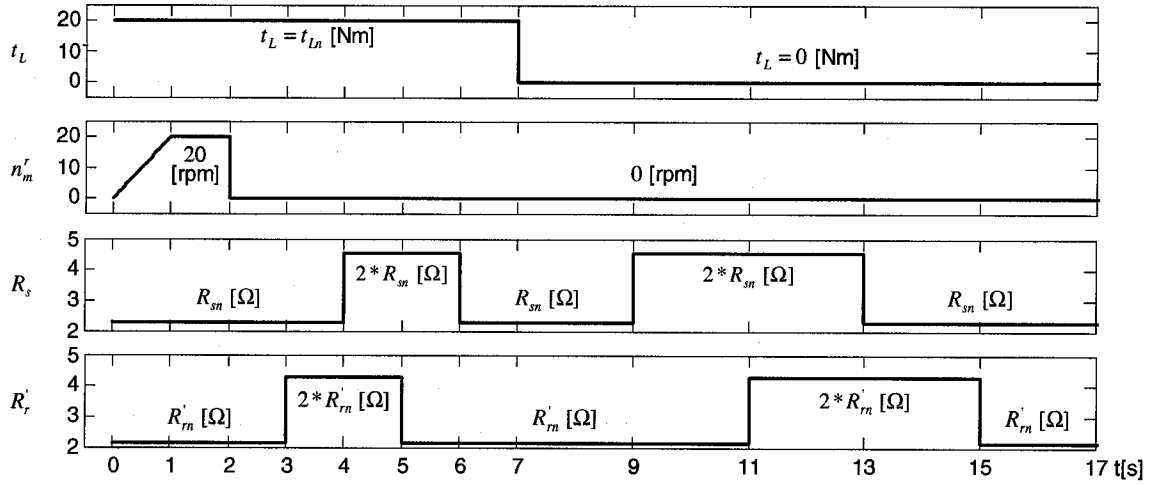
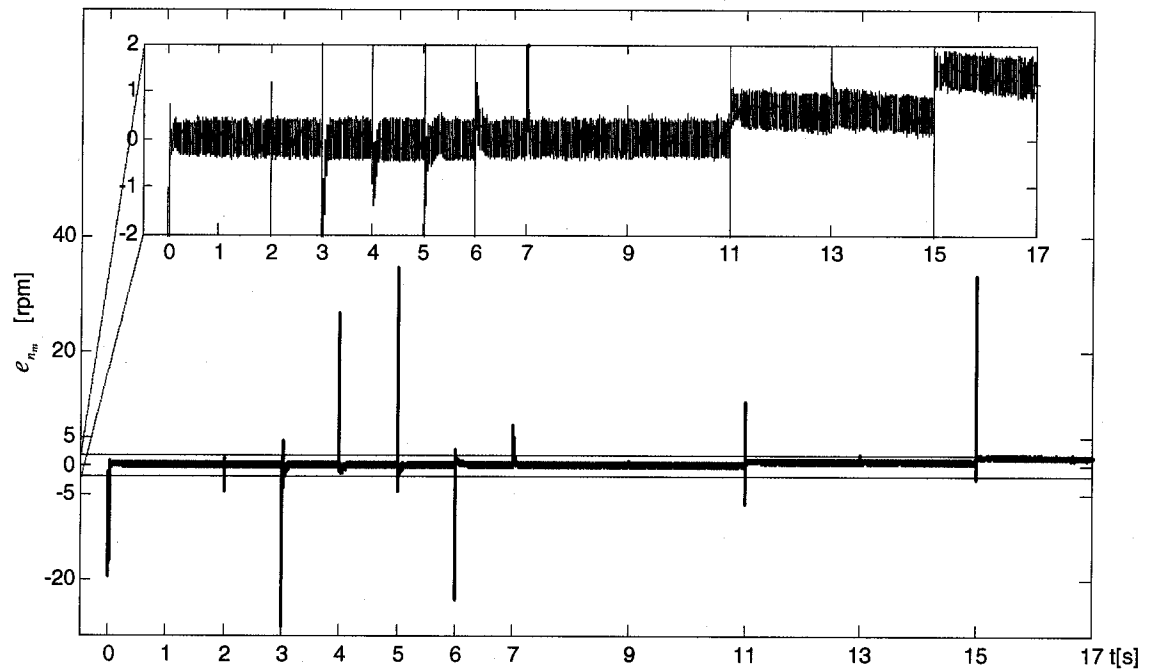
(a) Variation of the $|\hat{\psi}_r|$ (b) Variation of the field controller input, $\Delta|\bar{\psi}_r|$ (c) Variation of the estimation error of $|\hat{\psi}_r|$, $e_{|\bar{\psi}_r|} = |\bar{\psi}_r| - |\hat{\psi}_r|$

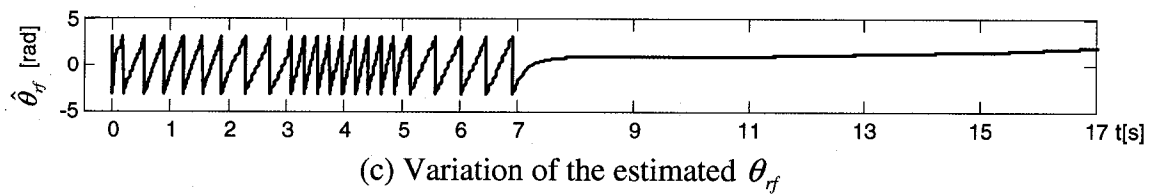
Fig. 4.8 Simulation results for the estimation of flux obtained with the Switching EKF estimator and DVC



(a) Variation of the applied load torque, t_L , the reference speed value, n_m^r , the stator resistance, R_s , and the rotor resistance, R_r' , for zero speed range



(b) Variation of the estimation error of n_m , $e_{n_m} = n_m - \hat{n}_m$



(c) Variation of the estimated θ_{rf}

Fig. 4.9 Simulation results for combined Switching EKF estimation and DVC for the zero speed range

- ◆ In spite of no *a priori* information on the estimated states and parameters, except for stator resistance initialization in the interval of 0-1 [sec], the estimation performances of the Switching EKF's are quite good, even under challenging variations of velocity reference and the load torque as well as matched and unmatched resistance variations.
- ◆ As mentioned before, the estimation and control algorithms are challenged with the unmatched variations. Even under extreme conditions, it has been demonstrated that the proposed estimation algorithm combined with sensorless DVC performs quite well as can be seen at $t = 2.01$ [sec] and $t = 4$ [sec] under the scenarios given in Fig. 4.3. On the other hand, with matching algorithms and parameter variations, better transient and steady state performances are obtained with the proposed algorithm as can be seen at $t = 14$ [sec], when $R_s : 2 * R_{sn} \rightarrow R_{sn}$, while R_s estimation is *on* and at $t = 16.01$ [sec], when $R_r : 2 * R_m \rightarrow R_m$ while R_r estimation is active.
- ◆ The new estimation technique has performed quite well also with problematic zero speed operation [37], as can be seen in the time interval of $18[\text{sec}] \leq t \leq 22[\text{sec}]$ for the scenarios given in Fig. 4.3, and in the interval of $2[\text{sec}] \leq t \leq 17[\text{sec}]$ for the scenarios given in Fig. 4.9a. Moreover, it has been observed that the source of the estimation error of the velocity, $e_{n_m} = n_m - \hat{n}_m$, in the time interval $11[\text{sec}] \leq t \leq 17[\text{sec}]$ is the step shaped extreme variations of the R_r , $R_r : R_m \rightarrow 2 * R_m$ or $R_r : 2 * R_m \rightarrow R_m$, which also affect the estimation of t_L , especially when $t_L = 0$ [Nm] and $n_m = 0$ [rpm]. However, this error also converges to zero as can be seen in Fig. 4.9b. Additionally, in the time interval of $7[\text{sec}] \leq t \leq 17[\text{sec}]$ in Fig. 4.9c, which constitutes the dc condition, it can be observed that the proposed estimation technique has performed well under the most challenging operating condition inherent to the speed-sensorless control of IMs.

- ◆ The t_L is considered constant in the EKF extended models and the algorithm is challenged with a linear t_L variation in the time interval $11[\text{sec}] \leq t \leq 13[\text{sec}]$. In spite of this mismatch, satisfactory results have been obtained with the new technique.
- ◆ The proposed scheme also facilitates the indirect evaluation of uncertainties that have the same variation as the state or parameter that is being estimated. In this study, the viscous friction ($F_v = \beta_L \omega_m$) is taken into account in the simulation model representing the system but not in the extended model; thus, the estimated t_L as a constant state is expected to include also the viscous friction value once the steady-state is reached. This fact can be demonstrated easily as follows:

In the intervals, $1[\text{sec}] \leq t \leq 7[\text{sec}]$, $13[\text{sec}] \leq t \leq 18[\text{sec}]$ and $23[\text{sec}] \leq t \leq 24[\text{sec}]$, during which both the velocity reference and load torque are given positive constant values, the error in the torque estimation is $e_{t_L} \cong -0.1571$ or $e_{t_L} = -0.0021$. In the interval $9[\text{sec}] \leq t \leq 11[\text{sec}]$, where both the velocity and torque reference are given negative values, the error is found to be $e_{t_L} = 0.1571$. Thus, considering the viscous friction coefficient, $\beta_L = 0.001$ used in the model and the interval $1[\text{sec}] \leq t \leq 2[\text{sec}]$ (high speed range), the actual angular velocity is calculated as

$$\omega_m(\infty) = \hat{\omega}_m(\infty) + e_{\omega_m(\infty)} = 2\pi(1500.5 - 0.3223)/60 = 157.0982 [\text{rad/s}] \quad (4.12)$$

In the steady-state, e_{t_L} should be equal to the friction taken into account in the model; hence,

$$\begin{aligned} e_{t_L} &= -\beta_L \omega_m(\infty) \\ -0.1571 &= -0.001 \times 157.0982 \rightarrow -0.1571 [\text{Nm}] \cong -0.1570982 [\text{Nm}]. \end{aligned} \quad (4.13)$$

which is almost equal to the e_{t_L} in Fig. 4.5(b) at $t = 2$ [sec].

Similar analysis can be conducted in the interval $16[\text{sec}] \leq t \leq 18[\text{sec}]$ (the very low speed range) during which,

$$\omega_m(\infty) = \hat{\omega}_m(\infty) + e_{\omega_m(\infty)} = 2\pi(19.8785 - 0.1875)/60 = 2.0620[\text{rad/s}] \quad (4.14)$$

$$\begin{aligned} e_{t_L} &= -\beta_L \omega_m(\infty) \\ &= -0.0021 = -0.001 \times 2.0620 \\ &= -0.0021 [\text{Nm}] \cong -0.0020620 [\text{Nm}]. \end{aligned} \quad (4.15)$$

This fact should also be taken into consideration in the evaluation of the load torque estimation. By inspecting the t_L estimation, it can be observed that linear variations and reversals of t_L give rise to some estimation error for relatively short transient durations; however, in the intervals with constant velocity reference and constant t_L , this error is much lower and almost zero, once the F_v component is subtracted from t_L .

- ◆ Simulations are performed to compare the performance of the Switching EKF algorithm with the individual EKF- \hat{R}_s (with R_s estimation only) and EKF- \hat{R}_r (with R_r estimation only) for both high and low velocity operation as can be seen in Fig. 4.10. Two switching durations are considered to this purpose: $1 \times T$ and $100 \times T$, the latter of which gives rise to a lower estimation error, $e_{n_m} = n_m - \hat{n}_m$. As the highest velocity estimation error has occurred at the rated load torque, t_{LN} , this value is considered in the simulation model for the comparative scenarios. Also, it is demonstrated that the initial performance of the switching operation is independent of

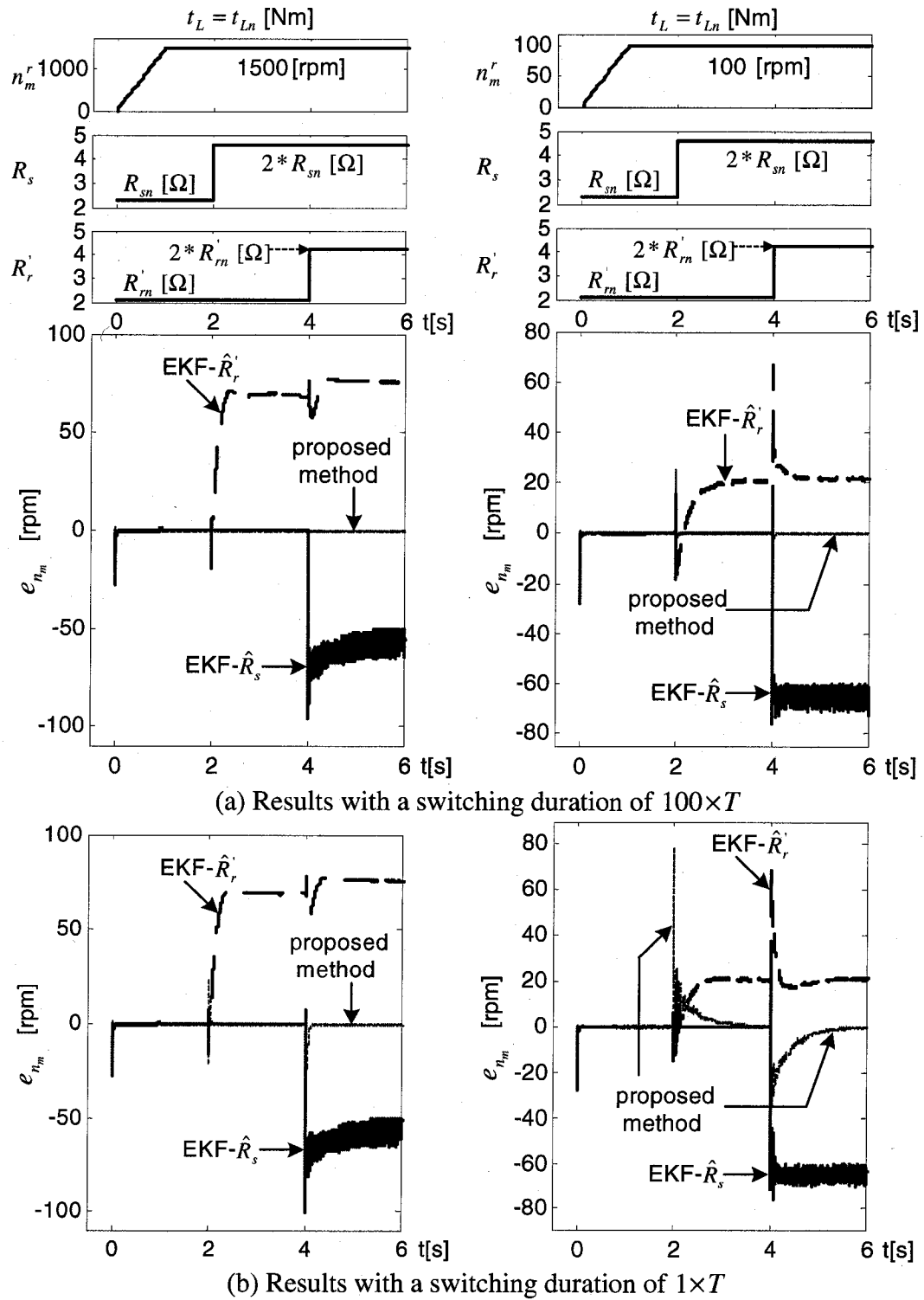


Fig. 4.10 Comparative results in the high and low velocity range with the EKF- \hat{R}_s , EKF- \hat{R}_r and proposed method

the initial value of the R_s estimation, which is taken as 0 and R_{sn} in the simulations to demonstrate this property.

Inspection of the results demonstrates the improved performance of the new algorithms in both the high and low velocity range. The performance deterioration is also obvious with individual EKF- \hat{R}_s and EKF- \hat{R}_r algorithms particularly when the speed reference approaches zero, as can be seen with calculations at 6[sec] based on the data given in Fig. 4.10a.

For $n_m^r = 1500$ [rpm],

$$e_{n_m}(\%) \text{ of EKF-}\hat{R}_r = \frac{75.6375}{1500} \times 100 = 5.0425\% \text{ [rpm]}$$

$$e_{n_m}(\%) \text{ of EKF-}\hat{R}_s = \frac{-62.4519}{1500} \times 100 = -4.1635\% \text{ [rpm]}$$

$$e_{n_m}(\%) \text{ of the proposed method} = \frac{0.2718}{1500} \times 100 = 0.0181\% \text{ [rpm]}$$

For $n_m^r = 100$ [rpm],

$$e_{n_m}(\%) \text{ of EKF-}\hat{R}_r = \frac{21.5239}{100} \times 100 = 21.5239\% \text{ [rpm]}$$

$$e_{n_m}(\%) \text{ of EKF-}\hat{R}_s = \frac{-64.0109}{100} \times 100 = -64.0109\% \text{ [rpm]}$$

$$e_{n_m}(\%) \text{ of the proposed method} = \frac{0.1178}{100} \times 100 = 0.1178\% \text{ [rpm]}$$

4.6 Conclusion

In this study, a Switching EKF algorithm is developed for the estimation of two parameters which are critical for the high performance sensorless control of IMs, namely R_s and R_r . The estimation of these two parameters is often reported as a challenge in sensorless IM control. The switching algorithm developed to this aim also estimates the uncertain load torque and velocity as well as the flux and current components. In this

study, the proposed algorithm is run in combination with the speed-sensorless direct vector control (DVC) of IMs; however, it could be used with a variety of other methods applied for the sensorless control of IMs.

Besides the proper updates of R_s and R_r which improve the flux and speed estimation, the performance of the switching algorithm also benefits from the estimation of velocity via the equation of motion, as opposed to its estimation as a constant in most past studies. This approach helps restore the lost rotor information on the stator side, hence, improving the very low and zero speed operation. This aspect of the study is an extension of the authors' previous research presented in [26] and [27].

The performance of the algorithm is tested in the very low and zero speed region and also evaluated with 17 scenarios developed by giving step-type and linear variations to the load torque and angular velocity reference. The robustness of the algorithm to stator resistance, R_s , and rotor resistance, R_r variations is tested with step-type changes imposed on R_s and R_r . As a result, the estimation of both R_s and R_r with the new algorithm has yielded a better performance in comparison to individual EKF- \hat{R}_s and EKF- \hat{R}_r algorithms, which conduct R_s or R_r estimation only.

The system performance is observed to be quite well under step-type variations and reversals in the load-torque and step and linear changes and reversals in the angular velocity. The system has also demonstrated the expected robustness to step-type variations forced on R_s and R_r , and acceptable errors are obtained even with the linear variations and reversals of the load torque. The estimation of the load torque, t_L , as a constant state in this algorithm, also accounts for mechanical uncertainties which is the viscous friction torque in this case, thereby, improving the estimation performance.

Finally, an important advantage of the proposed method over previous methods is that R_s and R_r estimations can be performed both in transient and steady state without signal injection and/or algorithm changes based on parameters or speed. Other multiple model based methods, such as [28], [29] and [30] are executable only during the steady state and cannot handle large load torque or speed variations as also stated by the authors. Moreover, when considering studies such as [31], [32] and [33], it should be noted that adjusting the value of R_r with respect to the estimated R_s means using only an approximate value of the actual R_r , which does not include the frequency based variations in R_r . Thus, the proposed Switching EKF method addresses all the above deficiencies by demonstrating a good performance under large uncertainties and load or speed variations in the transient and steady state.

References

- [1] Ortega R, Barabanov N, Escobar G, Valderrama E. Direct torque control of induction motors: stability analysis and performance improvement. *IEEE Trans on Automatic Control* 2001;46(8):1209–1222.
- [2] Denai MA, Attia SA. Intelligent control of an induction Motor. *Electric Power Components & Systems* (Taylor&Francis) 2002;30(4): 409–427.
- [3] Buja GS, Kazmierkowski MP. Direct torque control of PWM inverter-fed AC motors -a survey. *IEEE Trans on Industrial Electronics* 2004;51(4):744–757.
- [4] Takahashi I, Noguchi T. A new quick-response and high-efficiency control strategy of an induction motor. *IEEE Trans on Industry Applications* 1986;22(5):820–827.
- [5] Novotnak RT, Chiasson J, Bodson M. High-performance motion control of an induction motor with magnetic saturation. *IEEE Trans on Control Systems Technology* 1999;7(3):315–327.
- [6] Sabanovic A and Izosimov DB. Application of sliding modes to induction motor control. *IEEE Trans on Industry Applications* 1981;IA-17(1):41–49.

- [7] Wang W-J, Chen J-Y. Passivity-Based Sliding Mode Position Control for Induction Motor Drives IEEE Trans on Energy Conversion 2005;20(2):316–321.
- [8] Holtz J, Quan J. Drift- and parameter-compensated flux estimator for persistent zero-stator-frequency operation of sensorless-controlled induction motors. IEEE Trans on Industry Applications 2003;39(4):1052–1060.
- [9] Lascu C, Boldea I, Blaabjerg F. Direct torque control of sensorless induction motor drives: a sliding-mode approach. IEEE Trans on Industry Applications 2004;40(2):582–590.
- [10] Guidi G, Umida H. A novel stator resistance estimation method for speed-sensorless I drives. IEEE Trans on Industry Applications 2000;36(6):1619–1627.
- [11] Du T, Brdys MA. Shaft speed, load torque and rotor flux estimation of induction motor drive using an extended Luenberger observer. In: Proceedings of IEEE-IEMDC'93 Annual Meeting 1993;376:179–184.
- [12] Faiz J, Sharifian MBB. Different techniques for real time estimation of an induction motor rotor resistance in sensorless direct torque control for electric vehicle. IEEE Trans on Energy Conversion 2001;16(1):104–109.
- [13] Lin F-J. Robust speed-controlled induction motor drive using EKF and RLS estimators. IEE Proceedings—Electric Power Applications 1996;143(3):186–192.
- [14] Wade S, Dunnigan MW, Williams BW. Modeling and simulation of induction machine vector control with rotor resistance identification. IEEE Trans on Power Electronics 1997;12(3):495–506.
- [15] Finch JW, Atkinson D J, Acarnley P P. Full-order estimator for induction motor states and parameters. IEE Proceedings—Electric Power Applications 1998;145(3):169–179.
- [16] Wade S, Dunnigan MW, Williams BW. Comparison of stochastic and deterministic parameter identification algorithms for indirect vector control. IEE Colloquium on Vector Control and Direct Torque Control of Induction Motors 1995;2:1–5.

- [17] Salvatore L, Stasi S, Tarchioni L. A New EKF-based algorithm for flux estimation in induction machines. *IEEE Trans on Industrial Electronics* 1993;40(5):496–504.
- [18] Bogosyan O S, Gokasan M, Hajiyeve C. An application of EKF for the position control of a single link arm. In: *Proceedings of IEEE-IECON'01 Annual Meeting* 2001;1:564–569.
- [19] Barut M, Bogosyan O S, Gokasan M. EKF based estimation for direct vector control of induction motors. In: *Proceedings of IEEE-IECON'02 Annual Meeting* 2002; 2:1710–1715.
- [20] Kim Y-R, Sul S-K, Park M-H. Speed sensorless vector control of induction motor using extended Kalman filter. *IEEE Trans on Industry Applications* 1994;30(5):1225–1233.
- [21] Shi KL, Chan TF, Wong YK, Ho SL. Speed estimation of an induction motor drive using an optimized extended Kalman filter. *IEEE Trans on Industrial Electronics* 2002;49(1):124–133.
- [22] Lee C-M, Chen C-L. Observer-based speed estimation method for sensorless vector control of induction motors. *IEE Proceedings—Control Theory and Applications* 1998;145(3):359–363.
- [23] Wenqiang Y, Zhengchun J, Qiang X. A new algorithm for flux and speed estimation in induction machine. In: *Proceedings of IEEE-ICEMS 2001 Annual Meeting* 2001;2:698–701.
- [24] Qiongxuan G, Zhiyue F. Speed estimated for vector control of induction motor using reduced-order extended Kalman filter. In: *Proceedings of IEEE-PIEMC 2000 Annual Meeting* 2000;1:138–142.
- [25] El Moucary Ch, Garcia Soto G, Mendes E. Robust rotor flux, rotor resistance and speed estimation of an induction machine using the extended Kalman filter. In: *Proceedings of IEEE ISIE'99 Annual Meeting* 1999;2:742–746.

- [26] Barut M, Bogosyan, OS, Gokasan M. Speed sensorless direct torque control of IMs with rotor resistance estimation. *Energy Conversion and Management* (Elsevier) 2005;46(3):335-349.
- [27] Barut M, Bogosyan OS, Gokasan M. An EKF based estimator for speed sensorless vector control of induction motors. *Electric Power Components & Systems* (Taylor&Francis) 2005;33(7):727-744.
- [28] Ha I-J, Lee S-H. An online identification method for both stator-and rotor resistances of induction motors without rotational transducers. *IEEE Trans on Industrial Electronics* 2000;47(4):842-853.
- [29] Tajima H, Guidi G, Umida H. Consideration about problems and solutions of speed estimation method and parameter tuning for speed-sensorless vector control of induction motor drives. *IEEE Trans on Industry Applications* 2002;38(5):1282-1289.
- [30] Zhen L, Xu L. Sensorless field orientation control of induction machines based on a mutual MRAS scheme. *IEEE Trans on Industrial Electronics* 1998;45(5):824-831.
- [31] Cirrincione, M.; Pucci, M.; Cirrincione, G.; Capolino, G.-A. An adaptive speed observer based on a new total least-squares neuron for induction machine drives. *IEEE Transactions on Industry Applications* 2006;42(1):89-104.
- [32] Lascu, C.; Boldea, I.; Blaabjerg, F. Very-low-speed variable-structure control of sensorless induction machine drives without signal injection. *IEEE Transactions on Industry Applications* 2005;41(2):591-598.
- [33] Ohyama, K.; Asher, G.M.; Sumner, M. Comparative analysis of experimental performance and stability of sensorless induction motor drives. *IEEE Transactions on Industrial Electronics* 2005;53(1):178-186.
- [34] Chen F, Dunnigan MG. Comparative study of a sliding-mode observer and Kalman filters for full state estimation in an induction machine. *IEE Proceedings-Electric Power Applications* 2002;149(1):53-64.

- [35] Goodwin GC, Sin KS. Adaptive filtering prediction and control, New Jersey: Prentice-Hall Inc; 1984.
- [36] Vas P. Sensorless Vector and direct torque control, New York: Oxford University press, 1998.
- [37] Holtz J. Sensorless control of induction motors-performance and limitations. In: Proc IEEE ISIE 2000 Annual Meeting 2000;1:PL12–PL20.

Chapter 5:

Experimental Evaluation of Braided EKF for Sensorless Control of Induction Motors^{*}

Abstract— Temperature and frequency dependent variations of the rotor (R_r') and stator (R_s) resistances pose a challenge in the accurate estimation of flux and velocity in the sensorless control of induction motors (IMs) over a wide speed range. Solutions have been sought to the problem by signal injection and/or by the use of different algorithms for the different parameters and states of the same motor. In this study, a novel Extended Kalman Filter (EKF) based estimation technique is developed for the solution of the problem based on the consecutive operation of two EKF algorithms at every time step. The proposed “braided” EKF technique is experimentally tested under challenging parameter and load variations in a wide speed range, including low speed. The results demonstrate a significantly increased accuracy in the estimation of R_s and R_r' , as well as load torque, flux, and velocity in transient and steady state, when compared with single EKFs or other approaches taken to estimate these parameters and states in the sensorless control of IMs. The improved results also motivate the utilization of the new estimation approach in combination with a variety of control methods which depend on accurate knowledge of a high number of parameters and states.

Index Terms— *Induction motor, Extended Kalman Filter, speed-sensorless control, rotor resistance and stator resistance estimation, load torque estimation.*

5.1 Introduction

Induction motor (IM) parameters vary significantly with operating conditions. Besides the load torque that can vary from no load to full load, stator (R_s) and rotor (R_r')

^{*} Barut, M., Bogosyan, S. and Gokasan, M. (2006d), “Experimental Evaluation of Braided EKF for Sensorless Control of Induction Motors”, *IEEE Transactions on Industrial Electronics*. (In press)

resistances change with temperature and frequency, while inductances tend to saturate at high current levels. The effects of parameter and model uncertainties become even more relevant with speed-sensorless control, calling for sophisticated methods for the estimation of flux and velocity. The benefits of sensorless control are the increased reliability of the overall system with the removal of mechanical sensors, thereby reducing sensor noise and drift effects as well as cost and size. However, to exploit the benefits of sensorless control, the developed estimation methods must achieve robustness against parameter and model uncertainties over a wide speed range. Parameters of particular concern in the sensorless control literature are the frequency dependent, R_r' , temperature dependent, R_s and the load torque, all of which are very effective on the accurate estimation of flux and velocity.

To address the parameter sensitivity problem in IM sensorless control, a variety of approaches have been proposed and problems have been reported. Studies based on sliding mode observers with [1] estimating the R_r' and [2] estimating the R_s , studies on speed adaptive flux observers as in [3], in which R_s is also estimated, and [4], [5] and [6], which adjust the value of R_r' in proportion to the estimated R_s have been reported in the literature.

There are also Extended Kalman Filter (EKF) applications in the literature for the sensorless control of IMs. Model uncertainties and nonlinearities inherent in IMs are well suited to the stochastic nature of EKFs [7]. With this method, it is possible to make the online estimation of states while performing the simultaneous identification of parameters in a relatively short time interval [8–10], by also taking system and process and measurement noises directly into account. This is the reason why the EKF has found wide application in sensorless control of IMs, in spite of its computational complexity. Among recent sensorless studies using EKF estimation for IMs, [11], [12] and [13] estimate the flux and velocity, while [14] uses an adaptive flux observer in combination

with a second order Kalman filter for the same purpose. None of these studies estimate the load torque and motor resistances, resulting in a performance that is sensitive to the variation of these parameters. In [11], [12], [13], and [15–17] which present reduced-order estimators, the velocity is estimated as a constant parameter, which gives rise to a significant estimation error in the velocity during the transient state, especially under instantaneous load variations, although the performance is improved in the steady state. While [15] and [16] are sensitive to rotor resistance variations, [17] also estimates the rotor resistance. However, the estimation of rotor resistance is performed by the injection of low amplitude, high frequency signals to the flux reference in the direct vector control, (DVC) of IMs. This has caused fluctuations in the motor flux, torque and speed. Finally, recent studies of the authors [18, 19] estimating the velocity via the consideration of the equation of motion in the EKF model, in addition to the estimation of rotor resistance and mechanical uncertainties demonstrate improved results over a wide speed range. However, the results are sensitive to the variations of stator resistance, indicating the necessity of an approach to estimate rotor resistance and stator resistance simultaneously, as well as the load torque.

Studies achieving the simultaneous estimation of R_s and R_r in the sensorless control of IMs are only a few; in fact, [20] states that simultaneous estimation of R_s and R_r give rise to instability in the speed-sensorless case. As a solution, [21] presents a model reference adaptive system based on 3 models, of which one is used for the estimation of the rotor time constant via high frequency signal injection and the other 2 models are used interchangeably by enabling the stator resistance estimation only during short intervals, during which the rotor speed has reached the steady state. In studies such as [22] and [23], the speed and rotor flux are estimated as well as the stator resistance and rotor resistance by injecting high frequency signals into the flux and magnetizing current commands. However, in [22], the algorithm identifying the resistances, which is used in a feedback linearization controller is applicable only when the sensorless speed control system is in steady state, and not when the load torque is varying largely or when the

speed command is being changed, as also stated by the authors. On the other hand in [23], it is stated that the proposed drive can compete with a speed sensor equipped drive only if accuracy in steady-state is not essential and operation under high loads is not a requirement. Recently, [24] presented a sensorless control scheme using an open-loop estimator to calculate R_r' and a model reference adaptation for R_s . However, the performance of the parameter estimation is not demonstrated and only evaluated indirectly via the estimated velocity and flux. The above listed studies, to the authors' best knowledge, are among the most significant reported IM sensorless control studies estimating R_s and R_r' simultaneously as the two most effective parameters on estimation and control performance. However, the results require either signal injection or design of different algorithms based on the velocity range or based on the parameters and states to be estimated, R_s or R_r' .

The major contribution of this study is the development of an EKF based novel observer approach, which achieves the simultaneous estimation of R_s and R_r' and hence, the accurate estimation of flux, torque and velocity for the speed-sensorless control of induction motors without the need for signal injection or algorithm changes as in most previous studies. The observer involves the consecutive use of two EKF algorithms at every time step by what could be called a "braided" technique. The two EKF algorithms have exactly the same configuration and are derived based on the same extended model except for one state; therefore, R_s in one is replaced by R_r' in the other. Persistency of excitation required for parameter convergence in the steady state and provided by signal injection in most previous methods, is thus fulfilled by the system noise (or modeling error), which is inherently taken into account in all EKFs. The Braided EKF technique exploits this characteristic as well as the fast convergence property of EKFs. The proposed approach also offers a solution against the well known decreased estimation accuracy problem faced when a high number of states and parameters are to be estimated with a single EKF. The fast convergence rate and high estimation accuracy demonstrated

in the experimental results indicate that the proposed technique can address the challenge of R_s and R_r estimation in the sensorless control of IMs and improve estimation of flux and velocity over a wide speed range.

The study is organized as follows. After a discussion of previous literature on sensorless estimation and control in Section I, Section II proceeds with the derivation of the extended models for the new EKF algorithm. Next, the development of the multiple-model Braided EKF is introduced in Section III, which is followed by experimental results presented for various scenarios in Section IV. Finally, conclusions and future directions are discussed in Section V.

5.2 Extended Mathematical Models for Braided EKF

Sensorless schemes developed for IMs require the estimation of rotor flux components, $\psi_{r\alpha}$, $\psi_{r\beta}$, angular velocity, ω_m and stator current components $i_{s\alpha}$ and $i_{s\beta}$, which are also measured as output. However, as mentioned in Section I, the accurate estimation of these states is very much dependent on how well the system parameters are known, particularly the rotor (R_r) and stator (R_s) resistances over a wide speed range. To this purpose, in this study, two extended models are developed: one which is developed for the estimation of the rotor resistance, R_r and the other, for the stator resistance, R_s , with an additional set of estimated states which are the same in both models. The extended models to be used in the development of the two EKF algorithms can be given (as referred to the stator stationary frame) in the following general form:

$$\begin{aligned}\dot{\underline{x}}_{ei}(t) &= \underline{f}_{ei}(\underline{x}_{ei}(t), \underline{u}_e(t)) + \underline{w}_{i1}(t) \\ &= \underline{A}_{ei}(\underline{x}_{ei}(t))\underline{x}_{ei}(t) + \underline{B}_e \underline{u}_e(t) + \underline{w}_{i1}(t)\end{aligned}\quad (5.1)$$

$$\begin{aligned}\underline{Z}(t) &= \underline{h}_{ei}(\underline{x}_{ei}(t)) + \underline{w}_{i2}(t) \text{ (measurement equation)} \\ &= \underline{H}_e \underline{x}_{ei}(t) + \underline{w}_{i2}(t)\end{aligned}\quad (5.2)$$

Where, $i=1,2$, extended state vector \underline{x}_{ei} represents the estimated states. \underline{f}_{ei} is the nonlinear function of the states and inputs. \underline{A}_{ei} is the system matrix; \underline{u}_e is the control input vector. \underline{B}_e is the input matrix. \underline{w}_{i1} is the process noise. \underline{h}_{ei} is the function of the outputs. \underline{H}_e is the measurement matrix. \underline{w}_{i2} is the measurement noise.

Based on the general form in (5.1) and (5.2), the detailed matrix representation of the two IM models can be given as below:

Model 1: Extended model of IM derived for the estimation of R_s , (Model- R_s):

$$\begin{bmatrix} \dot{i}_{s\alpha} \\ \dot{i}_{s\beta} \\ \dot{\psi}_{r\alpha} \\ \dot{\psi}_{r\beta} \\ \dot{\omega}_m \\ \dot{i}_L \\ \dot{R}_s \end{bmatrix} = \underbrace{\begin{bmatrix} -\left(\frac{R_s + \frac{L_m^2 \dot{R}_r}{L_\sigma L_r^2}}\right) & 0 & \frac{L_m \dot{R}_r}{L_\sigma L_r^2} & \frac{L_m}{L_\sigma L_r} p_p \omega_m & 0 & 0 & 0 \\ 0 & -\left(\frac{R_s + \frac{L_m^2 \dot{R}_r}{L_\sigma L_r^2}}\right) & -\frac{L_m}{L_\sigma L_r} p_p \omega_m & \frac{L_m \dot{R}_r}{L_\sigma L_r^2} & 0 & 0 & 0 \\ L_m \frac{\dot{R}_r}{L_r} & 0 & \frac{\dot{R}_r}{L_r} & -p_p \omega_m & 0 & 0 & 0 \\ 0 & L_m \frac{\dot{R}_r}{L_r} & p_p \omega_m & \frac{\dot{R}_r}{L_r} & 0 & 0 & 0 \\ \frac{3 p_p L_m}{2 J_L L_r} \psi_{r\beta} & \frac{3 p_p L_m}{2 J_L L_r} \psi_{r\alpha} & 0 & 0 & 0 & \frac{1}{J_L} & 0 \\ 0 & 0 & 0 & 0 & 0 & 0 & 0 \\ 0 & 0 & 0 & 0 & 0 & 0 & 0 \end{bmatrix}}_{\underline{A}_{e1}} \begin{bmatrix} i_{s\alpha} \\ i_{s\beta} \\ \psi_{r\alpha} \\ \psi_{r\beta} \\ \omega_m \\ t_L \\ R_s \end{bmatrix} + \underbrace{\begin{bmatrix} \frac{1}{L_\sigma} & 0 \\ 0 & \frac{1}{L_\sigma} \\ 0 & 0 \\ 0 & 0 \\ 0 & 0 \\ 0 & 0 \\ 0 & 0 \end{bmatrix}}_{\underline{B}_e} \begin{bmatrix} v_{s\alpha} \\ v_{s\beta} \end{bmatrix} + \underline{w}_{11}(t) \quad (5.3)$$

$$\underbrace{\begin{bmatrix} i_{s\alpha} \\ i_{s\beta} \end{bmatrix}}_{\underline{z}} = \underbrace{\begin{bmatrix} 1 & 0 & 0 & 0 & 0 & 0 & 0 \\ 0 & 1 & 0 & 0 & 0 & 0 & 0 \end{bmatrix}}_{\underline{H}_e} \begin{bmatrix} i_{s\alpha} \\ i_{s\beta} \\ \psi_{r\alpha} \\ \psi_{r\beta} \\ \omega_m \\ t_L \\ R_s \end{bmatrix} + \underline{w}_{12}(t) \quad (5.4)$$

Model 2: Extended model of IM derived for the estimation of R_r' , (Model- R_r'):

$$\underbrace{\begin{bmatrix} \dot{i}_{s\alpha} \\ \dot{i}_{s\beta} \\ \dot{\psi}_{r\alpha} \\ \dot{\psi}_{r\beta} \\ \dot{\omega}_m \\ \dot{i}_L \\ \dot{R}_r' \end{bmatrix}}_{\underline{\dot{x}}_{e2}} = \underbrace{\begin{bmatrix} -\left(\frac{R_s}{L_\sigma} + \frac{L_m^2 R_r'}{L_\sigma L_r'^2}\right) & 0 & \frac{L_m R_r'}{L_\sigma L_r'} & \frac{L_m}{L_\sigma L_r'} p_p \omega_m & 0 & 0 & 0 \\ 0 & -\left(\frac{R_s}{L_\sigma} + \frac{L_m^2 R_r'}{L_\sigma L_r'^2}\right) & -\frac{L_m}{L_\sigma L_r'} p_p \omega_m & \frac{L_m R_r'}{L_\sigma L_r'^2} & 0 & 0 & 0 \\ L_m \frac{R_r'}{L_r'} & 0 & \frac{R_r'}{L_r'} & -p_p \omega_m & 0 & 0 & 0 \\ 0 & L_m \frac{R_r'}{L_r'} & p_p \omega_m & -\frac{R_r'}{L_r'} & 0 & 0 & 0 \\ \frac{3 p_p L_m}{2 J_L L_r'} \psi_{r\beta} & \frac{3 p_p L_m}{2 J_L L_r'} \psi_{r\alpha} & 0 & 0 & 0 & \frac{1}{J_L} & 0 \\ 0 & 0 & 0 & 0 & 0 & 0 & 0 \\ 0 & 0 & 0 & 0 & 0 & 0 & 0 \end{bmatrix}}_{\underline{A}_2} \underbrace{\begin{bmatrix} i_{s\alpha} \\ i_{s\beta} \\ \psi_{r\alpha} \\ \psi_{r\beta} \\ \omega_m \\ t_L \\ R_r' \end{bmatrix}}_{\underline{x}_{e2}} + \underbrace{\begin{bmatrix} \frac{1}{L_\sigma} & 0 \\ 0 & \frac{1}{L_\sigma} \\ 0 & 0 \\ 0 & 0 \\ 0 & 0 \\ 0 & 0 \\ 0 & 0 \end{bmatrix}}_{\underline{B}_e} \underbrace{\begin{bmatrix} v_{s\alpha} \\ v_{s\beta} \end{bmatrix}}_{\underline{u}_e} + \underline{w}_{21}(t) \quad (5.5)$$

$$\underbrace{\begin{bmatrix} i_{s\alpha} \\ i_{s\beta} \end{bmatrix}}_{\underline{z}} = \underbrace{\begin{bmatrix} 1 & 0 & 0 & 0 & 0 & 0 & 0 \\ 0 & 1 & 0 & 0 & 0 & 0 & 0 \end{bmatrix}}_{\underline{H}_e} \underbrace{\begin{bmatrix} i_{s\alpha} \\ i_{s\beta} \\ \psi_{r\alpha} \\ \psi_{r\beta} \\ \omega_m \\ t_L \\ R_r' \end{bmatrix}}_{\underline{x}_{e2}} + \underline{w}_{22}(t) \quad (5.6)$$

Where, p_p is the number of pole pairs. $L_\sigma = \sigma L_s$ is the stator transient inductance; $\sigma = 1 - \frac{L_m^2}{L_s L_r}$ is the leakage or coupling factor. L_s and R_s are the stator inductance and resistance, respectively. L_r' and R_r' are the rotor inductance and resistance, referred to the stator side, respectively. $v_{s\alpha}$ and $v_{s\beta}$ are the stator stationary axis components of stator voltages. $i_{s\alpha}$ and $i_{s\beta}$ are the stator stationary axis components of stator currents. $\psi_{r\alpha}$ and $\psi_{r\beta}$ are the stator stationary axis components of rotor flux. J_L is the total inertia of the IM and load. ω_m is the angular velocity. As can be seen from (5.3)-(5.4) and (5.5)-(5.6), the only differences between the two extended vectors, \underline{x}_{e1} and \underline{x}_{e2} , are

the constant states R_s and R_r , respectively. $i_{s\alpha}$ and $i_{s\beta}$ are the measured variables in both algorithms. The load torque and stator or rotor resistances are assumed to have a slow variation with time and therefore, are taken into consideration as constant parameters.

5.3 Development of the Braided EKF Algorithm

In this section, the two EKF algorithms used in the Braided EKF technique will be derived using the extended model in (5.3-5.4) and (5.5-5.6). For nonlinear problems such as the one in consideration, the Kalman Filter (KF) method is not strictly applicable, since linearity plays an important role in its derivation and performance as an optimal filter. The EKF technique attempts to overcome this difficulty by using a linearized approximation where the linearization is performed about the current state estimate. This process requires the discretization of (5.3) and (5.4) –or (5.5) and (5.6) as below;

$$\underline{x}_{ei}(k+1) = \underline{f}_{ei}(\underline{x}_{ei}(k), \underline{u}_e(k)) + \underline{w}_{i1}(k) \quad (5.7)$$

$$\underline{Z}(k) = \underline{H}_e \underline{x}_{ei}(k) + \underline{w}_{i2}(k) \quad (5.8)$$

For the linearization of (5.7-5.8), the current estimated states, $\hat{\underline{x}}_{ei}(k)$ and inputs $\hat{\underline{u}}_e(k)$ are used as below;

$$\underline{F}_{ei}(k) = \left. \frac{\partial \underline{f}_{ei}(\underline{x}_{ei}(k), \underline{u}_e(k))}{\partial \underline{x}_{ei}(k)} \right|_{\hat{\underline{x}}_{ei}(k), \hat{\underline{u}}_e(k)} \quad (5.9)$$

$$\underline{F}_{ui}(k) = \left. \frac{\partial \underline{f}_{ei}(\underline{x}_{ei}(k), \underline{u}_e(k))}{\partial \underline{u}_e(k)} \right|_{\hat{\underline{x}}_{ei}(k), \hat{\underline{u}}_e(k)} \quad (5.10)$$

Thus, the EKF algorithm can be given in the following recursive relations:

$$\underline{N}_i(k) = \underline{F}_{ei}(k) \underline{P}_i(k) \underline{F}_{ei}^T(k) + \underline{F}_{ui}(k) \underline{D}_u \underline{F}_{ui}^T(k) + \underline{Q}_i \quad (5.11a)$$

$$\underline{P}_i(k+1) = \underline{N}_i(k) - \underline{N}_i(k) \underline{H}_e^T (\underline{D}_\xi + \underline{H}_e \underline{N}_i(k) \underline{H}_e^T)^{-1} \underline{H}_e \underline{N}_i(k) \quad (5.11b)$$

$$\hat{\underline{x}}_{ei}(k+1) = \hat{\underline{f}}_{ei}(\underline{x}_{ei}(k), \hat{\underline{u}}_e(k)) + \underline{P}_i(k+1) \underline{H}_e^T \underline{D}_\xi^{-1} (\underline{Z}(k) - \underline{H}_e \hat{\underline{x}}_{ei}(k)) \quad (5.11c)$$

Here, \underline{Q}_i is the covariance matrix of the system noise, namely model error. \underline{D}_ξ is the covariance matrix of the output noise, namely measurement noise. \underline{D}_u is the covariance matrix of the control input noise ($v_{s\alpha}$ and $v_{s\beta}$), namely input noise. \underline{P}_i and \underline{N}_i are the covariance matrix of state estimation error and extrapolation error, respectively.

The algorithm involves two main stages: prediction and filtering. In the prediction stage, the next predicted states $\hat{\underline{f}}_{ei}(\cdot)$ and predicted state error covariance matrices, $\underline{P}_i(\cdot)$ and $\underline{N}_i(\cdot)$ are processed, while in the filtering stage, the next estimated states, $\hat{\underline{x}}_{ei}(k+1)$, obtained as the sum of the next predicted states and the correction term (2nd term in (5.11c)) are calculated.

The flowchart of the Braided EKF algorithm is given in Fig. 5.1, demonstrating the consecutive use of the two EKF algorithms. While one algorithm estimates R_s and the other, R_r , both algorithms also estimate load torque, velocity, flux and current components as the common states. After the initialization of the states, the algorithms are run by switching them on and off consecutively and at each time step. The final values of $\underline{P}_i(k+1)$ and $\hat{\underline{x}}_{ei}(k+1)$ calculated for one EKF algorithm at the end of each switching period are passed over to the next EKF algorithm as the initial values of the covariances and states. The resistance, R_s or R_r , estimated during the previous period is also passed on to the next EKF algorithm and is assumed to be constant in the new EKF model throughout the whole switching period.

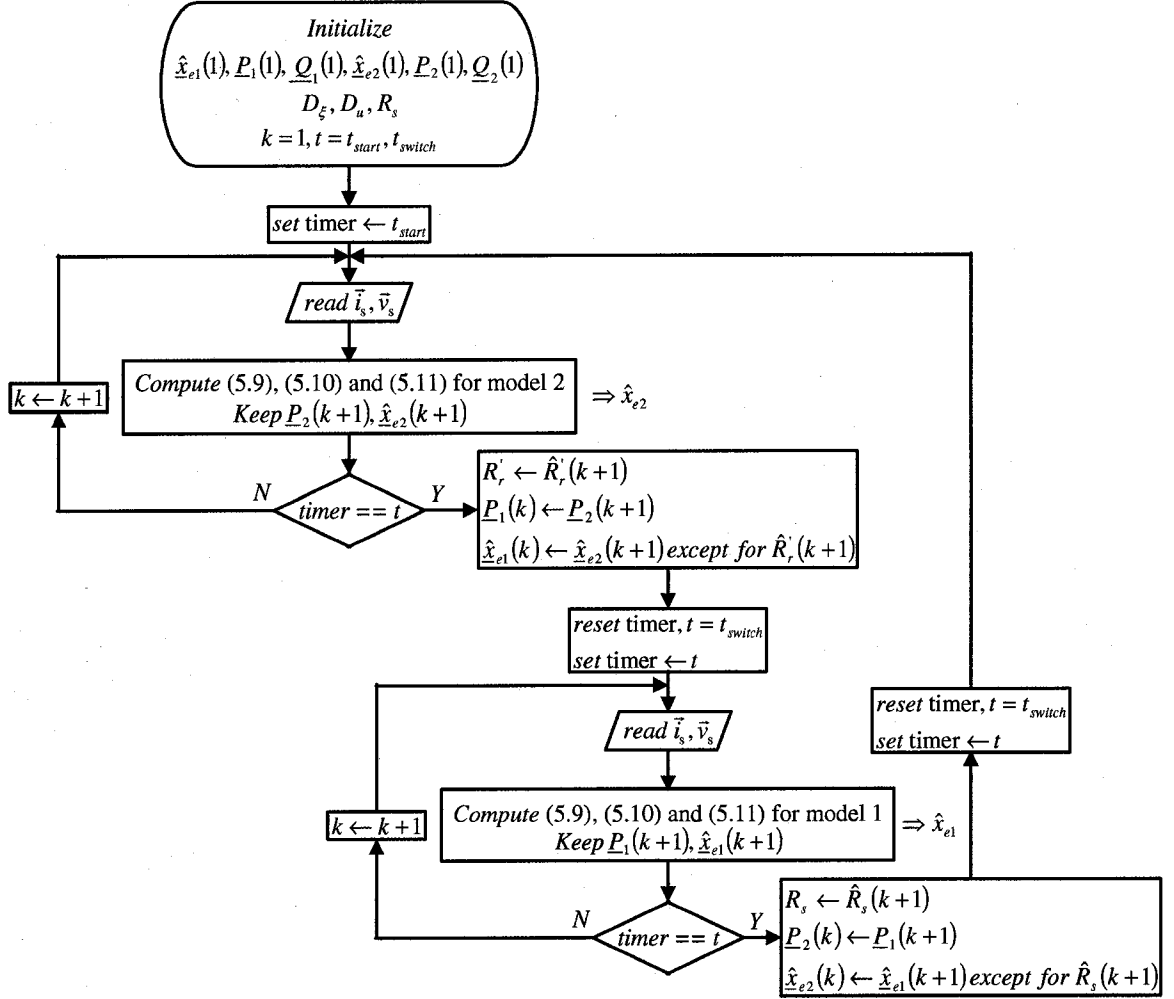


Fig.5.1 Flow-chart of the Braided EKF algorithm.

5.4 Experimental Results and Observations

In this section, the performance of the Braided EKF will be evaluated against the single EKF algorithms designed for R_r estimation ($EKF - R_r$) and R_s estimation ($EKF - R_s$).

The experimental setup used for the sensorless estimation tests is presented in Fig. 5.2. The induction motor under consideration is 3 phase, 8 pole, 3 [HP]/2.238 [kW], with its specification details given in Table 5.1a. The EKF algorithm and all analog signals are developed and processed on a Power PC based DS1104 Controller Board, offering a 4-channel, 16-bit (multiplexed) ADC and four 12-bit ADC units. The controller board

processes floating-point operations at a rate of 250 [MHz]. A torque transducer rated at 50 [N.m] and an encoder with 3600 [counts/rev], are also used for the verification of the load torque and velocity estimation and hence, for the performance evaluation of the Braided EKF. The phase voltages and currents are measured with high band voltage and current sensors from LEM Inc.

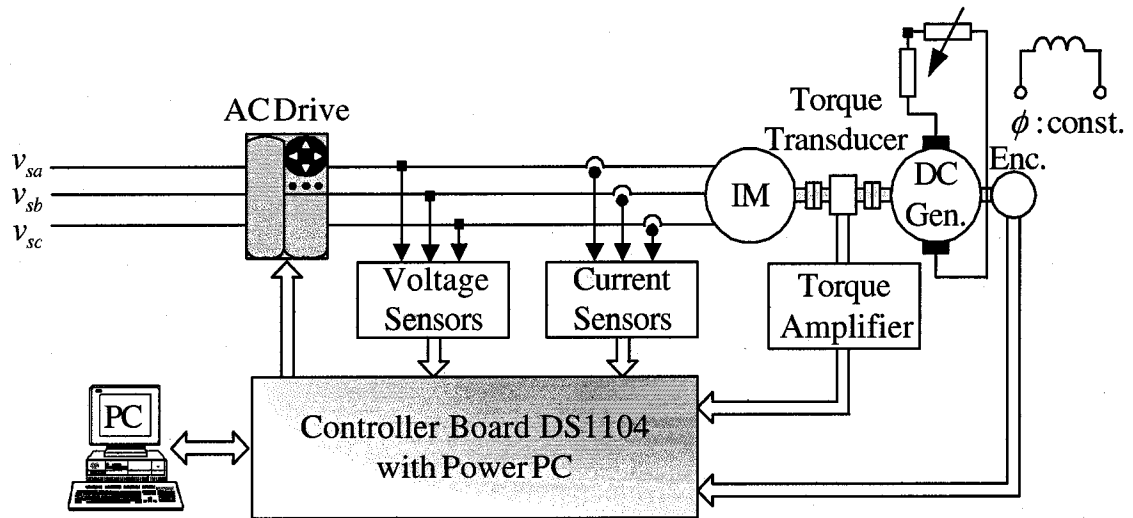


Fig. 5.2 Schematic representation of the experimental setup.

Table 5.1a Rated values and parameters of the induction motor used in the experiments.

P [kW]	f [Hz]	$* J_L$ [kg.m ²]	p_p	V [V]	I [A]
2.238	60	0.2595	4	230	12

R_s [Ω]	R_r [Ω]	L_s [H]	L_r [H]	L_m [H]	N_m [rpm]	t_L [Nm]
0.6619	0.7322	0.0375	0.0376	0.0334	850	25.1

* J_L is the total inertia in the experimental test-bed.

The load is generated through a DC machine operating in generator mode coupled to the IM. An array resistor connected to the armature terminals of the dc machine is used to

vary the load torque applied to the IM based on the relationship as $t_L = k_t^2 \omega / R$, where k_t is the torque constant of the dc machine; ω is angular velocity and R is the total resistance (switched array + armature). The value of the resistance is adjusted to 7.8 [Ω] to generate a load torque, t_L , of 20.73 [N.m], at approximately 819 [rpm]. The parameters for the DC generator used in experiments is listed in Table 5.1b.

Table 5.1b Rated values and parameters of the DC machine used in the experiments.

P [kW]	V [V]	I [A]	N_m [rpm]	t_L [Nm]
3	125	24	1150	24.91

The initial values of the \underline{P}_i and \underline{Q}_i in the EKF algorithms are found by trial-and-error to achieve a rapid initial convergence as well as the desired transient and steady state performance for the estimated states and parameters; while the $\underline{D}_\varepsilon$ and \underline{D}_u , on the other hand, are determined taking into account the measurement errors of the current and voltage sensors and the quantization errors of the ADCs, respectively.

For Model-1 ($EKF - R_s$),

$$\underline{Q}_1 = \text{diag} \left\{ 10^{-8} [A^2] \quad 10^{-8} [A^2] \quad 4 \times 10^{-17} [(V.s)^2] \quad 4 \times 10^{-17} [(V.s)^2] \quad 10^{-14} [(rad/s)^2] \right. \\ \left. 10^{-15} [(Nm)^2] \quad 10^{-16} [\Omega^2] \right\}$$

$$\underline{P}_1 = \text{diag} \left\{ 1 [A^2] \quad 1 [A^2] \quad 1 [(V.s)^2] \quad 1 [(V.s)^2] \quad 1 [(rad/s)^2] \quad 1 [(Nm)^2] \quad 1 [\Omega^2] \right\}$$

For Model-2 ($EKF - R_r$):

$$\underline{Q}_2 = \text{diag} \left\{ 1.5 \times 10^{-11} [A^2] \quad 1.5 \times 10^{-11} [A^2] \quad 0 [(V.s)^2] \quad 0 [(V.s)^2] \quad 10^{-14} [(rad/s)^2] \right. \\ \left. 7 \times 10^{-15} [(Nm)^2] \quad 10^{-16} [\Omega^2] \right\}$$

$$\underline{P}_2 = \text{diag} \left\{ 1 [A^2] \quad 1 [A^2] \quad 1 [(V.s)^2] \quad 1 [(V.s)^2] \quad 1 [(rad/s)^2] \quad 1 [(Nm)^2] \quad 1 [\Omega^2] \right\}$$

For both models,

$$\underline{D}_i = \text{diag}\{2.6 \times 10^{-4} [A^2] \quad 2.6 \times 10^{-4} [A^2]\}, \quad \underline{D}_u = \text{diag}\{2.3 \times 10^{-5} [V^2] \quad 2.3 \times 10^{-5} [V^2]\}$$

For a realistic evaluation, the performance of the IM is tested in open-loop with PWM input voltages and currents as can be seen in Fig. 5.3. The EKF algorithms take as input the transformed components of the current and voltage. The following is a generalized description of this transformation; $x_\alpha = x_a$; $x_\beta = (1/\sqrt{3})(x_b - x_c)$ where: $x : i$ and v for current and voltage, respectively.

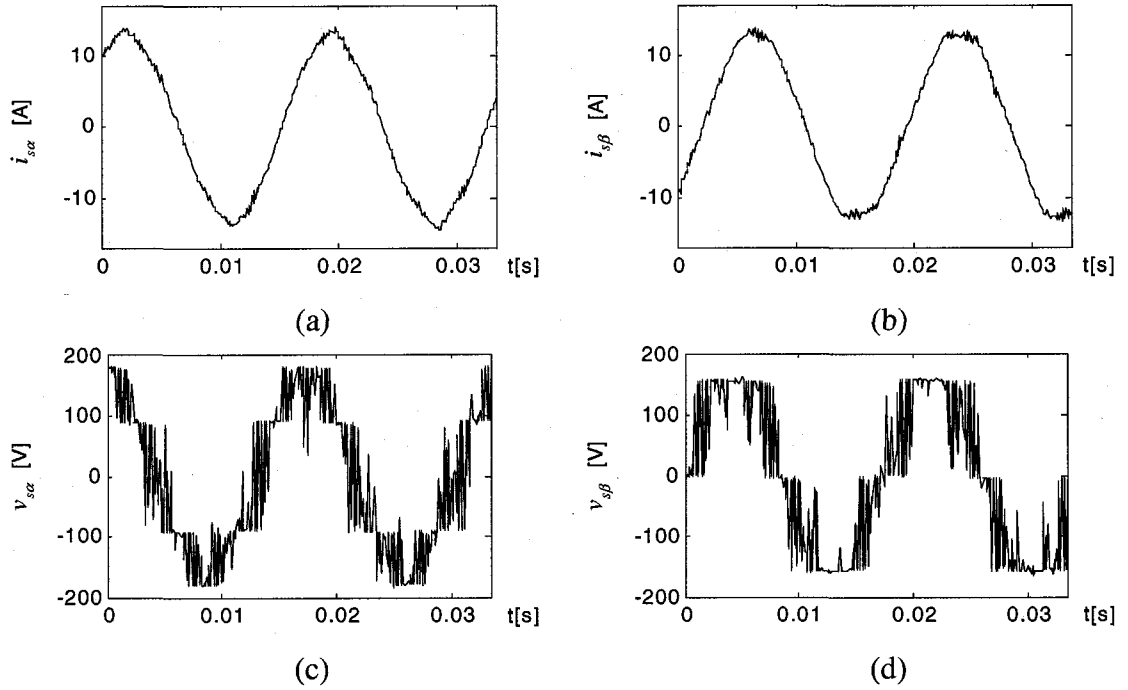


Fig. 5.3 Stator currents and voltages applied to the IM through the AC drive.

Fig. 5.3 demonstrates the transformed current and voltage at 60 [Hz], 230 [V] for a t_L of approximately 21.06 [N.m].

To test the performance of the Braided EKF against the conventional $EKF - R_s$ and $EKF - R_r$ algorithms, five scenarios are developed, which impose challenging R_s , R_r ,

load torque and velocity variations on the motor in the high and low speed range. All algorithms are started with initial parameter and state estimations of zero. The sampling period for all algorithms is $T_{sample} = 110 [\mu s]$.

The resulting performances are presented with the variations of n_m & \hat{n}_m , t_{ind} & \hat{t}_L , $\hat{\psi}_{r\alpha}$, $\hat{\psi}_{r\beta}$, \hat{R}_r , \hat{R}_s , $e_{i_{s\alpha}}$ & $e_{i_{s\beta}}$, $e_{n_m} \triangleq n_m - \hat{n}_m$ and $e_{t_L} \triangleq t_{ind} - \hat{t}_L$, namely, the measured and estimated velocity, the induced torque as obtained from the torque-meter and estimated load torque, the estimated α and β components of the rotor flux, estimated rotor resistance, estimated stator resistance, estimation errors in $(i_{s\alpha})$ and $(i_{s\beta})$, and estimation errors of velocity and load torque, respectively.

Scenario I – Load torque & stator resistance variations for EKF – R_r , (Fig. 5.4):

This scenario aims to test the performance of *EKF – R_r* , under R_r and R_s variations. To this purpose, while the IM is running at 849.5 [rpm] under no-load, and the switched array resistance of 7.8 [Ω] is connected to the armature, the field supply of the dc generator is switched on at $t = 1.8$ [sec]. The IM is loaded with 20.2 [N.m] at 817.2 [rpm], which also causes an increase in R_r . To also test the algorithm under R_s uncertainties, the following variations are given to R_s at $t = 16.2$ [sec], $R_s : R_{sn} \rightarrow 2 \times R_{sn}$, at $t = 24.7$ [sec], $R_s : 2 \times R_{sn} \rightarrow R_{sn}$. Finally, the scenario is switched back to its initial status at $t = 31.75$ [sec].

Inspecting the results, it can be seen that due to the instantaneous switching effects created by the challenging variations, the maximum errors of $i_{s\alpha}$ and $i_{s\beta}$ jump to peak values of 3.1 [mA], however, the errors of both currents remain within a band of ± 2 [mA]. The estimated values of velocity and load torque also track their measured values quite closely with a reasonable relationship observed between the load torque estimation error and that of the velocity. In the time interval of $0[\text{sec}] \leq t \leq 16.2[\text{sec}]$ and

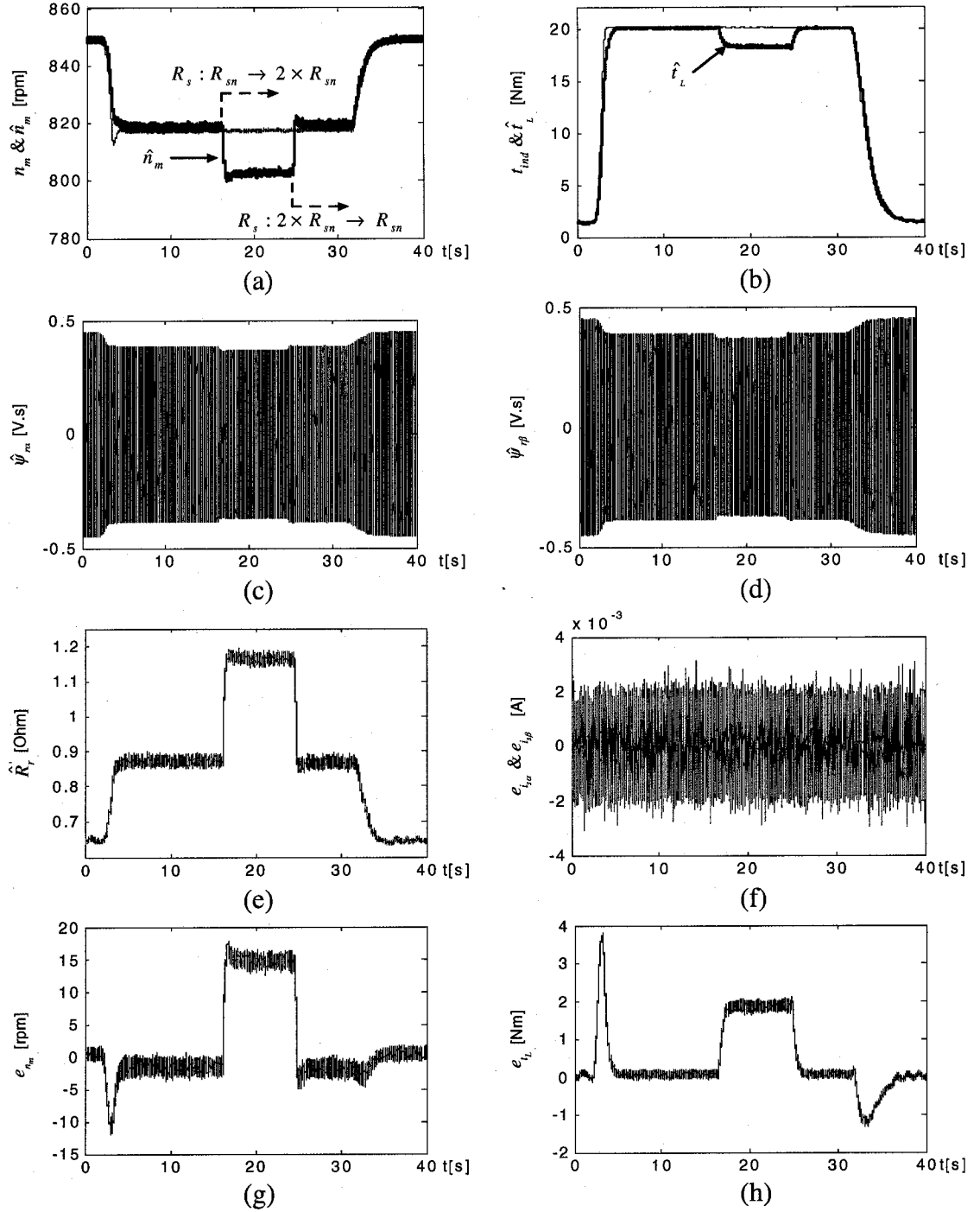


Fig. 5.4 Experimental results of $EKF - \hat{R}_r$ for load torque & stator resistance variations: (a) The variation of n_m and \hat{n}_m ; (b) the variation of t_{ind} and \hat{t}_L ; (c) the variation of $\hat{\psi}_{r\alpha}$; (d) the variation of $\hat{\psi}_{r\beta}$; (e) the variation of \hat{R}_r ; (f) the variation of $e_{i_{s\alpha}}$ & $e_{i_{s\beta}}$; (g) the variation of e_{n_m} ; and (h) the variation of e_{t_L} .

31.75[sec] ≤ t ≤ 40[sec] in Fig. 5.4 (e), it can be noted that the estimated rotor resistance, \hat{R}_r , has demonstrated a variation in harmony with the rotor frequency which is close to linear, and consequently, with the load torque, as has been stated in [19], [25]. However, under the challenging R_s variation $R_s : R_{sn} \rightarrow 2 \times R_{sn}$ at $t = 16.2$ [sec], a considerable amount of error occurs in the estimated load torque and, consequently, in the estimated velocity and flux. The error is corrected at $t = 24.7$ [sec], when the R_s value is switched back to its nominal value, R_{sn} used in the extended model. While the operation of the IM over a long duration is expected to cause a similar increase in the R_s value even at high speeds, the temperature dependent increase in R_s is even more critical at low speeds. Therefore, proper and continuous updates of R_s are essential for the $EKF - R_r$ algorithm throughout the whole speed range for accurate estimations of flux, load torque and velocity.

Scenario II – Load torque & rotor resistance variations for $EKF - R_s$, (Fig. 5.5):

In this section, the $EKF - R_s$ algorithm will be tested for load torque and rotor resistance variations. To this aim, while the IM is running at 849.5 [rpm] under no-load, and the switched array resistance of 7.8 [Ω] is connected to the armature, the field supply of the dc generator is switched on at $t = 2$ [sec.]. The IM is loaded with 20.9 [N.m] at 815.5 [rpm]. The variation of the load torque inherently varies R_r , and since the extended model of $EKF - R_s$ assumes R_r to be constant, a considerable amount of error occurs in the estimated load torque and, consequently, in the estimated velocity and flux. However, $i_{s\alpha}$ and $i_{s\beta}$ errors remain within a very small band of ± 0.4 [mA], as can be seen in Fig. 5.5(f). The resulting performance of this scenario is presented in Fig. 5.5(a), (b), (c), (d), (e), (f), (g) and (h).

To demonstrate the importance of proper \hat{R}_r updates for the performance of the

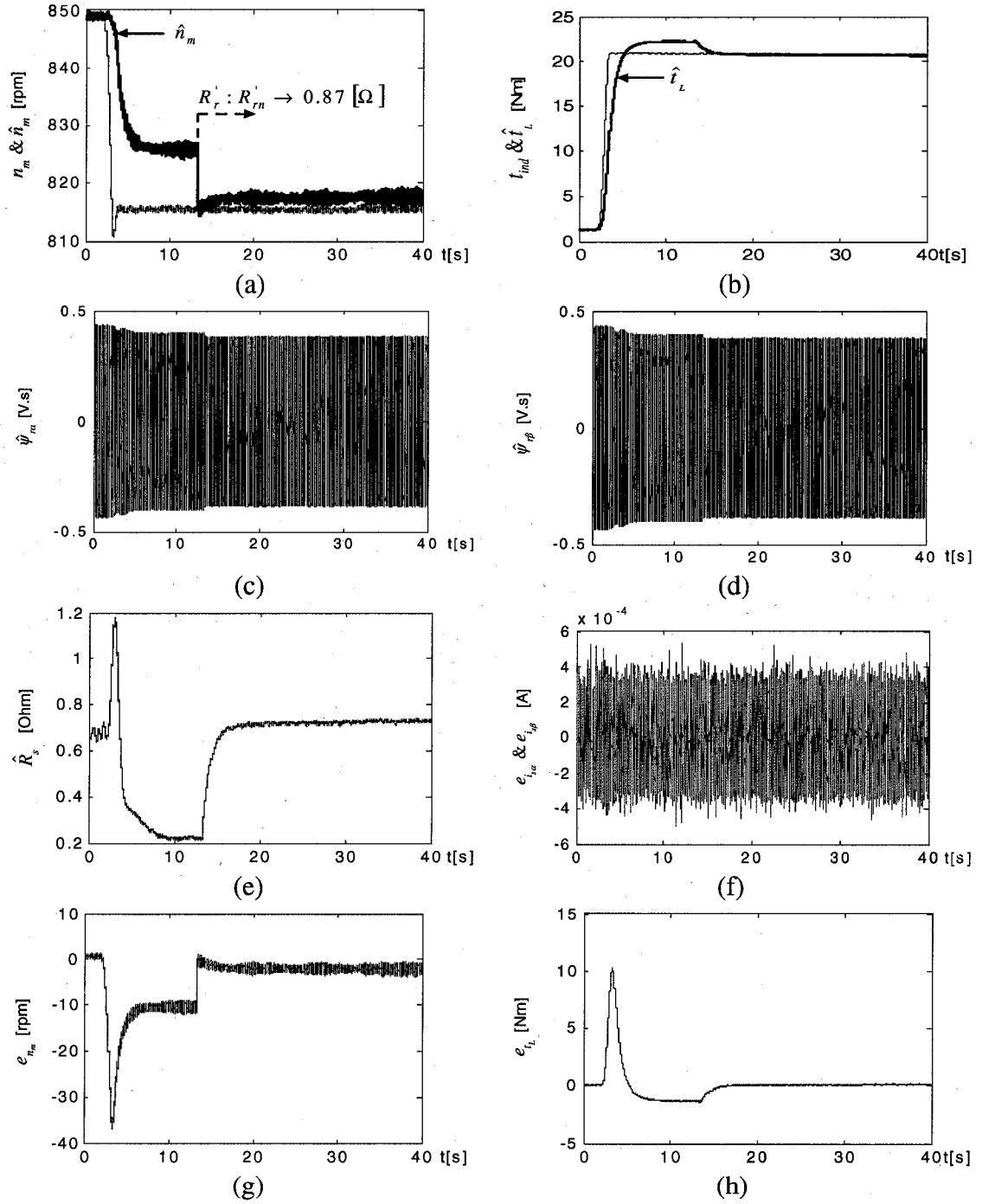


Fig. 5.5 Experimental results of $EKF - R_s$ for load torque & rotor resistance variations: (a) The variation of n_m and \hat{n}_m ; (b) the variation of t_{ind} and \hat{t}_L ; (c) the variation of $\hat{\psi}_{r\alpha}$; (d) the variation of $\hat{\psi}_{r\beta}$; (e) the variation of \hat{R}_s ; (f) the variation of $e_{i_{s\alpha}}$ & $e_{i_{s\beta}}$; (g) the variation of e_{n_m} ; and (h) the variation of e_{t_L} .

$EKF - R_s$ algorithm, starting at $t = 13.3$ [sec] the algorithm is updated with the accurate \hat{R}_r values, obtained from $EKF - R_r$ in Scenario I. The velocity and torque estimation errors, which were at a significant level prior to \hat{R}_r updates at 13.3 [sec], start converging towards zero. Thus, this scenario indicates the importance of accurate R_r values for the performance of the $EKF - R_s$ algorithm and also emphasizes the need for simultaneous R_s and R_r updates.

Scenario III – Load torque & rotor resistance variations under Braided EKF, (Fig. 5.6):

In this section, the performance of the Braided EKF algorithm will be evaluated under rotor resistance variations. To this aim, while the IM is running at 849.5 [rpm] under no-load, and the switched array resistance of 7.8 [Ω] is connected to the armature, the field supply of the dc generator is switched on at $t = 7.2$ [sec.]. The IM is loaded with 20.74 [N.m] at 818.7 [rpm], which also causes an increase in R_r . At $t = 19$ [sec.], the scenario is switched to its initial status by switching off the DC generator field supply. The resulting performance is given in Fig. 5.6(a), (b), (c), (d), (e), (f), (g) and (h).

Inspecting the results, it can be seen that, the Braided EKF has in fact achieved a significantly improved performance over individual EKFs, with the simultaneous estimation of R_s and R_r throughout the operation. Hence, in spite of R_r variations between $t = 7$ and 19 [sec], the estimation errors are significantly lower (and almost zero) in comparison to the errors obtained with $EKF - R_s$ only, which performs R_s estimation only while R_r variations are taking place.

Scenario IV – Stator resistance variations under Braided EKF, (Fig. 5.7):

In this section, the performance of the Braided EKF will be evaluated under R_s variations. To this aim, the scenario is started with an incorrect initialization of $R_s(0^+) = 2 \times R_{sn}$, while only $EKF - R_r$ is running and at $t = 7.27$ [sec.], the Braided

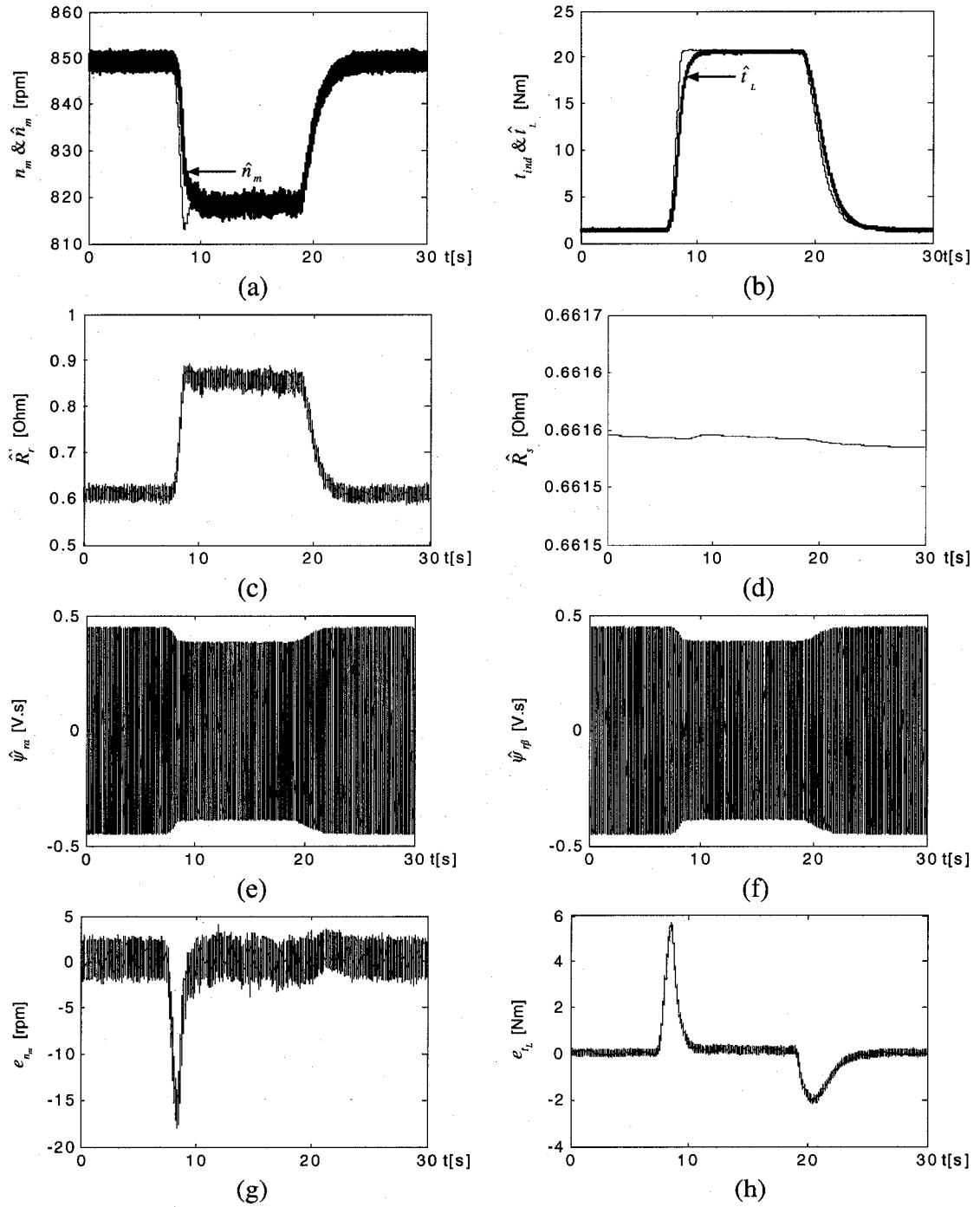


Fig. 5.6 Experimental results of Braided EKF for load torque variations at constant velocity: (a) The variation of n_m and \hat{n}_m ; (b) the variation of t_{ind} and \hat{t}_L ; (c) the variation of \hat{R}_r ; (d) the variation of \hat{R}_s ; (e) the variation of $\hat{\psi}_{ra}$; (f) the variation of $\hat{\psi}_{rb}$; (g) the variation of e_{n_m} ; and (h) the variation of e_{t_L} .

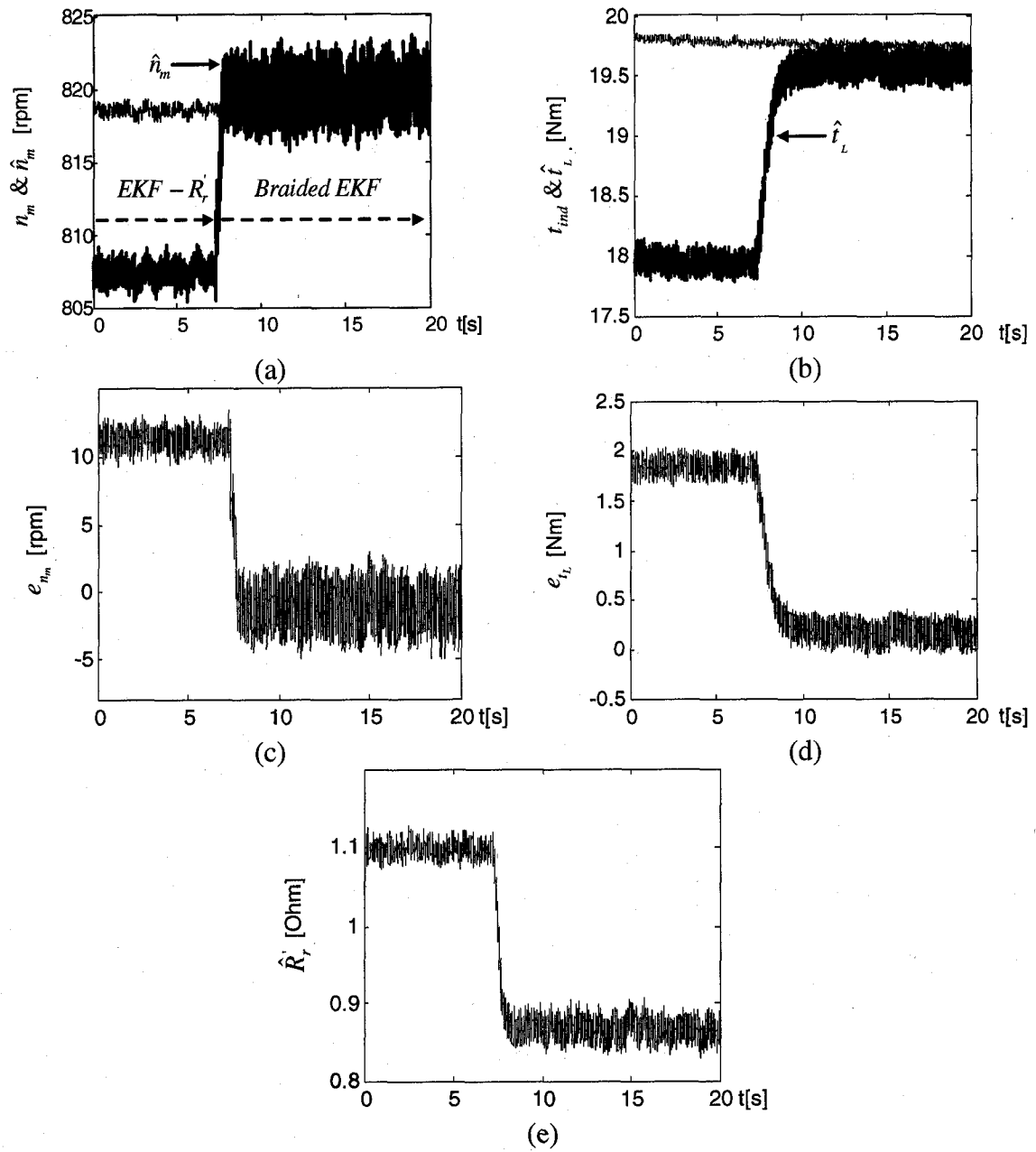


Fig. 5.7 Experimental results of Braided EKF for steady state with incorrect $R_s(0^+) = 2 \times R_{sn}$: (a) The variation of n_m and \hat{n}_m ; (b) the variation of t_{ind} and \hat{t}_L ; (c) the variation of e_{n_m} ; (d) the variation of e_{t_L} ; and (e) the variation of \hat{R}_r .

algorithm starts. The resulting performance of this scenario is given in Fig. 5.7(a), (b), (c), (d) and (e).

Inspecting the results, the following can be noted: the estimation error obtained in the initial period when only the $EKF - R_r'$ algorithm is on under a variation in R_s , is significantly reduced as soon as the Braided EKF algorithm is switched on. As can be seen from Fig. 5.7, all errors quickly approach zero as soon as the Braided EKF is switched on, in spite of the variation in R_s .

Scenario V – Low speed operation under Braided EKF (Fig. 5.8):

Finally, the performance of the Braided EKF algorithm is tested in low speed operation. While the IM is running at 821.7 [rpm] under a load torque of 19.17 [N.m], the velocity and load torque are decreased to 54.5 [rpm] and 2.85 [N.m], respectively, with a linear variation given to the velocity reference on the ac drive. At $t = 22$ [sec] the scenario is switched back to the initial status. The resulting performance is given in Fig. 5.8(a), (b), (c), (d), (e), (f), (g) and (h).

Inspecting the estimation errors of the velocity and load torque in Fig. 5.8(f) and (g), respectively, it can be noted that the Braided EKF outperforms the individual $EKF - R_s$ and $EKF - R_r'$ algorithms. Hence, the benefits of the Braided EKF algorithm over individual EKF algorithms are evident in the whole velocity range, especially under unmatched R_s and R_r' variations, therefore, R_r' variations while $EKF - R_s$ is running or R_s variations when the estimator is $EKF - R_r'$. The switching action provided by the Braided algorithm at every time step ensures better prediction and correction against all uncertainties and parameter variations.

5.5 Conclusion

The proper estimation of temperature and frequency based uncertainties of R_s and R_r' is known to be essential for the accuracy of flux and velocity estimation in IM sensorless control; however, the simultaneous estimation of R_s and R_r' has frequently been reported as a challenge in previous literature on sensorless IM control.

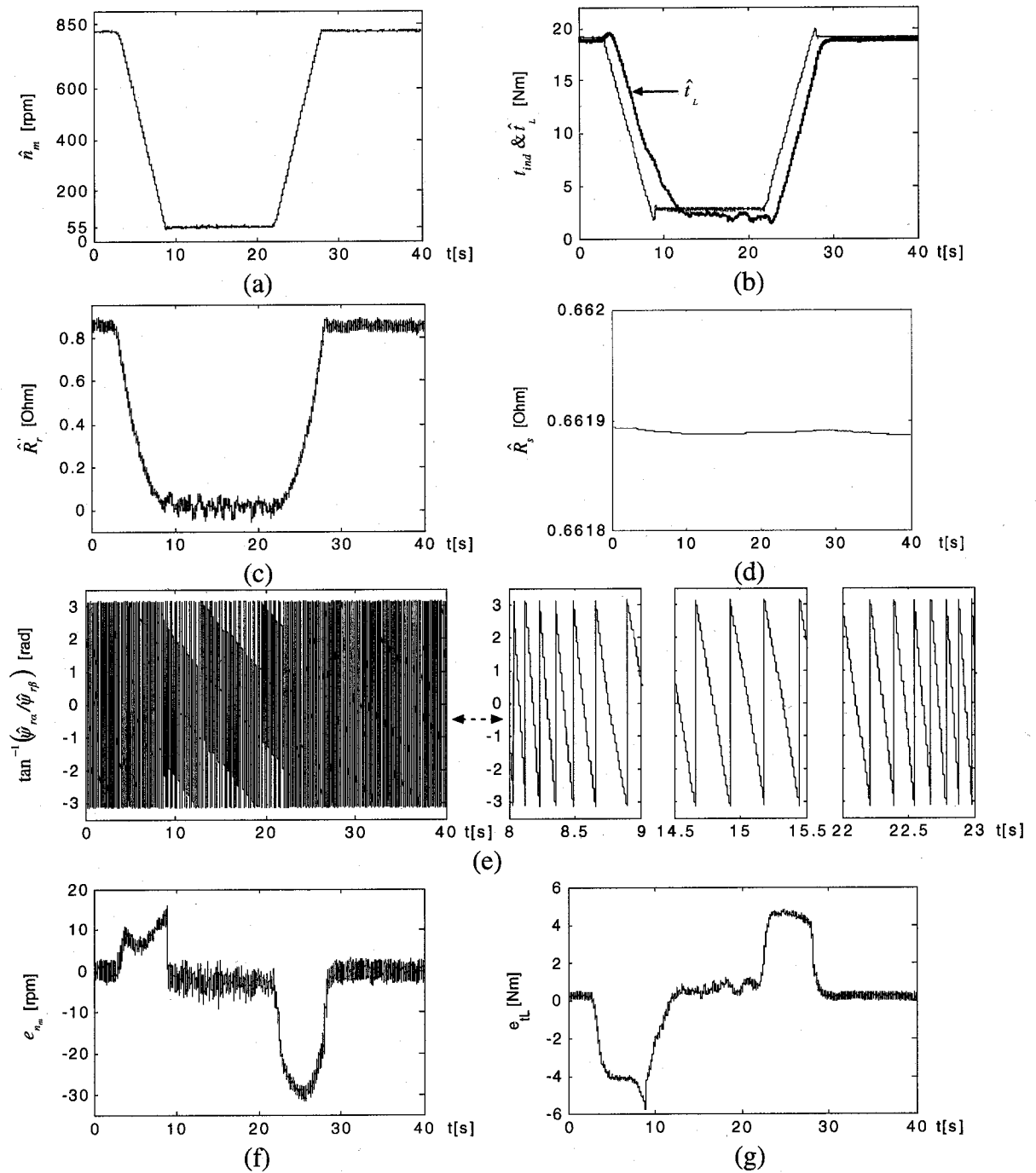


Fig. 5.8 Experimental results for Braided EKF for low speed operation: (a) The variation of n_m and \hat{n}_m ; (b) the variation of t_{ind} and \hat{t}_L ; (c) the variation of \hat{R}_r ; (d) the variation of \hat{R}_s ; (e) the variation of the estimated position of the flux with reference to the stator stationary axis; (f) the variation of e_{n_m} ; and (g) the variation of e_{t_L} .

There have been only a few studies achieving the simultaneous estimation of R_s and R_r in sensorless control, -either by the use of open-loop estimators or by developing different estimation techniques for different states and parameters in the IM model or by signal injection, which requires additional and customized measures to be taken. In this study, a more flexible approach is proposed to the solution of the problem that does not require signal injection or algorithm changes and is based on the consecutive use of two EKF algorithms of the same nature and configuration for the simultaneous estimation of R_s and R_r in addition to the load torque, flux and velocity.

The solution offered by the braided approach exploits the fast convergence rate of EKFs as well as the persistent excitation properties introduced by the model (or system) noise and measurement noise inherent to EKF, increasing estimation accuracy in steady-state and eliminating the need for external signal injection. However, the computational complexity and deteriorated performance of EKFs with the increased number of estimated states is also a well-known fact. To overcome this problem in this study, the two EKF algorithms estimating R_s and R_r are utilized in a braided manner, thus achieving the accurate estimation of a high number of parameters and states than would have been possible with a single EKF algorithm.

Experimental results taken under challenging scenarios demonstrate the performance achieved by the proposed algorithm in a wide speed range with significantly increased accuracy in the estimation of flux and velocity, in comparison to single EKF algorithms which estimate R_s or R_r only or other approaches taken in previous studies. The results also motivate the utilization of the proposed estimation technique in combination with a variety control methods for IMs or other electrical machines which require the accurate knowledge of a large number of parameters.

References

- [1] A. Derdiyok, "Speed-sensorless control of induction motor using a continuous control approach of sliding-mode and flux observer," *IEEE Transactions on Industrial Electronics*, vol. 52, no. 4, pp. 1170–1176, Aug. 2005.
- [2] C. Lascu, I. Boldea, and F. Blaabjerg, "Direct torque control of sensorless induction motor drives: a sliding-mode approach," *IEEE Transactions on Industry Applications*, vol. 40, no. 2, pp. 582–590, March-April 2004.
- [3] G. Guidi and H. Umida, "A novel stator resistance estimation method for speed-sensorless induction motor drives," *IEEE Transactions on Industry Applications*, vol. 36, no. 6, pp. 1619–1627, Nov.-Dec. 2000.
- [4] M. Cirrincione, M. Pucci, G. Cirrincione, and G.-A. Capolino, "An adaptive speed observer based on a new total least-squares neuron for induction machine drives," *IEEE Transactions on Industry Applications*, vol. 42, no. 1, pp. 89–104, Jan.-Feb. 2006.
- [5] C. Lascu, I. Boldea and F. Blaabjerg, "Very-low-speed variable-structure control of sensorless induction machine drives without signal injection," *IEEE Transactions on Industry Applications*, vol. 41, no. 2, pp. 591–598, March-April 2005.
- [6] K. Ohyama, G.M. Asher and M. Sumner, "Comparative analysis of experimental performance and stability of sensorless induction motor drives," *IEEE Transactions on Industrial Electronics*, vol. 53, no. 1, pp. 178 – 186, Dec. 2005.
- [7] S. Wade, M.W. Dunnigan and B.W. Williams, "Comparison of stochastic and deterministic parameter identification algorithms for indirect vector control," *IEE Colloquium on Vector Control and Direct Torque Control of Induction Motors*, London, U.K., vol. 2, pp. 1–5, 1995.
- [8] L. Salvatore, S. Stasi and L. Tarchioni, "A new EKF-based algorithm for flux estimation in induction machines," *IEEE Transactions on Industrial Electronics*, vol. 40, no. 5, Oct. 1993, pp. 496–504.

- [9] O. S. Bogosyan, M. Gokasan and C. Hajiyeve, "An application of EKF for the position control of a single link arm," *Proc. IEEE-IECON'01 Annual Meeting*, Denver, Colorado, vol. 1, 2001, pp. 564–569.
- [10] M. Barut, O. S. Bogosyan, M. Gokasan, "EKF based estimation for direct vector control of induction motors," *Proc. IEEE-IECON'02 Annual Meeting*, Sevilla, vol. 2, 2002, pp. 1710–1715.
- [11] B. Akin, U. Orguner, A. Ersak and M. Ehsani, "A comparative study on non-linear state estimators applied to sensorless AC drives: MRAS and Kalman filter," *Proc. IEEE-IECON'04 Annual Meeting*, Busan, Korea, vol. 3, 2004, pp. 2148–2153.
- [12] K. Young-Real, S. Seung-Ki and P. Min-Ho, "Speed sensorless vector control of induction motor using extended Kalman filter," *IEEE Transactions on Industry Applications*, vol. 30, no. 5, Sept.-Oct. 1994, pp. 1225–1233.
- [13] K.L. Shi, T.F. Chan, Y.K. Wong, and S.L. Ho, "Speed estimation of an induction motor drive using an optimized extended Kalman filter," *IEEE Transactions on Industrial Electronics*, vol. 49, no. 1, Feb. 2002, pp. 124–133.
- [14] C.-M. Lee and C.-L. Chen, "Observer-based speed estimation method for sensorless vector control of induction motors," *IEE Proceedings-Control Theory and Applications*, vol. 145, no. 3, May 1998, pp. 359–363.
- [15] Y. Wenqiang, J. Zhengchun and X. Qiang, "A new algorithm for flux and speed estimation in induction machine," *Proc. IEEE-ICEMS 2001 Annual Meeting*, Shenyang, China, vol. 2, 2001, pp. 698–701.
- [16] G. Qiongquan and F. Zhiyue, "Speed estimated for vector control of induction motor using reduced-order extended Kalman filter," *Proc. IEEE-PIEMC 2000 Annual Meeting*, Beijing, China, vol. 1, 2000, pp. 138–142.
- [17] Ch. El Moucary, G. Garcia Soto, and E. Mendes, "Robust rotor flux, rotor resistance and speed estimation of an induction machine using the extended Kalman filter". *Proc. IEEE-ISIE'99 Annual Meeting*, Bled, Slovenia, vol. 2, pp. 742–746.

- [18] M. Barut, S. Bogosyan, and M. Gokasan, "Speed sensorless direct torque control of IMs with rotor resistance estimation," *Energy Conversion and Management (Elsevier)*, vol. 46, no. 3, Feb. 2005, pp. 335-349.
- [19] M. Barut, S. Bogosyan, and M. Gokasan, "An EKF based estimator for speed sensorless vector control of induction motors," *Electric Power Components & Systems, formerly Electric Machines And Power Systems (Taylor-Francis)*, vol. 33, no. 7, July 2005, pp. 727-744.
- [20] J. Faiz and M.B.B. Sharifian, "Different techniques for real time estimation of an induction motor rotor resistance in sensorless direct torque control for electric vehicle," *IEEE Transactions on Energy Conversion*, vol. 16, no. 1, March 2001, pp. 104-109.
- [21] L. Zhen and L. Xu, "Sensorless field orientation control of induction machines based on a mutual MRAS scheme," *IEEE Transactions on Industrial Electronics*, vol. 45, no. 5, Oct. 1998, pp. 824-831.
- [22] H. In-Joong and L. Sang-Hoon, "An online identification method for both stator-and rotor resistances of induction motors without rotational transducers," *IEEE Transactions on Industrial Electronics*, vol. 47, no. 4, Aug. 2000, pp. 842-853.
- [23] H. Tajima, G. Guidi, and H. Umida, "Consideration about problems and solutions of speed estimation method and parameter tuning for speed-sensorless vector control of induction motor drives," *IEEE Transactions on Industry Applications*, vol. 38, no. 5, Sept.-Oct. 2002, pp. 1282-1289.
- [24] G. Edelbaher, K. Jezernik and E. Urlep, "Low-speed sensorless control of induction machine," *IEEE Transactions on Industrial Electronics*, vol. 53, no. 1, Feb. 2006, pp. 120-129.
- [25] A.B. Proca and A.Keyhani, "Identification of variable frequency induction motor models from operating data," *IEEE Transactions on Energy Conversion*, vol. 17, no. 1, March 2002, pp. 24-31.

Chapter 6:

Sensorless Sliding Mode Position Control of Induction Motors Using Braided Extended Kalman Filters *

Abstract— This study is aimed at designing a sensorless sliding mode position control system for the rotor flux oriented Direct Vector Control (DVC) strategy of induction motors (IMs). For this purpose, a novel sliding mode controller (SMC) with reduced chattering is designed for the control of the flux and angular position of the motor. All the states required for DVC in addition to the step-shaped load torque, stator resistance and rotor resistance are estimated using Braided EKF based observers. The performance of the new SMC is compared against a previously developed chattering-free SMC scheme. The simulation results demonstrate an improved robustness in the system response against parameter and load variations. It has also been demonstrated that the new Braided EKF technique used in the proposed sliding mode position control system also increases estimation accuracy of estimations when compared with chattering-free SMC under challenging variations of 100 % in the load and stator & rotor resistance.

Index Terms— *Sliding mode control, reduced chattering, position control, sensorless vector control, Extended Kalman filter, induction motor, estimator, observer.*

6.1 Introduction

The development of sensorless induction motor (IM) drives based on vector control or field-oriented control (FOC) has reached a level of maturity in recent years. However, the ongoing problem is to improve the dynamic behaviour of the drive under load and parameter variations for a wide speed range including zero speed for motion control applications of IM, such as robots, manipulators, electric vehicles, elevators, cranes, and

* Barut, M. and Bogosyan, S. (2007), "Sensorless Sliding Mode Position Control of Induction Motors Using Braided Extended Kalman Filters", *Proceedings of the IEEE International Symposium on Industrial Electronics (ISIE 2007)*. (To be submitted)

numerically controlled (NC) machine tools. Therefore, control tasks can be summarized as

- design of robust controllers against parameter/model uncertainties of IMs
- design of robust estimators for the determination of IM states and parameters for sensorless control.

PID controllers are widely used in motor control and other industrial applications because they provide a simple structure, design and implementation, while also ensuring a good control performance [1, 2, 3]. However, the parameter-tuning of the controller is quite a difficult task for highly nonlinear systems, such as IMs under parameter variations and external disturbances, when the aim is to track a desired dynamics [4, 5]. Therefore, artificial intelligence based studies, as in [5-7], have also been proposed recently for the position control of IMs. Although these methods improve performance of the designed controller, generally speaking, they need computationally complex algorithms, network architecture or fuzzy rules, which are constructed by a time-consuming trial-and-error tuning procedure.

The SMC is a very effective approach for the solution of the problem due to its well-established design criteria, easy implementation, fast dynamic response, and robustness to parameter variations when a system is in a sliding mode [8, 9, 10, 11]. However, the well-known drawback of the SMC is chattering, which is due to high-frequency control activity, and may excite unmodeled plant dynamics. Thus, to reduce chattering, several modifications have been proposed in previous studies related to the sliding mode position control of IMs: [12, 13, 14, 15] use Slotine's SMC approach, first-order low-pass filter (LPF), a pseudo sliding technique, an adaptive law for estimating the load torque disturbance, respectively. In [12], the tracking error is kept in a thin boundary layer; while [13] gives a sluggish response in transient state. Electrical uncertainty effects on performance of the controller have not been addressed at all in [14], while [15] is sensitive to variations in the rotor time constant. This study also does not address the sinusoidal tracking performance of the controller. Moreover, in all studies mentioned above, position sensors have been used. Among previous studies using SMC for the

sensorless position control of IMs, [16] presents a chattering-free SMC based on the average-equivalent control approach. The simulation results have been obtained under variations of 20% and %8 in rotor and stator resistance at rated load; however, the performance of the scheme step-type references has not been addressed at all, while step performance is known to be critical in the sensorless control of IM. Moreover, it should be noted that there is a trade-off between robustness and chattering reduction as pointed out in [17].

In this study, a novel reduced chattering SMC law is developed for the sensorless position control of IMs. The developed control combines the concept of power rate reaching law in [9] and average-equivalent control law in [16], [18] and [19]. In the proposed control law, the equivalent control represents the average control signal which is required to keep the switching variable on the switching surface. The power rate switching term aims to make the controller robust against matched uncertainties and to attain sliding mode in a short time. However, although the control law is robust against parameter variations, in sensorless control, the performance is very much dependent on how well the states are estimated. This, in turn, calls for reliable estimation methods that can account for stator and rotor resistance variations as well as the load torque. To this aim, the developed controller is combined with the novel Braided EKF estimation technique developed in [20]. Finally, the obtained simulation results show that the proposed SMC and estimator combination provides a superior performance over the sliding mode based control and observer in [16].

6.2 Mathematical Model of the IM

The model of IM in synchronous axis (dq) can be given as follows:

$$\frac{di_{sd}}{dt} = \dot{i}_{sd} = -k_1 i_{sd} + \omega_s i_{sq} + k_2 \psi_{rd} + k_3 \omega_m \psi_{rq} + k_4 v_{sd} \quad (6.1a)$$

$$\frac{di_{sq}}{dt} = \dot{i}_{sq} = -k_1 i_{sq} - \omega_s i_{sd} + k_2 \psi_{rq} - k_3 \omega_m \psi_{rd} + k_4 v_{sq} \quad (6.1b)$$

$$\frac{d\psi_{rd}}{dt} = \dot{\psi}_{rd} = k_5 i_{sd} - k_6 \psi_{rd} + (\omega_s - p_p \omega_m) \psi_{rq} \quad (6.2a)$$

$$\frac{d\psi_{rq}}{dt} = \dot{\psi}_{rq} = k_5 i_{sq} - k_6 \psi_{rq} - (\omega_s - p_p \omega_m) \psi_{rd} \quad (6.2b)$$

A. Design of SMCs design with reduced chattering

In this section, two sliding mode controllers (SMCs) are designed; one for the flux control, and one for the position control. To this aim, initially a sliding manifold is defined for each:

$$\text{i) } \sigma_d = |\psi_r|^{ref} - \psi_d \quad (6.4a)$$

$$\text{ii) } \sigma_q = (\dot{\theta}_m^{ref} - \dot{\theta}_m) + c(\theta_m^{ref} - \theta_m) = \dot{e}_q + ce_q \quad (c > 0) \quad (6.4b)$$

The controllers to be designed must take the controlled states to the manifolds and keep them there as the errors go to zero in spite of parameter and model uncertainties. To ensure stability conditions, the derivations of the controllers are based on Lyapunov Theory; to this aim, a positive definite Lyapunov function is chosen as below:

$$V = \frac{1}{2}\sigma_d^2 + \frac{1}{2}\sigma_q^2 \rightarrow \dot{V} = \sigma_d\dot{\sigma}_d + \sigma_q\dot{\sigma}_q \quad (6.5)$$

At this point, the following selection is made to ensure that \dot{V} is negative definite and consequently, that the sliding mode will occur in the intersection of the surfaces with, $\sigma_d = 0$ and $\sigma_q = 0$:

$$\sigma_d\dot{\sigma}_d = -k_d|\sigma_d|^{1/n_d}|\sigma_d| \rightarrow \dot{\sigma}_d = -k_d|\sigma_d|^{1/n_d} \text{sgn}(\sigma_d) \quad (6.6a)$$

$$\sigma_q\dot{\sigma}_q = -k_q|\sigma_q|^{1/n_q}|\sigma_q| \rightarrow \dot{\sigma}_q = -k_q|\sigma_q|^{1/n_q} \text{sgn}(\sigma_q) \quad (6.6b)$$

(where $k_d > 0, k_q > 0, 0 < n_d < 1$ and $0 < n_q < 1$)

By using (6.2a), (6.3), (6.4a) & (6.4b), $\dot{\sigma}_d$ and $\dot{\sigma}_q$ can be found as follows:

$$\dot{\sigma}_d = \frac{d|\psi_r|^{ref}}{dt} - \bar{k}_s i_{sd} - \Delta k_5 i_{sd} + k_6 \psi_{rd} + (\omega_s - p_p \omega_m) \psi_{rq} = -\bar{k}_s i_{sd} + f_d(.) \quad (6.7a)$$

$$\begin{aligned}
\dot{\sigma}_q &= \dot{\omega}_m^{ref} - \dot{\omega}_m + c\dot{e}_q \\
&= -\bar{k}_7 \psi_{rd} i_{sq} + \bar{k}_7 \psi_{rq} i_{sd} + \Delta k_7 (\psi_{rd} i_{sq} - \psi_{rq} i_{sd}) + k_8 \omega_m + k_9 t_L \\
&= -\bar{k}_7 |\psi_r|^{ref} i_{sq} + f_q(.)
\end{aligned} \tag{6.7b}$$

(where \bar{k}_5 and \bar{k}_7 are known; Δk_5 and Δk_7 unknown)

When the control input i_{sd} (or i_{sq}) attains its *equivalent* value ($i_{sd} = i_{sd(eq)}$; $i_{sq} = i_{sq(eq)}$), $\dot{\sigma}_d$ (or $\dot{\sigma}_q$) becomes zero. Therefore, $i_{sd(eq)}$ and $i_{sq(eq)}$ are determined by

$$i_{sd(eq)} = \frac{f_d(.)}{\bar{k}_5} \tag{6.8a}$$

$$i_{sq(eq)} = \frac{f_q(.)}{\bar{k}_7 |\psi_r|^{ref}} \tag{6.8b}$$

Substituting (6.8a) and (6.8b) into (6.7a) and (6.7b), $\dot{\sigma}_d$ and $\dot{\sigma}_q$ can be rewritten as

$$\dot{\sigma}_d = \bar{k}_5 (i_{sd(eq)} - i_{sd}) \tag{6.9a}$$

$$\dot{\sigma}_q = \bar{k}_7 |\psi_r|^{ref} (i_{sq(eq)} - i_{sq}) \tag{6.9b}$$

Finally, using the backward Euler discrete time versions of (6.6a) & (6.9a) and (6.6b) & (6.9b) under the assumptions of $i_{sd(eq)}(k) \cong i_{sd(eq)}(k-1)$ and $i_{sq(eq)}(k) \cong i_{sq(eq)}(k-1)$, the control laws for the flux and position are determined as

$$i_{sd}(k) = i_{sd}(k-1) + \frac{\sigma_d(k) - \sigma_d(k-1)}{\bar{k}_5 T} + \frac{k_d |\sigma_d(k)|^{1/n_d} \text{sgn}(\sigma_d(k))}{\bar{k}_5} \tag{6.10a}$$

$$i_{sq}(k) = i_{sq}(k-1) + \frac{\sigma_q(k) - \sigma_q(k-1)}{\bar{k}_7 T |\psi_r|^{ref}} + \frac{k_q |\sigma_q(k)|^{1/n_q} \text{sgn}(\sigma_q(k))}{\bar{k}_7 |\psi_r|^{ref}} \tag{6.10b}$$

(where T is sampling time.)

B. Braided EKF Based Observers

In this section, the Braided EKF technique proposed in [20] is used to estimate the states required by the developed SMC; however, to improve the performance of sensorless estimation, the R_s and R_r parameters are also estimated with the braided technique. The extended model of induction motor used in each EKF algorithm is defined as follows [20]:

-*Model1* with $\dot{\underline{x}}_{e1} = [\dot{i}_{s\alpha} \ \dot{i}_{s\beta} \ \dot{\psi}_{r\alpha} \ \dot{\psi}_{r\beta} \ \dot{\omega}_m \ \dot{i}_L \ \dot{R}_s]^T$ (For the estimation of R_s), which is obtained by taking $\omega_s = 0$ in Eq. 1a, 1b, 2a, 2b and 3, and by taking $\frac{dt_r}{dt} = \dot{i}_L = 0$ and $\frac{dR_r}{dt} = \dot{R}_s = 0$.

-*Model2* with $\dot{\underline{x}}_{e2} = [\dot{i}_{s\alpha} \ \dot{i}_{s\beta} \ \dot{\psi}_{r\alpha} \ \dot{\psi}_{r\beta} \ \dot{\omega}_m \ \dot{i}_L \ \dot{R}_r]^T$ (For the estimation of R_r), which is obtained by taking $\omega_s = 0$ in Eq. 1a, 1b, 2a, 2b and 3, and by taking $\frac{dt_L}{dt} = \dot{i}_L = 0$ and $\frac{dR_s}{dt} = \dot{R}_r = 0$.

The estimation process requires the discretization of model1 and model2 as below;

$$\underline{x}_{ei}(k+1) = \underline{f}_{ei}(\underline{x}_{ei}(k), \underline{u}_e(k)) + \underline{w}_{i1}(k) \quad (6.11a)$$

$$\underline{Z}(k) = \underline{H}_e \underline{x}_{ei}(k) + \underline{w}_{i2}(k) \quad (6.11b)$$

($i=1,2$; extended state vector \underline{x}_{ei} representing the estimated states. \underline{w}_{i1} is the process noise. \underline{w}_{i2} is the measurement noise. \underline{H}_e is the measurement matrix.)

For the linearization of (6.12a-b), the current estimated states, $\hat{\underline{x}}_{ei}(k)$ and inputs $\hat{\underline{u}}_e(k)$ are used as below;

$$\underline{F}_{ei}(k) = \left. \frac{\partial f_{ei}(\underline{x}_{ei}(k), \underline{u}_e(k))}{\partial \underline{x}_{ei}(k)} \right|_{\hat{\underline{x}}_{ei}(k), \hat{\underline{u}}_e(k)} \quad (6.12a)$$

$$\underline{F}_{ui}(k) = \left. \frac{\partial f_{ei}(\underline{x}_{ei}(k), \underline{u}_e(k))}{\partial \underline{u}_e(k)} \right|_{\hat{\underline{x}}_{ei}(k), \hat{\underline{u}}_e(k)} \quad (6.12b)$$

Thus, the EKF algorithm can be given in the following recursive relations;

$$\underline{N}_i(k) = \underline{F}_{ei}(k) \underline{P}_i(k) \underline{F}_{ei}^T(k) + \underline{F}_{ui}(k) \underline{D}_u \underline{F}_{ui}^T(k) + \underline{Q}_i \quad (6.13a)$$

$$\underline{P}_i(k+1) = \underline{N}_i(k) - \underline{N}_i(k) \underline{H}_e^T (\underline{D}_\xi + \underline{H}_e \underline{N}_i(k) \underline{H}_e^T)^{-1} \underline{H}_e \underline{N}_i(k) \quad (6.13b)$$

$$\hat{\underline{x}}_{ei}(k+1) = \hat{\underline{f}}_{ei}(\underline{x}_{ei}(k), \hat{\underline{u}}_e(k)) + \underline{P}_i(k+1) \underline{H}_e^T \underline{D}_\xi^{-1} (\underline{Z}(k) - \underline{H}_e \hat{\underline{x}}_{ei}(k)) \quad (6.13c)$$

Where, \underline{Q}_i is the covariance matrix of the system noise, namely model error. \underline{D}_ξ is the covariance matrix of the output noise, namely measurement noise. \underline{D}_u is the covariance matrix of the control input noise ($v_{s\alpha}$ and $v_{s\beta}$), namely input noise. \underline{P}_i and \underline{N}_i : covariance matrix of state estimation error and extrapolation error, respectively.

The flowchart of Braided EKF algorithm [20] is given in Fig. 6.2, demonstrating the consecutive use of the two EKF algorithms; thus, while one algorithm estimates R_s and the other, R_r , both algorithms also estimate load torque, velocity, flux and current components as the common states. After the initialization of the states, the algorithms are run by switching them on and off consecutively and at each sampling interval. The final values of $\underline{P}_i(k+1)$ and $\hat{\underline{x}}_{ei}(k+1)$ calculated for one EKF algorithm at the end of each switching period are passed over to the next EKF algorithm as the initial values of the covariances and states. The resistance, - R_s or R_r - estimated during the previous period is also passed on to the next EKF algorithm and is assumed to be constant in the new EKF model throughout the whole switching period.

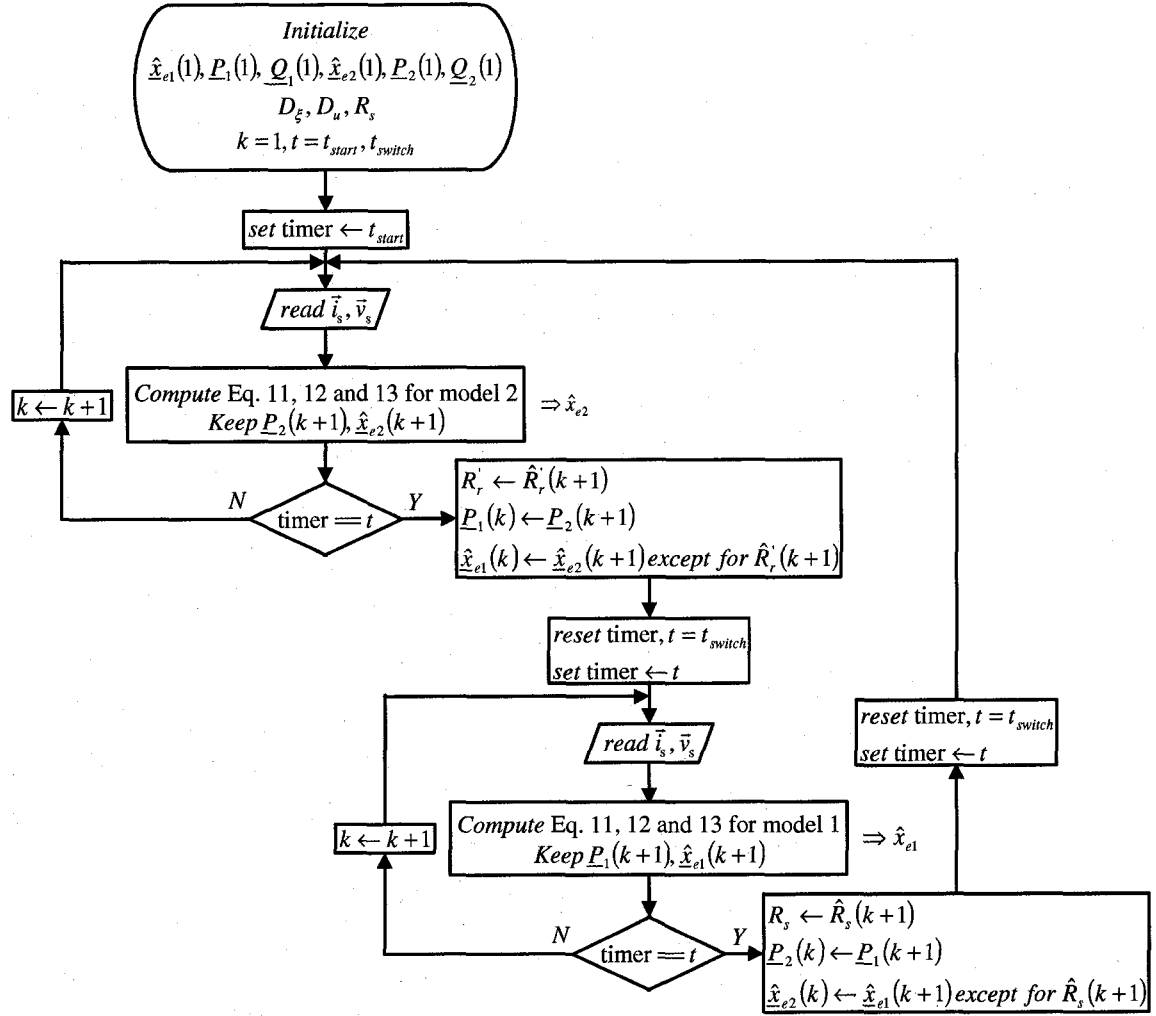


Fig. 6.2 Flow-chart of the Braided EKF algorithm.

6.4 Simulation Results and Observations

To test the performance of the proposed SM position control system, simulations were performed on an IM with the following rated parameters;

$$R_{sN} = 2.283 \Omega, \quad R_{rN} = 2.133 \Omega, \quad L_s = 0.23 H, \quad L_r = 0.23 H, \quad L_m = 0.22 H,$$

$$J_L = 0.005 \text{ kg.m}^2, \quad p_p = 2, \quad t_{LN} = 20 \text{ Nm}, \quad N_{mN} = 1430 \text{ rpm}$$

$$\beta_L = 0.001 \text{ Nm/(rad/s)} \text{ (total viscous friction coefficient),}$$

For a good evaluation of the novel reduced chattering SMC, its performance is compared with the chattering-free SMC (CF-SMC) developed in [16] with the following control input laws;

$$i_{sd}(k) = i_{sd}(k-1) + \frac{[(1+D_d T)\sigma_d(k) - \sigma_d(k-1)]}{k_s T} \quad (6.14a)$$

$$i_{sq}(k) = i_{sq}(k-1) + \frac{[(1+D_q T)\sigma_q(k) - \sigma_q(k-1)]}{k_7 T |\psi_r|^{ref}} \quad (6.14b)$$

(where $D_d > 0$, $D_q > 0$, and T is sampling time.)

Design parameters for the SMCs are as below:

$$k_d = 0.015, k_q = 0.010, n_d = n_q = 0.5, c = 17, D_d = 1, D_q = 50$$

The system covariance matrixes used in the Braided EKF algorithm are follows:

$$\underline{Q}_i = \text{diag}(10^{-9} \quad 10^{-9} \quad 10^{-9} \quad 10^{-9} \quad 10^{-4} \quad 10^{-4} \quad 10^{-5})$$

$$\underline{P}_i = \text{diag}(9 \quad 9 \quad 9 \quad 9 \quad 9 \quad 9 \quad 9)$$

Variances, $\underline{D}_\xi = \text{diag}\{10^{-6}[A^2] \quad 10^{-6}[A^2]\}$ and $\underline{D}_u = \text{diag}\{10^{-6}[V^2] \quad 10^{-6}[V^2]\}$

Sampling time, $T = 100 \mu s$.

To test the performance of the developed schemes, simulations are performed for 3 different scenarios; In the *first scenario*, the position reference, θ_m^{ref} , is stepped up gradually from 0.5 [rad] to 1.5 [rad] with rated load and rated parameters of the IM. Moreover, in order to test the performance of the controllers under parameter variations at $t=2$ [sec], $\bar{k}_5 = \frac{R_r}{L_r} L_m$ and $\bar{k}_7 = \frac{3}{2} \frac{p_p}{J_L} \frac{L_m}{L_r}$ are increased to $5 \times \bar{k}_5$ and $5 \times \bar{k}_7$. The resulting performances of the two SMC schemes for position and flux control are demonstrated in Fig. 6.3 (a) and (b), respectively.

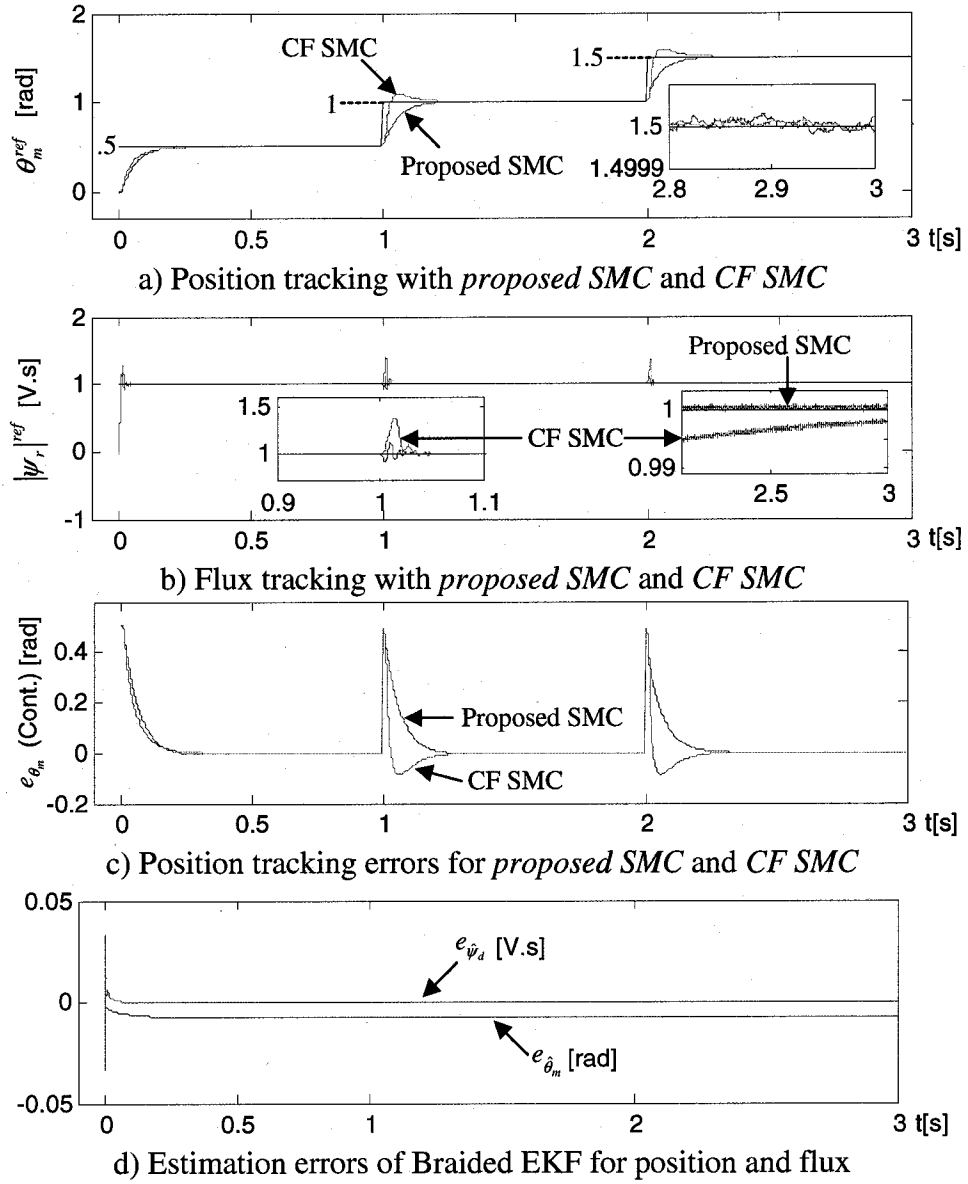


Fig. 6.3 Step-type tracking performance for proposed SMC and CF SMC

While Fig. 6.3 (c) depicts position tracking errors, e_{θ_m} , estimation errors for flux and position, $e_{\hat{\psi}_d}$ and $e_{\hat{\theta}_m}$, are given in Fig. 6.3 (d). The error signals, $e_{(\cdot)}$, give the deviations between the actual and estimated states. Comparing the performances of both SMCs under step-type changes in the position reference and parameters, it can be noted that the

proposed SMC demonstrates improved performance robustness under uncertainties imposed onto the system.

The controllers are also tested for sinusoidal type position references with similar changes in the reference and parameters as before. The results depicted in Fig. 6.4 demonstrate the improved performance of the proposed SMC particularly in transient state.

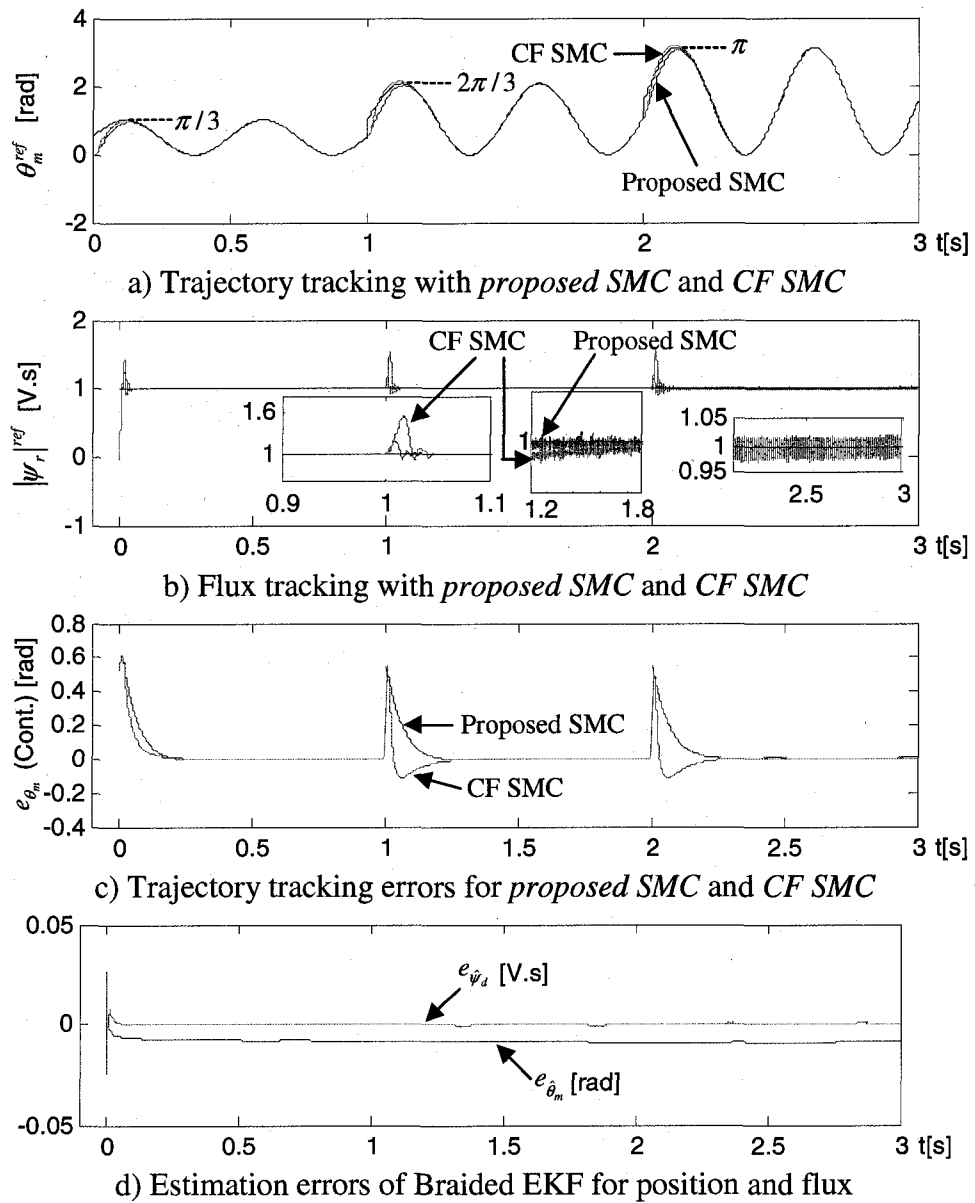


Fig. 6.4 Sinusoidal tracking performance for proposed SMC and CF SMC

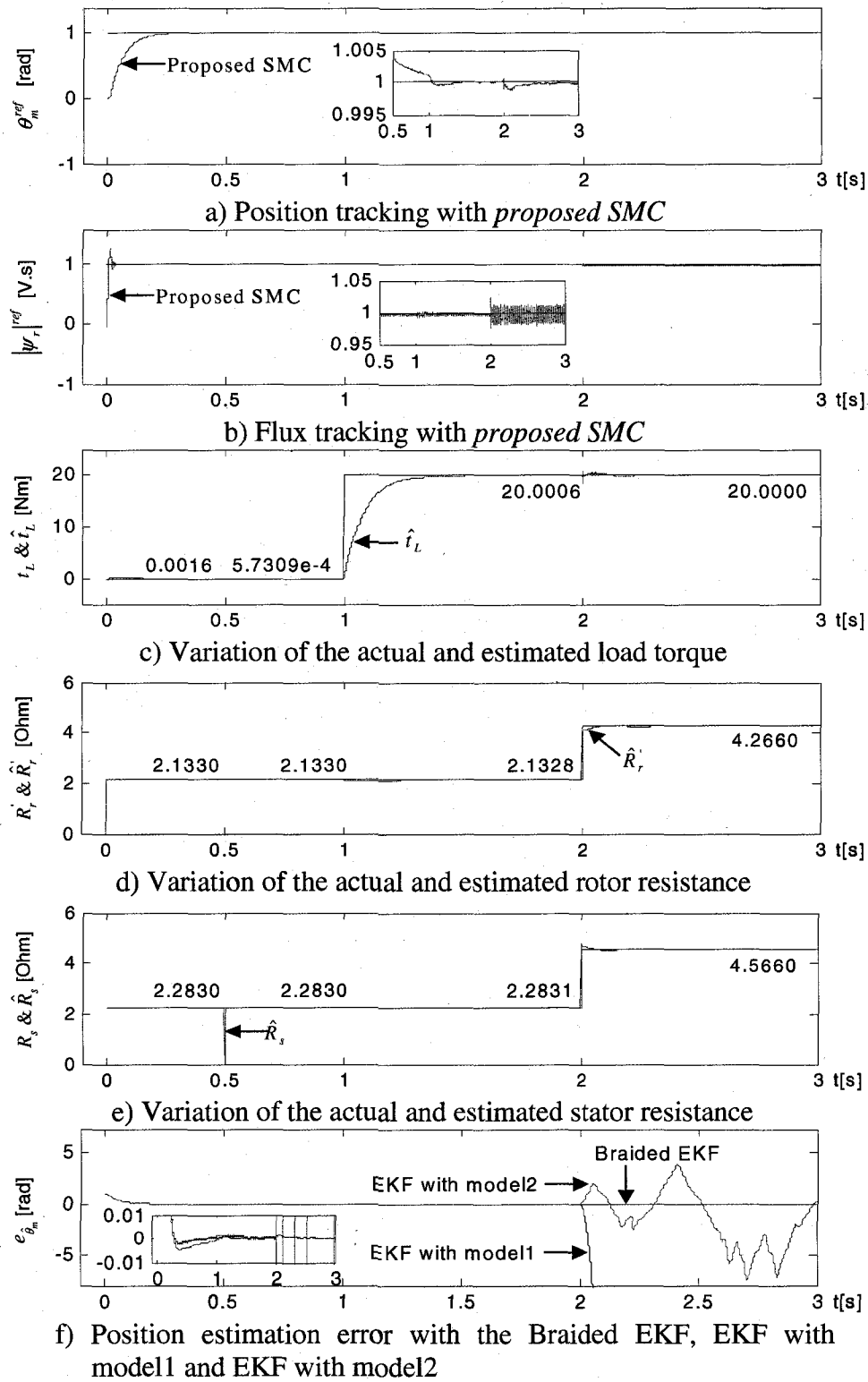


Fig. 6.5 The performance of the proposed SM control system under variation of stator resistance, rotor resistance and load torque variations.

Finally, simulations are performed to evaluate the proposed SMC performance under variations of 100 % in stator resistance, rotor resistance and load torque. To this aim, the IM is given a start for a unit step reference under no-load at rated parameters. Then, t_L and R_s & R_r are stepped up to $t_L = t_{LN}$ at 1 [sec] and at 2 [sec] $R_s \rightarrow 2 \times R_{sN}$ & $R_r \rightarrow 2 \times R_{rN}$, respectively. After 0.5 [sec], EKF with model1 and EKF with model2 are run by switching them on and off consecutively. The resulting position and tracking performance of the proposed SMC are given in Fig. 6.5 (a) and (b), respectively. Fig. 6.5 (b), (c), (d), and (e) depict the variations of the actual and estimated load torque (t_L & \hat{t}_L), actual and estimated rotor resistance (R_r & \hat{R}_r), and actual and estimated stator resistance (R_s & \hat{R}_s), respectively. Fig. 6.5 (f) demonstrates the comparative performance of the Braided EKF scheme, EKF with model1 (R_s estimation only) and EKF with model2 (with R_r estimation only). Inspection of the results demonstrates that the proposed SMC scheme combined with the Braided EKF estimation technique yields superior performance even under zero frequency, zero load conditions as can be seen in the interval $0 \leq t < 1$.

6.5 Conclusion

In this study, a sensorless sliding mode position control method is developed for the rotor flux oriented Direct Vector Control (DVC) of IM. The new sliding mode controller is a combination of power rate reaching law and average-equivalent control law, and aims to maintain robustness and increased accuracy by decreasing the chattering effect. The obtained simulation results for step- and sinusoidal-type reference trajectories demonstrate that the proposed sensorless sliding mode position control system can perform well even under 100 % variations of the stator resistance, rotor resistance and load torque. The method is also demonstrated to be more robust in comparison to the chattering-free SMC used in the sensorless position control of IMs in [16].

References

- [1] K.J. Astrom and T. Hagglund, "The future of PID control," *Control Engineering Practice*, vol. 9, no. 11, Nov. 2001, pp. 1163-1175.
- [2] D.D. Kukolj, S.B. Kuzmanovi, and E. Levi, "Design of a PID-like compound fuzzy logic controller," *Engineering Applications of Artificial Intelligence*, vol. 14, no. 6, Dec. 2001, pp. 785-803.
- [3] S.-M. Kim and W.-Y. Han, "Induction motor servo drive using robust PID-like neuro-fuzzy controller," *Control Engineering Practice*, vol. 14, no. 5, May 2006, pp. 481-487.
- [4] B. Heber, X. Longya, and Y. Tang, "Fuzzy logic enhanced speed control of an indirect field-oriented induction machine drive," *IEEE Transactions on Power Electronics*, vol. 12, no. 5, Sept. 1997, pp. 772-778.
- [5] R.-J Wai, "Supervisory genetic evolution control for indirect field-oriented induction motor drive," *IEE Proceedings-Electric Power Applications*, vol. 150, no. 2, March 2003, pp. 215-226.
- [6] R.-J. Wai and H.-H. Chang, "Backstepping wavelet neural network control for indirect field-oriented induction motor drive," *IEEE Transactions on Neural Networks*, vol. 15, no. 2, March 2004, pp. 367-382.
- [7] T. Khaorapapong and P. Ariyadirek, "Application of fuzzy logic in the position control of induction motor for bending and cutting machine," in *Proc. IEEE-ISCIT 2004*, vol. 1, 2004, pp. 378-382.
- [8] V.I. Utkin, "Sliding mode control design principles and applications to electric drives," *IEEE Transactions on Industrial Electronics*, vol. 40, no. 1, Feb. 1993, pp. 23-36.
- [9] J.Y. Hung, W. Gao , and J.C. Hung, "Variable structure control: a survey," *IEEE Transactions on Industrial Electronics*, vol. 40, no. 1, Feb. 1993, pp. 2-22.

- [10] O. Kaynak, K. Erbatur and M. Ertugrul, "The fusion of computationally intelligent methodologies and sliding-mode control-a survey," *IEEE Transactions on Industrial Electronics*, vol. 48, no. 1, Feb. 2001, pp. 4-17.
- [11] L.-G. Shiau and J.-L. Lin, "Stability of sliding-mode current control for high performance induction motor position drives," *IEE Proceedings-Electric Power Applications*, vol. 148, no. 1, Jan. 2001, pp. 69-75.
- [12] M.W. Dunnigan, S. Wade, B.W. Williams, and X. Yu, "Position control of a vector controlled induction machine using Slotine's sliding mode control approach," *IEE Proceedings-Electric Power Applications*, vol. 145, no. 3, May 1998, pp. 231-238.
- [13] Y. Xia, X. Yu and W. Oghanna, "Adaptive robust fast control for induction motors," *IEEE Transactions on Industrial Electronics*, vol. 47, no. 4, Aug. 2000, pp. 854-862.
- [14] K.B. Goh, M.W. Dunnigan, and B.W. Williams, "Sliding mode position control of a vector-controlled induction machine with nonlinear load dynamics," in *Proc. IEEE-PEMD 2004*, vol. 1, 2004 pp. 87-92.
- [15] W.-J. Wang and J.-Y. Chen, "Passivity-based sliding mode position control for induction motor drives," *IEEE Transactions on Energy Conversion*, vol. 20, no. 2, June 2005, pp. 316-321.
- [16] C. Sahin, A. Sabanovic, and M. Gokasan, "Robust position control based on chattering-free sliding modes for induction motors," in *Proc. IEEE-IECON*, vol. 1, 1995, pp. 512-517.
- [17] A. Suyitno, J. Fujikawa, H. Kobayashi, and Y. Dote, "Variable-structured robust controller by fuzzy logic for servomotors," *IEEE Transactions on Industrial Electronics*, vol. 40, no. 1, Feb. 1993, pp. 80-88.
- [18] S. Bogosyan, M. Gokasan, and A. Sabanovic, "Robust-Adaptive Linearization with Torque Ripple Minimization for a PMSM Driven Single Link Arm," in *Proc. IEEE-IECON'97 Annual Meeting*, vol. 1, 1997, pp. 102-107.

- [19] S. Bogosyan, M. Gokasan, and E.M. Jafarov, "A sliding mode controllers for a nonlinear time-varying motion control system", in *Proc. IEEE-IECON'99 Annual Meeting*, vol. 2, 1999, pp. 1008–1013.

- [20] M. Barut, S. Bogosyan, and M. Gokasan, "Experimental evaluation of Braided EKF for sensorless control of induction motors," *IEEE Transactions on Industrial Electronics*. (In press)

Chapter 7:

General Conclusion

In this thesis, novel control and estimation algorithms were developed to address the well-known problems related to the sensorless position and velocity control of induction motors (IMs). Challenges holding the low cost, low maintenance IMs back from being a more viable choice, in comparison to their high cost permanent-magnet rotor competitors, in demanding high performance motion control applications are the following characteristics inherent to IMs and their control:

- *Position control requires reliable performance particularly in low and zero speed operation, with and without load. The major challenge in IM sensorless position and velocity control lies in the fact that the sole source of feedback, which is the stator current, ceases to convey information on the rotor due to the reduced levels of rotor currents and voltages around zero stator frequency. Therefore, most past studies in sensorless position control present no results for zero speed and zero load operation although good results are obtained under different combinations of load torque and velocity.*
- *Significant parameter variations exist in an already highly nonlinear system with model uncertainties, the most effective of which are the temperature and frequency based variations of the stator and rotor resistances. This is defined as the major source of IM model uncertainties on the electrical side. Most past studies in sensorless IM estimation and control take into consideration either one of the two uncertainties and only very few deal with both.*
- *There are mechanical uncertainties related to load torque and various types of friction, which is common to all motion control systems. Although several studies have dealt with load torque uncertainties in IMs, to the authors' knowledge, there is no IM sensorless position control study addressing problems related to friction.*

- *Conditions and challenges arise related to the simultaneous estimation of a high number of parameters due to the lack of persistency of excitation in steady-state and hence, the loss of estimation accuracy. The few studies with acceptable results in simultaneous R_s and R_r' estimation have used different algorithms for different parameters and/or used signal injection, which is a source for other problems.*
- *Signal acquisition errors and noise, particularly at low and zero speed operation are also a problem.*

Resulting performances and outcomes of the proposed algorithms are:

- ◆ Results obtained over a large speed range via *Studies 1 & 2* indicate the expected benefits of the approach, also including zero speed, zero load torque operation, which was depicted as being problematic in most past literature (Holtz, 2000; Holtz 2006) on sensorless control. However, the experiments have also demonstrated the well-known effects of the rotor resistance uncertainties, indicating a requirement for the estimation of both resistances in high performance sensorless motion control with IMs.
- ◆ A significant improvement has been achieved with the estimation scheme in *Study 3* which combines the EKF scheme with a look up table for R_r' . Experimental results taken under challenging parameter and load variations over a whole velocity range, including zero speed, motivate the utilization of the approach in practice, in cases where one single EKF might not be adequate to handle the high number of parameters to be estimated, thereby compromising estimation accuracy. Nevertheless, the performance of the approach has to be further improved by increasing the “sensitivity” of the R_r' look-up table to velocity, torque and temperature variations or, even better, by incorporating a second on-line EKF scheme which runs in parallel or consecutively with the first, to estimate the additional parameters.

- ◆ The performance of the novel Switching EKF algorithm in *Study 4* to address the above mentioned problems is tested in the high, very low and zero speed regions with different scenarios developed by giving step-type and linear variations to the load torque and angular velocity reference beside the step-type changes imposed on R_s and R_r' in simulations. As a result, the simultaneous estimation of R_s and R_r' with the new algorithm has yielded a better performance in comparison to individual EKF- \hat{R}_s and EKF- \hat{R}_r' algorithms, which conduct R_s or R_r' estimation only.

The motivation for the development of the novel EKF scheme based on the switching of algorithms every n sampling periods ($n \times T$) is mostly to perform the estimation of a high number of parameters, preferably with relatively slow variation rates; however, the motivation also stems from an interest to investigate the limits of the switching algorithm when the number of EKFs are increased beyond two. Thus, the good results obtained for $100 \times T$ also suggest the possibility of using more than two EKFs in the switching algorithm if it is required to estimate a higher number of parameters.

- ◆ The Braided EKF technique developed in *Studies 5* and *6* aims for an even higher estimation accuracy when fast changing parameters are involved, such as rotor resistances. Experimental results taken with this method in the low and high speed range for the DVC of IMs in *Study 5*, and also at zero speed for DTC of IMs in *Study 6* demonstrate the expected performance of the braided algorithm in a wide speed range with significantly increased accuracy in the estimation of flux and velocity, in comparison to other approaches taken in previous studies or the single EKF algorithms which estimate R_s or R_r' only.

The results obtained with both Braided and Switching EKF schemes motivate the utilization of the proposed estimation technique in combination with a variety of

control methods for IMs or other motion control applications which require the accurate knowledge of a large number of parameters.

- ◆ An important advantage of the proposed method, which includes more than one EKF algorithm, over previous methods is that R_s and R_r' estimations can be performed both in transient and steady state under large load and speed variations without any signal injection.
- ◆ For all of the estimation methods developed in this thesis, it has been observed that the estimation of the velocity via the equation of motion is another factor that helps reflect the rotor information to the stator side, especially at zero speed and zero load torque operation, without the need for injecting any high frequency signal and white noise. This issue has been depicted as being problematic in most of the previous literature (Holtz, 2000; Holtz, 2006) on sensorless control of IMs.
- ◆ Another benefit of the proposed estimation techniques in this thesis is the approach taken for the estimation of the viscous and Coulomb friction at constant velocity in steady-state. The estimation of the load torque as a constant state in all EKF schemes also helps in the accurate determination of the friction effects in steady-state, which is known to be a performance deteriorating factor in motion control.
- ◆ The new reduced chattering SMC in *Study 7* is compared against a previously developed chattering-free SMC, which is proven to be effective in various motion control applications as well as in sensorless position control of IMs. The simulation results demonstrate an improved robustness in the system response against parameter and load variations. The new Braided EKF technique used in combination with the proposed sliding mode position control also gives rise to higher robustness when compared with the chattering-free SMC in Sahin et al. (1995), under challenging variations of 100% in load and stator and rotor resistance, and also at persistent zero

speed operation. This operation mode is not addressed at all in Sahin et al. (1995), which combines chattering-free SMC and estimation.

Some suggestions for future work are listed below:

- ◆ Uncertainties of the magnetizing inductance and inertia also have important effects on the high performance motion control of IMs. In this dissertation, all velocity and position control applications consider a constant and well-known inertia value and negligible saturation. However, in most motion control applications inertia variation is to be expected. Also, the magnetizing inductance of IMs tends to decrease with saturation; this effect becomes crucial especially at very low and zero speed. Therefore, for certain motion control applications, Braided or Switching EKF algorithms should be developed to estimate the inertia and magnetic inductance as well.
- ◆ An interesting point open for research is the determination of the covariance matrix related to the model error in EKFs. In order to achieve a desired transient and steady state performance for the estimated states and parameters, values of the covariance matrix usually have been found by trial-and-error methods as in this thesis. This procedure may become highly time consuming as the number of estimated states and parameters increase. Hence, the development of a systematic method of determining these matrix components could be an important breakthrough for EKF algorithms in general.
- ◆ Additional improvements could be made in calculating the control design parameters for the SMC based on adaptive or intelligent methods.

In summary, this thesis offers novel and flexible solutions for sensorless speed or position control of IMs in order to increase robustness to the variations in rotor or/and stator resistance beside load torque including friction effects, particularly Coulomb and

viscous friction at the steady-state. The proposed methods offer solutions for estimation and control over the whole speed range including persistent zero speed operation, which is regarded as highly problematic (Holtz, 2000; Faiz and Sharifian, 2001; Holtz, 2002; Holtz and Quan, 2003; Rashed and Stronach, 2004; Holtz, 2006).

Finally, the novel EKF based estimation techniques in the scope of this work could be used with a variety of other methods applied to the sensorless speed and position control of IMs or other electrical machines, which require the accurate knowledge of a large number of parameters. Similarly, the developed SMC scheme with reduced chattering could offer high robustness and accuracy in many demanding motion control applications.

References

- Faiz, J. and Sharifian, M.B.B. (2001), "Different techniques for real time estimation of an induction motor rotor resistance in sensorless direct torque control for electric vehicle", *IEEE Transactions on Energy Conversion*, Vol. 16 No. 1, pp. 104–109.
- Holtz, J. (2000), "Sensorless control of induction motors-performance and limitations", *Proceedings of the IEEE-ISIE 2000 Annual Meeting*, Vol. 1, pp. PL12–PL20.
- Holtz, J. (2002), "Sensorless control of induction motor drives", *Proceedings of the IEEE*, Vol. 90 No.8, pp. 1359–1394.
- Holtz, J. and Quan, J. (2003), "Drift- and parameter-compensated flux estimator for persistent zero-stator-frequency operation of sensorless-controlled induction motors", *IEEE Transactions on Industry Applications*, Vol. 39 No. 4, pp. 1052–1060.
- Holtz, J. (2006), "Sensorless control of induction machines —with or without signal injection?", *IEEE Transactions on Industrial Electronics*, Vol. 53 No. 1, pp. 7–30.

Rashed, M. and Stronach, A.F. (2004) "A stable back-EMF MRAS-based sensorless low speed induction motor drive insensitive to stator resistance variation", *IEE Proceedings-Electric Power Applications*, Vol. 151 No.6, pp. 685–693.

Sahin, C., Sabanovic, A. and Gokasan, M. (1995), "Robust position control based on chattering-free sliding modes for induction motors", *Proceedings of the IEEE-IECON'95 Annual Meeting*, Vol. 1, pp. 512–517.

Appendix A:

Sensorless Estimation of Induction Motors in Wide Speed Range*

Abstract:

Purpose – This study aims an improved performance in the estimation of velocity and flux in the sensorless control of induction motors (IM) over a wide speed range, including low and zero speed.

Design/methodology/approach – Temperature and frequency dependent variations of stator (R_s) and rotor (R_r) resistances are very effective on estimation performance in sensorless control over a wide speed range. To this aim, an Extended Kalman Filter (EKF) is designed, which estimates the stator resistance, R_s , load torque, t_L , velocity and flux. To provide robustness against R_r variations, the extended model is also continuously updated with R_r values from a look-up table, built via EKF estimation (Barut et al., 2005).

Findings – As demonstrated by the experimental results, the estimated states and parameters undergo a very short transient and attain their steady-state values accurately, with no need for signal injection due to the inherent noise introduced by EKF.

Originality/value – The value of this study is in the development of an EKF based scheme, which solves the R_s - R_r estimation problem in IM sensorless control. The successful experimental results obtained with the combined EKF and look-up table approach also offer a solution to all EKF based estimation schemes which involve a high number of estimated parameters, hence, compromising estimation accuracy.

* Bogosyan, S., Barut, M., and Gokasan, M. (2006a), "Sensorless estimation of induction motors in wide speed range", *The International Journal for Computation and Mathematics in Electrical and Electronic Engineering (COMPEL)*. (In review)

Index Terms – *EKF estimation, sensorless-speed control, low/zero speed operation, stator resistance and load torque estimation, rotor resistance, look-up table.*

A.1 Introduction

Sensorless vector control (Guidi and Umida, 2000) and direct torque control (DTC) (Lascu et al., 2004) of induction motors (IMs) require the accurate estimation of speed and torque, as well as the rotor or stator flux. The performance of estimation and hence, the success of sensorless control in IMs is also dependent on the accurate knowledge of parameters such as stator (R_s) (Holtz 2005) and rotor resistances (R_r) (Barut et al., 2002; Wang et al. 2005) that vary significantly with temperature and frequency, respectively.

In this study, for the accurate estimation of velocity and flux in IM sensorless control over a wide speed range, an EKF scheme is developed to estimate R_s and load torque (t_L), beside velocity and flux. To further improve estimation accuracy, the extended model of the EKF algorithm is continuously updated with R_r values from a look-up table, also built using EKF estimation from the authors' previous study (Barut et al., 2005). The experimental results taken under challenging parameter and load variations demonstrate the improved estimation accuracy of velocity and flux achieved with the EKF based estimation scheme.

A.2 Extended Mathematical Model of the IM

Speed-sensorless control schemes developed for IM require the estimation of rotor flux components, $\psi_{r\alpha}$, $\psi_{r\beta}$, angular velocity, ω_m and stator current components $i_{s\alpha}$ and $i_{s\beta}$, which are also measured as output. In this study, an EKF based estimation algorithm is developed against R_s , R_r and t_L variations, which are known to degrade the control performance. R_s is estimated on-line along with t_L , velocity, $\psi_{r\alpha}$, $\psi_{r\beta}$, $i_{s\alpha}$ and $i_{s\beta}$. The

latter two are also measured as outputs. The extended model is continuously updated from a look-up table developed via an EKF algorithm estimating R_r .

The extended model is derived as follows;

$$\begin{aligned}\dot{\underline{x}}_e(t) &= \underline{f}_e(\underline{x}_e(t), \underline{u}_e(t)) + \underline{w}_1(t) \\ &= \underline{A}_e(\underline{x}_e(t))\underline{x}_e(t) + \underline{B}_e\underline{u}_e(t) + \underline{w}_1(t)\end{aligned}\quad (\text{A-1})$$

Here, the extended state vector is the $\underline{x}_e = (i_{s\alpha} \ i_{s\beta} \ \psi_{r\alpha} \ \psi_{r\beta} \ \omega_m \ t_L \ R_s)^T$. \underline{f}_e is the nonlinear function of the states and inputs. \underline{A}_e is the system matrix. \underline{u}_e is the control input vector. \underline{B}_e is the input matrix. \underline{w}_1 is the process noise representing modeling error due to the uncertain parameters/states.

The constant state used for the load torque aims to capture system uncertainties of constant nature i.e. Coulomb and viscous friction at steady-state:

$$\begin{aligned}\begin{bmatrix} \dot{i}_{s\alpha} \\ \dot{i}_{s\beta} \\ \dot{\psi}_{r\alpha} \\ \dot{\psi}_{r\beta} \\ \dot{\omega}_m \\ \dot{t}_L \\ \dot{R}_s \end{bmatrix}_{\underline{\dot{x}}_e} &= \underbrace{\begin{bmatrix} -\left(\frac{R_s}{L_\sigma} + \frac{L_m^2 R_r}{L_\sigma L_r^2}\right) & 0 & \frac{L_m \dot{R}_r}{L_\sigma L_r^2} & \frac{L_m}{L_\sigma L_r} p_p \omega_m & 0 & 0 & 0 \\ 0 & -\left(\frac{R_s}{L_\sigma} + \frac{L_m^2 R_r}{L_\sigma L_r^2}\right) & -\frac{L_m}{L_\sigma L_r} p_p \omega_m & \frac{L_m \dot{R}_r}{L_\sigma L_r^2} & 0 & 0 & 0 \\ L_m \frac{\dot{R}_r}{L_r} & 0 & \frac{\dot{R}_r}{L_r} & -p_p \omega_m & 0 & 0 & 0 \\ 0 & L_m \frac{\dot{R}_r}{L_r} & p_p \omega_m & \frac{\dot{R}_r}{L_r} & 0 & 0 & 0 \\ \frac{3 p_p L_m}{2 J_L L_r} \psi_{r\beta} & \frac{3 p_p L_m}{2 J_L L_r} \psi_{r\alpha} & 0 & 0 & 0 & \frac{1}{J_L} & 0 \\ 0 & 0 & 0 & 0 & 0 & 0 & 0 \\ 0 & 0 & 0 & 0 & 0 & 0 & 0 \end{bmatrix}}_{\underline{A}_e} \begin{bmatrix} i_{s\alpha} \\ i_{s\beta} \\ \psi_{r\alpha} \\ \psi_{r\beta} \\ \omega_m \\ t_L \\ R_s \end{bmatrix}_{\underline{x}_e} + \underbrace{\begin{bmatrix} \frac{1}{L_\sigma} & 0 \\ 0 & \frac{1}{L_\sigma} \\ 0 & 0 \\ 0 & 0 \\ 0 & 0 \\ 0 & 0 \\ 0 & 0 \end{bmatrix}}_{\underline{B}_e} \underbrace{\begin{bmatrix} v_{s\alpha} \\ v_{s\beta} \end{bmatrix}}_{\underline{u}_e} + \underline{w}_1(t)\end{aligned}\quad (\text{A-2})$$

$$\underline{Z}(t) = \underline{h}_e(\underline{x}_e(t)) + \underline{w}_2(t) \text{ (measurement equation)} = \underline{H}_e \underline{x}_e(t) + \underline{w}_2(t)$$

$$= \underbrace{\begin{bmatrix} 1 & 0 & 0 & 0 & 0 & 0 & 0 \\ 0 & 1 & 0 & 0 & 0 & 0 & 0 \end{bmatrix}}_{H_e} \begin{bmatrix} i_{s\alpha} \\ i_{s\beta} \\ \psi_{r\alpha} \\ \psi_{r\beta} \\ \omega_m \\ t_L \\ R_s \end{bmatrix} + \underline{w}_2(t) \quad (\text{A-3})$$

where \underline{h}_e is the function of the outputs. \underline{H}_e is the measurement matrix. \underline{w}_2 is the measurement noise (error). p_p is the number of pole pairs. $L_\sigma = \sigma L_s$ is the stator transient inductance. σ is the leakage or coupling factor. L_s and R_s are the stator inductance and resistance, respectively. L_r and R_r are the rotor inductance and resistance, referred to the stator side, respectively. $v_{s\alpha}$ and $v_{s\beta}$ are the stator stationary axis components of stator voltages.

A.3 Development of the EKF Algorithm

An EKF algorithm is developed for the estimation of the states in the extended IM model given in (A-2) and (A-3), to be used in the sensorless control of the IM using measured phase currents and voltage values. The Kalman filter is a well-known recursive algorithm that takes the stochastic state-space model of the system together with measured outputs to achieve the optimal estimation of states (Chen and Dunnigan, 2002) in multi-input, multi-output systems. The filter takes system and measurement noises into account in the form of white noise. The optimality of the state estimation is achieved with the minimization of the mean estimation error. The process requires the discretization of (A-2) and (A-3) as below;

$$\underline{x}_e(k+1) = \underline{f}_e(\underline{x}_e(k), \underline{u}_e(k)) + \underline{w}_1(k) \quad (\text{A-4})$$

$$\underline{Z}(k) = \underline{H}_e \underline{x}_e(k) + \underline{w}_2(k) \quad (\text{A-5})$$

The EKF uses the current estimation of states $\hat{\underline{x}}_e(k)$ and $\hat{\underline{u}}_e(k)$ to derive the Jacobien matrices for the linearization of (A-4) and (A-5), as below;

$$\underline{F}_e(k) = \left. \frac{\partial \underline{f}_e(\underline{x}_e(k), \underline{u}_e(k))}{\partial \underline{x}_e(k)} \right|_{\hat{\underline{x}}_e(k), \hat{\underline{u}}_e(k)} \quad (\text{A-6})$$

$$\underline{F}_u(k) = \left. \frac{\partial \underline{f}_e(\underline{x}_e(k), \underline{u}_e(k))}{\partial \underline{u}_e(k)} \right|_{\hat{\underline{x}}_e(k), \hat{\underline{u}}_e(k)} \quad (\text{A-7})$$

Thus, the EKF algorithm can be given in the following recursive relations (Bogosyan et al., 2001):

$$\underline{N}(k) = \underline{F}_e(k) \underline{P}(k) \underline{F}_e(k)^T + \underline{F}_u(k) \underline{D}_u \underline{F}_u(k)^T + \underline{Q} \quad (\text{A-8a})$$

$$\underline{P}(k+1) = \underline{N}(k) - \underline{N}(k) \underline{H}_e^T (\underline{D}_\xi + \underline{H}_e \underline{N}(k) \underline{H}_e^T)^{-1} \underline{H}_e \underline{N}(k) \quad (\text{A-8b})$$

$$\hat{\underline{x}}_e(k+1) = \hat{\underline{f}}_e(\underline{x}_e(k), \underline{u}_e(k)) + \underline{P}(k+1) \underline{H}_e^T \underline{D}_\xi^{-1} (\underline{Z}(k) - \underline{H}_e \hat{\underline{x}}_e(k)) \quad (\text{A-8c})$$

Here, \underline{Q} : covariance matrix of the system noise, namely model error; \underline{D}_ξ : covariance matrix of the output noise, namely measurement noise; \underline{D}_u : covariance matrix of the control input noise ($v_{s\alpha}$ and $v_{s\beta}$), namely input noise; \underline{P} , \underline{N} : covariance matrix of state estimation error and extrapolation error, respectively.

The algorithm involves two main stages: prediction and filtering. In the prediction stage, the next predicted states $\hat{\underline{f}}_e(.)$ and predicted state error covariance matrices, $\underline{P}(.)$ and $\underline{N}(.)$ are processed, while in the filtering stage, next estimated states, $\hat{\underline{x}}_e(k+1)$, obtained as the sum of the next predicted states and the correction term (2nd term in (A-8c)) are calculated. The schematic representation of the new EKF algorithm is given in Fig. A-1. The algorithm also takes into account the frequency and temperature dependent

variations (Barut et al., 2005) of R_r' , by updating its value in the extended model via the *interpolation look-up table* as given in Table A-1. The (2-D) table is developed via the EKF algorithm in Barut et al. (2005) for the estimation of R_r' .

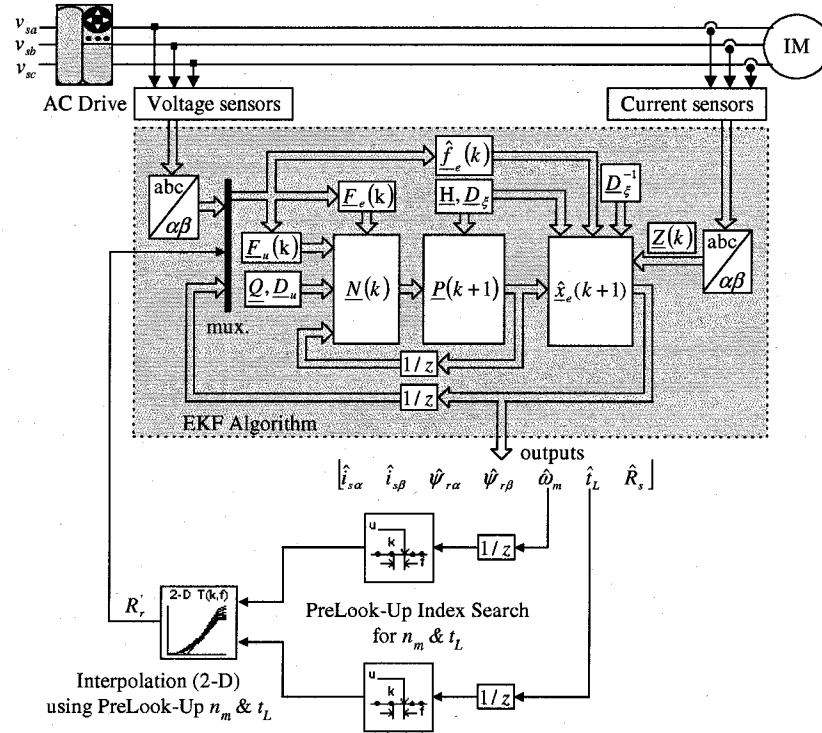


Fig. A-1 Structure of the proposed EKF algorithm

Table A-1. An interpolation (2-D) table with prelook-up index search to obtain variations in rotor resistance.

$t_L[Nm]/n_m[rpm]$	1.435	3.7	5.1	7.21	9.45	11.65	13.85	14.9	17.2	19.4
8.5	0.085Ω	0.085Ω	0.085Ω	0.085Ω	0.085Ω	0.085Ω	0.085Ω	0.085Ω	0.085Ω	0.085Ω
150	0.113Ω	0.115Ω	0.115Ω	0.121Ω	0.121Ω	0.123Ω	0.125Ω	0.125Ω	0.126Ω	0.126Ω
200	0.13Ω	0.135Ω	0.135Ω	0.136Ω	0.145Ω	0.146Ω	0.146Ω	0.148Ω	0.149Ω	0.151Ω
300	0.18Ω	0.185Ω	0.19Ω	0.195Ω	0.2Ω	0.205Ω	0.21Ω	0.215Ω	0.22Ω	0.225Ω
400	0.25Ω	0.26Ω	0.262Ω	0.265Ω	0.27Ω	0.285Ω	0.295Ω	0.295Ω	0.305Ω	0.315Ω
500	0.335Ω	0.345Ω	0.35Ω	0.355Ω	0.366Ω	0.375Ω	0.385Ω	0.39Ω	0.405Ω	0.415
600	0.445Ω	0.455Ω	0.46Ω	0.47Ω	0.48Ω	0.495Ω	0.51Ω	0.515Ω	0.535Ω	0.55Ω
700	0.575Ω	0.582Ω	0.59Ω	0.605Ω	0.615Ω	0.635Ω	0.65Ω	0.66Ω	0.685Ω	0.71Ω
800	0.695Ω	0.7Ω	0.705Ω	0.71Ω	0.73Ω	0.755Ω	0.775Ω	0.795Ω	0.835Ω	0.885Ω
816	0.705Ω	0.71Ω	0.71Ω	0.715Ω	0.745Ω	0.765Ω	0.805Ω	0.82Ω	0.875Ω	0.915Ω

A.4 Hardware Configuration

The experimental test-bed for the EKF based estimator is given in Fig. A-2. The IM in consideration is a 3 phase, 4 poles, 3 HP/2.238 kW motor, the detailed specifications of which will be given in the experimental results. The EKF algorithm and all analog signals are developed and processed on a Power PC based DS1104 Controller Board, offering a 4-channel, 16-bit (multiplexed) ADC and four 12-bit ADC units. The controller board processes floating-point operations at a rate of 250 MHz. A torque transducer rated at 50 N.m and an encoder with 3600 counts/rev, is also used, but for evaluation purposes only and for the verification of the load torque and velocity estimations. The phase voltages and currents are measured with high band voltage and current sensors from LEM.

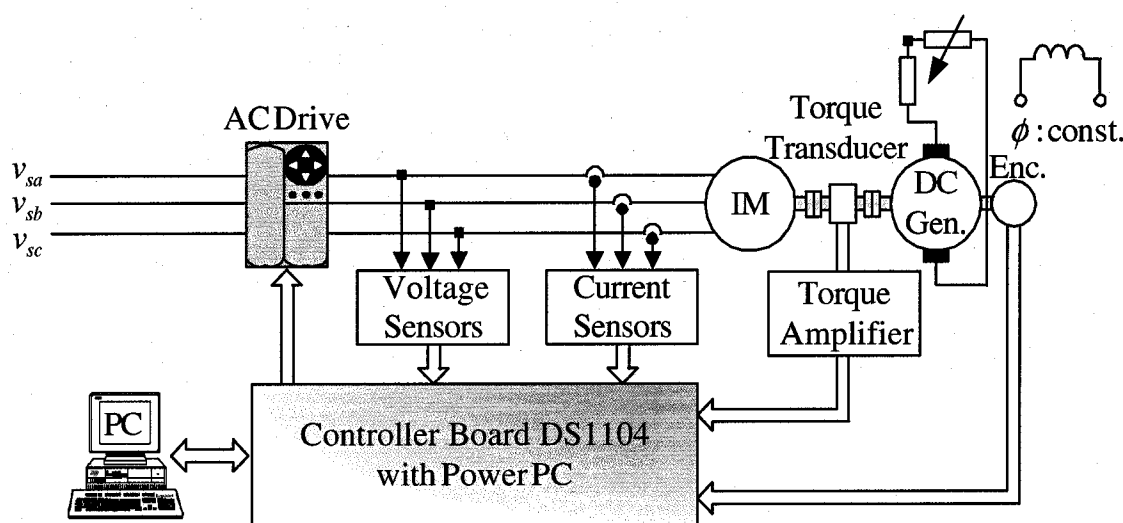


Fig. A-2 Schematic representation of the experimental setup

In the experiments, the IM is fed via an ac drive with a constant V/f PWM voltage instead of a sinusoidal input voltage to achieve a more realistic performance test. By using an ac drive in open-loop, voltages with different frequency values can be varied linearly with the acceleration and deceleration times of the driver, which also allows

velocity reversal. The load is generated through a DC machine operating in generator mode coupled to the IM. An array resistor connected to the armature terminals of the dc machine is used to vary the load torque applied to the IM, as $t_L = k_t^2 \omega / R$, where k_t is torque constant of dc machine, ω is angular velocity and R is the total resistance (switched array + armature). The value of the resistance is adjusted to 7.8 [Ω] to generate a load torque, t_L of 20.73 [N.m], at approximately 819 [rpm].

A.5 Experimental Results and Observations

The parameters for the IM and DC generator used in experiments are listed in Table A-2a and Table A-2b;

Table A-2a. Rated values and parameters of the induction motor used in the experiments.

P [kW]	f [Hz]	$* J_L$ [kg.m ²]	p_p	V [V]	I [A]
2.238	60	0.2595	4	230	12

R_s [Ω]	R_r [Ω]	L_s [H]	L_r [H]	L_m [H]	N_m [rpm]	t_L [Nm]
0.6619	0.7322	0.0375	0.0376	0.0334	850	25.1

* J_L : total inertia in the experimental test-bed.

Table A-2b. Rated values and parameters of the DC machine used in the experiments.

P [kW]	V [V]	I [A]	N_m [rpm]	t_L [Nm]
3	125	24	1150	24.91

The values of system parameters and covariance matrix elements are very effective on the performance of the EKF estimation. In this study, to avoid computational complexity, the covariance matrix of the system noise \underline{Q}_i is chosen in diagonal form, also satisfying the condition of positive definiteness. According to the Kalman filter theory, the \underline{Q}_i , $\underline{D}_\varepsilon$ (measurement error covariance matrix) and \underline{D}_u (input error covariance matrix) have to

be obtained by considering the stochastic properties of the corresponding noises (Vas, 1998). However, since these are usually not known, in most cases the covariance matrix elements are used as weighting factor or tuning parameters. In this study, for both EKF algorithms, the tuning of the initial values of the \underline{P}_i and \underline{Q}_i is done by trial-and-error to achieve a rapid initial convergence and the desired transient and steady state behaviors of the estimated states and parameters, while the \underline{D}_ξ and \underline{D}_u are determined taking into account the measurement errors of the current and voltage sensors and the quantization errors of the ADCs, as given below:

$$\begin{aligned}\underline{Q} &= \text{diag}\{10^{-10}[A^2] \quad 10^{-10}[A^2] \quad 4 \times 10^{-17}[(V.s)^2] \quad 4 \times 10^{-17}[(V.s)^2] \quad 10^{-14}[(rad/s)^2] \\ &\quad 10^{-15}[(Nm)^2] \quad 10^{-16}[\Omega^2]\} \\ \underline{P} &= \text{diag}\{1[A^2] \quad 1[A^2] \quad 1[(V.s)^2] \quad 1[(V.s)^2] \quad 1[(rad/s)^2] \quad 1[(Nm)^2] \quad 1[\Omega^2]\} \\ \underline{D}_\xi &= \text{diag}\{2.6 \times 10^{-4}[A^2] \quad 2.6 \times 10^{-4}[A^2]\} \\ \underline{D}_u &= \text{diag}\{2.3 \times 10^{-5}[V^2] \quad 2.3 \times 10^{-5}[V^2]\}\end{aligned}$$

The performance of the IM is tested in open-loop with PWM input voltages/currents given in Fig. A-3. The EKF algorithm takes as input the transformed components of the current and voltage. The following is a generalized description of this transformation;

$$x_\alpha = x_a; \quad x_\beta = (1/\sqrt{3})(x_b - x_c)$$

where x represents i and v for current and voltage, respectively. Fig. A-3 demonstrates the transformed current and voltage at 60 [Hz], 230 [V] for a t_L of approximately 21.06 [N.m].

First, the performance of the developed algorithm is experimentally evaluated under four scenarios at a sampling rate, $T_{sample} = 110 [\mu s]$.

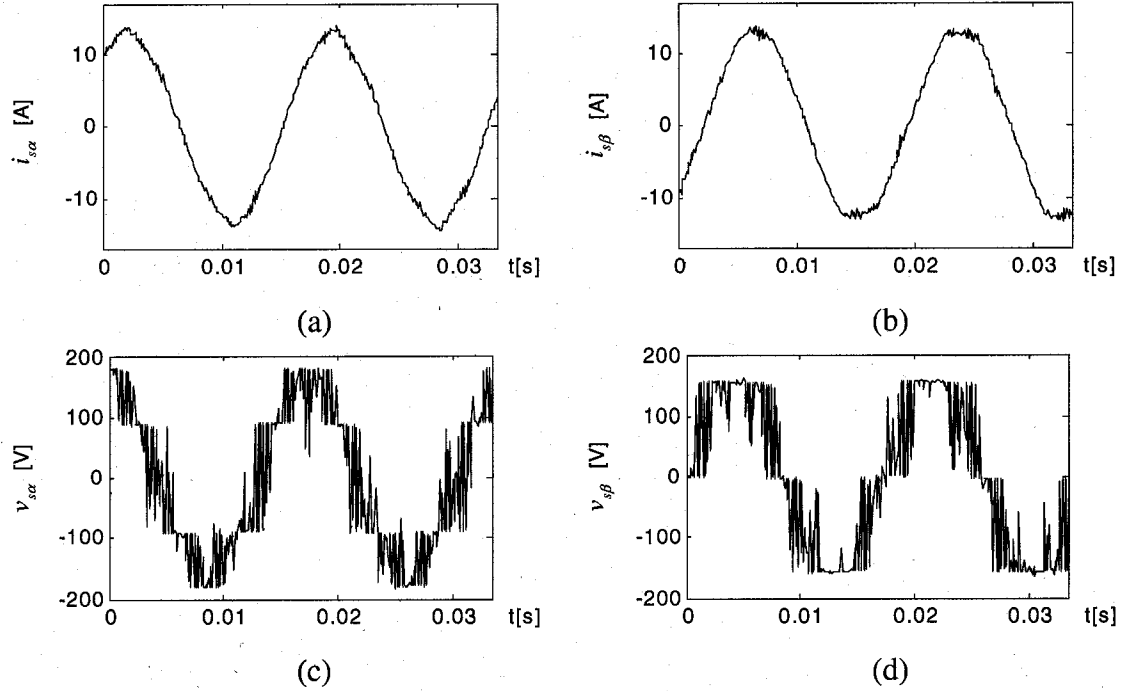


Fig. A-3 Stator currents and voltages applied to the IM through the AC drive

To demonstrate the need for R_s estimation for an improved estimation performance in IM sensorless control (even when R_r' is being updated), in scenarios where no R_s estimation is involved the EKF scheme developed in the authors' previous study (Barut et al., 2005) is used to update R_r' instead of the less dynamic look-up table. Thus, it is aimed to emphasize the need for R_s updates even when a more dynamic approach is taken towards R_r' updates. In scenarios or intervals where EKF based R_s estimation is switched on, the scheme uses R_r' updates from the look-up table instead of taking R_r' estimation from the EKF_ R_r' algorithm, as the high performance controller can not accommodate 2 EKF schemes running in parallel. The estimation of all states and parameters are started with an initial value of zero.

Scenario I– Performance of R_s -estimation with and without R_r' updates:

This scenario is developed to demonstrate the importance of R_r' updates on the performance of the EKF estimation scheme. To this aim, the IM is initially run at 849.6

[rpm] under no-load with R_s estimation only and using a constant initial value for R_r' . At $t = 13.3$ [sec.], the IM is loaded with 20.1 [N.m] via the dc generator, giving rise to a drop in the velocity to 818 [rpm]. To show the importance of R_r' updates on estimation performance, at $t=35.1$ [sec.], the R_r' - look-up table is switched on to provide continuous updates of R_r' and finally at $t = 58.6$ [sec.], the IM operation is switched to no-load by switching off the DC generator field supply.

The resulting performance is given in Fig. A-4(a), (b), (c), (d), (e), (f), (g), (h) and (i), which demonstrate the variations of n_m & \hat{n}_m , t_{ind} & \hat{t}_L , \hat{R}_s , \hat{R}_r , $\hat{\psi}_{r\alpha}$, $\hat{\psi}_{r\beta}$, $e_{n_m} \triangleq n_m - \hat{n}_m$, $e_{t_L} \triangleq t_{ind} - \hat{t}_L$ and the variation of $e_{i_{sa}}$ & $e_{i_{s\beta}}$; namely, the measured and estimated velocity, the induced torque as obtained from the torque-meter and estimated load torque, estimated stator resistance, estimated rotor resistance, the estimated α and β components of the rotor flux, estimation error of velocity, estimation error of load torque and the estimation errors in (i_{sa}) and $(i_{s\beta})$, respectively.

As can be seen from Fig. A-4(a), an error of 10 [rpm] has occurred in the estimation of velocity (with a corresponding error in the calculation of t_L) in the interval of $13.3[\text{sec.}] < t < 35.1[\text{sec.}]$; in this interval no updates are used for R_r' . However, once the look-up table is switched on for R_r' at $t=35.1$ [sec.], a significant improvement is achieved with the estimation of t_L and hence, with velocity.

Scenario II- Performance in 4 region operation:

This scenario aims to demonstrate the performance of the algorithm under ramp-type velocity/torque reversals. To this aim, the velocity/load torque are reversed by changing the input frequency from 60 [Hz] to -60 [Hz], while the motor is running at 816.5 [rpm] under 19.8 [N.m]. Then, the scenario is switched to its initial status by changing the input frequency from -60 [Hz] to 60 [Hz]. The slope of these variations is determined with the

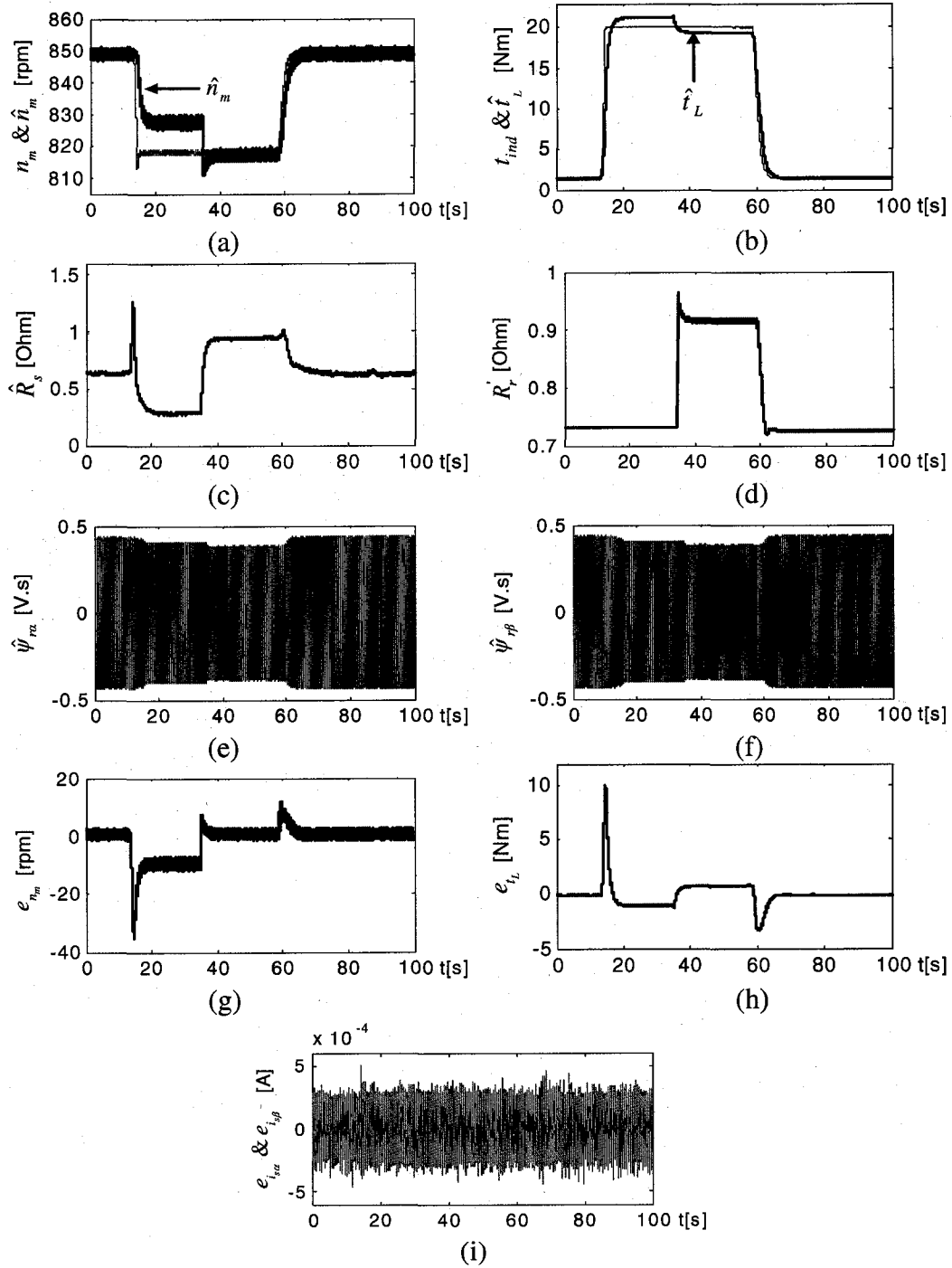


Fig. A-4 Experimental results demonstrating R_r update requirement: (a) Variation of n_m and \hat{n}_m ; (b) variation of t_{ind} and \hat{t}_L ; (c) variation of \hat{R}_s ; (d) variation of \hat{R}_r ; (e) variation of $\hat{\psi}_{r\alpha}$; (f) variation of $\hat{\psi}_{r\beta}$; (g) variation of e_{n_m} ; (h) variation of e_{t_L} ; and (i) variation of $e_{i_{\alpha}}$ & $e_{i_{\beta}}$

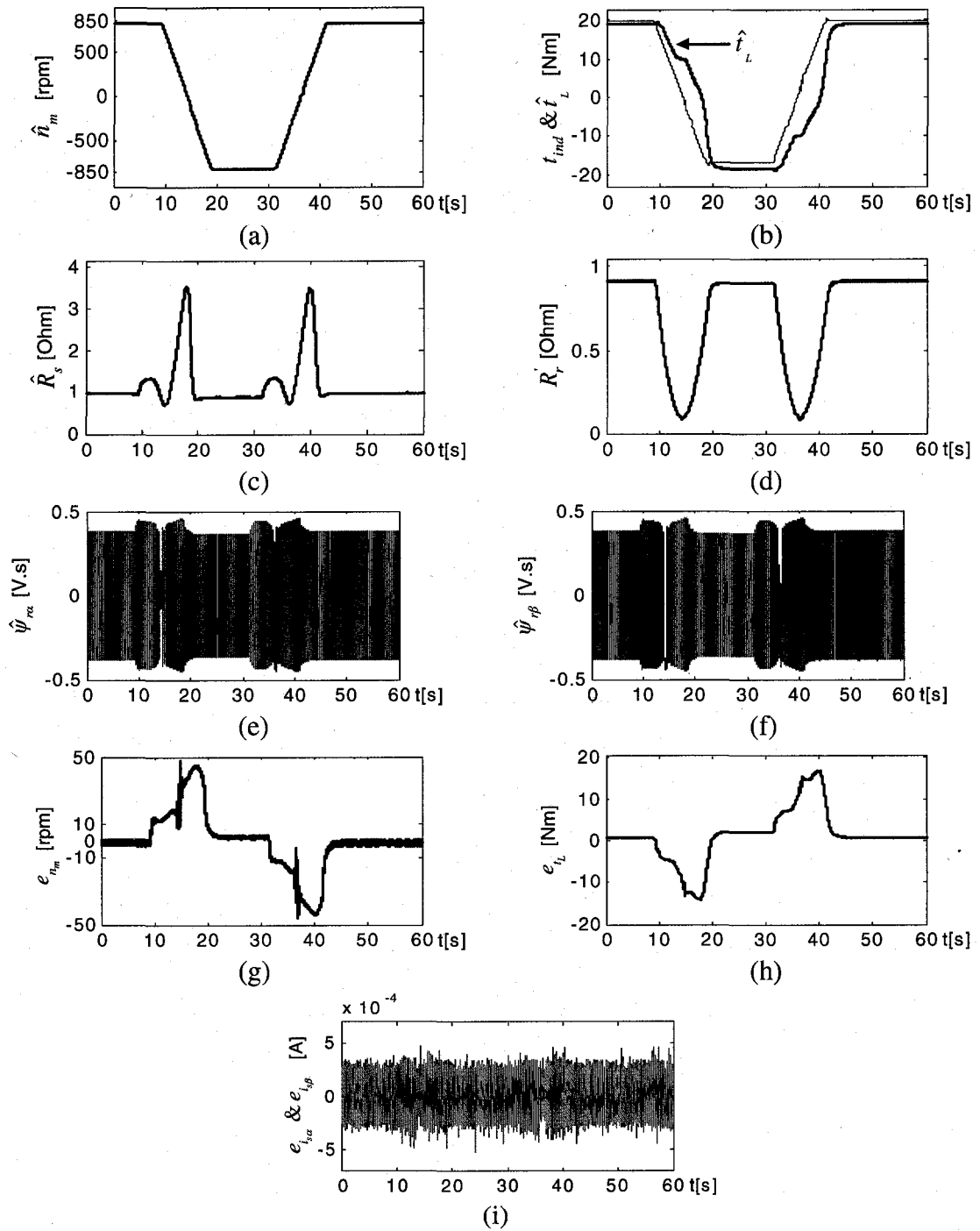


Fig. A-5 Experimental results demonstrating 4 region operation: (a) Variation of \hat{n}_m ; (b) variation of t_{ind} and \hat{t}_L ; (c) variation of \hat{R}_s ; (d) variation of R_r ; (e) variation of $\hat{\psi}_{ra}$; (f) variation of $\hat{\psi}_{r\beta}$; (g) variation of e_{n_m} ; (h) variation of e_{t_L} ; and (i) variation of $e_{i_{s\alpha}}$ & $e_{i_{s\beta}}$

arbitrary choice of the acceleration/deceleration rate given as an option on the ac drive. Fig. A-5(a), (b), (c), (d), (e), (f), (g), (h) and (i) demonstrate the variations of n_m & \hat{n}_m , t_{ind} & \hat{t}_L , \hat{R}_s , \hat{R}_r , $\hat{\psi}_{r\alpha}$, $\hat{\psi}_{r\beta}$, $e_{n_m} \triangleq n_m - \hat{n}_m$, $e_{t_L} \triangleq t_{ind} - \hat{t}_L$ and the variation of $e_{i_{s\alpha}}$ & $e_{i_{s\beta}}$.

Inspecting the results of this scenario, it can be noted that the load torque and velocity estimations track the variations of the measured torque/velocity in steady-state; however, during the transient state at velocity reversal, there is a maximum error of 48 [rpm] and 16.55 [N.m] in the estimation of the velocity and load torque, respectively. This is because the induced torque, t_{ind} , which is obtained through the torque transducer for verification, also includes the acceleration/deceleration torque together with total load torque. Another reason for the increase in the t_L estimation error is that the load torque is considered as a constant state in the EKF algorithm. The variation in the rotor resistance, \hat{R}_r , in Fig. A-5(d), demonstrates a decline with the decreasing rotor frequency, f_r , in the low velocity range, and an incline as the rotor frequency increases. This result is also in harmony with the $R_r - f_r$ relationship as stated in Proca and Keyhani (2002) and Barut et al. (2005).

Scenario III – Performance with and without R_s estimation in high speed region:

As is well-known with induction motors, R_s undergoes significant variations with temperature, ranging from 0.7 to 1.7 of the rated R_{sn} value, around rated speed (Byeong-Seok and Krishnan, 1998). Two scenarios are run in this section, –one without R_s estimation and with R_s estimation- to highlight the importance of accurate R_s updates on the estimation performance. In both scenarios, arbitrary variations are imposed on R_s by the external addition of resistances to the phase windings, since an increase in R_s is normally expected due to heating over long periods of operation. In the scenario with the EKF estimation of R_s , \hat{R}_r values are provided from the EKF scheme in Barut et al., (2005).

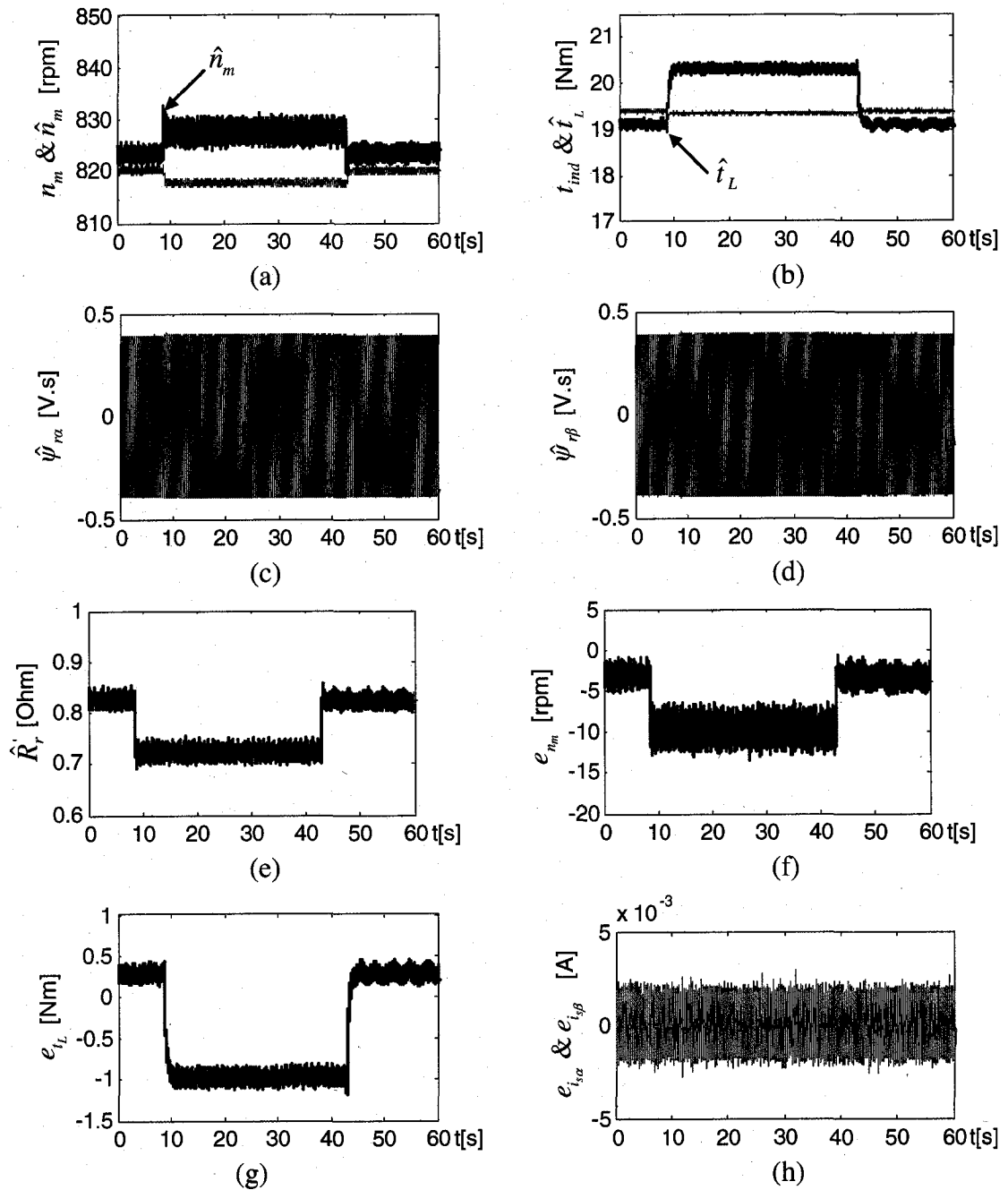


Fig. A-6 Experimental results at high speed with EKF- \hat{R}_r and without R_s estimation: (a) Variation of \hat{n}_m ; (b) variation of t_{ind} and \hat{t}_L ; (c) variation of $\hat{\psi}_{r\alpha}$; (d) variation of $\hat{\psi}_{r\beta}$; (e) variation of \hat{R}_r ; (f) variation of e_{n_m} ; (g) variation of e_{t_L} ; and (h) variation of $e_{i_{s\alpha}}$ & $e_{i_{s\beta}}$

First, while the IM is running at 820.2 [rpm] under a load torque of 19.4 [N.m], at $t=8.6$ [sec.], the R_s is increased to 1.4Ω (approximately $2 R_{sn}$) by connecting additional resistors to the IM terminals. At $t=42.7$ [sec.] the additional resistors are shorted via a switch. Fig. A-6(a), (b), (c), (d), (e), (f), (g) and (h) demonstrate the variations of n_m & \hat{n}_m , t_{ind} & \hat{t}_L , \hat{R}_r , $\hat{\psi}_{r\alpha}$, $\hat{\psi}_{r\beta}$, $e_{n_m} \triangleq n_m - \hat{n}_m$, $e_{t_L} \triangleq t_{ind} - \hat{t}_L$ and the variation of $e_{i_{s\alpha}}$ & $e_{i_{s\beta}}$.

Inspecting the results in Fig. A-6, it can be noted that when R_s variations are occurring, R_r' estimation alone is not sufficient to achieve a good estimation performance and hence, considerable errors occur in the estimation of velocity and all other states/parameters; however, system stability is still maintained.

In the next section, the scenario is repeated with similar variations imposed on R_s , but with the EKF based R_s estimation switched on, as well as R_r' updates from the look-up table. The results indicate that R_s estimation is also necessary for improved performance even for the less problematic high speed operation. Fig. A-7 presents the results obtained with EKF based R_s estimation and R_r' updates from the look-up table. Fig. A-7(a), (b), (c), (d), (e), (f), (g), (h) and (i) demonstrate the variations of n_m & \hat{n}_m , t_{ind} & \hat{t}_L , \hat{R}_s , \hat{R}_r , $\hat{\psi}_{r\alpha}$, $\hat{\psi}_{r\beta}$, $e_{n_m} \triangleq n_m - \hat{n}_m$, $e_{t_L} \triangleq t_{ind} - \hat{t}_L$ and the variation of $e_{i_{s\alpha}}$ & $e_{i_{s\beta}}$.

As can be seen from the results, the EKF estimation of R_s improves the estimation of velocity and all other estimated variables/parameters significantly. It can also be observed that the estimated R_s has attained its accurate value, which can easily be verified by measurements.

Scenario IV – Performance with and without R_s estimation at low and zero speed:

This scenario aims to demonstrate the importance of R_s estimation in the problematic low

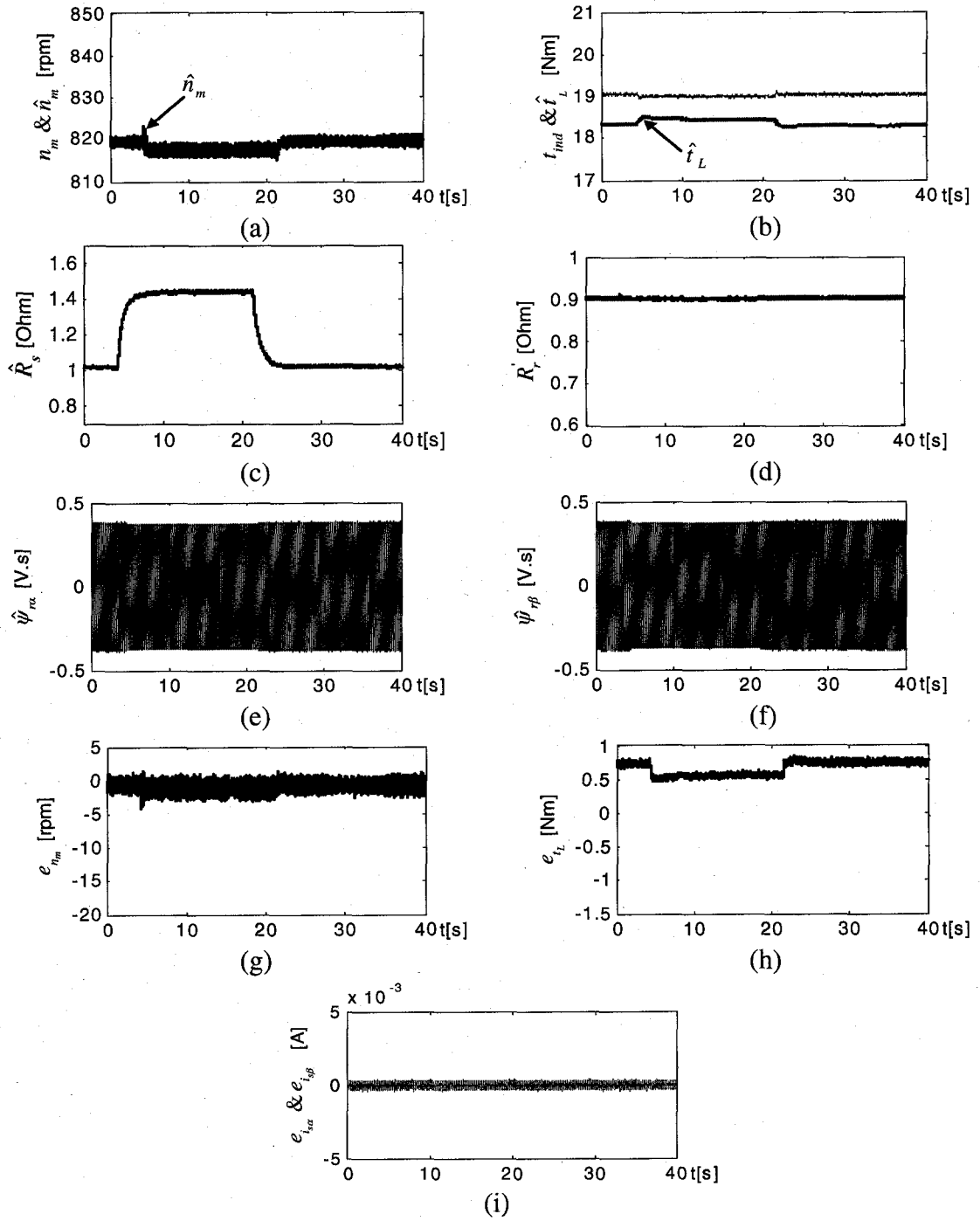


Fig. A-7 Experimental results at high speed with R_s estimation and R_r look-up table: (a) Variation of \hat{n}_m ; (b) variation of t_{ind} and \hat{t}_L ; (c) variation of \hat{R}_s ; (d) variation of R_r ; (e) variation of $\hat{\psi}_{r\alpha}$; (f) variation of $\hat{\psi}_{r\beta}$; (g) variation of e_{n_m} ; (h) variation of e_{t_L} ; and (i) variation of $e_{i_{s\alpha}}$ & $e_{i_{s\beta}}$

speed region, where no R_s estimation is provided, but only R_r' updates from the look-up table.

Initially, when the motor is running at 51 [rpm] under a load torque of 3.9 [N.m], at $t=7.8$ [sec.], the R_s is increased to 1.4 [Ω] by connecting additional resistors to the IM terminals. Fig. A-8(a), (b), (c), (d), (e), (f), (g) and (h) demonstrate the variations of n_m & \hat{n}_m , t_{ind} & \hat{t}_L , \hat{R}_r , $\hat{\psi}_{r\alpha}$, $\hat{\psi}_{r\beta}$, $e_{n_m} \triangleq n_m - \hat{n}_m$, $e_{t_L} \triangleq t_{ind} - \hat{t}_L$ and the variation of $e_{i_{s\alpha}}$ & $e_{i_{s\beta}}$.

As can be seen from Fig. A-8, the effect of R_s uncertainties becomes more significant in low speed operation, deteriorating overall estimation performance when there is only R_r' estimation, and no R_s estimation.

Next, the improvement achieved with the EKF based R_s estimation is demonstrated for very low and zero speed operation, by switching on R_s estimation in addition to R_r' updates. For this purpose, while the IM is running at 28 [rpm] under a load torque of 2.3 [N.m], at $t=5.5$ [sec.], n_m is stepped down to 0 [rpm]. Next, at $t=14.4$ [sec.], the R_s is increased to 1.4 Ω by connecting additional resistors to the IM terminals and at $t=53.7$ [sec.], the resistors are shorted via a switch. The resulting performance given in Fig. A-9 (a), (b), (c), (d), (e), (f), (g), (h) and (i) demonstrate the variations of n_m & \hat{n}_m , t_{ind} & \hat{t}_L , \hat{R}_s , \hat{R}_r , $\hat{\psi}_{r\alpha}$, $\hat{\psi}_{r\beta}$, $e_{n_m} \triangleq n_m - \hat{n}_m$, $e_{t_L} \triangleq t_{ind} - \hat{t}_L$ and the variation of $e_{i_{s\alpha}}$ & $e_{i_{s\beta}}$.

Inspecting the results, it can be noted that during the zero speed operation interval of approximately 58.5 [sec], the increase in R_s to 1.4 [Ω] is very closely tracked by estimation, resulting in an overall improved estimation performance for velocity and load torque in Fig. A-9(g) and (h).

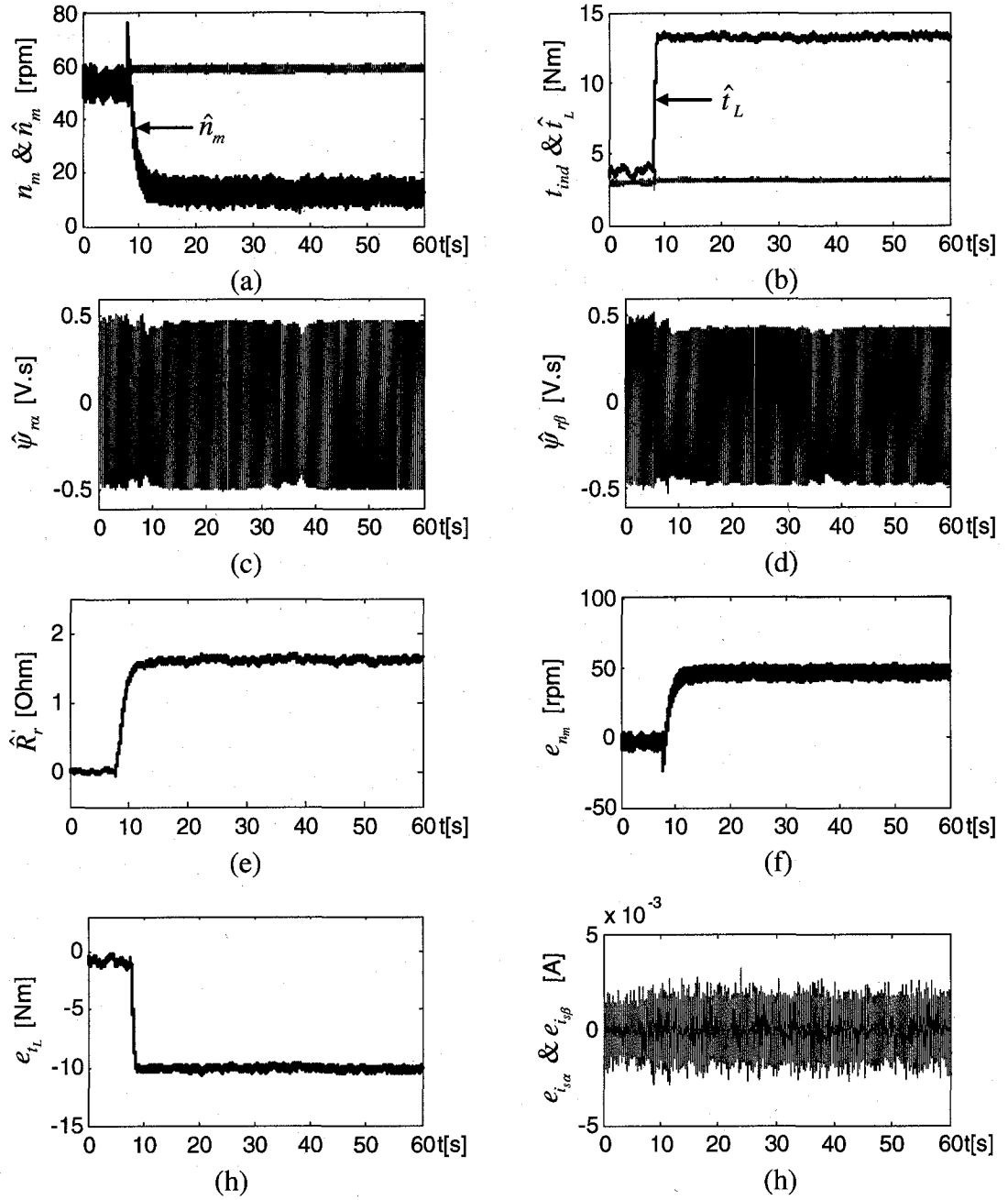


Fig. A-8 Experimental results at very low speed without R_s estimation: (a) Variation of \hat{n}_m ; (b) variation of t_{ind} and \hat{t}_L ; (c) variation of $\hat{\psi}_{r\alpha}$; (d) variation of $\hat{\psi}_{r\beta}$; (e) variation of \hat{R}_r ; (f) variation of e_{n_m} ; (g) variation of e_{t_L} ; and (h) variation of $e_{i_{s\alpha}}$ & $e_{i_{s\beta}}$

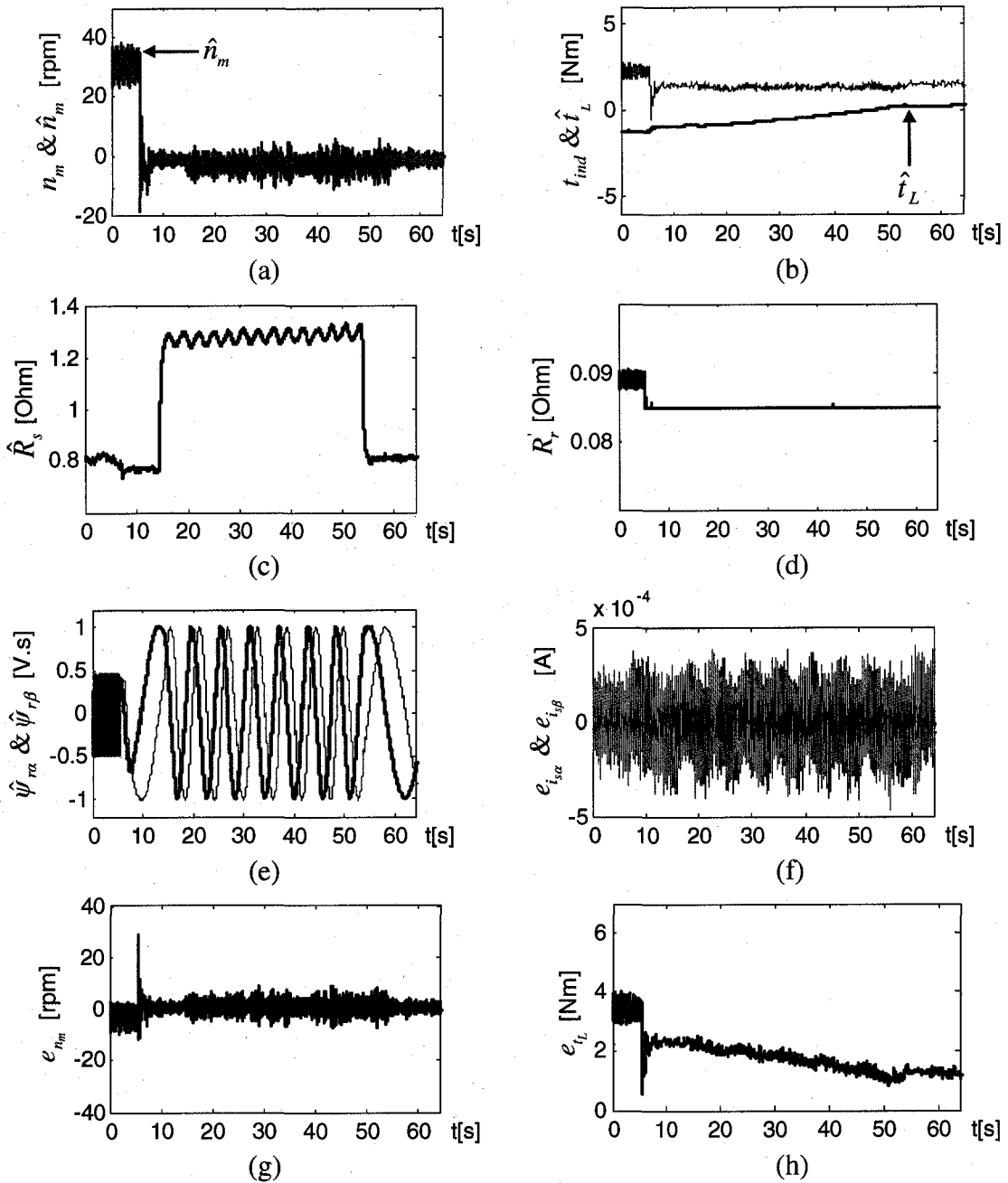


Fig. A-9 Experimental results at very low/zero speed with R_s estimation: (a) Variation of \hat{n}_m ; (b) variation of t_{ind} and \hat{t}_L ; (c) variation of \hat{R}_s ; (d) variation of R_r ; (e) variation of $\hat{\psi}_{r\alpha}$ & $\hat{\psi}_{r\beta}$; (f) variation of $e_{i\alpha}$ & $e_{i\beta}$; (g) variation of e_{n_m} ; (h) variation of e_{t_L} ; and (i) variation of the estimated position of the flux with reference to the stator stationary axis.

A.6 Conclusion

The major contribution of this study is the development and experimental implementation of an EKF based scheme which provides on-line estimates for R_s and continuous updates for R_r from a look-up table for an improved estimation performance in IM sensorless control over a wide speed range. The look-up table is built via the EKF estimation of R_r from the authors' previous study (Barut et al., 2005). The temperature and frequency related uncertainties of both R_s and R_r are known to be very effective on sensorless estimation and control performance in IMs. In that sense, to the authors' best knowledge, this is the first known study in the sensorless control of induction motors, using both R_s and R_r estimations simultaneously, for improved performance.

The significant improvement achieved with the estimation scheme over a wide speed range motivates the utilization of the approach in practice, in cases where one single EKF might not be adequate to handle the high number of parameters to be estimated, thereby compromising estimation accuracy.

The performance of the approach can be further improved by increasing the “sensitivity” of the R_r look-up table to velocity, torque and temperature variations or even better by incorporating a second on-line EKF scheme which runs in parallel or consecutively with the first, to estimate the additional parameters.

References

- Barut, M. Bogosyan, O.S. and Gokasan, M. (2002), “EKF based estimation for direct vector control of induction motors”, *Proceedings of IEEE-IECON02*, Vol. 2, pp. 1710–1715
- Barut, M. Bogosyan, O.S. and Gokasan, M. (2005), “An EKF based estimator for speed sensorless vector control of induction motors,” *Electric Power Components & Systems, formerly Electric Machines and Power Systems*, Taylor–Francis, Vol. 33, No. 7, pp. 727–744.

Bogosyan, S., Gokasan, M. and Hajiyeve, C. (2001), "An application of EKF for the position control of a single link arm", *Proceedings of IEEE-IECON'01 Annual Meeting*; Vol. 1, pp. 564–569.

Chen, F. and Dunnigan, M.W. (2002), "Comparative study of a sliding-mode observer and Kalman filters for full state estimation in an induction machine", *IEE Proceedings-Electric Power Applications*, Vol. 149, No. 1, pp. 53–64

Guidi, G. and Umida, H. (2000), "A novel stator resistance estimation method for speed-sensorless induction motor drives", *IEEE Transactions on Industry Applications*, Vol. 36, No. 6, pp. 1619–1627

Holtz, J. (2005), "Sensorless control of induction machines—with or without signal injection?", *IEEE Transactions on Industrial Electronics*, Vol. 53, No. 1, pp. 7 – 30

Kojabadi, H.M., Chang, L. and Doriaswami, R. (2002), "Recent progress in sensorless vector-controlled induction motor drives", *Proceedings of IEEE-LESCOPE02*, pp. 80–85

Lascu, C., Boldea, I. and Blaabjerg, F. (2004), "Direct torque control of sensorless induction motor drives: a sliding-mode approach", *IEEE Trans on Industry Applications*, Vol. 40 No. 2, pp. 582–590

Proca A.B. and Keyhani A. (2002), "Identification of variable frequency induction motor models from operating data", *IEEE Transactions on Energy Conversion*, Vol. 17, No. 1, pp. 24–31

Vas, P. (1998), *Sensorless vector and direct torque control*, Oxford University Press, New York

Wang, H., Xu, W., Shen, T. and Yang, G. (2005), "Stator flux and torque decoupling control for induction motors with resistances adaptation", *IEE Proceedings-Control Theory Applications*, Vol. 152, No. 4, pp. 363-370

Appendix B:

Braided Extended Kalman Filters for Sensorless Estimation in Induction Motors at High-Low/Zero Speed*

Abstract—In this study, an Extended Kalman Filter (EKF) based estimation approach is developed for the simultaneous estimation of rotor (R_r) and stator (R_s) resistances, the uncertainties of which are commonly known to cause problems in flux and velocity estimation for sensorless control over a wide speed range. The proposed “braided” EKF approach in this paper is based on the consecutive operation of two EKF algorithms running in turn, at each sampling interval and is the first reported study in IM sensorless control achieving the accurate estimation of R_s , R_r , which is reported as a challenge in the literature. The Braided EKF also improves the estimation of flux and velocity over a wide range, including persistent operation at zero speed. The proposed algorithm is tested with simulations and experiments at high, low and zero speed under challenging load torque, velocity and R_s , R_r variations. A significant improvement is achieved over conventional single EKF schemes and compatible, if not better results are obtained with previously reported sensorless estimation methods, with no need for signal injection or for different algorithms for different parameters and speed ranges.

Index Terms—Induction motor, Braided Extended Kalman Filters, sensorless control, rotor resistance and stator resistance estimation, load torque estimation, zero speed operation.

B.1 Introduction

The benefits of sensorless control are increased reliability of the overall system with the removal of mechanical sensors, thereby reducing sensor noise and drift effects as well as

* Bogosyan, S., Barut, M., and Gokasan, M. (2006b), “Braided Extended Kalman Filters for Sensorless Estimation in Induction Motors at High-Low/Zero Speed”, *IEE Proceedings Control Theory & Applications*. (In review)

cost and size. However, the effect of parameterization errors and model uncertainties become more relevant with speed/position-sensorless control and require sophisticated estimation methods. Speed/position-sensorless control of IMs also gives rise to control and estimation problems at and around zero stator frequency. This is mainly due to the fact that all flux estimation methods rely on the effect of the rotor induced voltages on the measured variables of the stator side and that those effects almost vanish with decreasing stator frequency [1]. Increased noise-to-signal ratios in measured output voltage and input currents, especially under low or no load conditions, also affect the performance negatively at low/zero speed operation. Moreover, the persistency of excitation of the input signal, which is essential for accurate estimation/identification, is also reduced at low speeds, giving rise to erroneous steady-state performance and drifts, particularly when a high number of parameters are to be estimated. Thus, in the design of observers for sensorless control of IMs not only robustness against parameter and model uncertainties must be achieved, but solutions must be sought for operation at and around zero speed.

To address the problems in the low and zero speed range, some reported studies exploit the motor anisotropies either via the injection of high frequency signals [2], [3] or by direct use of the inverter PWM signals [4]. A major disadvantage of the former approach is the requirement for additional high frequency signals, dependence on system parameters, dynamic delay caused by phase-locked loop (PLL), low-signal-to-noise ratio and magnetic saturation due to the fundamental field. The PWM approach, on the other hand, makes use of the high frequency components of the inverter PWM signals, thereby providing a higher signal-to-noise ratio and is quite effective for the position control of IMs (in the very low and zero speed region); however, it requires special measures to be taken in the high speed region.

Recently, for the solution of the problem at zero/very low speed, model based estimation methods have also been proposed such as in [5], [6] and [7], specifically addressing

persistent operation at zero speed. Among those studies, [5] uses a total least square (TLS) based speed adaptive flux observer which enables zero stator frequency operation over an interval of 60 sec., with mean and maximum estimation error values of 1.34 [rpm] and 38 [rpm], respectively at zero load; [6] uses model reference adaptive system (MRAS) based linear neural networks presenting results with a maximum velocity estimation error of 95 [rpm] during a persistent operation interval of 60 [sec] at zero speed; [7] utilizes a continuous sliding mode approach, for which zero stator frequency results are obtained under load and presented only for a very short interval of 4 sec.

Temperature and frequency based variations of stator (R_s) and rotor (R_r) resistances play an important role in the rotor and stator oriented IM models and their variations influence the estimation and control performance significantly.

To address this problem in IM sensorless control, a variety of approaches have been proposed and problems have been reported. To mention a few, the study in [8] states that simultaneous estimation of the stator, R_s and rotor resistances, R_r , give rise to instability. In another study [9], taking a model reference adaptive approach the individual estimation of ω_m with R_s or R_r has yielded good results, while the simultaneous R_s , R_r and ω_m estimation has led to inaccurate estimation values. Studies based on sliding mode (SM) observers (SMO), such as [10] estimate the R_r and [11] estimate the R_s and [12] estimate the R_s and develop a SM flux observer that does not require speed adaptation. Satisfactory results are obtained in the 3-6 rpm operation region. Some studies develop speed adaptive flux observers, such as [13] in which R_s is also estimated and [14], [12] and [15] which adjust the value of R_r in proportion to the estimated R_s . None of those studies address persistent operation at zero speed, except [14], as already discussed under zero speed studies.

Model uncertainties and nonlinearities inherent to IMs are also well suited for the stochastic nature of Extended Kalman Filters (EKF). With this method, it is possible to

make the on-line estimation of states while simultaneously performing identification of parameters in a relatively short time interval. The EKF is also known for its high convergence rate, which improves transient response significantly. Moreover, EKFs meet the requirement of high frequency signals for accurate estimation and convergence in steady-state with the model and measurement noises inherently included in the extended model of EKFs. On the other hand, the major limitations of the EKF technique appear to be its computational complexity and reduced estimation accuracy when a high number of parameters are to be estimated with a single EKF with limited number of measurements as is the case with sensorless control. While the former issue is no longer a problem thanks to the high performance processors of our day, the latter issue remains a problem and requires that special measures be taken, as is the case in this study.

In spite of the numerous EKF studies in IM sensorless control, only those which are most relevant to the presented study will be mentioned here due to space limitations: i.e. [16], [17], [18], [19], [20], [21], are some studies estimating the flux and velocity; [22] estimates the rotor resistance by injecting of low amplitude, high frequency signals to the flux reference giving rise to fluctuation in the flux, torque and speed. Most of these studies estimate the velocity as a constant parameter, giving rise to a poor estimation performance in transient state. Recently, the authors' studies in [23] and [24] estimating the velocity via the consideration of the equation of motion in the EKF model, in addition to the estimation of rotor resistance and mechanical uncertainties demonstrate improved results over a wide speed range. However, the results are sensitive to the variations of stator resistance, indicating the necessity of an approach to estimate rotor resistance and stator resistance simultaneously, as well as the load torque. To the authors' best knowledge, simultaneous R_s - R_r estimation and/or persistent operation at zero speed in sensorless IM control have yet not been reported in any EKF based sensorless estimation study.

In IM sensorless control, only a few studies have achieved the simultaneous estimation of R_s and R_r ; among these studies, [25] presents a model reference adaptive system (MRAS) based on 3 models, of which one is used for the estimation of rotor time constant via high frequency signal injection and the other 2 models are used interchangeably by enabling the stator resistance estimation only during short intervals, during which the rotor speed has reached the steady state. In studies such as [26], [27] the speed and rotor flux are estimated as well as the stator resistance and rotor resistance, by injecting high frequency signals to the flux and magnetizing current commands. Recently, [28] presents a sensorless control scheme using an open-loop estimator to calculate R_r and a model reference adaptation for R_s . However, the performance of the parameter estimation is not demonstrated and only evaluated indirectly via the estimated velocity and flux. The above listed studies, to the authors' best knowledge, are the only reported IM sensorless control studies estimating R_s and R_r simultaneously as the two most effective parameters on estimation and control performance; however, the results require either signal injection or the design of different algorithms based on the velocity range or based on the parameters/states to be estimated, R_s or R_r .

The major contribution of this study is the development of a novel EKF implementation technique, which achieves the simultaneous estimation of R_s and R_r , hence improving the accuracy of estimated flux, torque, and velocity in IM sensorless estimation over a wide speed range, including persistent operation at zero speed. The developed “braided” EKF approach involves the consecutive use of two EKF algorithms at every sampling interval; the two EKF algorithms have exactly the same configuration and are derived based on the same extended model and estimated states except for one state; i.e. R_s in one model is replaced by R_r in the other. Both EKFs also estimate velocity, load torque, stator flux and current components. The algorithm is tested using simulations and experiments in different velocity ranges under challenging parameter and load variations and very promising results have been obtained, without the need for signal injection or algorithm changes as in most previous studies yielding acceptable performance.

B.2 Extended Mathematical Models of the IM

In this study, two extended models are developed for the EKF based estimation scheme. Both models estimate stator flux components, $\psi_{s\alpha}$ and $\psi_{s\beta}$, angular velocity, ω_m , the load torque, t_L and stator current components $i_{s\alpha}$ and $i_{s\beta}$, which are also measured as output. Additionally, one of the models includes R_s , while the other has R_r - with both resistances and load torque taken into consideration as constant variables under the assumption of slow variation in time. Thus, the so-called extended models developed in this study can be obtained (as referred to the stator stationary frame) in the following general form:

$$\begin{aligned}\dot{\underline{x}}_{ei}(t) &= \underline{f}_{ei}(\underline{x}_{ei}(t), \underline{u}_e(t)) + \underline{w}_{i1}(t) \\ &= \underline{A}_{ei}(\underline{x}_{ei}(t))\underline{x}_{ei}(t) + \underline{B}_e \underline{u}_e(t) + \underline{w}_{i1}(t)\end{aligned}\quad (\text{B-1})$$

$$\begin{aligned}\underline{Z}(t) &= \underline{h}_{ei}(\underline{x}_{ei}(t)) + \underline{w}_{i2}(t) \quad (\text{measurement equation}) \\ &= \underline{H}_e \underline{x}_{ei}(t) + \underline{w}_{i2}(t)\end{aligned}\quad (\text{B-2})$$

Here, \underline{x}_{ei} is the extended state vector for both models. \underline{f}_{ei} is the nonlinear function of the states and inputs. \underline{A}_{ei} is the system matrix. \underline{u}_e is the control input vector. \underline{B}_e is the input matrix. \underline{w}_{i1} is the process noise. \underline{h}_{ei} is the function of the outputs. \underline{H}_e is the measurement matrix. \underline{w}_{i2} is the measurement noise.

Based on the general form in (B-1) and (B-2), the detailed matrix representation of the two IM models can be given as below:

Model for R_s Estimation, Model- R_s :

$$\begin{bmatrix} \dot{i}_{s\alpha} \\ \dot{i}_{s\beta} \\ \dot{\psi}_{s\alpha} \\ \dot{\psi}_{s\beta} \\ \dot{\omega}_m \\ \dot{t}_L \\ \dot{R}_s \end{bmatrix} = \underbrace{\begin{bmatrix} -\left(\frac{R_s}{L_\sigma} + \frac{R_s L_s}{L_\sigma L_r}\right) & -p_p \omega_m & \frac{R_r}{L_r L_\sigma} & \frac{p_p \omega_m}{L_\sigma} & 0 & 0 & 0 \\ p_p \omega_m & -\left(\frac{R_s}{L_\sigma} + \frac{R_r L_s}{L_\sigma L_r}\right) & \frac{p_p \omega_m}{L_\sigma} & \frac{R_r}{L_r L_\sigma} & 0 & 0 & 0 \\ -R_s & 0 & 0 & 0 & 0 & 0 & 0 \\ 0 & -R_s & 0 & 0 & 0 & 0 & 0 \\ \frac{3 p_p}{2 J_L} \psi_{s\beta} & \frac{3 p_p}{2 J_L} \psi_{s\alpha} & 0 & 0 & 0 & \frac{1}{J_L} & 0 \\ 0 & 0 & 0 & 0 & 0 & 0 & 0 \\ 0 & 0 & 0 & 0 & 0 & 0 & 0 \end{bmatrix}}_{\Delta_1} \begin{bmatrix} i_{s\alpha} \\ i_{s\beta} \\ \psi_{s\alpha} \\ \psi_{s\beta} \\ \omega_m \\ t_L \\ R_s \end{bmatrix} + \underbrace{\begin{bmatrix} \frac{1}{L_\sigma} & 0 \\ 0 & \frac{1}{L_\sigma} \\ 1 & 0 \\ 0 & 1 \\ 0 & 0 \\ 0 & 0 \\ 0 & 0 \end{bmatrix}}_{B_e} \underbrace{\begin{bmatrix} v_{s\alpha} \\ v_{s\beta} \end{bmatrix}}_{\underline{u}_e} + \underline{w}_{11}(t) \quad (\text{B-3})$$

$$\underbrace{\begin{bmatrix} i_{s\alpha} \\ i_{s\beta} \end{bmatrix}}_{\underline{z}} = \underbrace{\begin{bmatrix} 1 & 0 & 0 & 0 & 0 & 0 & 0 \\ 0 & 1 & 0 & 0 & 0 & 0 & 0 \end{bmatrix}}_{H_e} \begin{bmatrix} i_{s\alpha} \\ i_{s\beta} \\ \psi_{s\alpha} \\ \psi_{s\beta} \\ \omega_m \\ t_L \\ R_s \end{bmatrix} + \underline{w}_{12} \quad (\text{B-4})$$

Model for R_r Estimation, Model- R_r :

$$\begin{bmatrix} \dot{i}_{s\alpha} \\ \dot{i}_{s\beta} \\ \dot{\psi}_{s\alpha} \\ \dot{\psi}_{s\beta} \\ \dot{\omega}_m \\ \dot{t}_L \\ \dot{R}_r \end{bmatrix} = \underbrace{\begin{bmatrix} -\left(\frac{R_s}{L_\sigma} + \frac{R_s L_s}{L_\sigma L_r}\right) & -p_p \omega_m & \frac{R_r}{L_r L_\sigma} & \frac{p_p \omega_m}{L_\sigma} & 0 & 0 & 0 \\ p_p \omega_m & -\left(\frac{R_s}{L_\sigma} + \frac{R_r L_s}{L_\sigma L_r}\right) & \frac{p_p \omega_m}{L_\sigma} & \frac{R_r}{L_r L_\sigma} & 0 & 0 & 0 \\ -R_s & 0 & 0 & 0 & 0 & 0 & 0 \\ 0 & -R_s & 0 & 0 & 0 & 0 & 0 \\ \frac{3 p_p}{2 J_L} \psi_{s\beta} & \frac{3 p_p}{2 J_L} \psi_{s\alpha} & 0 & 0 & 0 & \frac{1}{J_L} & 0 \\ 0 & 0 & 0 & 0 & 0 & 0 & 0 \\ 0 & 0 & 0 & 0 & 0 & 0 & 0 \end{bmatrix}}_{\Delta_2} \begin{bmatrix} i_{s\alpha} \\ i_{s\beta} \\ \psi_{s\alpha} \\ \psi_{s\beta} \\ \omega_m \\ t_L \\ R_r \end{bmatrix} + \underbrace{\begin{bmatrix} \frac{1}{L_\sigma} & 0 \\ 0 & \frac{1}{L_\sigma} \\ 1 & 0 \\ 0 & 1 \\ 0 & 0 \\ 0 & 0 \\ 0 & 0 \end{bmatrix}}_{B_e} \underbrace{\begin{bmatrix} v_{s\alpha} \\ v_{s\beta} \end{bmatrix}}_{\underline{u}_e} + \underline{w}_{21}(t) \quad (\text{B-5})$$

$$\underbrace{\begin{bmatrix} i_{s\alpha} \\ i_{s\beta} \end{bmatrix}}_{\underline{z}} = \underbrace{\begin{bmatrix} 1 & 0 & 0 & 0 & 0 & 0 & 0 \\ 0 & 1 & 0 & 0 & 0 & 0 & 0 \end{bmatrix}}_{H_e} \begin{bmatrix} i_{s\alpha} \\ i_{s\beta} \\ \psi_{s\alpha} \\ \psi_{s\beta} \\ \omega_m \\ t_L \\ R_r \end{bmatrix} + \underline{w}_{22} \quad (\text{B-6})$$

Here, p_p is the number of pole pairs. $L_\sigma = \sigma L_s$ is the stator transient inductance. σ is the leakage or coupling factor. L_s , L_r : stator and rotor inductances, respectively. $v_{s\alpha}$, $v_{s\beta}$: stator voltages. J_L : total inertia of the IM and load.

As can be seen from (B-3), (B-4) and (B-5), (B-6), the difference between the two extended vectors, \underline{x}_{e1} and \underline{x}_{e2} is due to the consideration of R_s or R_r . Since for both models $i_{s\alpha}$ and $i_{s\beta}$ are the measured variables, the measurement noises \underline{w}_{12} and \underline{w}_{22} are equal.

B.3 Development of Braided EKF Algorithm

In this section, the derivation of the EKF algorithm is given, using the two extended models, - Model_ R_s and Model_ R_r developed in Section II:

The Kalman filter is a well-known recursive algorithm that takes the stochastic state space model of the system into account, together with measured outputs to achieve the optimal estimation of states in multi-input, multi-output systems. The system and measurement noises are considered to be in the form of white noise. The optimality of the state estimation is achieved with the minimization of the covariance of the estimation error. As is well known, the Kalman Filter (KF) is not strictly applicable to nonlinear systems, such as IMs, since linearity plays an important role in its derivation and performance as an optimal filter. The EKF attempts to overcome this difficulty by using

a linearized approximation where the linearization is performed about the current state estimate. This process requires the discretization of (B-3) and (B-4) –or (B-5) and (B-6) as below;

$$\underline{x}_{ei}(k+1) = \underline{f}_{ei}(\underline{x}_{ei}(k), \underline{u}_e(k)) + \underline{w}_{i1}(k) \quad (\text{B-7})$$

$$\underline{Z}(k) = \underline{H}_e \underline{x}_{ei}(k) + \underline{w}_{i2}(k) \quad (\text{B-8})$$

As mentioned before, EKF involves the linearized approximation of the nonlinear model (B-7 and B-8) and uses the current estimation of states $\hat{\underline{x}}_{ei}(k)$ and inputs $\hat{\underline{u}}_e(k)$ in linearization by using,

$$\underline{F}_{ei}(k) = \left. \frac{\partial \underline{f}_{ei}(\underline{x}_{ei}(k), \underline{u}_e(k))}{\partial \underline{x}_{ei}(k)} \right|_{\hat{\underline{x}}_{ei}(k), \hat{\underline{u}}_e(k)} \quad (\text{B-9})$$

$$\underline{F}_{ui}(k) = \left. \frac{\partial \underline{f}_{ei}(\underline{x}_{ei}(k), \underline{u}_e(k))}{\partial \underline{u}_e(k)} \right|_{\hat{\underline{x}}_{ei}(k), \hat{\underline{u}}_e(k)} \quad (\text{B-10})$$

Thus, the EKF algorithm can be given in the following recursive relations:

$$\underline{N}_i(k) = \underline{F}_{ei}(k) \underline{P}_i(k) \underline{F}_{ei}(k)^T + \underline{F}_{ui}(k) \underline{D}_u \underline{F}_{ui}(k)^T + \underline{Q}_i \quad (\text{B-11a})$$

$$\underline{P}_i(k+1) = \underline{N}_i(k) - \underline{N}_i(k) \underline{H}_e^T (\underline{D}_\xi + \underline{H}_e \underline{N}_i(k) \underline{H}_e^T)^{-1} \underline{H}_e \underline{N}_i(k) \quad (\text{B-11b})$$

$$\hat{\underline{x}}_{ei}(k+1) = \hat{\underline{f}}_{ei}(\hat{\underline{x}}_{ei}(k), \hat{\underline{u}}_e(k)) + \underline{P}_i(k+1) \underline{H}_e^T \underline{D}_\xi^{-1} (\underline{Z}(k) - \underline{H}_e \hat{\underline{x}}_{ei}(k)) \quad (\text{B-11c})$$

Here, \underline{Q}_i is the covariance matrix of the system noise, namely model error. \underline{D}_ξ is the covariance matrix of the output noise, namely measurement noise. \underline{D}_u is the covariance

matrix of the control input noise ($v_{s\alpha}$ and $v_{s\beta}$), namely input noise. \underline{P}_i and \underline{N}_i are the covariance matrix of state estimation error and extrapolation error, respectively.

The algorithm involves two main stages: prediction and filtering. In the prediction stage, the next predicted states $\hat{f}_{ei}(\cdot)$ and predicted state error covariance matrices, $\underline{P}_i(\cdot)$ and $\underline{N}_i(\cdot)$ are processed, while in the filtering stage, next estimated states, $\hat{x}_{ei}(k+1)$, obtained as the sum of the next predicted states and the correction term (2nd term in (B-11c)), are calculated.

The Braided EKF scheme is comprised of two EKF algorithms running consecutively, with each EKF estimating the same set of variables, but a different resistor value, R_s or R_r . This estimated resistance value is passed on to the other EKF model in the next step, which, in turn, estimates the other resistance value. The rest of the variables and covariances are calculated by each EKF algorithm and passed to the control scheme along with the updated resistance values. A flow chart of the Braided EKF can be seen in Figure B-1.

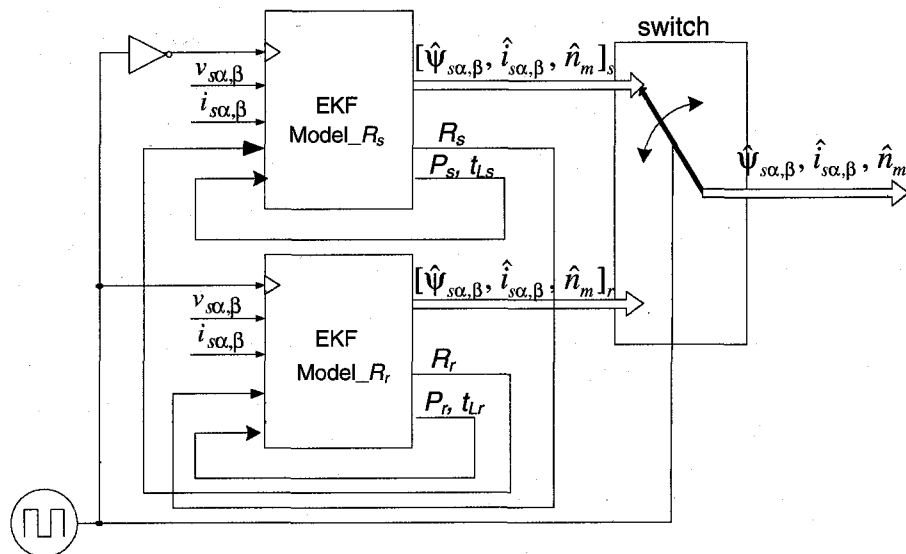


Fig. B-1 Braided EKF algorithm block diagram

B.4 Simulation and Experimental Results

To test the performance of the Braided EKF technique, proposed estimation method, simulations and experiments are performed on an induction motor with a DC machine providing the load, the parameters for which are given in Table B-1 and Table B-2, respectively.

Table B-1a. Rated values and parameters of the induction motor used in the experiments.

P [kW]	f [Hz]	$*J_L$ [kg.m ²]	p_p	V [V]	I [A]
2.238	60	0.2595	4	230	12

R_s [Ω]	R_r [Ω]	L_s [H]	L_r [H]	L_m [H]	N_m [rpm]	t_L [Nm]
0.6619	0.7322	0.0375	0.0376	0.0334	850	25.1

* J_L : total inertia in the experimental test-bed.

Table B-1b. Rated values and parameters of the DC machine used in the experiments.

P [kW]	V [V]	I [A]	N_m [rpm]	t_L [Nm]
3	125	24	1150	24.91

Tests are performed over the whole speed range, with special emphasis on the performance at and around zero speed. For a realistic evaluation of the proposed method, the results are compared with those obtained with EKF algorithms estimating either R_r or R_s , EKF- R_r and EKF- R_s respectively. Both algorithms also estimate the velocity, load torque, flux and current components and are tested under step type and linear variations of the velocity and load torque. R_r and R_s values are given increases of twice their rated values as well as half the rated value for R_r to further challenge the performance of the proposed method. A sampling time of $T=100$ μ sec is used.

Simulation Results:

High speed operation under load torque and R_r/R_s variations:

In this section, the performance of the Braided EKF is compared with the individual EKF- R_r and EKF- R_s algorithms for high speed operation and velocity and load torque reversals. To this aim, in the interval $0 < t < 20$ [sec], different load torque variations, velocity reversals as well as R_r and R_s variations of twice their rated values are imposed on the system and the obtained velocity estimation errors are compared for all three algorithms. As can be seen in Fig. B-2(c) and (d), the Braided EKF algorithm demonstrates an improved performance over EKF- R_r and EKF- R_s , particularly for unmatched parameter variations.

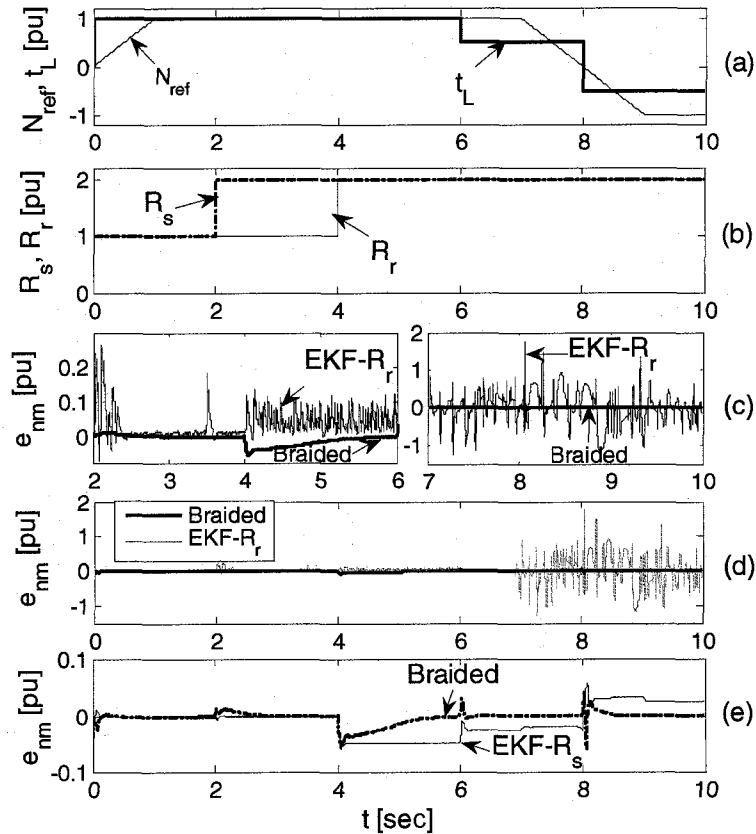


Fig B-2 Variation of velocity estimation errors, e_{nm} , at high speed operation under load torque variations, for three methods: a) N_m^{ref} , t_L , b) R_s , R_r , c) and d) e_{nm} with braided and EKF- R_r , ((c) detailed variation), e) e_{nm} with braided and EKF- R_s

Persistent operation at zero speed under zero load torque and R_r / R_s variations:

In this section, a similar comparison is performed between the three algorithms, while the velocity and load torque references are kept at zero and random decreases/increases are given to R_r and R_s . As can be seen in Fig. B-3, in the interval $0 < t < 30$ [sec], during which both R_r and R_s stepwise decreased from their rated values, the braided algorithm outperforms the EKF- R_r and EKF- R_s , as depicted by the velocity estimation error in Fig. B-3(c) and (d).

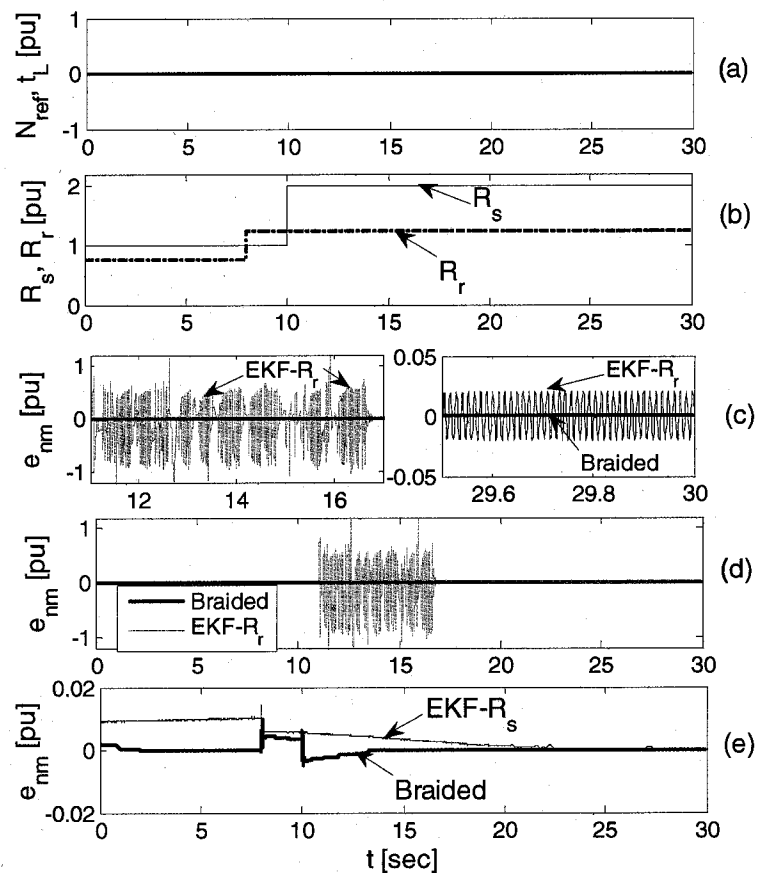


Fig. B-3 Variation of e_{nm} for zero speed and zero load for three methods: a) N_m^{ref} , t_L , b) R_s , R_r , c) and d) e_{nm} with braided and EKF- R_r , ((c) detailed variation), e) e_{nm} with braided and EKF- R_s

To provide a better explanation for the variations imposed on the system, per unit (pu) values are used for the results.

Experimental Results and Observations

The experimental setup depicted in Fig. B-4 includes a squirrel cage induction motor and driver, a host PC computer, a dS1104 Power PC processor and interface board, current and voltage sensors, a DC generator and resistor bank serving as the mechanical load and a torque transducer and encoder for the validation of estimated load torque and velocity.

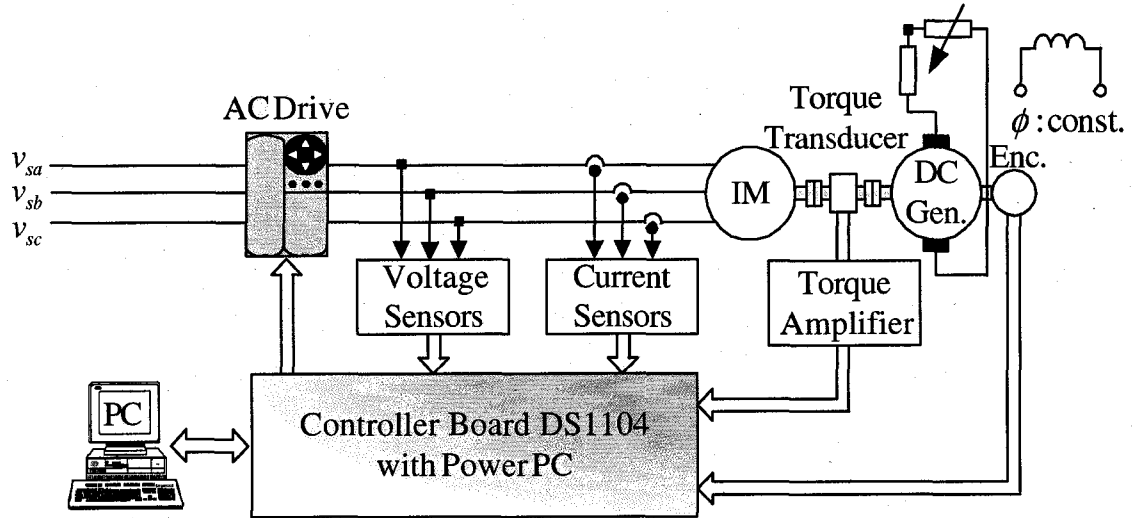


Fig. B-4 Schematic representation of the experimental setup.

High speed operation using EKF- R_r :

The experiments at high speed operation are initially conducted using the EKF- R_r algorithm only, which performs the estimation of R_r , velocity, load torque, stator flux and current components. To this aim, while the motor is operating at its rated speed under 75% load, the load torque is increased by 10%. This has naturally given rise to a drop in the measured velocity, while a faulty increase is obtained in the estimated velocity as can be seen in Fig. B-5(a). When the load torque assumes its original value, the velocity estimation error also drops to zero, as depicted in Fig. B-5(b). The measured and estimated torque, torque estimation error, estimated R_r (pu), estimation error of the current and flux components are given in Fig. B-5(c), (d), (e), (f) and (g), respectively.

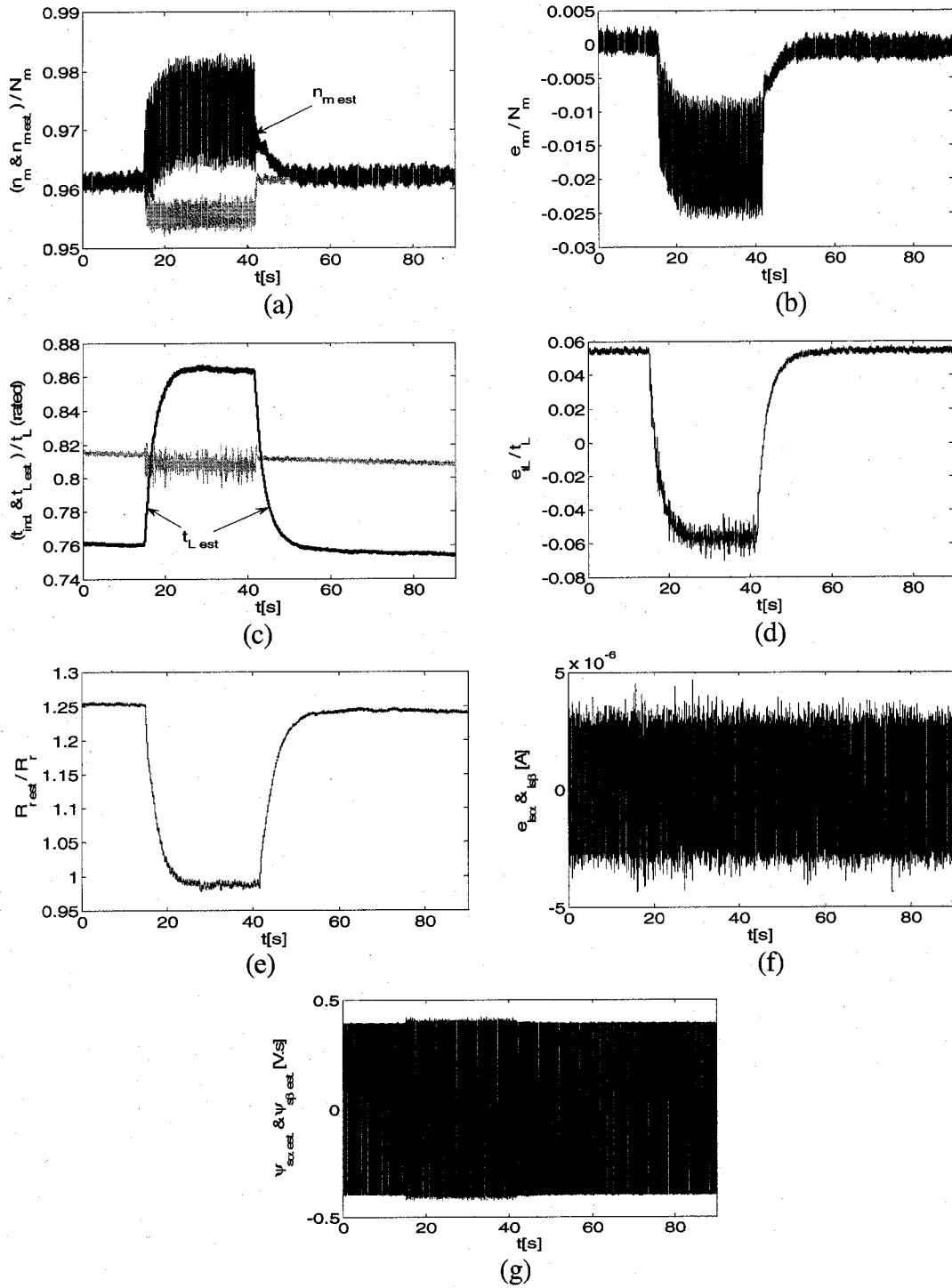


Fig. B-5 EKF-R_r results for high speed operation; variations of a) n_m , \hat{n}_m , b) $n_m - \hat{n}_m$, c) t_{ind} , \hat{t}_L , d) $t_{ind} - \hat{t}_L$, e) estimated rotor resistance, \hat{R}_r , f) $e_{is\alpha}$ and $e_{is\beta}$, g) $\psi_{s\alpha}$, $\psi_{s\beta}$

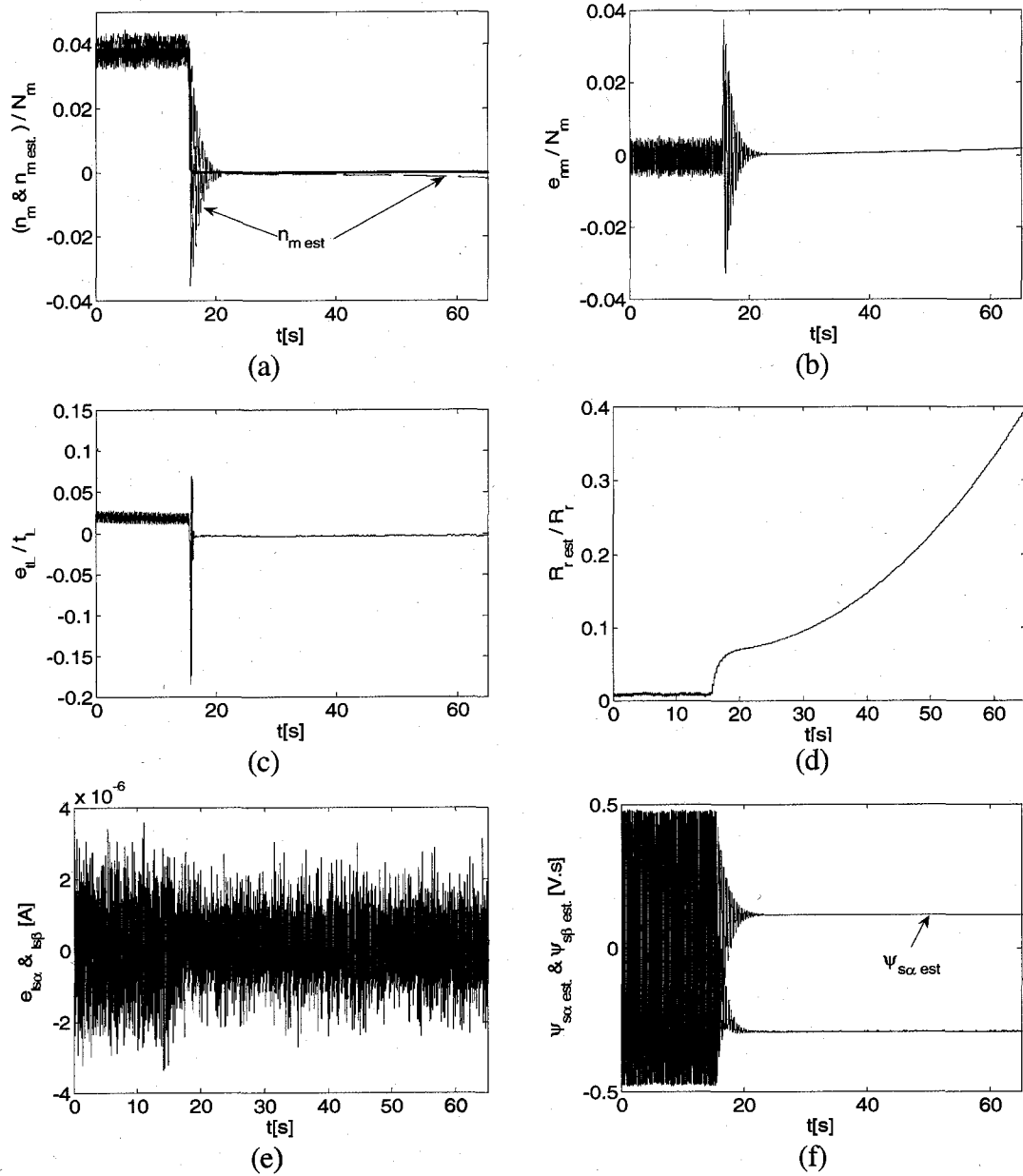


Fig. B-6 EKF- R_r results for low/zero speed operation; variations of a) n_m , \hat{n}_m , b) $n_m - \hat{n}_m$, c) $t_{ind} - \hat{t}_L$, d) \hat{R}_r , e) $e_{is\alpha}$ and $e_{is\beta}$, f) $\psi_{s\alpha}$, $\psi_{s\beta}$

Persistent operation at zero speed and load using EKF- R_r :

In this section, the performance EKF- R_r is also tested in zero speed operation. Initially, the velocity reference is maintained at low speed level (~ 0.04 pu) in Fig. B-6(a) and a constant value is obtained for the estimated R_r with an acceptably low velocity estimation

error (Fig. B-6(b)). However, when the velocity is given a stepwise decrease to zero, the estimated R_s and hence, the velocity estimation error start to drift (Fig. B-6(d)) due to the lack of updates of R_s .

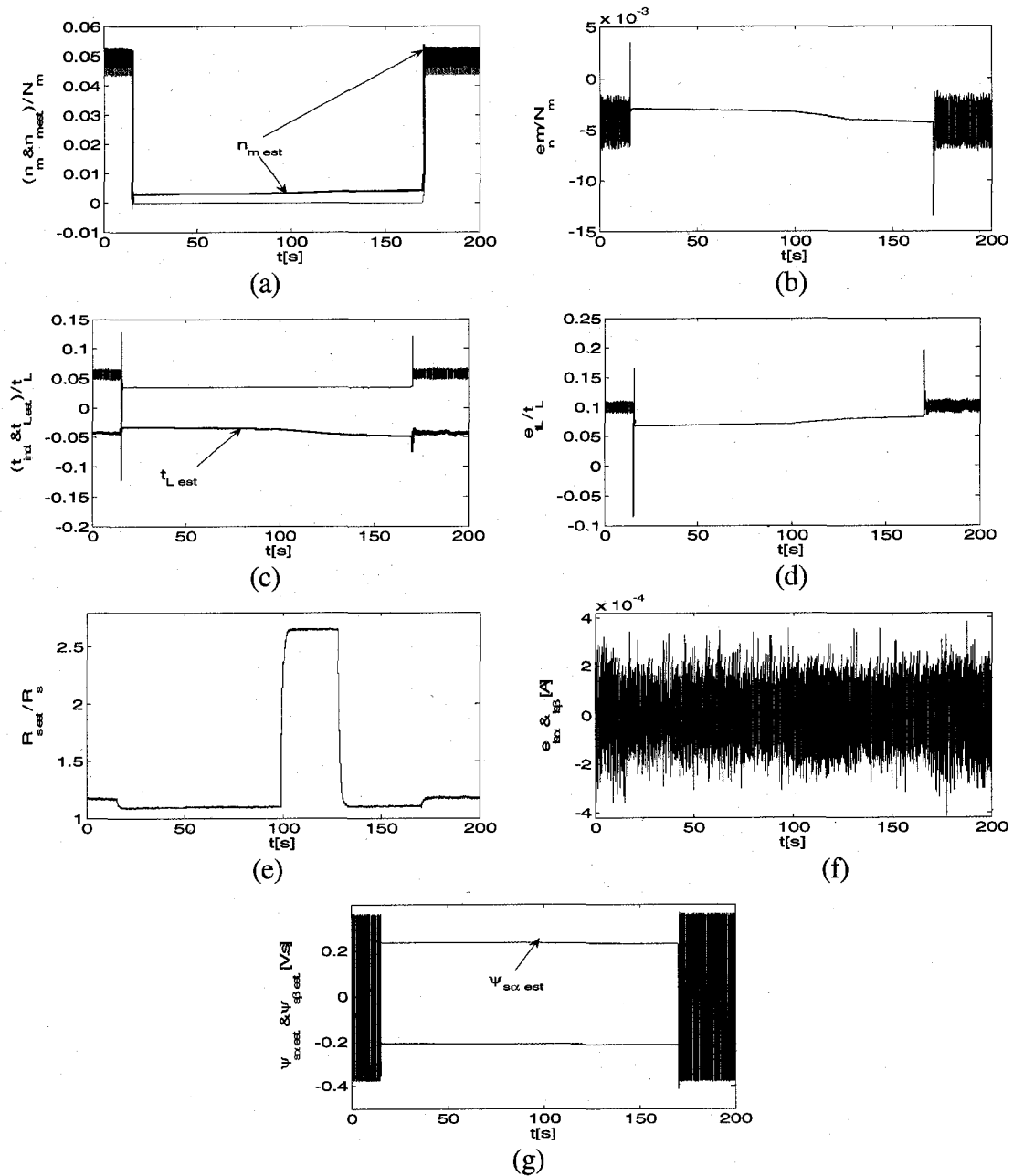


Fig. B-7 EKF- R_s results for low/zero speed operation; variations of a) n_m , \hat{n}_m , b) $n_m - \hat{n}_m$, c) t_{ind} , \hat{t}_L , d) $t_{ind} - \hat{t}_L$, e) \hat{R}_s , f) $e_{is\alpha}$ and $e_{is\beta}$, g) $\psi_{s\alpha}$, $\psi_{s\beta}$

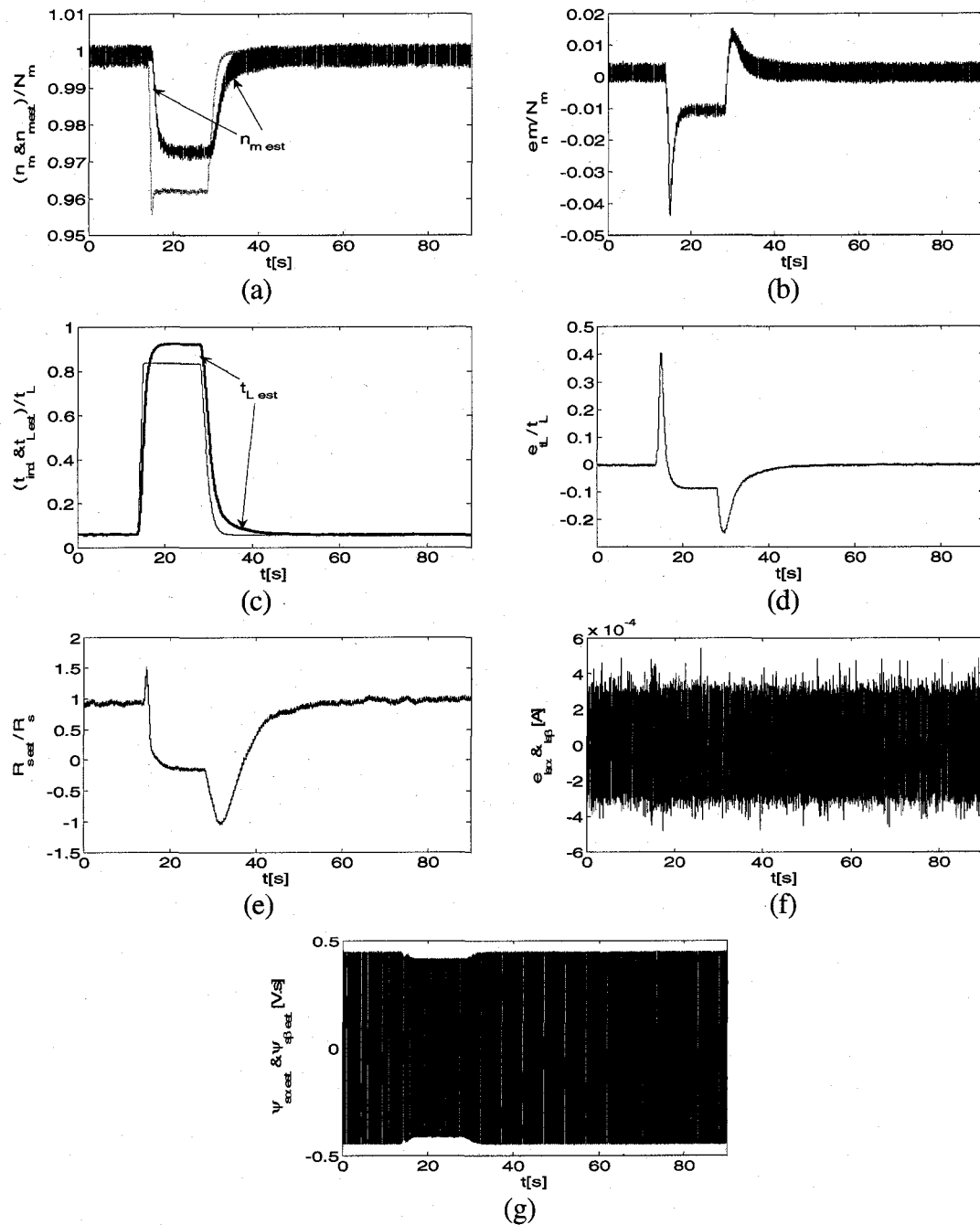


Fig. B-8 EKF- R_s results for high speed operation; variations of a) measured, n_m and estimated speed, \hat{n}_m , b) speed estimation error, $n_m - \hat{n}_m$, c) induced torque, t_{ind} and estimated torque, \hat{t}_L , d) torque error, $t_{ind} - \hat{t}_L$, e) estimated stator resistance, \hat{R}_s , f) observer errors ($e_{is\alpha}$ and $e_{is\beta}$), g) estimated flux components, $\psi_{s\alpha}$ and $\psi_{s\beta}$

Persistent operation at zero speed and zero load using EKF- R_s :

In this section, experiments are performed for zero speed operation using the EKF- R_s algorithm, since the R_s uncertainties are more effective in low speed operation. To further challenge the algorithm, the R_s value is instantaneously increased to 2.5 times its rated value by connecting serial resistances externally to the stator windings (Fig. B-7(e)). The EKF- R_s algorithm performs quite well in spite of the challenging R_s variation, yielding a very low velocity estimation error (Fig. B-7(b)).

High speed operation performance with EKF- R_s :

In this section the EKF- R_s algorithm is tested in high speed operation, under load torque and hence rotor resistance variations. In the interval where the load torque variation is imposed, a significant increase has occurred in the velocity estimation error as can be seen in Fig. B-8(b).

The experimental results obtained with individual EKF- R_r and EKF- R_s indicate that for an acceptable performance in sensorless estimation for IMs over the whole speed range, both R_r and R_s should continuously be updated. This observation motivates the development of the Braided EKF scheme.

High speed operation performance with the Braided EKF:

In this section, the Braided EKF algorithm is tested for high speed operation under load torque variations (from 5% to 85% of the rated load) as can be seen in Fig. B-9(c). From the figures, it can be seen that the load torque variations have also given rise to R_r variations in Fig. B-9(f), while the variations of R_s are much less in the high speed range, it can be seen in Fig. B-9(e). The experimental results indicate also that the Braided EKF performs very well under those variations yielding a very low estimation error for the velocity as can be seen in Fig. B-9(b). The very low estimation errors obtained for the current 9(g), velocity 9(a) and the torque 6(d) also indicate the accurate estimation of the flux components given in Fig. B-9(h).

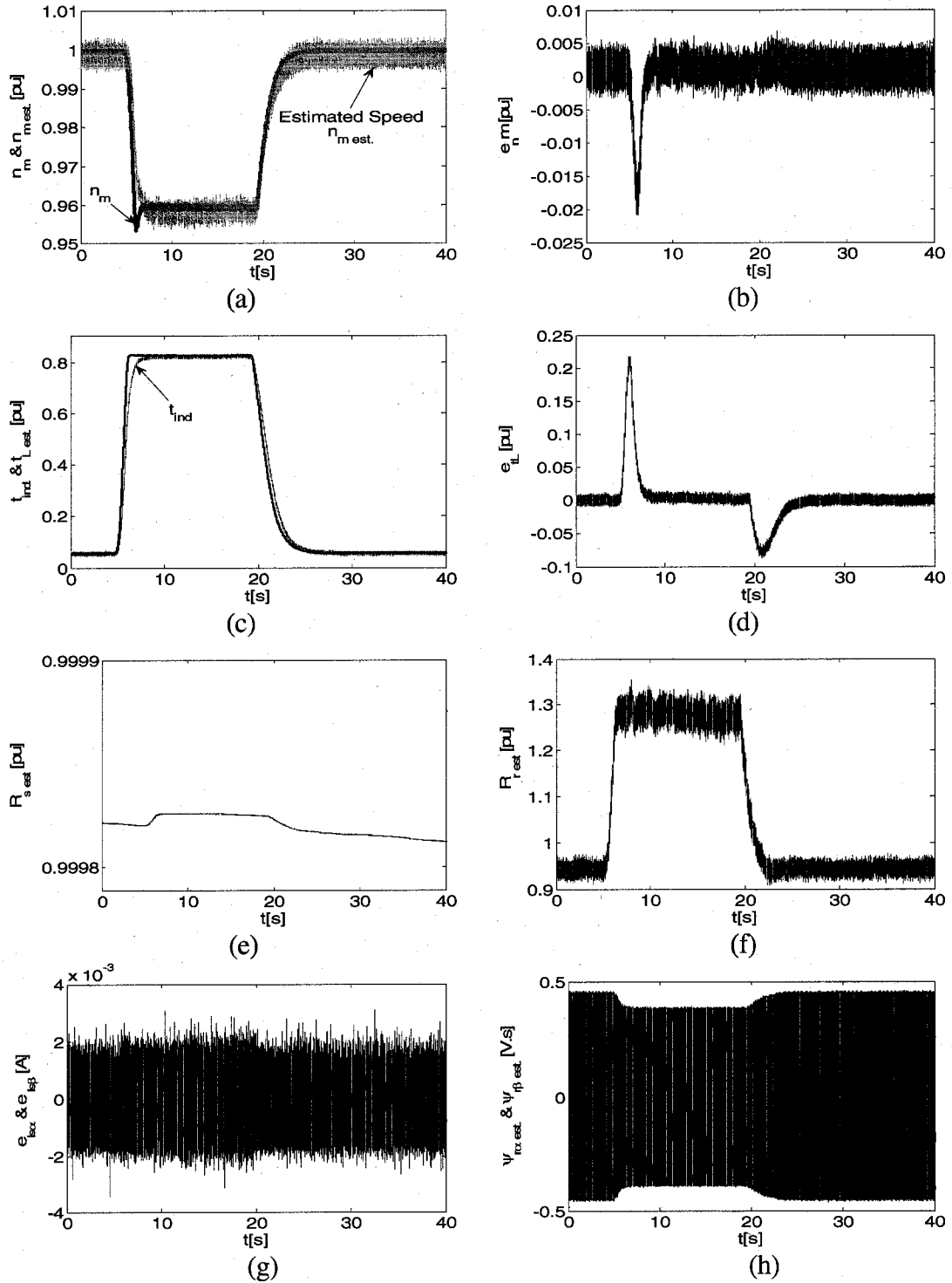


Fig. B-9 Braided EKF results for high speed operation; variations of a) n_m , \hat{n}_m , b) $n_m - \hat{n}_m$, c) t_{ind} , \hat{t}_L , d) $t_{ind} - \hat{t}_L$, e) \hat{R}_s , f) \hat{R}_r , g) $e_{is\alpha}$ and $e_{is\beta}$, h) $\psi_{s\alpha}$, $\psi_{s\beta}$

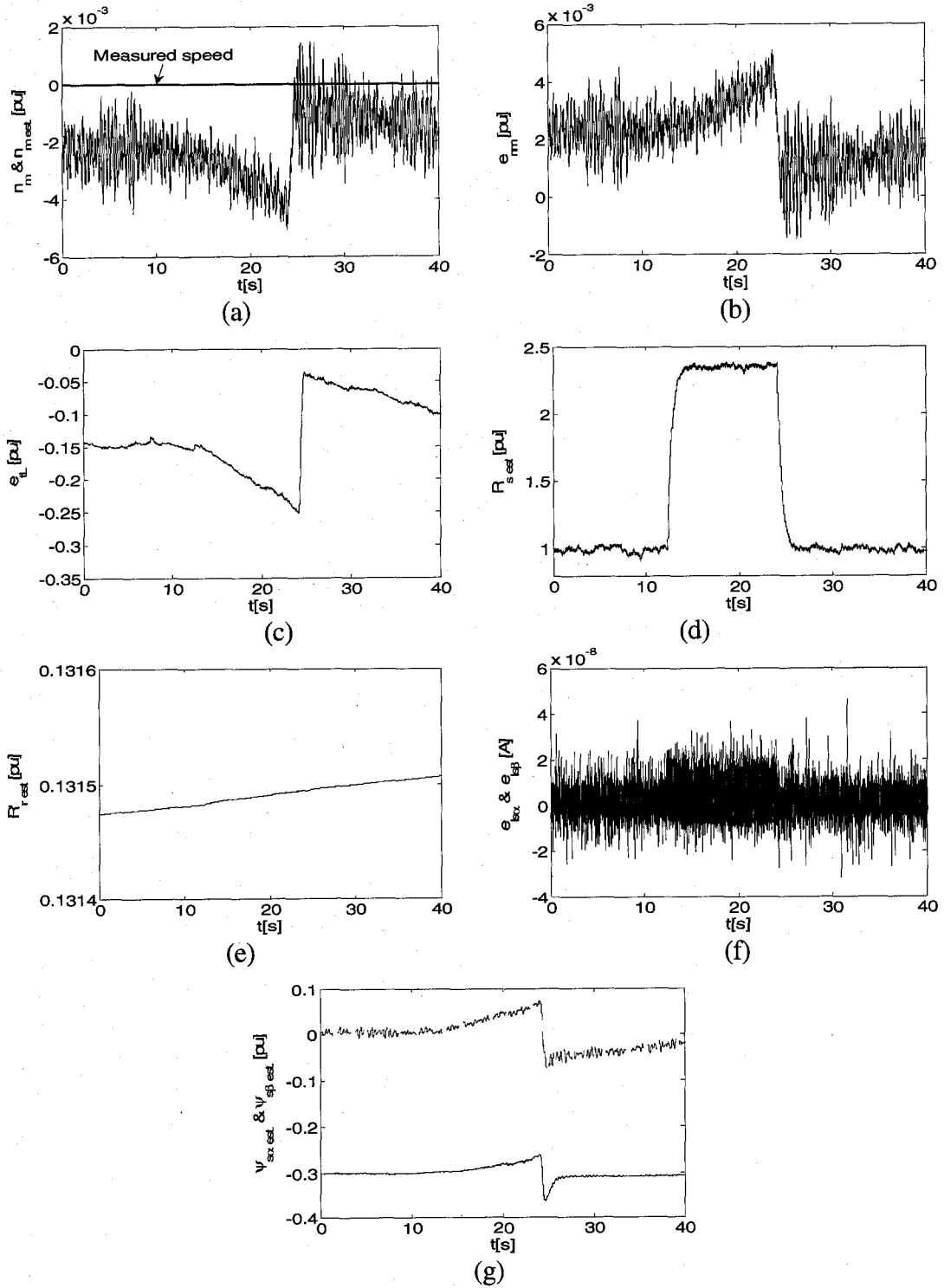


Fig. B-10 (a) Braided EKF results for zero speed operation; variations of a) n_m, \hat{n}_m , b) $n_m - \hat{n}_m$, c) $t_{ind} - \hat{t}_L$, d) \hat{R}_s , e) \hat{R}_r , f) $e_{is\alpha}$ and $e_{is\beta}$, g) $\psi_{s\alpha}, \psi_{s\beta}$

Persistent zero speed and zero load operation using Braided EKF:

In this section, the Braided EKF is also tested for persistent operation at zero speed under challenging external variations impressed on R_s (Fig. B-10(d)), which is increased to $2.4 R_{sn}$. It can be noted that the velocity estimation error remains within a very low error band, it can be seen in Fig. B-10(b), while velocity is zero (in Fig. B-10(a)).

In conclusion, it can be noted that the Braided EKF is superior to the individual EKF algorithms in terms of overall performance. The braided scheme also demonstrates a compatible and, most of the time, a better performance in one-on-one comparison with EKF- R_r in high speed, and with EKF- R_s in zero speed operation. Although stopped the end of 40 seconds, the experiments have also indicated that the persistent operation at zero speed can be extended over longer intervals, without causing drift or instability.

B.5 Conclusion

Temperature and frequency based variations of R_s and R_r induction motors become very effective on the estimation performance, particularly when speed-sensorless control is aimed. Due to problems arising from lack of persistency of excitation and decreased accuracy when a single algorithm is used to estimate a high number of parameters and states, the simultaneous estimation of R_s and R_r is often reported as a challenge in IM sensorless control. The problem of sensorless estimation is even more compounded at low and zero speed operation due to the decreased excitation in the input signals. The few reported studies overcoming these problems in the literature either use signal injection or different estimation methods for different states/parameters with a limited number of measurements as in sensorless control, in different speed ranges.

In this study, a multiple EKF based observer technique is developed for the estimation of R_s and R_r for use in the sensorless control of IMs. The approach is based on the consecutive use of two EKF algorithms derived from two extended models, which are comprised of one common and one different set of parameters. Thus the resulting

algorithm achieves the accurate estimation of a higher number of parameters than would be possible with a single EKF algorithm.

The Braided EKF technique exploits the model and measurement noise inherent to EKFs for the persistency of excitation required for convergence in steady-state. With the use of multiple EKFs in estimation, it also overcomes the limitation of a single EKF in estimating a high number of parameters with limited number of measurements, as is the case in sensorless control.

The simulation and experimental results obtained for sensorless estimation at high and low speed, as well as in persistent operation at zero speed, demonstrate significantly improved results over single EKF algorithms. The performance is comparable, if not better, than that for most previous studies, in terms of offering a more general and flexible solution over the whole speed range. The developed method can be extended to the estimation of any other set of parameters/states in IM sensorless control and may also be used with other control methods which require the accurate knowledge of a high number of parameters.

References

- [1] Holtz J.: "Sensorless control of induction machines -with or without signal injection?," IEEE Trans. Industrial Electronics, 2006, 53, (1), pp 7-30
- [2] Teske, N., Asher, G.M., Summer M. and Bradley K.: "Suppression of saturation saliency effects for the sensorless position control induction motor drives under loaded conditions," IEEE Trans. Industrial Electronics, 2000, 47 (1), pp. 1142-1149
- [3] Teske, N., Asher, G.M., Bradley K. and Summer M.: "Analysis and suppression of inverter clamping saliency in sensorless position controlled induction machine drives," Proc. of the IEEE-IAS Annual Meeting, Chicago, 2001, pp. 2629-2636

- [4] Holtz J. and Pan H.: "Elimination of saturation effects in sensorless position controlled induction motors," Proc. of the IEEE-IAS Annual Meeting, Pittsburgh, 2002, pp. 1695 - 1702.
- [5] Lascu, C., Boldea I., and Blaabjerg F.: "Direct torque control of sensorless induction motor drives: a sliding-mode approach," IEEE Trans. Industry Applications, 2004, 40, (2), pp. 582–590
- [6] Derdiyok, A., Guven, M.K., Rehman, H., Inanc, N., and Xu, L.: "Design and implementation of a new sliding-mode observer for speed-sensorless control of induction motor," IEEE Trans. Industrial Electronics, 2002, 49, (5), pp. 1177–1182
- [7] Kim, Y.-R., Sul, S.-K. and Park, M.-H.: "Speed sensorless vector control of induction motor using extended Kalman filter," IEEE Trans. Industry Applications, 1994, 30, (5), pp. 1225–1233
- [8] Faiz, J. and Sharifian, M.B.B.: "Different techniques for real time estimation of an induction motor rotor resistance in sensorless direct torque control for electric vehicle," IEEE Trans. Energy Conversion, 2001, 16, (1), pp.104–109
- [9] Zhuohui, T, Yongdong, L., and Zhiyan, J.: "Speed sensorless DTC and parameter estimation of induction motor based on a full-order MRAS method," Proc. of IEEE-PIEMC 2000; pp.1202–1206
- [10] Derdiyok, A.; "Speed-sensorless control of induction motor using a continuous control approach of sliding-mode and flux observer," IEEE Trans. Industrial Electronics, 2005, 52, (4), pp.1170–1176
- [11] Lascu, C., Boldea, I., and Blaabjerg, F.: "Direct torque control of sensorless induction motor drives: a sliding-mode approach," IEEE Trans. Industry Applications 2004; 40, (2), pp. 582–590
- [12] Lascu, C., Boldea, I., and Blaabjerg, F.: "Very-low-speed variable-structure control of sensorless induction machine drives without signal injection," IEEE Trans. Industry Applications, 2005, 41, (2), pp. 591–598

- [13] Guidi, G, and Umida, H.: "A novel stator resistance estimation method for speed-sensorless induction motor drives," *IEEE Trans. Industry Applications*, 2000; 36, (6), pp. 1619–1627
- [14] Cirrincione, M., Pucci, M., Cirrincione, G., and Capolino, G.-A.: "An adaptive speed observer based on a new total least-squares neuron for induction machine drives," *IEEE Trans. Industry Applications*, 2006, 42, (1), pp. 89–104
- [15] Ohyama, K., Asher, G.M., and Sumner, M.: "Comparative analysis of experimental performance and stability of sensorless induction motor drives," *IEEE Trans. Industrial Electronics*, 2005, 53, (1), pp. 178–186
- [16] Akin, B., Orguner, U., Ersak, A., and Ehsani, M.: "A comparative study on non-linear state estimators applied to sensorless AC drives: MRAS and Kalman filter," *Proc. of the IEEE-IECON 04*, Nov. 2004, pp. 2148 – 2153
- [17] Kim, Y.-R., Sul, S.-K., and Park, M.-H.: "Speed sensorless vector control of induction motor using extended Kalman filter. *IEEE Trans. Industry Applications*, 1994, 30, (5), pp. 1225–1233.
- [18] Shi, K.L., Chan, T.F., Wong, Y.K., and Ho, S.L.: "Speed estimation of an induction motor drive using an optimized extended Kalman Filter," *IEEE Trans. Industrial Electronics*, 2002, 49, (1), pp. 124–133
- [19] Lee, C-M, and Chen, C-L.: "Observer-based speed estimation method for sensorless vector control of induction motors," *IEE Proceedings—Control Theory and Applications*, 1998, 145, (3), pp. 359–363
- [20] Wenqiang, Y, Zhengchun, J, and Qiang, X.: "A new algorithm for flux and speed estimation in induction machine," *Proc. of the IEEE-ICEMS01*, 2001, pp. 698–701
- [21] Qiongquan, G., and Zhiyue, F.: "Speed estimated for vector control of IM using reduced-order EKF," *Proc. of the. IEEE-PIEMC'00*, 2000, pp. 138–142

- [22] El Moucary, Ch., Garcia Soto, G., Mendes, E.: "Robust rotor flux, rotor resistance and speed estimation of an induction machine using the extended Kalman Filter," Proc. of the IEEE-ISIE'99, 1999, pp. 742–746
- [23] Barut, M, Bogosyan, O.S., and Gokasan, M.: "Speed sensorless direct torque control of IMs with rotor resistance estimation," *Energy Conversion and Management*, Elsevier, 2005, 46, (3), pp. 335-349
- [24] Barut, M, Bogosyan, O.S., and Gokasan, M.: "An EKF based estimator for speed sensorless vector control of induction motors," *Electric Power Components & Systems*, Taylor–Francis, 2005, 33, (7), pp. 727–744
- [25] Zhen, L., and Xu, L.: "Sensorless field orientation control of induction machines based on a mutual MRAS scheme," *IEEE Trans. Industrial Electronics*, 1998, 45, (5), pp. 824–831
- [26] In-Joong, H., and Sang-Hoon, L.: "An online identification method for both stator- and rotor resistances of induction motors without rotational transducers," *IEEE Trans. Industrial Electronics*, 2000, 47, (4), pp. 842–853
- [27] Tajima, H, Guidi, G., and Umida, H.: "Consideration about problems and solutions of speed estimation method and parameter tuning for speed-sensorless vector control of IM drives," *IEEE Trans. Industry Applications*, 2002, 38, (5), pp. 1282–1289
- [28] Edelbaher, G., Jezernik, K. and Urlep, E.: "Low-speed sensorless control of induction machine," *IEEE Trans. Industrial Electronics*, 2006, 53, (1), pp. 120-129

Appendix C:**Definitions of Acronyms**

ADC	Analog-to-Digital Converter
AFO	Adaptive Flux Observer
CF-SMC	Chattering-Free Sliding-Mode Controller
DC	Direct Current
DTC	Direct-Torque Control
DVC	Direct Vector Control
EKF	Extended Kalman Filter
ELO	Extended Luenberger Observer
EMF	Electro-Motive Force
FOC	Field-Oriented Control
IM	Induction Motor
KF	Kalman Filter
LPF	Low-Pass Filter
MRAS	Model-Reference Adaptive System
PBC	Passivity-Based Control
PC	Personal Computer
PI	Proportional-Integral controller.
PID	Proportional-Integral-Derivative controller
PLL	Phase-Locked Loop
PWM	Pulse Width Modulation
SM	Sliding-Mode
SMC	Sliding-Mode Controller (or Control)
SMO	Sliding-Mode Observer
SVM	Space-Vector Modulation
TLS	Total Least Square
VC	Vector Control